Laser and Electron Beam Treatments for Corrosion Protection of Friction Stir Welds in Aerospace Alloys

by

Eirian Bethany Siggs

A thesis submitted to

The University of Birmingham

For the degree of

ENGINEERING DOCTORATE

School of Metallurgy and Materials

The University of Birmingham

2009

UNIVERSITY OF
BIRMINGHAM

University of Birmingham Research Archive

e-theses repository

This unpublished thesis/dissertation is copyright of the author and/or third parties. The intellectual property rights of the author or third parties in respect of this work are as defined by The Copyright Designs and Patents Act 1988 or as modified by any successor legislation.

Any use made of information contained in this thesis/dissertation must be in accordance with that legislation and must be properly acknowledged. Further distribution or reproduction in any format is prohibited without the permission of the copyright holder.

Abstract

Friction Stir Welding (FSW) is a suitable technology for aerospace structure development and is a possible replacement for mechanical fastening. To achieve the application of FSW, pre- and post-weld treatments are required.

A pre-weld treatment of surface preparation was required to ensure a weld with good mechanical properties. The surface preparation necessary is the removal of paint and anodising layers from aerospace alloys. Laser paint removal was assessed and designed to remove these layers with only an oxide remaining, which welded to produce high quality welds.

The post-weld treatment was essential to increase the corrosion resistance of the welded area. The improvement in corrosion resistance was achieved with High Power Beam Surface Modification (HPBSM), which created a homogeneous surface through rapid surface melting and solidification. The rapid thermal processing dissolved and dispersed the precipitate solute atoms which were retained in solid solution through planar solidification.

Electron beams and various lasers were used in the HPBSM processing. Excimer Laser Surface Melting (LSM) improved corrosion resistance but the layer depth was restricted by processing parameters. HPBSM processing studies using an electron beam, USP-CO_2 laser and Nd:YAG laser provided understanding on how processing parameters controlled the modified layer characteristics.

To Simon for always being his wonderful self.

Acknowledgements

There are many people to whom I owe a lot of thanks for all of their help and guidance throughout my doctorate. This project would not have been possible without the financial support of EPSRC, Airbus UK and BAE Systems. Particular thanks go to my industrial supervisors Dr Stephen Morgan and Dr Steve Harris of BAE Systems ATC and Mike Poad of Airbus UK. Thanks also to the rest of the people in the BAE Systems Materials and OLT departments for their help and assistance especially when things started to go wrong. I must also include in these thanks the people who made the project possible but also jumped ship during the course, Dr Debbie Price, Dr Simon Scott and Prof Stewart Williams of Cranfield University.

I owe a lot of thanks to Dr Alison Davenport of The University of Birmingham who provided the academic support. I would also like to thank the Applied Electrochemistry Group of the Univeristy of Birmingham who helped me out with testing, particularly Cristiano Padovani, Napachat Tareelap and Farkhanda Kauser.

This thesis was possible with the help of many different universities. Thanks are due to Cranfield University Welding Engineering Research Centre and Heriot Watt University School of Engineering and Physical Sciences for use of their lasers. Thanks are also due to the University of Manchester Prof Phil Prangnell and Dr Paul Ryan for the discussions and TEM expertise.

I have had considerable support away from the office from my family who have helped in all the ways they knew how. Enormous thanks go to Simon for helping, listening, distracting and

looking after me, I would have been lost without you. Thanks to Mum and Dad who have helped me all the way through my pursuit of the alien subject metallurgy. Thanks to Kylie, Dave and Dan for being a fantastic distraction. Not forgetting also thanks to my extended family for their patience, understanding and unending hospitality, Alan and Mandy.

Particular thanks go to the friends that took all my whinges, joys and problems with minimal complaint. Particular thanks go to Tiina for all of her support and guidance from the beginning. I also need to thank the girls Caroline, Jenny M, Jenny P, Carla and Pauline for the discussions and commiserations. Thanks to Taz, Nicke, Pete and Megan for the use of their dinning rooms and sharing of alcohol. Finally I owe more than thanks to Claire for the commaradery in modules and always being on the end of phone regardless of everything, you are a wonderful star to be treasured.

Table of Contents

List of Figures

List of Tables

Notation

CAA = Chromic Acid Anodising

EBSM = Electron Beam Surface Melting

EDX = Energy Dispersive Analysis of X-rays

FSW = Friction Stir Welding

GPB zones = Guinier-Preston-Bagaryatski zones

HAZ = Heat Affected Zone

HPBSM = High Power Beam Surface Modification

IGC = Inter Granular Corrosion

LSA = Laser Surface Alloying

LSM = Laser Surface Melting

MLA = Micro Lens Array

Nd:YAG Laser = Neodymium-doped Yttrium Aluminium Garnet Laser

PRF = Pulse Repetition Frequency

SEM = Scanning Electron Microscopy

SSSS = Super Saturated Solid Solution

TEA-CO_2 Laser = Transversely Excited Atmospheric Carbon Dioxide Laser

TMAZ = Thermo-Mechanically Affected Zone

TSA = Tartaric Sulphuric Acid Anodising

USP-CO_2 Laser = Ultra Super Pulse Carbon Dioxide Laser

1 Introduction

Aluminium alloys have been used since the 1920's in aerospace structures since they develop a high strength-to-weight ratio through precipitation hardening. However, the presence of precipitates within the alloys leads to poor corrosion resistance [1]. Therefore the application of aluminium alloys requires the development of treatments which improve their corrosion resistance; the most successful of currently available methods is anodising [2]. The chromic acid anodising (CAA) process is currently used but is under review as there is pending legislation on the restriction of usage of chromium (VI) and therefore alternative corrosion protection techniques are being considered [3, 4]. Currently, aluminium alloys on airframes are protected from the environment by multiple layers of anodising and paint, all of which tend to be chromate based [2].

Mechanical fastening by riveting is currently used in the joining of aircraft structures as aluminium alloys are not easily welded by traditional techniques owing to their tendency for solidification and liquation cracking [2, 5, 6]. The new technique of Friction Stir Welding (FSW) is suitable for the joining of aluminium alloys and it is a potential replacement for riveting [7-9]. The benefits for the replacement of riveting with FSW in airframes include: the formation of a continuous joint, which results in improvement to the mechanical properties, along with reductions in both airframe cost and weight. Disadvantages in the application of FSW include the necessity of a clean surface prior to welding (i.e. with no paint or anodising layers) and more detrimentally, low corrosion resistance of the resulting weld [10-12]. It has been proposed that laser treatment could be used to alleviate both of these issues with surface preparation and local surface modification.

Preparation of material to be joined in FSW requires the removal of any contaminants or layers from the surfaces. The benefit of using a laser for this removal is that the process is highly specific and controllable with minimal damage to the substrate material [10, 11].

Altering the substrate material by Laser Surface Melting (LSM) can improve the corrosion resistance of a friction stir weld. The improvement in corrosion resistance by LSM is from rapid solidification, due to rapid cooling by the bulk material, causing in homogenising of the surface composition and microstructure [12-17]. However, even this technique has possible problems: there are concerns with the application of LSM including the limitations of laser processing parameters that may affect the melt layer thickness as in many cases only relatively a thin modified layer have be produced [18]. The problem with a thin modified layer is that it can be easily damaged and will be consumed if the LSM process were to be combined with other corrosion protection techniques such as anodising.

Modelling has shown that a key parameter for increasing the LSM layer thickness is the pulse duration, which is an inherent property of the laser [19]. Therefore in order to maximise the LSM modified layer thickness the affect of pulse duration needs to be investigated and this would require the use of a number of different lasers.

Electron Beam Surface Melting (EBSM) is an alternative rapid solidification technique to LSM, which has a greater degree of flexibility in the processing parameters, including pulse duration [20]. As EBSM allows for variation in the pulse duration, modified layers of a range of thicknesses can be produced and the relationship between the pulse duration and layer

thickness can be studied. This technique could allow thicker modified layers to be produced that are more corrosion resistant and are thick enough to survive an anodising treatment.

The objective of the work described in this thesis is to investigate the use of high power beams for surface preparation prior to FSW and post weld treatment for improved corrosion protection.

The pre-weld treatment investigation into laser paint removal required the optimisation of processing parameters for removal of specific layers present on airframe materials which were; anodising, primer and paint top-coat.

The post-weld treatment investigation required the characterisation of the rapid solidification techniques, LSM and EBSM, in terms of the effect of processing parameters on the modified layer microstructure and corrosion resistance. In particular the effect of pulse duration in LSM was investigated using three different lasers; excimer, USP-CO_2 and Nd:YAG. A non-standard EBSM system was developed and characterised to investigate the effect of pulse duration on the microstructures which were then compared with those produced by LSM. All the investigations were performed on parent material of 2xxx and 7xxx series aluminium alloys, as opposed to welded material as there was more detailed understanding and control of the initial microstructures. Table 1.1 summarises the tests that were performed with the various high power beams including the material type.

The work described in this thesis begins with a review of the literature (Chapter 2) on FSW, LSM, EBSM, and rapid solidification theory with attention to the effect of processing

parameters on the microstructure and any affects on material corrosion resistance. The experimental chapter (Chapter 3) details the general techniques used throughout this thesis and then specific details for each technique are separated into the appropriate results chapters. The first results chapter (Chapter 4) describes work on the pre-treatment aluminium alloys using laser paint removal prior to FSW. The rapid solidification techniques are then separated into three different LSM investigations listed in order of increasing pulse duration (Chapters 5, 6 and 7) and EBSM (Chapter 8). Chapter 9 then discusses these rapid solidification techniques and their key features.

Table 1.1 Summary of power beam systems and materials used throughout this thesis.

	Pulse Duration	Lasing Medium	Application	Material
Excimer Laser	25ns	Excited Dimer	LSM Paint Removal	AA2024, AA7056, AA7150, AA7449,
TEA-CO_2 Laser	3μs	CO_2	Paint Removal	AA2024
Nd:YAG Laser	80-150ns	Nd:$Y_3Al_5O_{12}$ crystal	Paint Removal	AA2024
Nd:YAG Laser	0.2-50ms	Nd:$Y_3Al_5O_{12}$ crystal	LSM	AA2024
USP-CO_2 Laser	7-100μs	CO_2	LSM	AA2024, AA7150
Electron Beam	7-40μs	-	EBSM	AA2024

2 Literature Review

2.1 Aluminium Alloys

Aluminium alloys are widely used because their properties can be tailored to suit the requirements of many applications. The elements used to alloy aluminium are also used to classify the alloys into series by a four digit system, as shown in Table 2.1 [2]. The aluminium alloys series are further distinguished by their response to heat treatment through precipitation hardening (also shown in Table 2.1). The heat treatment used is characterised by a letter and number designation system and examples are shown in Table 2.2 [2, 21].

Alloys that undergo precipitation hardening due to heat treatment develop particularly high strength and are suitable for aerospace applications, such alloys are the 2xxx and 7xxx series. A widely used aerospace alloy is AA2024 and it is the main alloy of study in this thesis. Three 7xxx series alloys have also been investigated these are AA7056, AA7150 and AA7449.

Table 2.1 The American Aluminium Association four digit classification system used to differentiate between commercially available wrought aluminium alloy [2].

Series Designation	Alloying Element	Thermal Response
1xxx	99% Aluminium	Non-Heat Treatable
2xxx	Copper	Heat Treatable
3xxx	Manganese	Non-Heat Treatable
4xxx	Silicon	Heat Treatable
5xxx	Magnesium	Non-Heat Treatable
6xxx	Magnesium and Silicon	Heat Treatable
7xxx	Zinc	Heat Treatable
8xxx	Other – Lithium	Heat Treatable

Table 2.2 The temper designation system used to describe the thermal and mechanical treatments undergone by heat-treatable aluminium alloys [21].

Temper	Description
T1	Partial solution treatment and naturally aged
T2	Cold worked and naturally aged
T3	Solution heat treated, cold worked and naturally aged
T4	Solution heat treated and naturally aged
T5	Artificially aged
T6	Solution heat treated and artificial ageing
T7	Solution heat treated and stabilised
T8	Solution heat treated, cold work and artificial ageing
T9	Solution heat treated, artificial ageing and cold work

2.1.1 Metallurgy

2.1.2 AA2024

AA2024 is an extensively used aerospace material due to high strength and fracture toughness. The properties of aluminium alloys, are dependent on the alloy microstructure and composition (given for AA2024 in Table 2.3), in particular the second phase precipitates that are present.

Table 2.3 Nominal weight percentage for AA2024 chemical composition [22].

Element (wt%) / Material	Al	Cr	Cu	Fe	Mg	Mn	Si	Ti	Zn	Zr
AA2024	Bal	0.10	3.4-4.9	0.50	1.2-1.8	0.3-0.9	0.50	0.15	0.25	-

The primary alloying element in AA2024 is copper and the influence of copper alloying addition depends on its concentration (further discussed in Section 2.3.2) [23, 24].

The addition of copper along with magnesium has the detrimental affect on the alloy properties by increasing the alloys tendency for solidification and liquation cracking both of which decrease the alloy weldability (further discussed in Section 2.2) [25].

The advantage of a magnesium addition however is to accelerate the alloy response to precipitation hardening, by stimulating the nucleation of precipitates (discussed further later in this Section) [21].

Manganese is another alloying addition in AA2024 and it influences the alloy grain structure by forming fine dispersoid precipitates that restrict grain boundary movement [2, 21].

As briefly described above, each of the AA2024 alloying elements influence the precipitates and alloy microstructure that forms. Figure 2.1 shows a typical AA2024 microstructure with elongated grains, from material fabrication rolling processes, and different precipitate types.

The precipitates that form in aluminium alloys are separated by their nature and size into three classes [21, 26]:

- Constituent particles are large (1-10μm) equilibrium precipitates which are formed from low-solubility elements (Cu) and impurities (Fe, Si) during casting; these particles are then fragmented during rolling operations.
- Dispersoid particles (200-500nm) are insoluble precipitates which have high melting temperatures and form during homogenisation heat treatment (500°C, 12-24 hours) in

fabrication. The precipitates contain low diffusivity elements (Cr, Mn or Zr) and are used to refine the microstructure grain size.

- Strengthening particles (≤50nm) are formed in heat treatments (tempers) with their size and distribution being used to control the alloy strength.

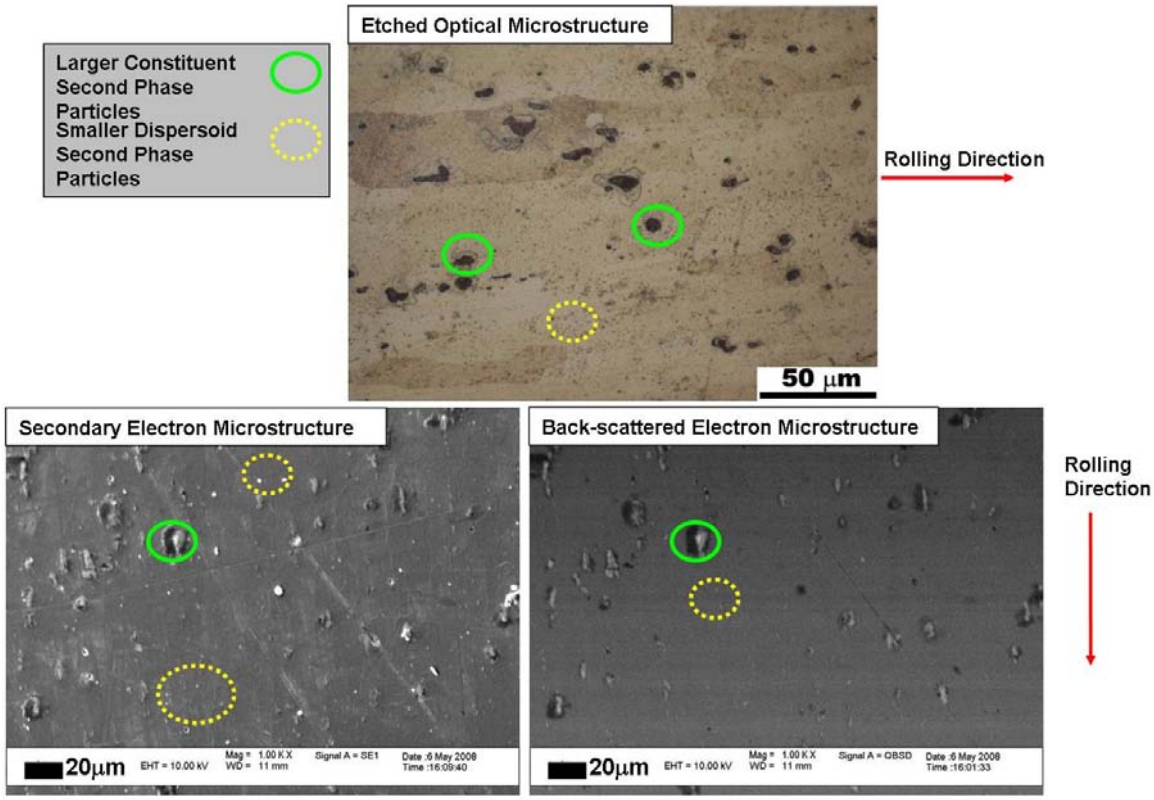

Figure 2.1 Microstructure cross-section of parent material AA2024 etched with Keller's reagent.

The main constituent precipitates present in AA2024 are [21, 26]:

- Al_2CuMg – S phase, round incoherent particles.
- Al_2Cu - θ phase, less common then S phase and varies in shape.
- Al-Cu- (Fe,Mn,Si) - α phase, which varies in composition and are irregularly shape.

The dispersoid precipitates in AA2024 have been identified as $Al_{20}Cu_2Mn_3$ or $Al_2(Mn,Fe)_3Si$ [27], and the strengthening precipitates have been identified as S phase [26].

Once constituent and dispersoid precipitates have formed during alloy fabrication, only heat treatments that are above the alloy melting temperature can affect them [21]. It is the strengthening precipitates that respond to lower temperature heat treatments and can be used to control the alloy strength through precipitation hardening.

The strengthening precipitates form in an alloy which contains elements (copper, zinc or magnesium) that decrease in solubility with a decrease in temperature and the elements need to be at a concentration which exceeds the solid solubility at room temperature [2].

The element concentration and decrease in solubility allows precipitation hardening to be achieved in three stages; solution heat treatment, quenching and ageing. The solution heat treatment stage is used to dissolve the alloying elements into solution and then quenching to room temperature obtains a super saturated solid solution (SSSS) [2, 21].

The SSSS decomposes into a fine dispersion of strengthening precipitates (S-phase) by a precipitation sequence, which has a number of intermediate precipitates that form before the final strengthening precipitates. The precipitation sequence for S-phase has been proposed as [21, 28]:

$$SSSS \longrightarrow GPB\ zones \longrightarrow GPB2 / S'' \longrightarrow S' \longrightarrow S$$

GPB zones (Guinier-Preston-Bagaryatski zones or GP(Cu, Mg) zones) are solute (copper and magnesium) rich clusters which are fully coherent with the matrix. GPB2/S″ is a coherent

intermediate precipitate whose existence is still under debate. S′ is an intermediate precipitate that is semi-coherent with the matrix and is the precursor to the incoherent S-phase equilibrium precipitate [28].

The precipitation process, while increasing the alloy strength, also has the affect of decreasing the alloy corrosion resistance [25, 29, 30]. This decrease in corrosion resistance from precipitation is due to the difference in electrochemical activity between precipitates and the matrix (this is further discussed in Section 2.2).

2.1.3 7xxx Series

The 7xxx series aluminium alloys contain, copper, zinc and magnesium. The alloys are used extensively due to their high response to precipitation hardening by the formation of Al-Zn-Mg and Zn-Mg phases [21]. The 7xxx series alloys used in this thesis are AA7056, AA7150 and AA7449, the composition for these alloys is given in Table 2.4.

Table 2.4 Nominal weight percentage chemical composition of 7xxx series alloys AA7056, AA7150 and AA7449 [22].

Element (wt%) / Material	Al	Cr	Cu	Fe	Mg	Mn	Si	Ti	Zn	Zr
AA7056	Bal	-	1.2-1.9	0.12	1.5-2.3	0.20	0.10	0.08	8.5-9.7	0.05-0.15
AA7150	Bal	0.04	1.9-2.5	0.15	2.0-2.7	0.10	0.12	0.06	5.9-6.9	0.08-0.15
AA7449	Bal	-	1.4-2.1	0.15	1.4-2.1	0.20	0.12	0.25	7.5-8.7	-

The compositions shown in Table 2.4 illustrates that there are elemental differences between the 7xxx series aluminium alloys used in this thesis, particularly chromium and zirconium. These elements are used for their influence on the alloy grain structure by forming dispersoid precipitates (β′ phase-Al_3Zr and $Al_{12}Mg_2Cr$) that restrict grain boundary movement and therefore also the grain size [2, 21, 31].

Of these elements, zirconium addition is favoured as the precipitates do not participate in the material fracture process. It should be noted that zirconium atoms also have a low diffusivity in aluminium even though they are small and coherent to the matrix [2].

The zirconium alloying content also affects the precipitation hardening response of the alloy as the strengthening phase is the η phase ($MgZn_2$) which decomposes from the SSSS by the precipitation sequence [31]:

$$SSSS \longrightarrow GPB\ zones \longrightarrow \eta' \longrightarrow \eta$$

2.2 Friction Stir Welding

Traditional fusion welding techniques (such as Tungsten Inert Gas welding (TIG) and Metal Inert Gas welding (MIG)) are not capable of efficiently joining high strength aluminium alloys because of the high welding temperatures involved and the alloys tendency for both solidification and liquation cracking [5, 25, 32].

Solidification cracking occurs in aluminium alloys as the material has a high thermal expansion and a wide solidification temperature range. It is these alloy characteristics that during welding initiate cracking within the weld fusion zone where there is high thermal stresses and shrinkage. Adjacent to the fusion zone is the partially melted weld region where low melting point phases form at grain boundaries and under sufficient stresses these phases tear in liquation cracking. Increasing the welding temperature causes an increase liquation cracking as the partially melted zone is widened [25].

Friction Stir Welding (FSW) is a solid state joining technique that uses a rotating tool to heat and soften material, through friction, this allows material to be mixed and form a joint upon cooling. In comparison to traditional welding techniques, FSW is a lower temperature solid state process which means that it is particularly suitable for the joining of high strength aluminium alloys [7-9]. The low temperature of FSW also means that the welds have low distortion, good mechanical properties and undergo minimal microstructural change [6, 9, 33, 34].

2.2.1 Process

FSW joins material by heating it into a plasticised state and Figure 2.2 shows the processing stages of plunging, welding and withdrawal. The necessary friction to achieve this is generated by the action of the FSW tool, which is a shouldered probe (Figure 2.2 stage 1).

For welding, the tool is rotated and plunged in between the material plates that are being joined up to the tool shoulder as shown in Figure 2.2 stage 1. Rotation of the tool causes friction between the tool shoulder and the material surface, which generates enough heat to soften but not melt the material. Once the material is softened it behaves plastically and can

flow around the tool. The tool can then be translated along the joint line, which mixes and transfers material around the tool to the trailing edge where it is forged by a downward force from the tool shoulder. As the tool is translated along the joint, more material is plasticised and mixed before being left to cool (Figure 2.2 stage 2) [34]. At the end of FSW the tool translation is stopped and the tool is retracted from the surface as shown in Figure 2.2 stage 3.

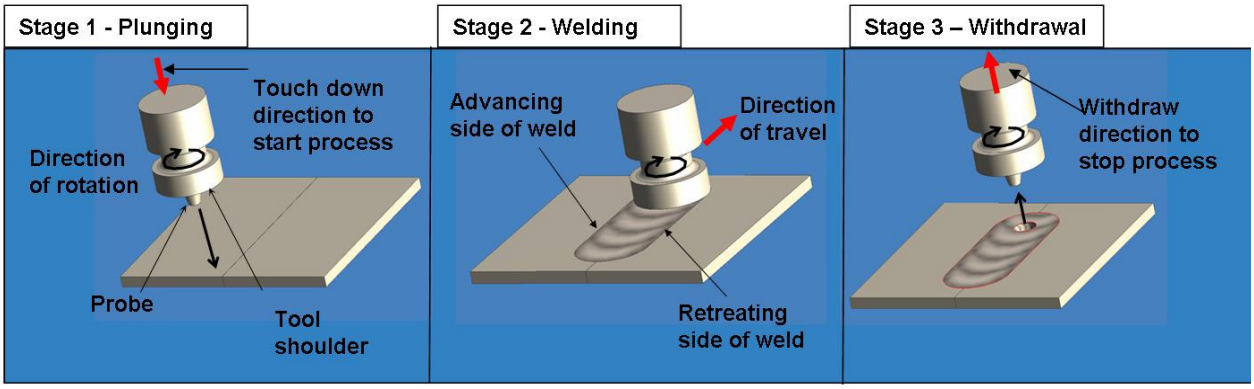

Figure 2.2 Schematic diagram showing the basic principles of the friction stir welding process.

2.2.2 Friction Stir Welding Preparation

FSW is capable of joining a variety of materials as long as the material surfaces are in a suitable condition [9, 14, 35]. The condition of the surface is important as the friction required for joining is generated by the tool shoulder rotating against the surface and a reduction in the friction can lead to incomplete mixing and weld defects. To avoid defects, it is therefore necessary to prepare surfaces for FSW by the removal of any surface layers that are present which can reduce friction. Surface layers such as paint and anodising are applied in the aerospace industry for environmental protection and would need to be removed prior to FSW.

The anodising process coars and protects by the immersion of the component to be coated in a chemical bath. Advances in the aerospace industry with the development of new aircraft such as the Airbus A380 mean that components of increasing size are being used. It can be the case then that the final component is too large for the chemical anodising bath and anodising must therefore be performed on the component parts before they are welded into the final structure.

If anodising and paint layers are applied before welding then there is a requirement for a localised technique to remove the surface layers in the region that is to be used in FSW.

Present industrial techniques for paint removal are machining, chemical-based strippers and grit blasting. However, none of these techniques are ideal. For example, both the chemical-based and the grit blasting techniques incur environmental and operator hazards from the generation of a large amount of waste [10, 11, 36-38]. Other disadvantages for grit blasting include substrate damage and the fact that the amount of material removed is difficult to control. In comparison, machining provides highly controllable removal but the process is unfavourable due to high cost (including labour costs) and large amounts of debris.

The ideal paint removal process would have the following characteristics:

- Reproducible clean surfaces
- Controllable accurate removal area and depth
- Minimal detrimental affects to substrate

Laser based paint removal processes can offer these advantages.

The use of lasers to remove paint layers from a surface has been under development for many years with a variety of lasers, paints and substrates [36, 37, 39, 40]. In the laser paint removal process there is a strong influence from the processing parameters, such as pulse duration (laser types and parameters are discussed in Section 2.6.1) [41]. Studies using excimer and CO_2 lasers to remove layers from aerospace structures have shown that laser paint removal is highly controllable with parameter optimisation for the specific paint and substrate combination[36-39]. Therefore laser paint removal could be used for FSW surface preparation.

2.2.3 Friction Stir Welding Microstructure

FSW produces a weld with three microstructural regions (shown in Figure 2.3) which are nugget, Thermo-Mechanically Affected Zone (TMAZ) and Heat Affected Zone (HAZ).

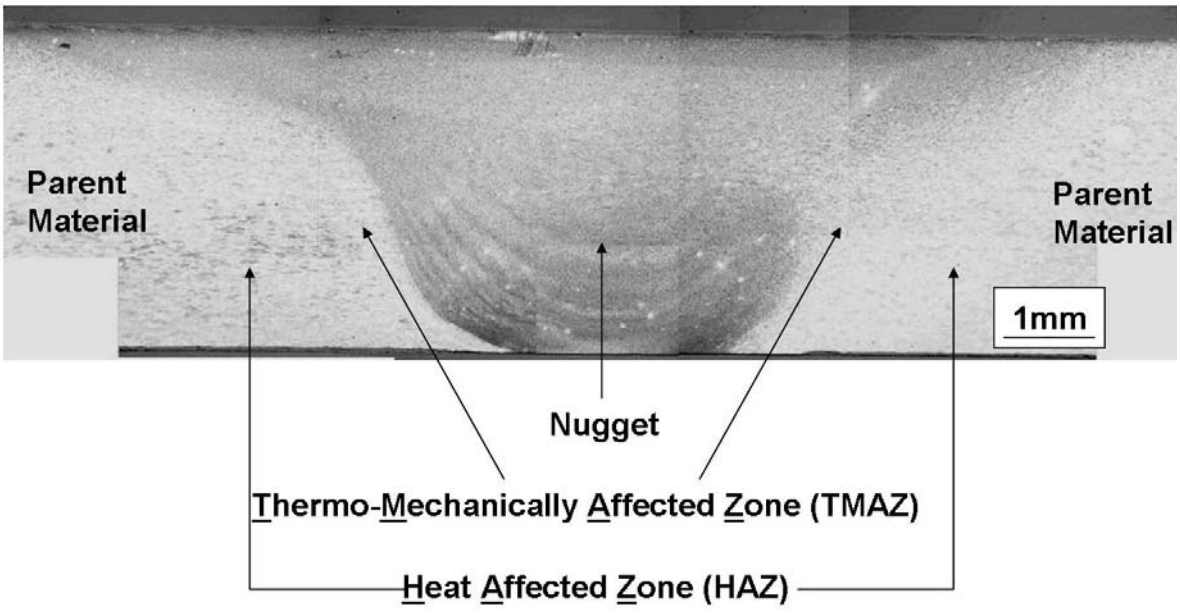

Figure 2.3 Cross section micrograph showing the microstructure regions of a friction stir weld in AA2024, etched using Keller's reagent.

The nugget region (in Figure 2.3) at the weld centre is subjected to high plastic deformation and a high enough temperature to initiate grain recrystallisation. Adjacent to the nugget and further from the weld centre is the TMAZ region, which is subjected to plastic deformation and a high temperature, which is not enough to initiate grain recrystallisation. The HAZ region is the furthest from the weld centre and is subjected only to the weld thermal cycle and there is no plastic deformation [42-44]. The thermal cycle of FSW can affect each of the weld regions in terms of microstructure and the precipitates that are present.

The two key parameters that determine the weld thermal cycle are the tool rotation rate and the traverse speed of the FSW tool. An increase in the heat input to the weld requires either an increase in the rotation speed or a decrease in the translation speed [35]. These parameters are sometimes combined into a "line energy" term, which is rotation speed divided by translation speed.

Changes in the weld line energy have shown that there are optimum welding parameters that alter the precipitates to provide high weld strength [45].

2.3 Corrosion of High Strength Aluminium Aerospace Alloys

Pure aluminium has a high corrosion resistance in neutral conditions (pH range 4-8.5) as it can form a highly stable surface oxide by Equation 2-1. The oxide provides protection as it is an insulator and therefore decreases cathodic reactivity by blocking electron conduction [23, 46].

$$2Al + 3H_2O \rightarrow Al_2O_3 + 6H^+ + 6e^- \quad (2\text{-}1)$$

The protection from the oxide can be lost however either by the presence of aggressive species such as chloride ions or changing the pH out of the neutral range, in acidic conditions the oxide is removed by Equation 2-2 whereas it is Equation 2-3 in alkaline conditions.

$$Al_2O_3 + 6H^+ \rightarrow 2Al^{3+} + 3H_2O \quad (2\text{-}2)$$

$$Al_2O_3 + 3H_2O + 2OH^- \rightarrow 2\ Al(OH)_4^- \quad (2\text{-}3)$$

Once the passive oxide has been breached, aluminium dissolution can occur at all pH values in anodic reactions shown in Equation 2-4 and Equation 2-5.

$$Al \rightarrow Al^{3+} + 3e^- \quad (2\text{-}4)$$

$$Al + 4OH^- \rightarrow Al(OH)_4^- + 3e^- \quad (2\text{-}5)$$

The metal ions released by Equation 2-4 into solution undergo water hydrolysis as shown in Equation 2-6, this reaction increases the acidity and can further propagate aluminium dissolution of Equation 2-4.

$$Al^{3+} + H_2O \rightarrow AlOH^{2+} + H^+ \quad (2\text{-}6)$$

The cathodic reactions that balance the anodic dissolution reactions also depend on the environment pH. In neutral and alkaline environments the cathodic reaction is oxygen reduction as shown in Equation 2-7. Whereas in an acidic environment the cathodic reaction is hydrogen evolution as shown in Equation 2-8.

$$O_2 + 2H_2O + 4e^- \rightarrow 4OH^- \quad (2\text{-}7)$$

$$2H^+ + 2e^- \rightarrow H_2 \quad (2\text{-}8)$$

In corrosion the reactions that take place depend on the environment, which in turn affects the stability of the surface oxide. Alloying of aluminium also affects the surface oxide as the formation of intermetallic particles can thin the surface oxide and increase electron conductivity between the anodic and cathodic reactions [46, 47].

For the electron transfer to occur between them, the anodic and cathodic reactions must be in electrical contact but they can be spatially separated, which can be electron contact through the alloys and ion transport through solution.

All of the electrons that are produced by the anodic reaction are consumed in the cathodic reaction which means that the anodic and cathodic reaction rates must be the same. The rate of one reaction, e.g. the cathodic reaction, can therefore limit the rate of the other reaction, i.e. the anodic dissolution rate.

2.3.1 Corrosion Mechanisms

Aluminium alloys undergo corrosion and the corrosion mechanism that occurs is influenced by the alloy composition and microstructure. Pitting and Intergranular Corrosion (IGC) are common forms of corrosion in aluminium alloys [48].

2.3.1.1 Pitting Corrosion

Pitting corrosion is a highly localised form of corrosion with the removal of metal to form small holes or pits. The pitting process is usually split into two stages; initiation and

propagation. The initiation mechanism for pitting is still under debate with a number of mechanisms proposed, as reviewed by Frankel [1]. However, there is a consensus that for aluminium alloys, pitting occurs due to a breakdown in the passive film and this is associated with constituent particles, e.g. S-phase in AA2024 [1].

The mechanism of pit propagation is more established and is shown schematically in Figure 2.4 [49]. The diagram illustrates the thinning affect that intermetallics have on the passive film, which allows for the cathodic reaction to take place and the cathodic current is the driving force for maintaining the pit and material dissolution [49]. The cathodic current is not supplied by just one intermetallic, though, as the diagram suggests, but it is generally supplied by many particles.

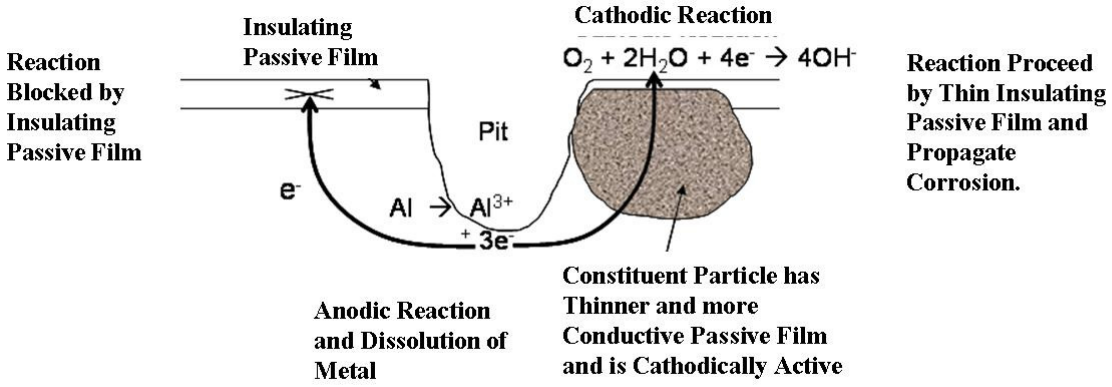

Figure 2.4 Representation of pitting corrosion propagation mechanism with constituent particles causing thinning of the passive surface oxide.

However, pits that initiate do not always propagate, but can re-passivate, stopping corrosion: this is known as metastable pitting. Once a pit is stable, propagation is autocatalytic as the process forms cations which attract aggressive anions, such as chlorides, into the pit to maintain the charge neutrality and these then undergo hydrolysis (Equation 2-6) which further

lowers the pH [50]. The combination of a high concentration of aggressive ions and a low pH favours dissolution of the metal (pit growth) over repassivation ("pit death").

2.3.1.2 Intergranular Corrosion

Intergranular corrosion (IGC) is the preferential dissolution of grain boundary regions without significant attack occurring within the grains. The grain boundary regions are sensitised to corrosion as they are favourable sites for precipitation. As precipitates form on grain boundaries, this causes solute depletion of the adjacent matrix, this sensitisation is illustrated in Figure 2.5 with the formation of copper precipitates [51]. The actual mechanism of IGC propagation is thought to be either the dissolution of a continuous path of reactive precipitates along the grain boundary (this is not the case for aluminium copper precipitates) [52] or the dissolution of the solute depleted matrix around the boundary[26, 47, 51, 53].

2.3.2 Aluminium Alloy Corrosion

Pure aluminium has high corrosion resistance due to having a protective oxide film. However aluminium alloying decreases the corrosion resistance due to the formation of constituent particles [23].

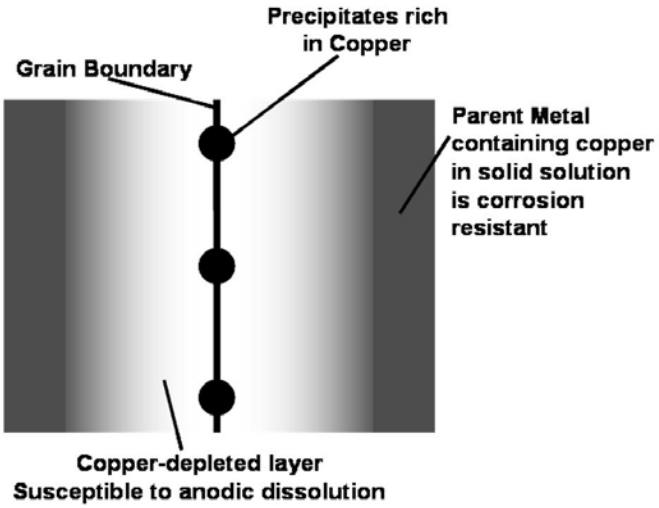

Figure 2.5 Grain boundary sensitisation to intergranular corrosion by precipitation of copper containing particles.

2.3.2.1 AA2024 Corrosion

AA2024 undergoes both pitting corrosion and IGC. The pitting corrosion on AA2024 occurs due to the influence of precipitates and a breakdown of the passive film [1].

The precipitates in AA2024 that contain copper or iron are preferential sites for cathodic reactions and initiate pitting and IGC [54]. The S-phase is particularly active and has been observed to be anodic as well as cathodic in nature. The anodic behaviour is generally observed on initial exposure which causes dissolution of magnesium and aluminium from the precipitate leaving behind copper. The copper particle that remains is then observed to be cathodic and can initiate rapid matrix dissolution [55].

The removal of all of these precipitates from the alloy surface would increase the alloy corrosion resistance [24].

2.3.2.2 7xxx Series Corrosion

The major alloying additions to 7xxx series aluminium alloys are magnesium, zinc and copper which form a number of precipitates of varying composition. The precipitates of interest to the corrosion behaviour contain copper as these are preferential sites for the cathodic reaction and cause pit initiation. Another precipitate of interest is the $MgZn_2$ phase which can continuously precipitate along grain boundaries and as this phase is highly reactive it can rapidly dissolve in IGC [56].

2.3.3 Corrosion of Friction Stir Welds

The FSW of 2xxx and 7xxx series aluminium alloys produces welds of lower corrosion resistance than the parent alloy [14, 42, 45, 57-59]. The corrosion occurs within the weld structure and is initiated by galvanic coupling between the weld microstructure regions (discussed in Section 2.2.3) [45, 60].

The specific location of corrosion within the weld varies, and some examples of corrosion locations in FSW of AA2024 include the nugget [60, 61] and the HAZ [14, 33]. The location of corrosion depends upon the activity (anodic and cathodic) of the separate weld regions and any differences in activity that occur between them. The relative activities of weld region depend on the precipitate distribution, which in turn is controlled by the FSW parameters [33, 45, 60-63].

In FSW, the rotation speed was found to be the primary factor influencing corrosion location whereas the translation speed altered the corrosion region width [45, 59]. Corrosion of the nugget was found to occur at low rotation speeds as the nugget had higher anodic activity then the HAZ. Increasing the rotation speed increased the anodic activity of the HAZ region and the cathodic reactivity of the nugget so the latter reactions region did not undergo dissolution [45, 59].

A high weld corrosion resistance has been achieved by using FSW parameters that provide the lowest heat input to the weld i.e. low rotation speed and high translation speed [45, 59]. However, welding at very low temperatures can cause incomplete mixing of material and the formation of weld defects, which can result in mechanical failure of the weld. It seems then that for the application of FSW to AA2024, additional corrosion protection would need to be applied to the weld surface.

2.4 Corrosion Prevention of Aerospace Alloys

Precipitation in aluminium alloys decreases their corrosion resistance, which means that the application of these alloys requires some form of environmental protection. Currently, in the aerospace industry, this is a multiple layer system of paint and conversion coatings [2].

A conversion coating is a surface film formed by a chemical reaction on the surface, which increases the corrosion resistance. It is also chemically bonded to the surface as it is created by converting part of the metal surface through a chemical or electrochemical process e.g. anodising. Currently in the aerospace industry chromate conversion coatings are in use.

Anodising is an electrolytic process used to increase corrosion resistance by increasing the surface oxide thickness. The anodising process operates by using the metal component as an anode in an electrolytic cell containing for example chromic (VI), phosphoric or sulphuric acid solution and when a current is passed through the cell oxygen is evolved at the anode increasing the oxide thickness. The anodised layer that is produced also has the benefit of having high adhesion to the next applied surface layer e.g. paint [3, 4].

The chemicals in the electrolytic cell greatly affect the properties of the resultant anodised layer. Chromic acid anodising (CAA) is widely used as the anodised layer is highly corrosion resistant. However, chromium (VI) is carcinogenic and alternative treatments are being sought [3, 4]. Research into chromium free coatings, to date, have not produced similar properties to CAA in terms of corrosion resistance and layer adherence without there being a detrimental effect on other properties [3, 4, 64-70].

In the aerospace industry, once an anodised layer has been created, more environmental protection is achieved by the application of paint layers, primer and top coat, onto the anodising. The overall result is a multiple layer environmental protection system that is applied over a component surface.

Problems arise with this traditional multiple layer protection system when components are welded into structures, as welding techniques disrupt the surface layers and reduce the environmental protection. Ideally the application of these protective layers needs to occur after welding. However, the final welded structure may be too large for anodising chemical baths to accommodate.

If the welded structure cannot have the environmental protection applied after welding, then an alternative approach is required. The proposed approach in this thesis is to apply enviromential protection before welding and use high power beams to prepare the surface for welding by locally removing these surface layers from the areas that are to be welded (laser paint removal) and then after welding apply localised corrosion protection to the welded area in High Power Beam Surface Modification (HPBSM).

The proposed post welding HPBSM process would increase corrosion resistance by using rapid solidification to form a homogeneous surface layer of uniform activity. Examples of HPBSM techniques include Laser Surface Melting (LSM) (discussed in Section 2.6), Laser Surface Alloying (LSA) (discussed in Section 2.6.9) and Electron Beam Surface Melting (EBSM) (discussed in Section 2.7).

Utilisation of these high power beam techniques to improve a material's corrosion resistance requires the understanding of rapid solidification theory and solidification parameters (discussed in Section 2.5).

2.5 Solidification Theory

The surface modification techniques of LSM, LSA and EBSM improve corrosion resistance by homogenising a surface microstructure and composition through localised melting and rapid solidification. To understand how a heterogeneous microstructure can be transformed into a more homogeneous one by rapid solidification requires an application of the following solidification phenomena; solidification parameters (Section 2.5.1), melt pool flow (Section

2.5.2), nucleation (Section 2.5.3) and solidification growth mechanisms (Section 2.5.4). This is because solidification behaviour controls the resulting microstructure in terms of grain size, shape, defect distribution and the extent of segregation [71].

2.5.1 Solidification Parameters

Transformation of a liquid phase into a solid phase is usually a two stage process which is nucleation followed by growth. Nucleation occurs when a small piece of solid forms in a liquid and growth occurs as atoms from the liquid attach to a solid. There is a certain minimum critical size of nuclei that experience growth. Critical parameters which influence this process include the thermal gradient across the solid/liquid interface, undercooling (the undercooling is the equilibrium freezing temperature minus the actual temperature of the liquid) and interface growth rate, which are described below.

The driving force for solidification results from the undercooling of liquid adjacent to the solid/liquid interface, and this can originate from a number of sources. In the rapid solidification of alloys it is the thermal and constitutional undercoolings that are important to consider and are described below.

Thermal undercooling (Δt) is the degree to which the liquid (at temperature t) is cooled below the equilibrium freezing temperature (t_m) before solidification takes place (i.e. undercooling $\Delta t = t_m - t$) and occurs during rapid solidification due to the high cooling rates involved.

In the solidification of alloys, the composition changes over the liquidus range. As the composition changes ahead of the solidification interface the actual temperature may not

match the temperature required by the alloy liquidus and this leads to constitutional undercooling. In alloy solidification it is the constitutional undercooling that has the greatest influence on the solidification structure [72, 73].

Once the driving force for solidification is established it is the thermal gradients (G) within both the solid (G_S) and the liquid at the interface (G_L) that influence the solidification structure.

The G_L value is critical as it controls the interface stability and morphology which in turn dictates the solidification structure discussed later. Any material movement by convection within the melt pool can greatly influence G_L and also the solidification structure.

The rate at which the solid/liquid interface advances into the liquid is the interface growth rate (R). While G_L determines the solidification structure it is R that influences the scale of the solidification structure, undercooling and solute distribution. The important G_L and R terms are combined as a product into one cooling rate term ($T= G_L.R$) which will be used in forthcoming discussions of solidification processes [72, 73].

2.5.2 Melt Pool Convective Flow

In rapid solidification techniques, convective liquid flow within the melt pool is required to achieve a homogeneous surface composition (discussed in Section 2.6.6) [74]. Convective material flow has been studied for welding applications and a number of controlling factors have been established, these are; buoyancy, electromagnetic forces and surface tension forces.

The effect of each of these forces on flow and melt pool shape is shown in Figure 2.6 and the occurrence of these forces is described below [72].

A buoyancy variation occurs across a melt pool due to changes in liquid density from different temperatures and compositions. The larger the buoyancy variation, the more material can flow.

Electromagnetic forces are found to influence liquid flow within the melt pool in processes (e.g. arc welding or electron beam welding) where there is a divergent current path with its associated magnetic field.

Most processes involving liquids are greatly influenced by surface tension forces resulting from a spatial variation in surface tension across the weld pool surface, which arises from temperature and composition changes. Out of the three factors, surface tension has the largest effect and can dominate material flow patterns [72].

Depending on the method of melting the surface there can also be an influence from mechanical forces e.g. in arc welding the arc's plasma jet will form a depression in the surface. There will be mechanical influences from laser and electron beams in high power beam surface modification and these will be discussed further in Sections 2.6.2.1 and 2.7.1 respectively.

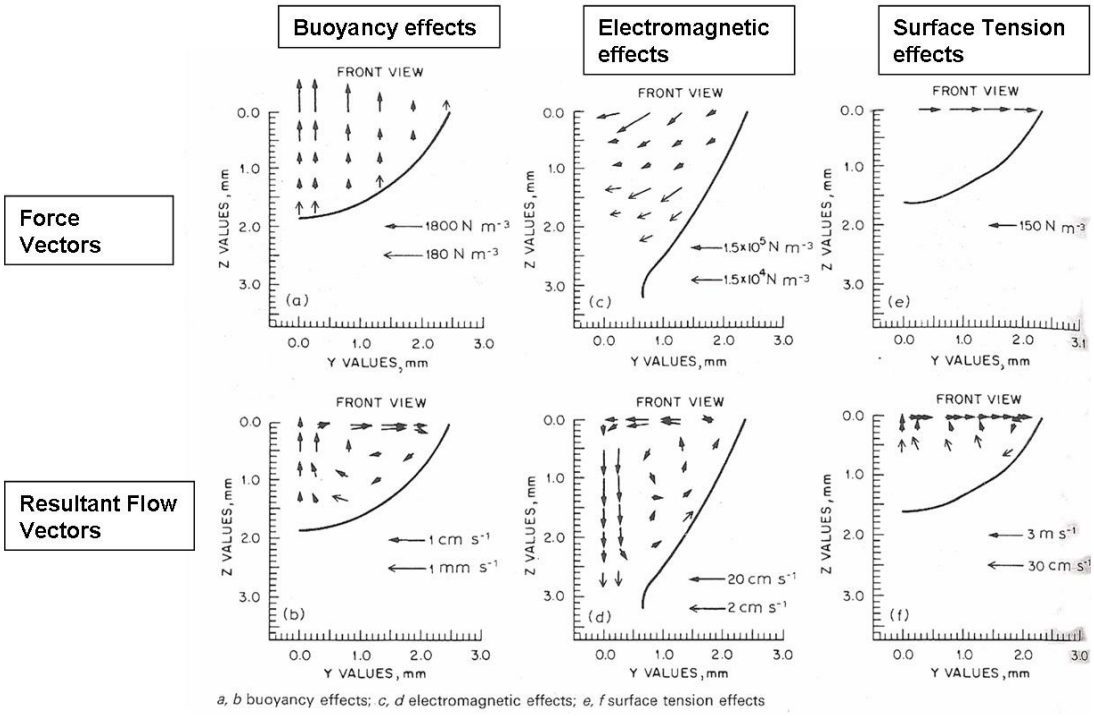

Figure 2.6 Calculated distribution of force vectors (a,c,e) and resultant flow vectors (b,d,f) in cross-section of aluminium alloy weld whilst in the liquid phase [72].

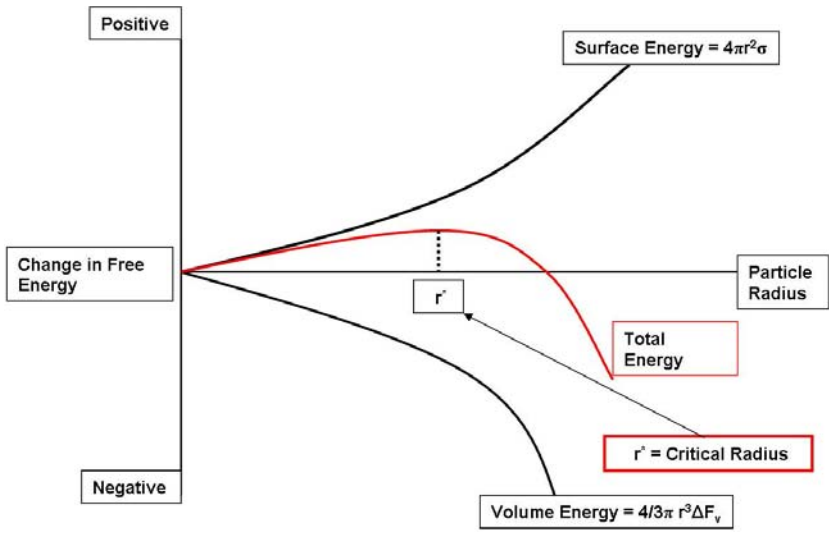

Figure 2.7 Graph of the variation in the total free energy of the solid-liquid system as the size of the solid changes. The solid is a stable nuclei if it has a radius above the critical value r^*. [75].

2.5.3 Nucleation

In HPBSM techniques, once the melt pool has been homogenised through mixing in the liquid state, the nucleation of a solid is required. The formation of a solid particle from a liquid is controlled by the change in total free energy of the system which is brought about by the nucleation of that particle i.e. the difference in the volume free energy of the particle and the surface free energy of the solid/liquid interface created. The relationship between the surface free energy, the volume free energy and the total energy is shown in Figure 2.7. In nucleation, Figure 2.7 shows that the volume free energy is negative and favours the nucleation process, whereas the surface free energy is positive and therefore an activation barrier for the formation of a stable nucleus. The energy barrier for nucleation can be overcome by an increase in undercooling which reduces the critical size for a stable nuclei (r^*) [75].

There are two types of nucleation: homogeneous and heterogeneous. Homogeneous nucleation occurs when atoms cluster together to form a stable nucleus, without the aid of foreign bodies such as impurities, inclusions or substrates. This means that a large amount of undercooling is required in homogeneous nucleation to supply the energy needed for the formation of the new surfaces.

In heterogeneous nucleation, less undercooling is required as this type of nucleation uses the surfaces of foreign bodies (e.g. particles suspended within the melt) to significantly reduce the surface energy requirement [72, 73]. Heterogeneous nucleation is the standard situation for most solidification [72].

Heterogeneous nucleation occurs in HPBSM processes as the liquid fully wets the solid substrate it is in contact with so there is no nucleation energy barrier and nucleation occurs spontaneously. The full wetting of the surface by the liquid also means that the solid that grows is influenced by the substrate e.g. epitaxial growth [76]. Epitaxy is the solidification condition where lattice planes on either side of a boundary are parallel to each other and there is unified crystal growth of one crystal layer on another.

2.5.4 Growth

Once a stable nucleus has formed, growth of the solid occurs at the interface with the addition of atoms from the liquid. The growth morphology that occurs with atom addition is controlled by the shape and stability of the solid/liquid interface. The interface shape that is stable for growth depends on conditions in its immediate vicinity including heat flow, thermal gradients, mass flow, composition gradients and growth rate [72, 73]. Typical growth morphologies are planar, cellular and dendritic; these are shown in Figure 2.8 [72].

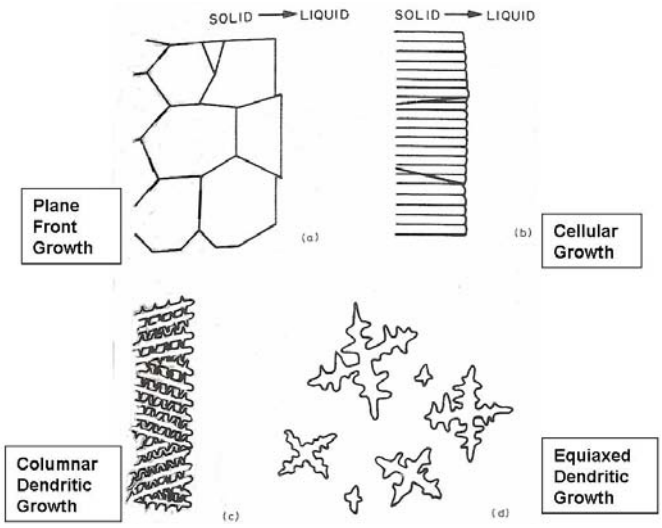

Figure 2.8 Various structural morphologies that can form through solidification [72].

Planar growth (Figure 2.8a) is where the direction of growth is perpendicular to the flat solidification front and parallel to the thermal gradient. In planar growth there is a lack of substructure development, except that there may be an epitaxial influence from the substrate. The role of crystallography in planar growth is limited but it can affect the growth rate, as some crystallographic directions can grow faster then others. The grains that are aligned in the faster growth direction will develop at a faster rate and can dominate the microstructure [72].

Cellular growth, like planar growth, (Figure 2.8b) is where the direction of grain growth is controlled by the heat flow conditions and there is only a small influence from crystallography. Cellular growth is different from planar growth as it occurs at faster cooling rates and this means that the solute in the alloy cannot re-distribute fast enough, leading to the rejection of solute ahead of the interface.

The solute rejection means that the composition ahead of the interface is changed and constitutional undercooling subsequently occurs. Constitutional undercooling means that the liquid ahead of the solidification front exists below its freezing temperature, so if a solid protrusion forms on the planar interface it has a greater stability and the protrusion can then grow into the liquid, which is illustrated on in the left-hand diagram in Figure 2.9 where a single solid protrusion grows into the liquid following the maximum thermal gradient. The growth of the first protrusion rejects solute laterally, which lowers the solidification temperature and creates recesses that trigger the formation of more protrusions. Once there are enough protrusions to break down the planar interface and form a cellular structure of

uniformly spaced cells, illustrated as cellular growth in the right-hand diagram Figure 2.9, which all grow parallel to the maximum thermal gradient. The spacing of the cells is related to the cooling rate, as an increase in cooling rate decreases the cell size [72, 73].

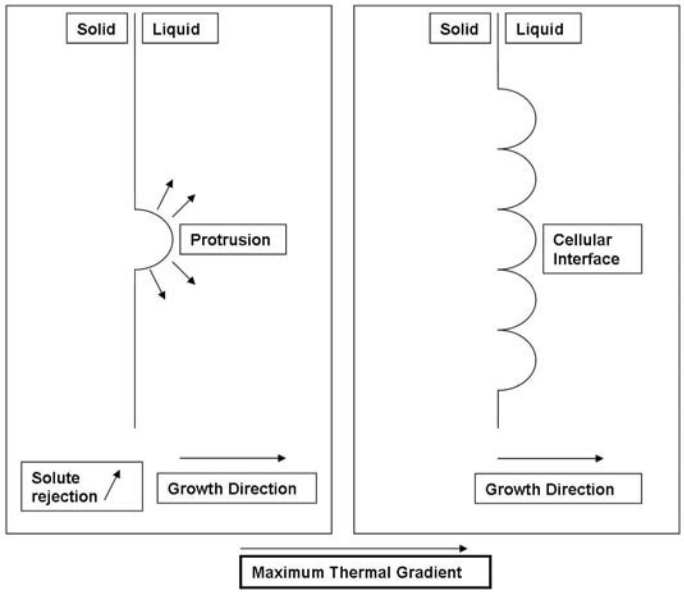

Figure 2.9 Schematic of solid/liquid interface with single protrusion and cellular growth.

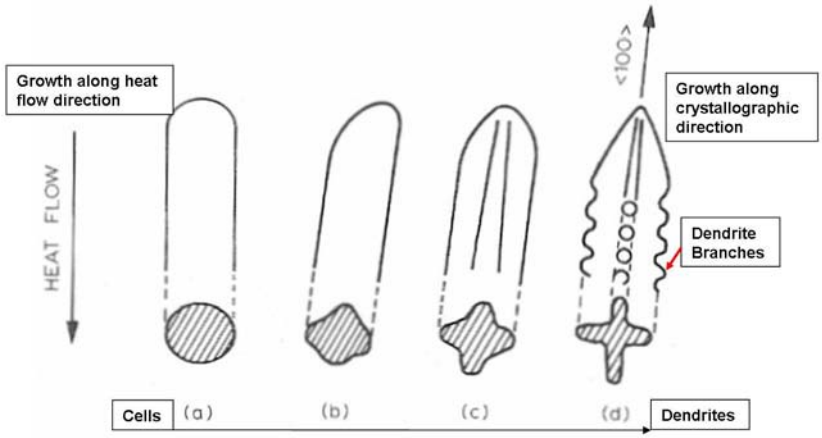

Figure 2.10 Schematic of solidification morphology transition from cells A, to cellular dendrites, B, and on to columnar, C, and to branched columnar dendrites, D, [72].

The transition from cellular to dendritic solidification structure is not fully understood but it is thought to be associated with the onset of constitutional undercooling between the cells causing instability perpendicular to the growth direction. This growth instability of the cell sides leads to branching and changes the cells into dendrites as shown in Figure 2.10 [72, 73]. The increase in interface instability, causing the transition from cells to dendrites, is related to an increase in the cooling rate. Another consequence of faster cooling rates, is that there is a greater influence from crystallography and the fast growth directions. Therefore a characteristic of dendritic growth morphology is that it occurs in specific crystallographic directions.

Dendritic growth is influenced by crystallography and has been identified in two forms, columnar and equiaxed. Columnar dendrites (Figure 2.8c) grow along the same crystallographic direction parallel to each other and this direction is not influenced by heat flow. Equiaxed dendrites (Figure 2.8d) grow in different but specific orientations depending on crystallography and the neighbouring dendrites are not necessarily parallel, so each dendrite is a separate grain [72, 77]. Although the dendritic structure is influenced by crystallography, there is still an influence from the cooling rate as the dendrite spacing decreases into a finer structure as the cooling rate increases.

There is a limit to the refinement of the dendritic structure with increasing cooling rate. This is due to the decrease in atom diffusion time with very high cooling rates [72, 78]. For the stable growth of a dendritic structure the liquid/solid interface must be able to form a number of stable perturbations along the interface. For an interface perturbation to be stable and grow it must be able to accumulate atoms by diffusion, which means that the distance between

interface perturbations must be less than the atomic diffusion distance during solidification. Increasing the solidification cooling rates reduces the diffusion distance to a point where, to create a smaller interface perturbation distance with many close perturbations would require a very high surface energy. Once the high surface energy for stable perturbations can no longer be reached planar growth again becomes stable, meaning there is a critical growth front velocity or ultimate stability limit beyond which planar growth is stable [72, 73]. Above the ultimate stability limit, planar growth produces a segregation-free microstructure by trapping the solute in solid solution. This results in a more uniform composition, across the melted layer with no second phases and extended element solubility limits.

2.5.5 Rapid Solidification Processes

Rapid solidification processes are characterised by high cooling rates that are above the ultimate stability for planar growth, and a solid of increased homogeneity can form. The increased homogeneity possible through rapid solidification is exploited in HPBSM techniques to create a surface layer of high corrosion resistance. To utilise fully HPBSM techniques, solidification theory has been investigated to get a deeper understanding of rapid solidification microstructures and processes [71, 78-81].

TEM microstructure studies on cw-CO_2 (laser types and parameters are discussed in Section 2.6.1) laser surface melting (LSM) treated eutectic Al-Cu alloy confirmed that microstructure morphology was a function of growth rate in rapid solidification [79]. Further to this work, more compositions of Al-Cu alloys were cw-CO_2 LSM treated which allowed a map to be created that correlated the microstructure to both the growth rate and the material composition [81]. A variation in solidification structure, due to composition and growth rate changes, has

been shown to occur through the thickness of modified layers produced by HPBSM techniques. For example a planar growth zone was observed at the base of modified layers in cw-Nd:YAG LSM of AA2014-T451, whereas the rest of the layer had a segregated cellular structure as shown in Figure 2.11 [82].

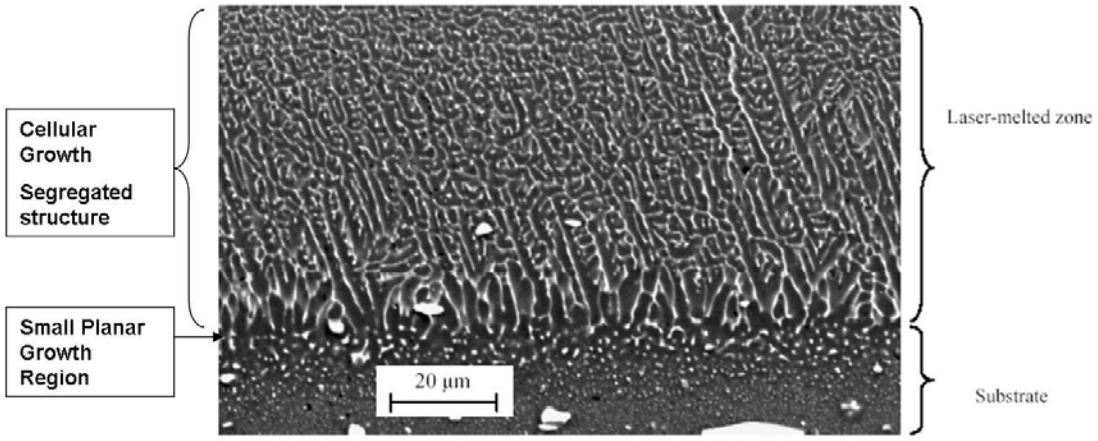

Figure 2.11 Regions of different solidification morphology that form in LSM layers obtained by 3kW cw-Nd:YAG LSM on AA2014-T451 [82]

The base of the modified layer is often referred to as the fusion boundary. Solidification initiates at the fusion boundary and from there the growth front accelerates from zero, therefore the fusion boundary experiences the slowest solidification (front velocity) of the entire modified layer. The fact that the solidification front accelerates from the fusion boundary means that the depth of the modified layer has an affect on the growth rate and the fastest solidification front velocity that can be achieved within it. The variation in solidification front velocity with solidification depth has been modelled by P. Ryan and the results are shown in Figure 2.12 [74]. The figure shows that there is an initial transient region of growth where the growth front, accelerates from zero and the speed is therefore below that speed required for planar solidification. The transient region forms regardless of modified

depth and with increasing depth there is a larger portion of the layer in this transient region. The modelling also estimated that the absolute stability criterion for planar growth occurred at a growth rate of 5m/s [74].

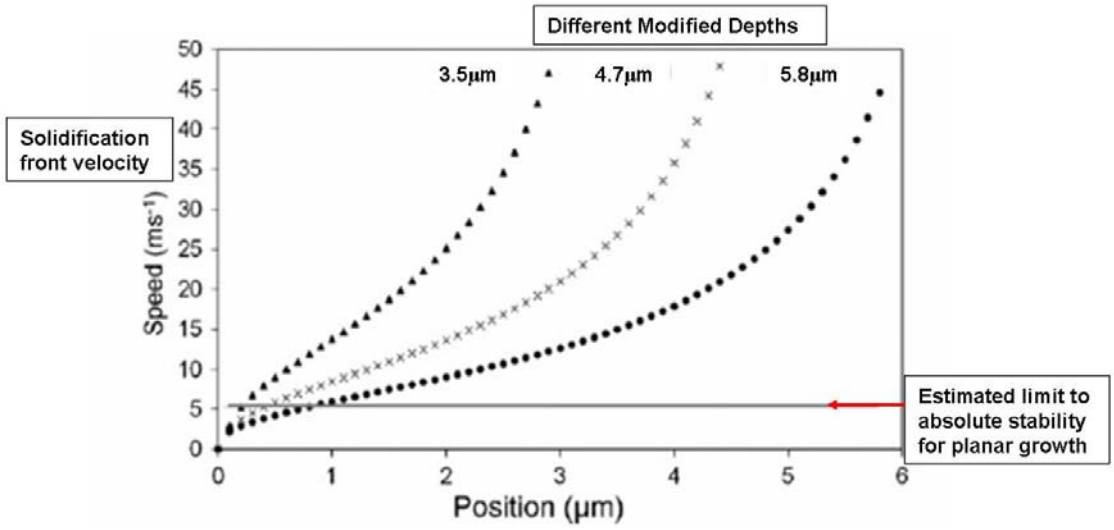

Figure 2.12 Results from modelling of excimer LSM of AA2024 for a single radiation pulse. Graph shows solidification growth velocity as a function of position within the modified layer, including modified layers of different thicknesses [74].

The growth rate throughout a modified layer though does not always vary enough to induce drastic changes to the solidification growth morphology. However, the effects of growth rate variation throughout the thickness of the modified layer can still be observed, as it affects the solidification structure scale [83]. This was illustrated in Nd:YAG LSM of AA2014-T451 where the variation in growth rate changed the dendrite arm spacing shown in Figure 2.13 [82]. This figure shows that with increasing distance into the layer there was an increase in the dendrite spacing from 2µm at the surface to 5µm at the fusion boundary [82]. However, Figure 2.14 shows that regardless of the growth rate or layer depth at which the dendrites are formed, element segregation to the dendrite boundaries always occurred in particularl copper [82]. This

segregation is undesirable in HPBSM techniques as it will limit the material corrosion resistance.

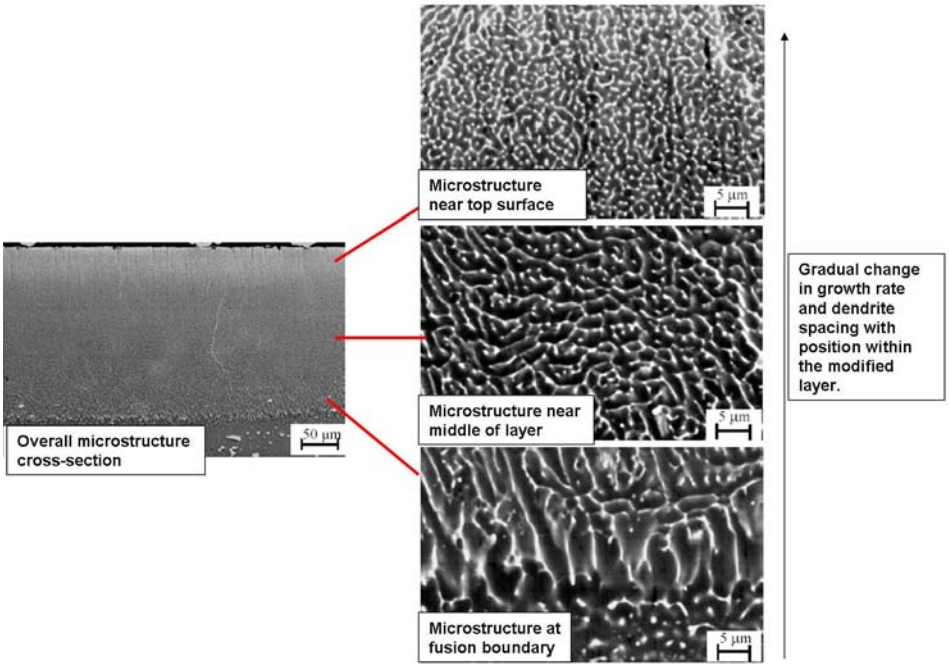

Figure 2.13 SEM images of 3kW cw-Nd:YAG LSM AA2014-T6 alloy showing variation in growth rate and dendrite spacing with position in modified layer [82].

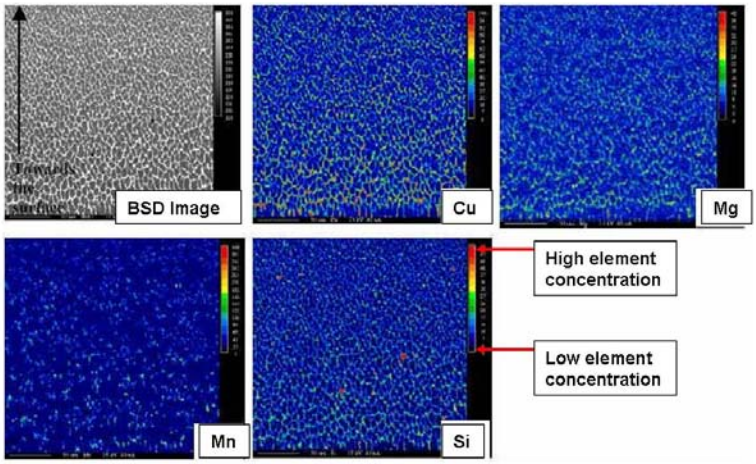

Figure 2.14 Electron probe micro-analysis X-ray mapping 3kW cw-Nd:YAG LSM AA2014-T451 alloy showing element segregation throughout modified layer [82].

As growth rate has been shown to vary throughout a modified layer depth this would lead to the conclusion that changing the modified layer thickness would also change the growth rate along with the solidification structure. Variations in layer thickness have been related to the solidification structure scale in Figure 2.15 [74] which used information from a range of HPBSM treatments of different pulse durations on AA2024-T3. This figure showed that an increase in layer thickness caused a decrease in growth rate which in turn increased the cell spacing [74].

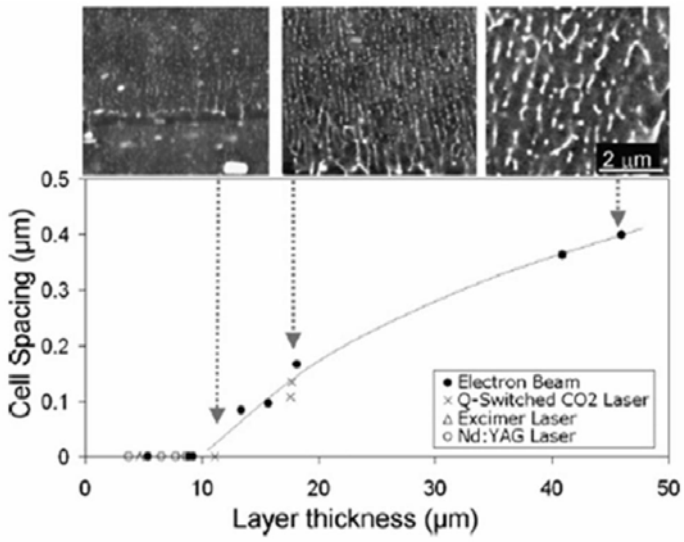

Figure 2.15 Variation in cell spacing with melt depth for AA2024-T3 using a variety of pulsed treatment methods with SEM images of microstructure at different depths [74].

The solidification structure and scale can be estimated from the growth rate but influences of the material substrate on solidification must also be taken into account [84]. A strong influence of the substrate material on solidification was shown in investigations of excimer LSM on AA2024 and AA7150 [74]. LSM of these two materials under identical processing conditions produced layers with different solidification structures, with planar growth taking place in the

AA2024 layers and cellular growth in the AA7150 layers. EBSD images of these layers in Figure 2.16 confirm these structures, with epitaxial growth from the underlying substrate in the AA2024 layer and cellular growth without crystallographic influence in the AA7150 layer [74]. Explanation for the difference in solidification structure with substrate material came from TEM investigations of the transient region on AA7150 which showed in Figure 2.17 that the cellular growth grew from an equiaxed grained region [74]. These equiaxed grains were nucleated from either seed grains that were coherent with the base layer or Al_3Zr particles that had solidified ahead of the solidification front both of which are shown in Figure 2.18 [74]. The presence of zirconium in the AA7150 was thought to be the main cause for cellular growth initiation and the drastic change in the solidification structure compared with AA2024. The substrate material must therefore always be considered with designing HPBSM techniques.

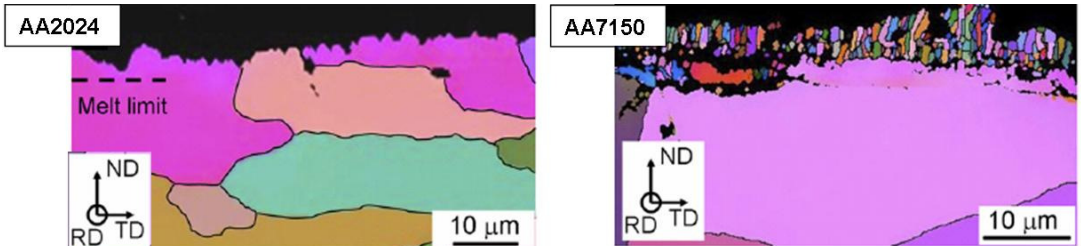

Figure 2.16 High resolution Euler contrast EBSD map showing morphology of LSM layers obtained with excimer laser treatments in Zr-free alloys (AA2024) and Zr-containing alloys (AA7150), [74].

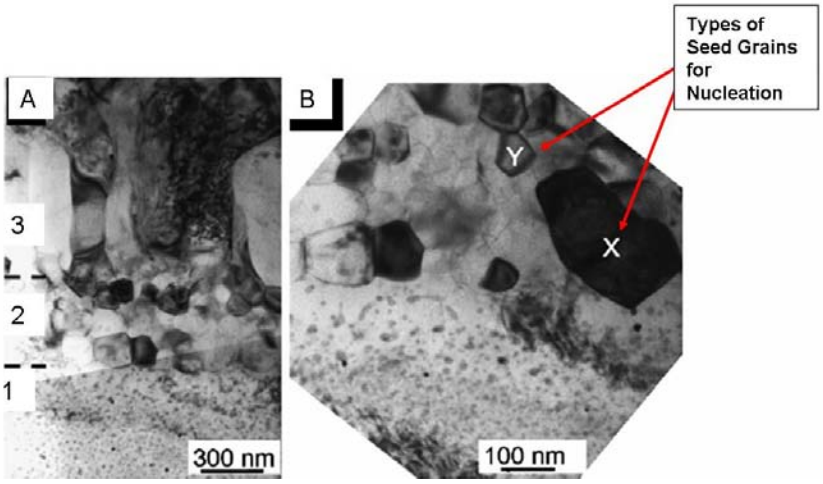

Figure 2.17 Cross-sectional TEM images through the base of a pulsed LSM layer formed by Excimer LSM on AA7150. A) shows grain structures at the base of the layer with three distinct regions. Region 1 is the coarse grained parent Region 2 equiaxed region of seed grains and Region 3 columnar grains formed from seed grains. Region 2 is magnified in B). [74].

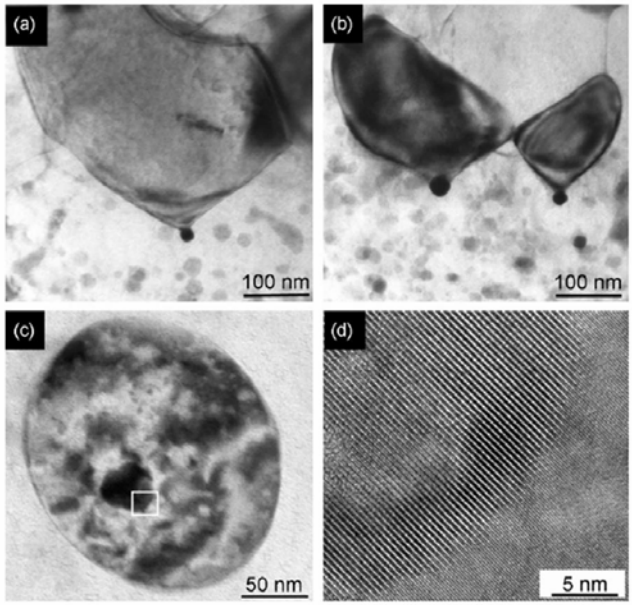

Figure 2.18 TEM imaging of excimer LSM AA7150 at the base of the modified layer including seed grains, in particular seed grains type X and Y from figure 2.15. A) type X seed grains nucleated from β′ particles at the melt base. B) An example of a Y seed grains nucleated from Al_3Zr dispersoids in the melt ahead of the growth front. D) a lattice image of epitaxial matching across the B′/α-Al interface from the highlighted area in C[74].

2.6 Laser Surface Melting

Laser Surface Melting (LSM) is an HPBSM technique which is used to alter material surface properties through rapid solidification.

LSM can be performed using many different lasers each of which has its own characteristics and processing capabilities (Sections 2.6.1 and 2.6.2). As a variety of lasers can be used for LSM, there is a wide range of processing parameters available (Section 2.6.3) which are selected to suit the material being processed (Section 2.6.4) and the material property being modified.

LSM can for example achieve an improvement in corrosion resistance by the formation of a homogeneous surface and, as identified in Section 2.5.2, this would require mixing of the molten material (Section 2.6.6). The degree of mixing required to improve corrosion resistance is not always achieved and this depends on the LSM processing parameters and the material being modified (Section 2.6.7).

An improvement in material corrosion resistance has been achieved by LSM on FSW surfaces (Section 2.6.8) and in Laser Surface Alloying (LSA) (Section 2.6.9) which is a similar process to LSM but has the incorporation of additional alloying elements into the molten layer before solidification.

2.6.1 Lasers

Lasers are suitable for surface modification processes as the laser radiation is highly coherent and collimated, so consequently can be focused to produce high power densities that can be used to heat a surface at high speeds [85]. This high level of surface heating occurs in LSM and produces a layer of novel microstructure that is strongly bonded to the substrate [86].

Laser surface modification has other benefits which include the absence of damage to the bulk material properties, non-contact processing, and the fact that there are few restrictions on component shape or treatment area. However, lasers have disadvantages which include the high initial investment cost, and the limitation that only a small volume of material can be treated at one time [17].

2.6.1.1 Laser Operation

Laser radiation is created in an excited lasing or gain medium which contains atoms or molecules that have specific discrete electron energy levels. It is electron movement between these discrete energy levels that causes the spontaneous emission of radiation.

For lasing to occur, a minimum of three electron energy levels are required: a ground state, a metastable level and a high level [31, 87], as illustrated in Figure 2.19. To initiate lasing, the electrons must be excited from the ground state to the high level with an energy input. The number of electrons in the high energy level must be increased until it is greater then the number of electrons in the ground state: this is referred to as a population inversion. To invert

the electron population requires that more than half of the electrons are raised to the high energy level.

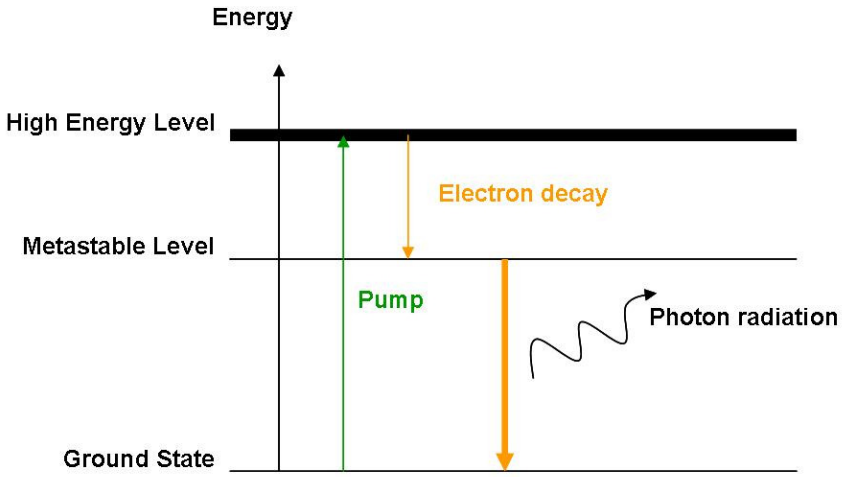

Figure 2.19 Energy level diagram for a three electron energy level laser system showing the electron transitions required for lasing.

Following the population inversion, electrons then lose energy and fall down the energy levels (electron decay), photons are emitted by electron movement from the metastable level down to the ground state. The rate of electron decay is called the relaxation rate.

To amplify the amount of photons produced, the decay of electrons is stimulated by the interaction of additional photons with the excited atoms in the gain medium. Once more than half of the electrons have decayed to the ground state the population inversion is destroyed and lasing stops. Lasing will not continue unless more energy is put into the system to re-invert the population.

In a three level energy system it takes a large energy input to maintain the population inversion, due to the fast electron relaxation rate. This large energy requirement means that for three energy level systems it is practical to input the energy in pulses, as this provides the same peak energy to invert the electron population but the overall average energy input is lower. As a result of this is that the lasing radiation is emitted in pulses [31, 87].

For continuous laser radiation emission, the energy required to invert the electron population must be reduced so that the inversion can be more easily maintained. A reduction in input energy is achieved by increasing the number of electron energy levels to a minimum of four energy levels with two metastable levels, as illustrated in Figure 2.20.

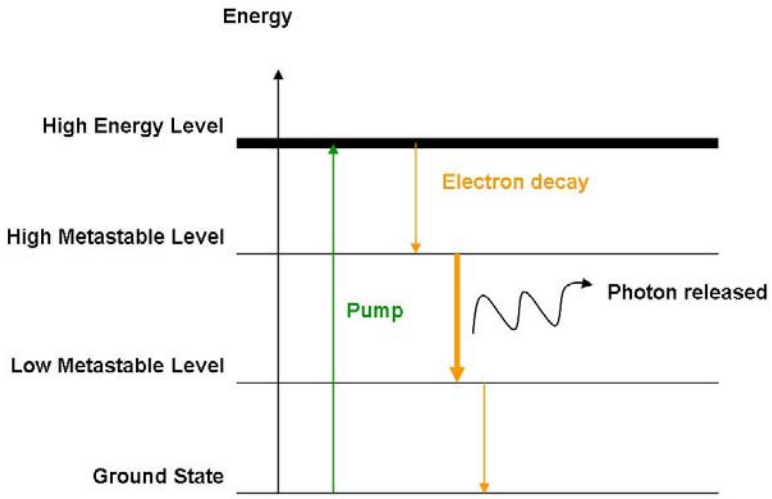

Figure 2.20 Energy level diagram for a four electron energy level laser system showing the electron transitions required for lasing.

In this four energy level system photon emission occurs between the two metastable levels and the population inversion only needs to be maintained between them. This means that less than half of the electrons need to be excited from the ground state to the higher energy levels

at any one time and overall less energy input is required compared with the three electron level system. It can be practical therefore to continuously provide the energy input to the system and produce continuous radiation.

Once continuous radiation has been produced it can be changed to provide radiation pulses by Q-switching. The Q factor of a laser cavity is a measure of its ability to store radiation, changing the Q level of a cavity controls the release of radiation which can be in the form of pulses [31, 87].

2.6.1.2 Laser Types

Different gain mediums and states can provide the energy levels required for lasing. Possible gain medium states include gas, solid and excited dimer (excimer) [87, 88]. The gain medium that is used in a laser is important as it dictates the laser characteristics in terms of radiation wavelength and pulse duration. It is the gain medium type and state therefore that defines a laser system. Table 2.5 shows some examples of laser types and their characteristics [89].

Table 2.5 Examples of lasers used in materials processing.

Laser	Wavelength	Mode of Operation	Pulse Length
Excimer XeCl	308nm	Pulsed	25ns
Excimer KrF	353nm	Pulsed	60ns
Ruby	0.6943μm	Pulsed	0.2-5ms
Nd:YAG	1.06μm	Repetitively Q-switched	200ns
Cw-Nd:YAG	1.06μm	Continuous	-
CO_2	10.6μm	Repetitively Q-switched	50-200ns
Cw-CO_2	10.6μm	Continuous	-
USP-CO_2	10.6μm	Pulsed	10-100μs

2.6.2 Laser Surface Melting Processes with Different Lasers

There are many different types of laser, each of which has its own characteristics including radiation wavelength and pulse duration. The laser gain medium produces these laser characteristics, which are then used as laser selection criteria for an application such as LSM.

As different lasers produce different wavelengths this means that certain lasers are more suited to particular materials and applications. Surface modification and LSM have been performed using a variety of different lasers [18, 90-92]. A summary of some of these are in Appendix 1 – Summary of Laser Surface Melting .

2.6.2.1 Laser Surface Interaction

In LSM, radiation is absorbed into a thin surface region and the thermal energy is then conducted away from the surface into the material bulk in all directions as shown by the arrows in Figure 2.21 [93]. This figure illustrates that the laser interaction with a material is at the surface.

In LSM the heating rates used are high enough to melt the surface region and a fusion interface then propagates down into the substrate. Further increases in the surface heating will result in vaporisation of material [89].

Vaporised material can cause problems in LSM as it creates an intense plasma which can deflect the laser beam lowering the energy density at the surface. Another effect of the vaporised material is that as it escapes a recoil pressure is created which affects the remaining

molten material, as when the recoil pressure is greater then the material surface tension sideways movement of material is induced within the melted area [17, 31, 94].

Once the laser radiation is removed from the material surface, rapid cooling occurs, which freezes the material to form non-equilibrium structures and compositions as there is insufficient time for diffusion or precipitation [84, 91, 95]. The fast cooling rates occur as the substrate acts as a heat sink and it has been shown that the cooling rates in excimer LSM can be in the order of 10^9C/s [96, 97].

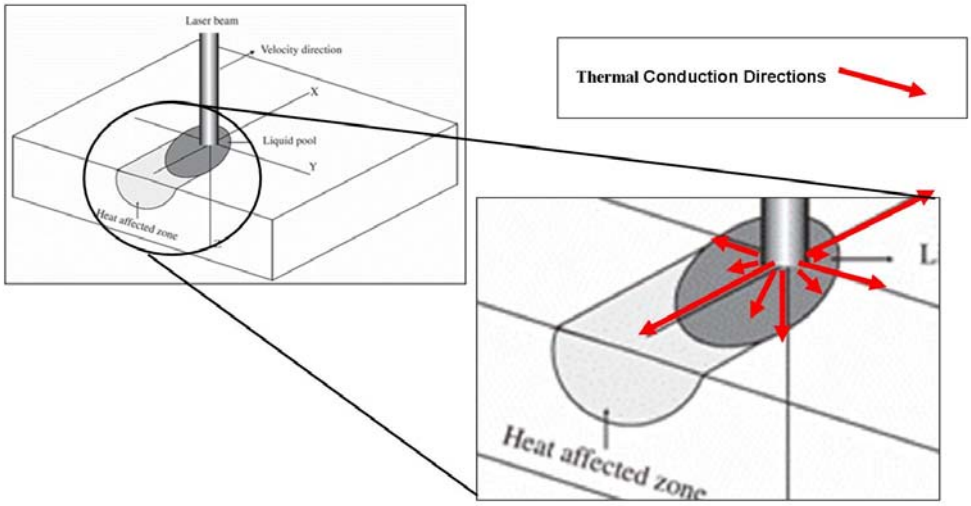

Figure 2.21 Schematic representation of laser interaction with a surface [93].

2.6.3 Effect of Processing Parameters

A laser's selection for an LSM process is usually based on its inherent characteristics. For most lasers these inherent characteristics include the pulse duration and wavelength. However, there are exceptions: some Nd:YAG lasers can vary the radiation wavelength between set values [87]. The pulse duration can also be varied in some lasers between certain

limits for example the USP-CO_2 laser, where changes in the gain medium excitation alters the resultant pulse duration [98].

If a laser that can vary its pulse duration or wavelength is selected for an LSM process, these variables must be taken into account along with the other LSM processing variables. These processing variables include: energy, number of pulses per unit area, atmosphere, scanning rate, beam overlap, spot size, and imaging arrangement [14]. The last three of these variables depend on the beam delivery optics and their affect on LSM processes have not been widely studied.

2.6.3.1 Wavelength

For LSM it is desirable to have efficient and maximum energy transfer from the laser into the sample surface [99]. The absorptivity of laser radiation into a surface is, particularly for continuous wave lasers, related to the radiation wavelength. For pulsed lasers there is not such a clear realtionship between wavelength and absorption due to an influence from pulse duration, but generally a decrease in pulse duration can decrease absorptivity [87, 100].

The surface to be processed can also affect the radiation absorptivity in a number of ways including: roughness, oxidation, temperature and state [89, 99-101]. For example generally there is higher radiation absorption when a surface oxide is present or there is a high surface roughness [85]. The application of an absorbent coating (e.g. graphite) can also be used in surface preparation to enhance absorptivity, particularly for highly reflective materials such as aluminium alloys [87].

2.6.3.2 Energy

The aim of laser processing is to initate surface modifications and the type of modification that is possible depends on the energy density or fluence (J/cm^2) as this quantifies the energy avaible for absorption and takes into account the laser spot size.

When laser processing is performed at low fluences there is not enough energy to induce material modifications. However, there may be enough energy available for the removal of any surface organic coatings [17, 102].

To induce material modification through surface melting requires an increase in the laser fluence up to the melting threshold value [98, 99, 103]. At the melting threshold value there is a step change in the material state and thus there is a change in some of the material properties such as radiation absorptivity [98].

An increase in fluence once the surface is melted causes an increase in the degree of surface heating which results in more material melting and thus the melted layer thickness is increased [89, 91, 96, 99, 104, 105]. The increase in modified layer thickness with fluence increase will continue until there is suffient energy for material vaporisation. There is therefore a maximum layer thickness that can be reached by increasing the laser fluence [105].

The change in radiation absorptivity on the melting of a surface means that in an LSM process the energy absorbed is not constant over the pulse duration. If the changes in absorption during LSM could be taken into account by varying the fluence over the laser pulse duration there would be an increase in the process efficiency and decrease in material vaporisation [98].

2.6.3.3 Pulse Duration and Interaction Time

LSM utilises both continuous wave (cw) and pulsed lasers. To compare the material irradiation times of these two laser types requires the calculation of the radiation interaction time. For pulsed lasers, the interaction time is the pulse duration whereas for cw lasers their interaction time is controlled by the translation speed of either the laser or the sample.

Generally the interaction time of cw lasers is longer than that of most pulsed lasers due to limitations in the mechanical scanning systems that have to be employed with cw lasers. It is found that the longer interaction times of the cw lasers tend to create modified layers that are thicker with a lower solidification rate and more segregation than the layers produced by the pulsed lasers [18, 84, 106].

Increased segregation in modified layers may be detrimental as it will cause a decrease in the corrosion resistance, so thinner layers produced by pulsed lasers may be more beneficial (as discussed in Section 2.6.7) [18]. Another advantage for pulsed lasers is that they produce more rapid cooling rates that have been shown not to form a HAZ, which would be beneficial in terms of corrosion resistance [107].

The layer thickness produced in LSM processes is influenced by both the interaction time and the energy density [96, 99]. This dual influence can be explained using the surface temperature and the vaporisation threshold [89, 99, 105].

In the initial stages of LSM the surface temperature is greater than the melting temperature but less than the vaporisation temperature, so the melt depth can be increased by an increase in energy and melting. This is until the temperature at the surface exceeds the vaporisation temperature and the maximum possible melt depth by increasing the energy has been achieved, as any further increase in energy will cause vaporisation and loss of material. At this point, the pulse duration becomes important as an increase in the pulse duration will further increase the melt depth at constant power [89]. This pulse duration influence is shown in Figure 2.22 in the LSM of pure metals [89].

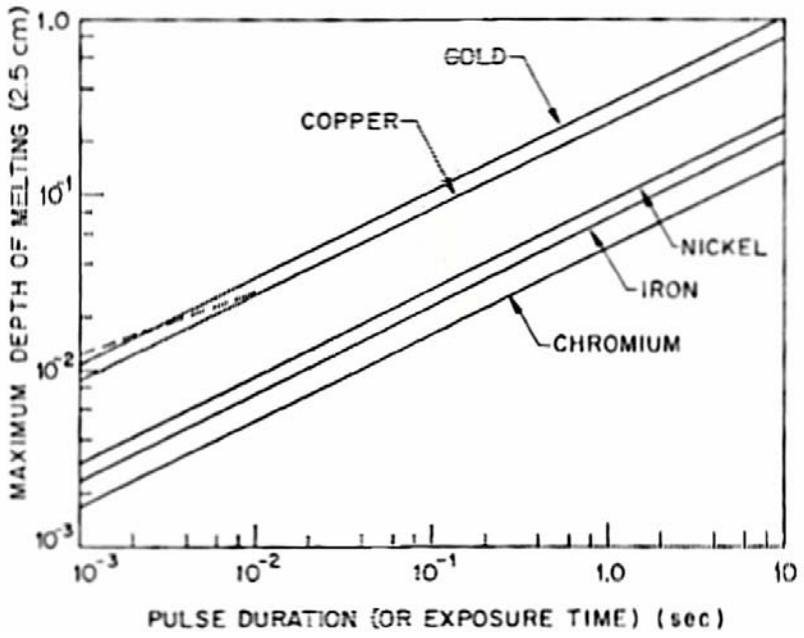

Figure 2.22 Maximum depth of LSM melting that may be produced in several metals with a pulse of given duration without evaporation occurring at the surface. [89].

When the LSM process is in this regime, where the surface temperature is just below the vaporisation temperature, there is optimum processing efficiency and the process is under pulse duration control. However it must be noted that the fluence value required for the

surface temperature to reach the vaporisation temperature will be dependent on the pulse duration [105, 108].

The processing variables of interaction time and laser energy have been shown to affect the melt layer thickness through changes in the surface heating and there will also be an influence from these variables on other aspects of the melted layer e.g. segregation, microstructure refinement, porosity and cracking [93, 96, 109-113].

An example of the relationship between these variables and the levels of layer cracking and porosity has been observed in cw-CO_2 LSM studies on aluminium alloys. This work identified an operating window for these variables which achieved no porosity or cracking within the modified layers shown in Figure 2.23 [110]. This figure shows that within the layer, porosity can form at both low and high traverse speeds where as cracking was only found to occur at high traverse speeds.

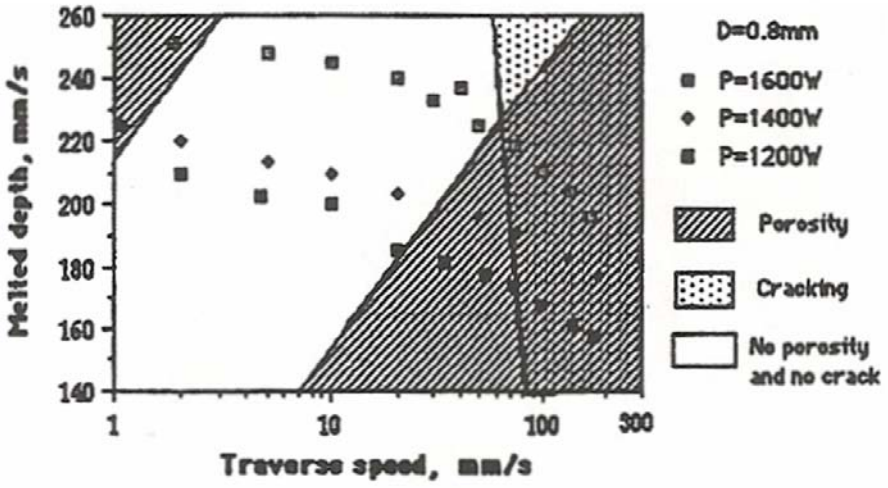

Figure 2.23 Graph of traverse speed vs. melt depth for CO_2 laser surface melting. With the highlighting of a processing parameter operating window that does not produce cracking or porosity within the modified layer [110].

The onset of cracking was along grain boundaries from the fusion line to the surface and this was due to the increase in the layer residual stresses with an increase in traverse speed and also a decrease in melt overlap [109, 110]. The cracking tended to occur from the fusion line as the residual stresses increase with modified layer depth [25].

Cracking does not occur at the lower traverse speeds as these allow for the relaxation of stresses within the melt pool as they have slower solidification growth [25].

An increase in translation speed, with small melt pools with fast growth, has been shown also to increase dislocation content and refine the microstructure causing an increase in material hardness [93, 111, 112].

2.6.3.4 Number of Pulses per Unit Area

Multiple pulses of radiation per unit area is often used to increase the overall energy input in to a surface and allow for areas larger then the laser beam size to be processed with the overlapping of adjacent pulses. The number of pulses per unit area used in LSM treatments has been observed to affect the modification in a number of ways.

It has been reported that there is a relationship between melt depth and number of pulses per unit area, as an increase in melt depth was caused by an increase in the number of pulses per unit area [85]. However, this result may be a misconception, as the peak modified layer thickness may have increased but not the average layer thickness.

The peak layer thickness can be increased with the number of pulses per unit area as every laser pulse causes movement to be induced in the liquid material (further discussed in Section 2.5.2), with material being pushed away from the laser beam. After each laser pulse therefore the surface condition is slightly changed, i.e. there is a slight depression in the surface where the laser has struck.

Subsequent laser pulses interact with this modified area and cause another slight change in surface condition. There can therefore be a large accumulation of material movement across a surface with the application of a large number of pulses.

As the movement is generally away from the laser beam material build ups and depressions can form which would result in an increase in the peak layer thickness and the surface roughness but not in the average layer thickness [14, 33, 98].

The amount of material movement within a layer can be related to the number of pulses per unit area through an accumulation of the effect from individual pulses. A cumulative effect would also be observed in other material properties if these were changed during a laser pulse. For example alloy composition can be changed during a laser pulse with the vaporisation of elements and this changes the composition which would accumulate with multiple pulses [98, 99].

This composition change can affect the processing further as different alloying elements can assist in heat absorption depending on their electrical properties as high thermal conductivity elements can increase the melt depth [98, 99].

2.6.3.5 Processing Atmosphere

In LSM the atmosphere used can affect the treatment by either inducing chemical reactions with the surface or changing the surface tension through the use of surface active elements [72].

Chemical reactions between a surface and an atmosphere has been observed in LSM of Ti-6Al-4V and AA8090 [114, 115]. In this case the use of a nitrogen atmosphere for the LSM of both of these alloys increased the amount of nitride precipitates within the modified layers, which was beneficial in terms of corrosion resistance for AA8090 as the nitride precipitates were insulating which impeded electron flow and decreased the cathodic current [114]. The nitride precipitates were not as beneficial though in the titanium alloy in terms of the corrosion resistance as when this alloy was treated in an argon atmosphere, which avoided nitride formation, there were benefits to the corrosion resistance as there was a decrease in solute partitioning and microstructure homogenisation [115].

2.6.3.6 Processing Parameter Modelling

In LSM there is a wide range of processing parameters available. For the application of LSM it is necessary to identify the effect of these processing parameters, in particular which parameters affect the modified layer thickness. To achieve this a numerical laser drilling model has been used to model the LSM modification of AA2024 [19]. The main advantage of using this model is that melt movement and the effects of material expulsion were included in the analysis. Although a small beam diameter was used in an attempt to reduce melt

movement. The model required certain assumptions which include: temperature-independent material properties, complete radiation absorption, one dimensional thermal affects, a clean surface, the absence of surface oxide and a rectangular pulse profile.

The main conclusion from the modelling was that there was a correlation between the pulse duration and the modified layer thickness, this is shown in Figure 2.24 [19]. The graph shows that increasing the pulse duration increases the modified layer thickness (melt depth), this result was produced for constant processing energy density values. Figure 2.24 also shows melt depths that were from experimental LSM tests using lasers with different pulse durations, it must be noted though that there is no account for the influence of wavelength on this data [19].

The correlation shown in Figure 2.24 will not continually increase the melt depth with pulse duration as there are other factors that will limit the melt depth. The modelling for example does not include the onset of cracking of the modified layer or any changes to the modified layer structure.

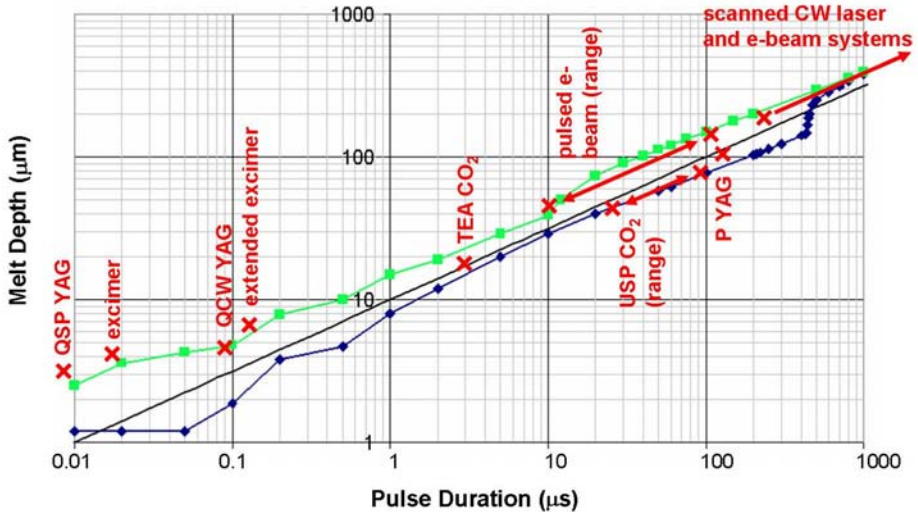

Figure 2.24 Modelling Results of Laser Pulse Duration Vs. Melt Depth [19].

2.6.4 Laser Surface Melting of Different Materials

LSM has been performed on many different materials with a variety of effects on the microstructure and properties depending on the processing parameters, examples are listed in Appendix 1 – Summary of Laser Surface Melting. Of interest to this discussion are the LSM treatments of aluminium alloys that have modified either the chemical or mechanical properties through changes in composition or microstructure.

Examples of modification in surface composition by LSM include CO_2 LSM of AA3003 (Al-Mn) and aluminium copper (15wt%) alloy where there is an extension in solid solubility and the formation of metastable phases [93, 116]. Such composition changes can have an effect on mechanical properties as seen in CO_2 and excimer LSM of aluminium copper alloys, where an increase in copper content caused an increase in the amount of θ phase which resulted in an increase in the surface hardness [113, 117]. In some cases, such as in excimer LSM of AA6013, composition changes with the production of a more homogeneous surface can be beneficial to

the mechanical properties as a homogeneous surface can increase the fatigue resistance as a result of an increase in the crack initiation resistance [118].

2.6.5 Laser Surface Melting of AA2024

The LSM production of a homogeneous surface also has the benefit of increasing the material's corrosion resistance (Section 2.2) and this has been achieved on AA2024 [18, 74, 119, 120]. The homogeneous layer causes an increase in corrosion resistance as a consequence of the removal of precipitates, an increase in the copper level in the matrix and an increase the oxide thickness (discussed further in 2.6.7) [18, 119, 120].

The level of homogeneity of the surfaces produced by excimer LSM on AA2024 has been shown to vary with layer thickness as layers less then 10μm thick had a high level of homogeneity and no phase separation due to partitionless planar growth. The small degree of heterogeneity that is present in these layers is in the form of bands of precipitates in the transient region, solute trails from insufficient precipitate mixing or dissolution and constituent precipitates in the lower part of the layer [74]. The layer heterogeneity is increased with an increase in layer depth to more then 10μm as the solidification structure changes and this would cause a decrease in the corrosion resistance [74].

2.6.6 Mixing in Laser Surface Melting

To improve a material's corrosion resistance by LSM requires surface homogenisation, before the onset of solidification, by the dissolution and dispersion of any precipitates that are present. The dispersion of elements can be achieved, in particular, by two mechanisms

convection movement and diffusion, of which the former is preferential as the dispersion rate is faster. Material movement has been observed in many LSM treatments by changes in the surface roughness and the formation of a rippled surface [31, 74, 98, 109, 116, 121].

For complete surface homogenisation there ideally needs to be enough mixing within the layer to fully disperse precipitates, but this does not always occur as observed in excimer LSM of AA2024 where solute trails remained after solidification shown in Figure 2.25 [74]. The solute trails were formed from precipitates being dissolved and then only partially dispersed, as the material was in the liquid state for an insufficient amount of time. To achieve complete dispersion requires material to be in the liquid state for a longer amount of time than that necessary for solute redistribution which varies with the dispersion mechanism involved [31].

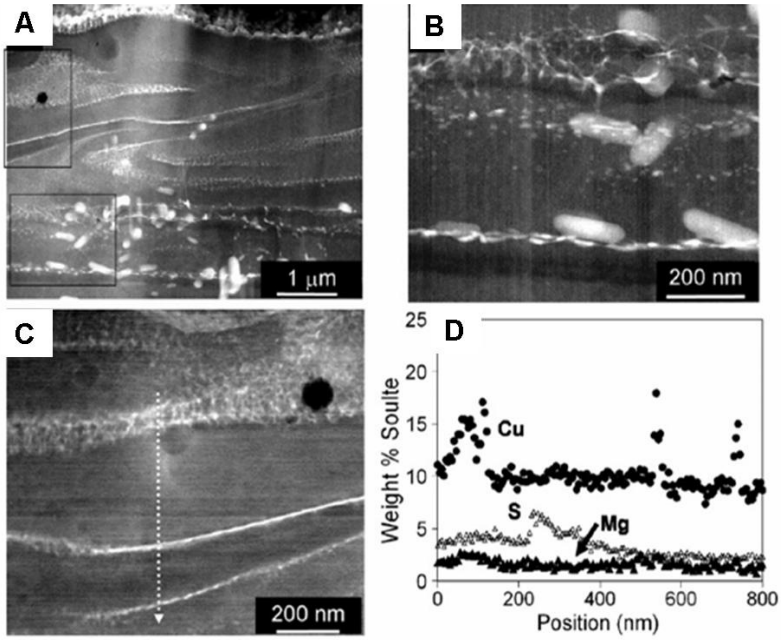

Figure 2.25 HAADF STEM (high angle annular dark field scanning transmission electron microscopy) images taken from cross-section through pulsed laser surface melting processed AA2024. A) General view of LSM region, B) Thin lateral precipitate bands at the base of the layer, C) the structure of the solute rich trails, D) EDX scan through the dotted line in C [74].

Modelling investigations into solute distribution by diffusion during LSM on AA2024 showed in Figure 2.26 that a liquid time of $7x10^{-7}$s would be required for diffusion to decrease by 20% the composition of the centre of a 4.4μm constituent particle. Distribution by diffusion alone would therefore require either using this excimer laser for 800 pulses or a laser with the minimum pulse duration of 0.56ms. This modelling concluded that to homogenise a surface by the rapid dispersion of precipitates required mixing by material movement to occur at a larger extent than that observed in this LSM process [74].

In laser processing it is the heat input from the laser interaction time and energy that initiates the thermal processes of diffusion, convection movement and vaporisation in a material. It is the extent of each of these processes that controls the type of surface modification possible

e.g. drilling or melting, as shown in Figure 2.27 [77]. Once the laser interaction time and energy have been selected to induce convection there are a number of other factors which must also be considered as these control the amount of material movement. These factors include; temperature gradients, surface tension gradients, buoyancy variation and surface temperature (previously discussed in Sections 2.5.2 and 2.6.2) [74, 77, 99, 122]. The modified layer features that have shown to be influenced by mixing include; melt pool shape, surface ripples, defect content, porosity, composition and heterogeneity [77].

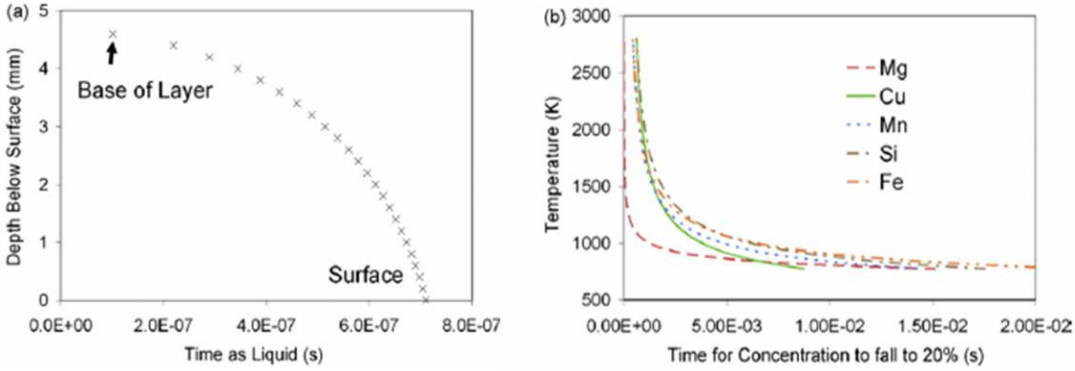

Figure 2.26 Modelling of LSM AA2024 liquid time. A) The estimated time spent as liquid plotted against position through thickness of melted layer for a single pulse. B) The time required for the composition at the centre of a constituent particle to decrease to 20% of its initial level by diffusion in the liquid [74].

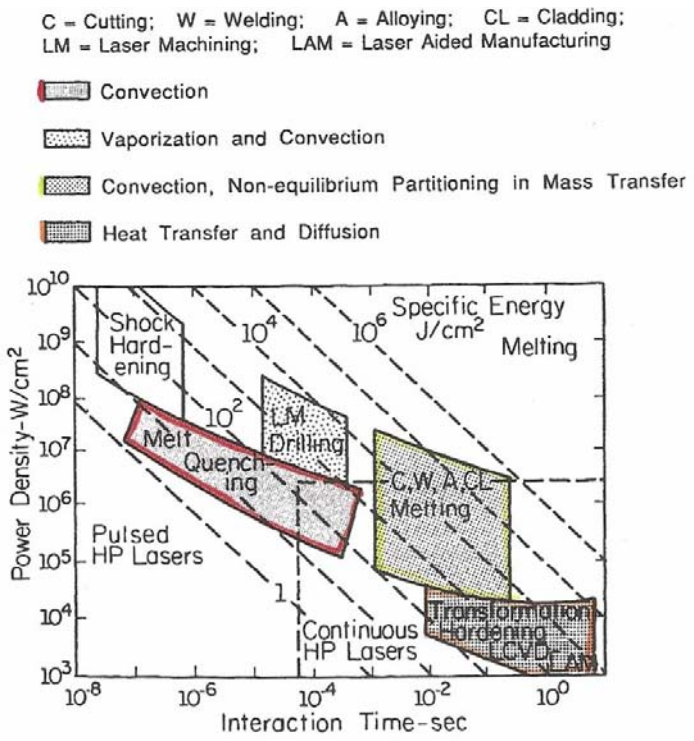

Figure 2.27 Graph of operational regimes and liquid transport in laser processing of materials with variation in interaction time and power density [77].

LSM requires convection movement to increase surface homogeneity to estimate the amount of movement required, modelling was performed using surface tension gradients to induce the convection movement. The modelled convection movement is shown in Figure 2.28 and this predicted a long particle trajectory shown in Figure 2.29 [77]. This predicted particle trajectory was thought to be sufficient for complete particle dissolution and the formation of a homogeneous surface, however particle size reduction and experimental comparisons were not included [77].

The amount of convection movement within an LSM layer that would cause complete particle dispersion has not been clearly established. However the complete dispersion of particles may not be required as a materials corrosion resistance could be improved even with some

level of heterogeneity present within the modified layers [18]. If the degree of dispersion necessary to increase corrosion resistance could be quantified then suitable LSM processing parameters could be selected, as long as these parameters also provided a cooling rate that did not produce a segregated solidification microstructure (Section 2.5.4) [96].

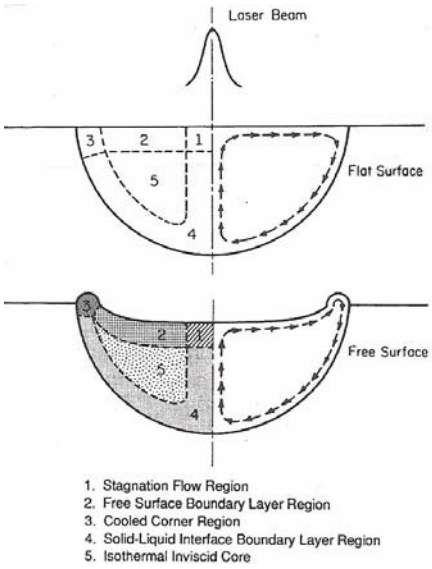

Figure 2.28 Modelled material flow regions in laser processing [77].

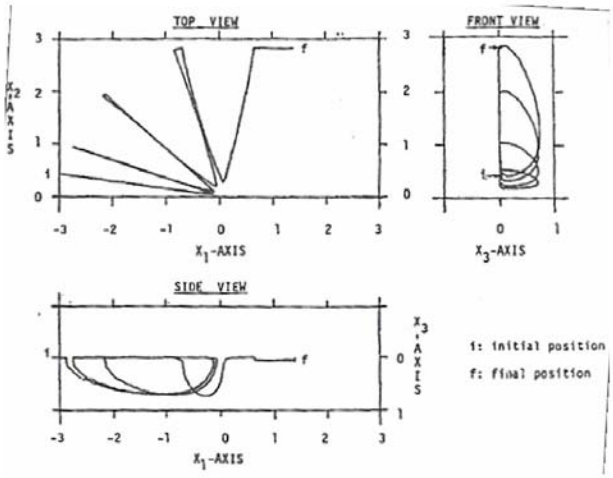

Figure 2.29 Modelled predicted particle trajectory in LSM as it enters, re-circulates and refreezes from material flow in Figure 2.26 [77].

2.6.7 Corrosion of Laser Surface Melted Surfaces

For many materials, precipitates have been linked to the initiation and propagation of corrosion; in aluminium alloys it is the constituent precipitates that act as cathodic sites and have been associated with the initiation of pitting and IGC [1, 106]. The removal of precipitates from a surface region has been highlighted as a key factor to improving a material's corrosion resistance [12, 15-17, 110, 114, 123, 124].

LSM can remove surface precipitates by dissolution into the matrix solid solution which can additionally further reduce corrosion by altering the activity of the matrix e.g. copper increase in the matrix will decrease the anodic activity [82, 125]. In most LSM studies complete removal of precipitates and surface homogenisation has not been achieved [18, 31, 98, 109]. LSM does however reduce the number of precipitates in the surface region and modifies the structure [31, 109].

The extent of precipitate dissolution, surface homogenisation and corrosion resistance improvement achievable by LSM depends on the laser processing parameters used and the solidification structure that they produce. The solidification parameters particularly the cooling rate, induced by LSM affect the resultant microstructure and any element segregation within the modified layer [72].

Corrosion has been noted in LSM layers to be associated with segregated regions within the layer, which means that the corrosion resistance improvement is limited by segregation, which is controlled by solidification growth morphology and the LSM processing parameters

[18, 82, 110]. Certain solidification structures are more likely to produce segregation e.g. cellular and dendritic structures and these arise from low cooling rates. Refinement of microstructure size, i.e. reduce dendrite or cell spacing though can lead to improvement in corrosion resistance [13, 15, 16, 106, 111, 126].

Other work has also reported that the corrosion resistance improvement by LSM is limited due to the formation of a layer that contained pores and cracks as these became sites for localised corrosion [120].

Another problem with cracks and accelerated localised corrosion is that once the base of the layer is reached, i.e. the transient zone there has been accelerated corrosion perpendicular to the surface along this region leading to layer de-lamination [18, 82, 110]. Even if there are not cracks layer de-lamination has been observed once uniform corrosion has occurred over the surface and exposed the transient region [18, 33].

The exposure of the substrate by cracks, scratches or layer de-lamination can decrease the corrosion resistance and accelerate substrate attack due to galvanic coupling between the LSM layer and the substrate [18, 31, 33, 127]. The galvanic coupling between the LSM treatment and the matrix does not always lead to accelerated corrosion and there is less of a risk if LSM layer has low cathodic reactivity [18].

Galvanic corrosion is even less of a risk if LSM layer acts as a sacrificial layer as in the case for zinc-containing aluminium alloys (7xxx series) where zinc goes into solid solution. In this case a scratched LSM layer of AA7449 underwent preferential anodic dissolution of the LSM

layer which meant that the layer dissolved and the exposed substrate was cathodically protected [18].

To protect large areas by LSM requires the overlapping of pulses due to the restricted small size of the laser beam. The regions where pulses are overlapped have also been shown to be sensitised to corrosion and localised attack. This is due to the re-heating of the area inducing further microstructure changes and causing micro-segregation within a small region [15, 123].

Ideally the LSM layer, to improve the corrosion resistance, would be smooth, crack free, protective barrier with complete precipitate removal with a uniform surface oxide and contain no regions of sensitisation from processing [12, 83, 91, 97, 128-130].

2.6.8 Laser Surface Melting of Friction Stir Welds

FSW can produce welds of poor corrosion resistance owing to sensitisation of the microstructure from precipitation and increased anodic activity across the weld, which was previously discussed in Section 2.3.3. LSM has been applied to FSW surfaces to increase the corrosion resistance by homogenising the surface through rapid solidification, as discussed in Section 2.6.7.

Excimer LSM has been applied to weld surfaces produced by the FSW of AA2024, AA2198, AA7010 and AA7449 aluminium alloys [14, 18, 33, 45, 58, 59, 127, 130, 131]. The LSM treatment suppressed corrosion over the welds by decreasing both the number and depth of corrosion attack sites [14, 18, 33, 58, 62, 132]. The corrosion resistance increase from LSM remains whilst the layer is intact, however investigations into LSM of FSW on AA2024 and AA7449 have

shown that once the layer is scratched there can be significant substrate attack in the weld's HAZ region [18].

2.6.9 Laser Surface Alloying

Laser Surface Alloying (LSA) is similar to LSM except for the addition of extra alloying elements into the final modified layer. For the case of aluminium alloys, this can be achieved by alloying with powder [120], sputtering metal layers [109] or formation of a chemical conversion coating on the layer [52, 107, 133, 134]. The incorporated elements in LSA can change the electrochemical reactivity of the laser treated layer and further increase the corrosion resistance [127]. This benefit has been shown in excimer laser treatments of AA2024 where the LSA layer had a higher corrosion resistance than the LSM layer that was produced using the same processing parameters [127].

2.6.9.1 Laser Surface Alloying AA2024

The elements that have been shown to provide an increase in corrosion resistance include; chromium, manganese, molybdenum, tantalum, tungsten, vanadium and zirconium [135, 136]. The effectiveness of an alloying element on the corrosion resistance depends on the stability and solubility of the oxidised species that the alloying element forms on the material being treated, as a stable insoluble oxide will provide high corrosion resistance [137].

The effect on corrosion resistance from excimer LSA of a wide variety of elements deposited by chemical dipping on AA2024-T351 has been investigated [52, 57, 107, 133, 134, 138] with the highest corrosion resistance achieved by alloying with manganese [52, 133, 134]. In this chemical

dipping process a conversion coating containing the required element in the oxidised form was deposited on the surface and upon melting the element was incorporated in the metallic form into the modified layer. The increase in corrosion resitance from LSA of manganese was due to an overall decrease in the surface passivity from a decrease in the cathodic activity [133].

Excimer LSA of AA2024 with sputtered layers of a range of elements was performed to further understand the effect of different elements on the corrosion improvement. It was found that the elements with a lower melting point such as manganese and chromium were more effective at increasing the breakdown potential with chromium achieving the highest. The less successful elements investigated with higher melting points were tungsten, tantalum and molybdenum. The corrosion attack that was observed on these LSA layers was similar to that of LSM layers with general attack occurring before de-lamination of the layers [127].

To increase the corrosion resistance of the surface by LSA there must be high element incorporation into the modified layer which is achieved more easily through sputtering deposition than by dip coating [127, 139, 140]. The thickness of the sputtered layers has also been shown to influence the degree of element incorporation with sputtered layers of 0.1µm producing higher element concentrations compared with thicker sputtered layers [127]. The higher element incorporation provides the increase in corrosion resistance [141, 142].

2.7 Electron Beam Surface Melting

Electron Beam Surface Melting (EBSM) is a HPBSM technique that uses a high energy beam of electrons to interact and modify a surface. The aim of EBSM is to melt and re-solidify the

surface to form through planar solidification a homogeneous layer of well controlled thickness. This layer would have improved corrosion resistance by the removal of reactive precipitates from the surface and retaining the elements in a solid solution. For such a modified layer to be achieved requires a careful understanding of the electron beam interaction and the affect of different processing parameters.

2.7.1 Electron Beam Surface Melting Processes

Electron beam energy is deposited in the top 5-10μm of a surface and sufficient energy can initiate melting [143]. Melting from the electron beam interaction has been shown by modelling of EBSM on aluminium to start below the surface [144-146].

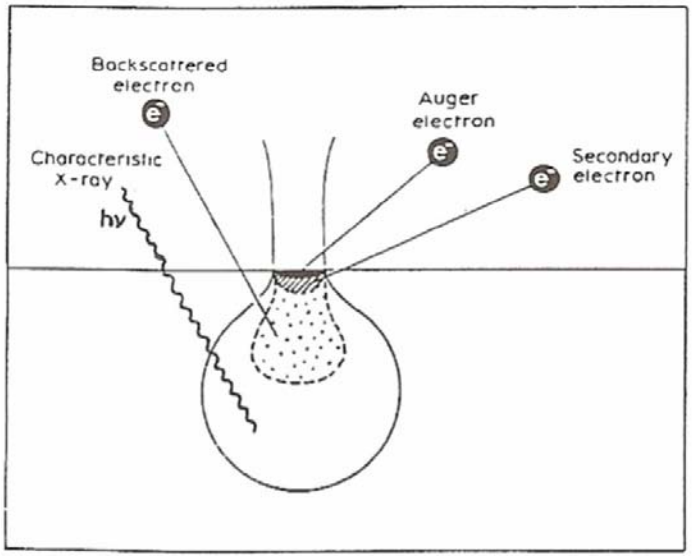

Figure 2.30 Diagram illustrating the interaction of an electron beam with a surface [20, 147, 148]

The electron beam deposits energy in the first few microns of material by electronic and lattice excitations. The accelerated electrons interact with the sample and lose energy through

scattering by elastic or inelastic collisions. The energy loss during these collisions causes the electrons to scatter and form a volume of interaction. The interaction of the electron beam with a surface is shown in Figure 2.30 [149]. The depth and volume of the electron interaction is influenced by a number of factors including the electron incident angle, current, accelerating voltage and average surface atomic number. It is the atomic number and voltage that have the most influence on the interaction volume [149].

2.7.2 BAE Systems Electron Beam System

BAE Systems has developed an electron beam system using a basic design taken from a system developed at The Institute of High Current Electronics at the Russian Academy of Sciences [143, 147, 148, 150-157]. The Russian design provided the key system features for processing which are shown in the schematic outline in Figure 2.31 and in a system photograph shown in Figure 2.32. Although the key features were taken from the Russian design the BAE Systems design was built to generate lower powers and have more flexible electronics.

A detailed discussion of the electron beam system can be found in Section 3.3, but there are some key features of the system that affect the materials processing efficiency and therefore need discussion. Such key features include; the cathode, the vacuum gases, the sample fixings and variable pulse duration.

The basic design of the system involves the movement of the sample surface underneath the pulsing electron beam. The design allows for movement of the sample in three directions to

provide focusing and treatment over an area. Focusing is also aided by mounting the sample at an angle to the beam as shown in Figure 2.31.

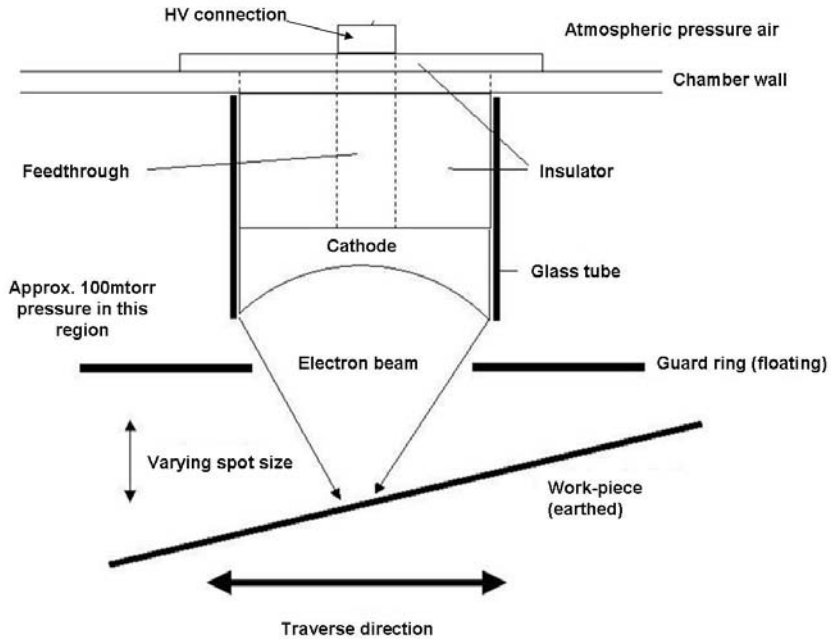

Figure 2.31 Schematic diagram of the pulsed, high power electron beam setup used for the treatment of specimens.

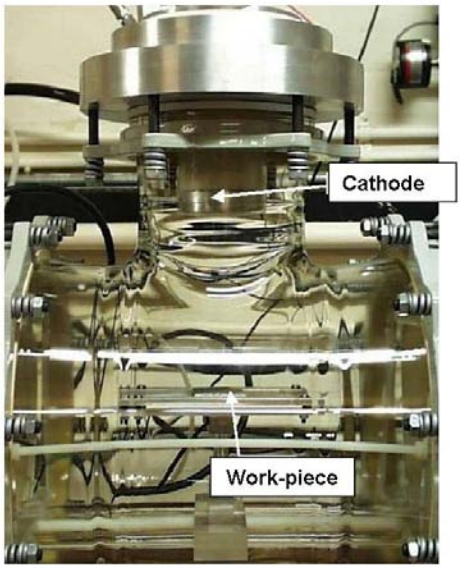

Figure 2.32 The BAE Systems electron beam apparatus highlighting key components.

Figure 2.31 also illustrates the shape of the system cathode which is a critical component and has been developed from previous work [158, 159]. The cathode of the system is important as its resistivity affects the electron discharge stability and its shape controls the beam focusing of this system. The system used a circular aluminium cathode with a radius of curvature on the side that faced down into the processing chamber. The concave shape was designed to increase the ability for the beam to self-focus and this would achieve high energy densities for processing at low cathode separations within a simple system [158, 159]. An aluminium cathode was used and it produced stable electron discharges until the cathode started to degrade by loss of oxide uniformity. Alternative cathodes could have been used that had higher resistivity that did not degrade but the advantage of using an aluminium cathode was that the discharge performance could be easily regenerated by simple mechanical processing (discussed in Section 3.3) [18, 148, 151]. The cathode stability was further increased as the system used a gas flow of a helium with 5% oxygen mixture [160]. The addition of oxygen was critical to maintaining the cathode stability and there was the added bonus that it also increased the electron discharge yield [160].

Once a stable electron discharge was produced EBSM could be performed by passing samples through the beam as shown in Figure 2.31. To pass the samples through the beam they were mounted on a platform either at an angle or flat. Samples were mounted at an angle to vary the cathode to sample separation as it moved through the beam. The variation in separation meant that there was also a change in the beam focus and energy density at the surface during treatment at set processing parameters such as energy, pulse duration or number of pulses per unit area. This variation in separation also aided experimental set-up with identification of the

focus. The system was designed to have changeable pulse duration so that the modified treatment depth could be varied and this would identify the optimum treatment that produced a thick, crack free, homogeneous layer [161].

2.7.3 Electron Beam Surface Melting Effect of Processing Parameters

The aim of EBSM in this thesis is to increase the corrosion resistance of a surface by the production of a homogeneous surface layer. The achievement of this requires the dissolution of reactive surface precipitates and also to create a solidification structure with minimal element segregation.

The tailoring of the modified surface properties depends upon the EBSM processing parameters which include; energy, pulse duration and number of pulses per unit area [162].

In a single radiation pulse the electron beam interaction induces a thermo-mechanical cycle in the surface [163] and once the material is melted there are significant microstructure changes [164].

Within the modified region the microstructure is not constant due to variation in the solidification growth conditions with depth and across the interaction This was observed in EBSM of stainless steel where the solidification structure varied over the modified depth with planar growth in the transient region beneath a segregated cellular structure [165]. There can also be variation in structure across the width of the modified region as shown in EBSM of

single crystal nickel material where there was cellular structure at the centre of the melt region and columnar dendrites at the edge [166].

The structures that form in EBSM have been shown to vary with the amount and rate of energy input [164]. Another affect on the modified layer of increasing the energy is that there is a greater degree of mixing induced. In the case of EBSM of 316L there was sufficient element movement induced by an energy increase that a defect free homogeneous microstructure was formed [167, 168].

As each single electron beam interaction changes the surface composition there is then also an overall effect on the modified layer from the number of pulses per unit area [169-171]. An example of this is provided by EBSM of D2 tool steels where an increase in the number of pulses per unit area was found to increase both the layer homogenisation and thickness. In this material, melting is initiated at the material carbides as they have a lower melting point compared with the matrix. The carbides initiate melting and are then partially dissolved during the electron beam pulse which means the initiation of melting by subsequent pulses requires a higher temperature. The carbide removal therefore changed the surface thermal properties and this formed a deeper modified layer with an increase in the number of pulses per unit area [171].

The presence of surface particles with low melting and vaporisation temperatures can also cause cratering of the surface. This occurs when the particles vaporise before the rest of the material so they erupt through the surface [168]. The production of craters affects the resulting surface roughness and depends on both the energy and number of pulses per unit area [169-171].

The energy, number of pulses per unit area and pulse duration have been shown to influence the modified layer thickness [33, 146, 158, 169-173]. An example of the influence from pulse duration is given by the EBSM of titanium alloys where variation in the scan speed affected the shape and size of the melted layer [173]. Other effects from scan speed include microstructure refinement as shown in EBSM of AISID3 tool steel where an increase in scan speed increased the defect density and decreased grain size [174].

2.7.4 Electron Beam Surface Melting and Laser Surface Melting

EBSM has more flexible processing parameters than LSM and LSA because electronics are used to control all of the beam characteristics. This is unlike lasers, where some parameters are dependent on the gain medium (discussed in Section 2.6.1). Other advantages of EBSM include high radiation absorption, low cost and the ability to treat reflective surfaces [120, 175]. The major disadvantage for EBSM is that a low pressure environment is required for beam propagation. However this could be overcome using moveable vacuum seals developed at BAE Systems in crawler robot technology [176].

2.7.5 Electron Beam Surface Melting Materials

Previous EBSM work has been on a variety of materials using a range of electron beam systems as shown in Appendix 2 – Summary of Electron Beam Surface Melting Treatments. The main bulk of the EBSM work has been for the improvement in wear or corrosion resistance of many different materials including pure metals, steels, aluminium bronzes, titanium alloys and aluminium alloys [79, 83, 143, 151, 156, 164, 165, 167, 168, 173, 174, 177-189].

The increase in wear resistance is achieved from microstructural refinement providing an increase in the surface hardness [173, 181, 187, 189]. Some problems have been encountered with improving the wear resistance due to poor surface finish, non-uniformity of treatment depth, and the presence of both pores and cracks within the modified layer [173].

The microstructure refinement that increases the wear resistance can also increase the corrosion resistance due to changes in the precipitate distribution [83, 143, 170, 180, 190]. The dissolution of reactive particles can also increase the corrosion resistance with the production of a homogeneous surface [143, 151, 170, 180, 186, 188, 191, 192].

2.7.6 Electron Beam Surface Melting AA2024

EBSM has been performed on AA2024 and AA6061 with limited improvement in the corrosion resistance as the modified layers produced contained micro-cracks, precipitates that were thought to have decomposed from the saturated solid solution, and in some cases a cellular segregated solidification structure [164, 169, 182].

There was some degree of precipitate dissolution but this was found to vary with precipitate size and depth within the layer [164, 169]. The limiting size for particle dissolution was identified as between 0.4 and 1μm and complete particle dissolution was only observed in the top 7μm of the layer [143, 164, 169, 182].

The variation in precipitate dissolution was attributed to the differing thermal gradient, liquid time and growth rate as these vary throughout the layer thickness. This was illustrated by the

presence of different solidification structures through an EBSM layer with epitaxial growth in the transient region and a mixture of dendrite and cells at the surface [165].

The number of micro-cracks present in the layer increased with energy, which was thought to be caused by the increase in residual stresses [143, 164, 169, 182]. In this work by Rotshtein cracking was not removed but as it was related to the processing parameters this suggests that characterisation of the full affects of the EBSM processing parameters on the modified layer would provide an indication of which processing parameters would be able to create a homogeneous, smooth, defect free corrosion resistant layer.

EBSM of AA2024 has not been shown to provide complete dissolution of precipitates. There has also not been an extensive study on that affect of different EBSM processing parameters on the precipitate distribution.

2.8 Summary

Friction stir welding (FSW) has been highlighted as a joining process suitable for high strength aluminium alloys [9]. FSW provides benefits over other joining techniques such as traditional welding processes and riveting as FSW has the capability to form long continuous joins with low labour intensity.

The benefit of continuous joining is of particular interest with the development of aircraft components of increasing size, such as for the A380. There are issues however, with the FSW of large structures that need to be overcome before their application in the aerospace industry.

For the efficient FSW of structures it has been identified that the surfaces to be joined need to be free of any surface layers that have been applied, i.e. environmental protection layers such as anodising or paint. These layers therefore have to be removed prior to welding. The problem is though that the resultant structure from FSW may be too large to have the environmental protection layers such as anodising applied as they would be too large to fit into the chemical bath.

A solution would be to apply the environmental protection layers before welding and then remove the layers from the specific areas required for welding. However, this would not be practical as it has been shown that FSW joints have a low corrosion resistance and it would be necessary to apply environmental protection after FSW [45].

The proposed solution under investigation in this thesis for the issues described above is the following process:

1. Apply traditional environmental protection layers to components.
2. Perform localised removal of the protective layers to the areas that are to be welded.
3. Perform FSW.
4. Locally apply a corrosion protection treatment over the welded area.

It is suggested that high power beam technology would be able to achieve stages two and four out of the proposed solution above.

The high power beam process that would achieve stage two in a FSW preparation technique is laser paint removal. There has been limited work into laser paint removal of the

environmental protection layers typical of aerospace components. The aim of investigations in this thesis was to identify a laser and processing parameters that could remove typical environmental protection layers of aerospace alloys and produce a surface that would be suitable for the production of high quality friction stir welds.

The suggested post-treatment for FSW to improve the corrosion resistance is High Power Beam Surface Modification (HPBSM) in either the form of Laser Surface Melting (LSM) or Electron Beam Surface Melting (EBSM).

HPBSM techniques use rapid solidification to increase the corrosion resistance of a material by the removal of reactive precipitates in the surface and the generation of a solidification structure that has minimal segregation [18].

Although HPBSM has been shown to be corrosion resistant the layers produced also have to have a reasonable damage tolerance in order to maintain environmental protection.

This thesis aims to investigate the HPBSM processing parameters and their effects on the modified layer properties, particularly the modified layer thickness. In order to achieve this, a number of different lasers were used along with an electron beam system.

The electron beam system was designed to provide a greater flexibility in the processing parameters compared with laser systems. The aim of this was to achieve a more detailed understanding of HPBSM and EBSM on aerospace alloy AA2024.

3 Experimental Method

Table 3.1 summarises the investigations performed in this thesis, and the experimental arrangements are described in this chapter for each of the high power beam techniques, along with the material characterisation methods used.

Table 3.1 Summary of high power beam systems and materials used throughout thesis.

	Pulse Duration	Application	Material
Excimer Laser	25ns	LSM Paint Removal	AA2024, AA7056, AA7150, AA7449,
TEA-CO_2 Laser	3μs	Paint Removal	AA2024
Nd:YAG Laser	80-150ns	Paint Removal	AA2024
Nd:YAG Laser	0.2-50ms	LSM	AA2024
USP-CO_2 Laser	7-100μs	LSM	AA2024, AA7150
Electron Beam	7-40μs	EBSM	AA2024

3.1 Materials

As illustrated in Table 3.1, a number of different aluminium alloys were used throughout investigations.

3.1.1 Materials for Laser Paint Removal

Initial processing parameter investigations into laser paint removal were carried out on material supplied by Airbus, which was AA2024-T351 plate with different forms of treatment on the upper and lower surfaces, as shown in Figure 3.1. The top side had a pure aluminium clad layer of 165μm thickness, a chromic acid anodising layer of approximately 3.5μm thickness and finally an AK30 Nobel primer paint of 28μm thickness. The underside however only had an anodising layer present.

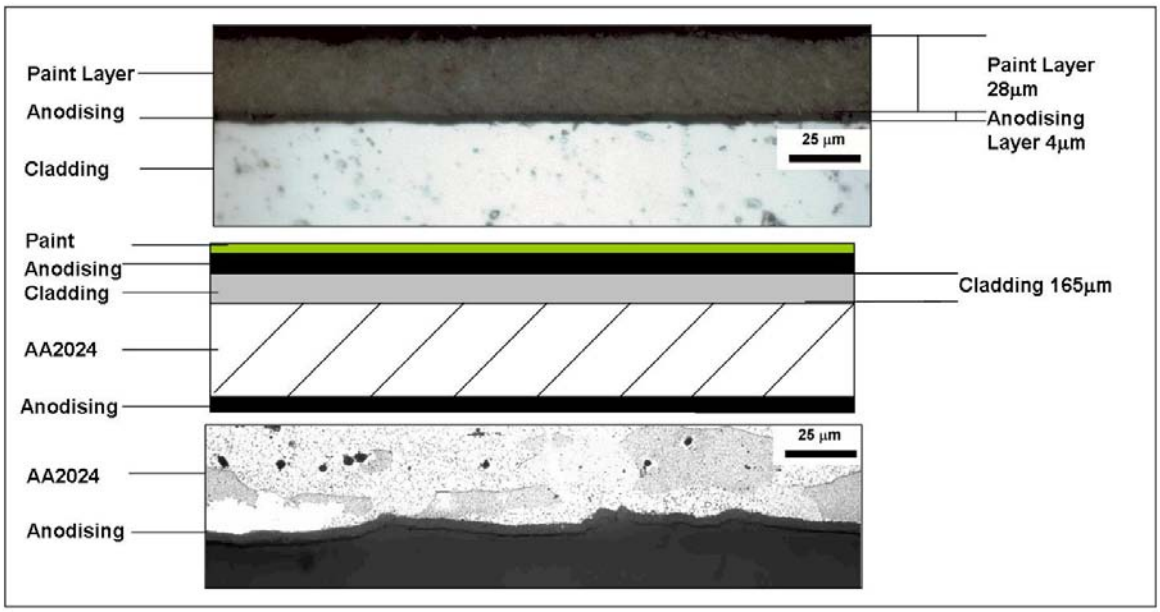

Figure 3.1 Diagram and micrographs of sample surface layers used in laser paint removal trials.

Both sides of the samples were used in testing as they allowed for the optimisation of laser parameters for the removal of specific layers, i.e. the underside was used to optimise parameters for the removal of anodising only.

The material used in the preparation of surfaces for FSW was not the same as that used in the processing parameter investigations as the presence of a clad layer was not suitable for FSW. Figure 3.2 shows the area and type of surface layers that had to be removed in preparation for FSW.

To test the effectiveness of the laser removal preparation technique, friction stir welds were also produced using surfaces prepared by LSM, machining and laser removal (further

discussed in Section 3.2.6). The same initial material was used for each of these removal methods.

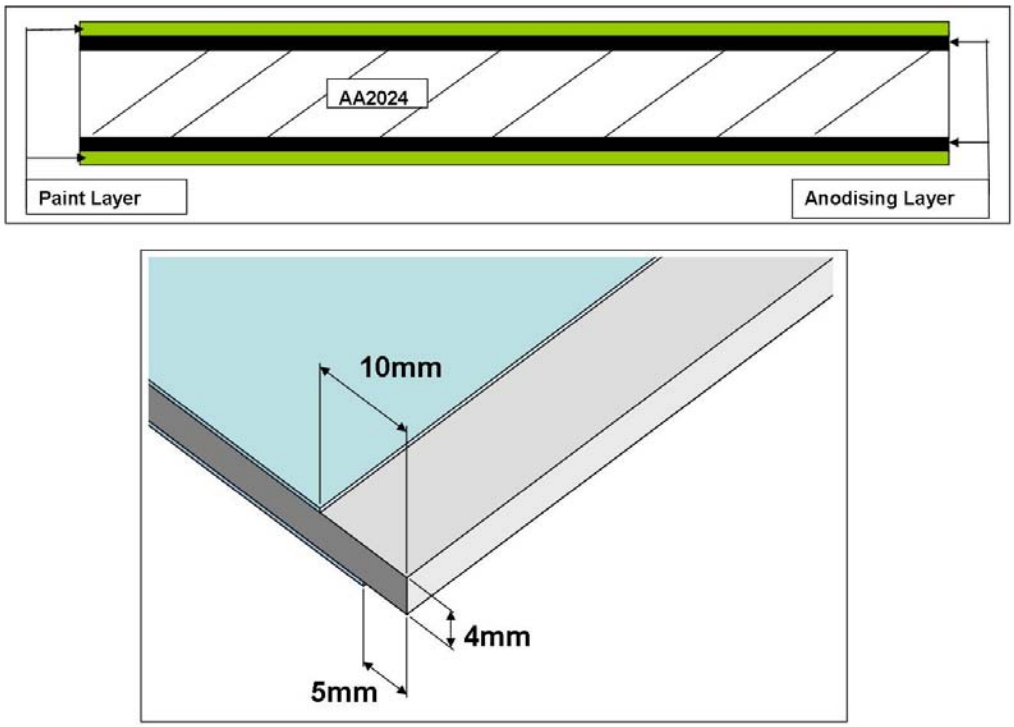

Figure 3.2 Diagram of layers samples used for Friction Stir Welding samples and the area of preparation.

3.1.2 Material for High Power Beam Surface Modification

The primary material used for surface modification studies was AA2024-T351, (supplied by All Metal Service) the average (from a minimum of three measurements) composition was measured by EDX and as shown in Table 3.2.

A range of 7xxx series alloys were also investigated: AA7056-T7651 (supplied by Apollo Metals Ltd), AA7150-T651 and AA7449-T7951 (both supplied by All Metal Service); their

average compositions are also shown in Table 3.2. There are differences between the 7xxx series alloy compositions, in particular AA7150 having a higher zirconium content when compared with AA7449 and AA7056.

The materials used were in plate form and the sample thickness varied between the alloys as shown in Table 3.3.

Table 3.2 Average weight percentage chemical composition (from a minimum of three measurements) of the aluminium alloys used in this study measured using EDX analysis.

Element (wt%) / Material	Al	Cu	Mg	Mn	O	Zn	Zr
AA2024	91.0	4.9	0.7	0.6	2.5	0.3	0.2
AA7056	89.3	1.2	0.9	0.1	3.0	8.8	0.1
AA7150	87.0	2.2	1.2	0.02	2.4	6.8	0.5
AA7449	86.1	2.4	1.4	0.00	1.3	8.8	0.2

Table 3.3 Thickness of aluminium alloy materials used throughout investigations.

Material	Thickness (mm)
AA2024	3.2 and 6
AA7056	6.4
AA7150	12
AA7449	14

The surface preparation used for samples depended upon the high power beam treatment being performed and will be discussed for LSM in Section 3.2.7 and for EBSM in Section 3.3.2.

3.2 Laser Processing

Throughout this work lasers from BAE Systems Advanced Technology Centre (ATC), Airbus Deutschland, Cranfield University and Heriot-Watt University have been used and the specifications for each of these lasers is shown in Table 3.4. The optical arrangement used in investigations varied with the laser, which will each be described in Sections 3.2.1 to 3.2.5.

Table 3.4 A summary of the lasers used and their general specifications

Laser	Pulse Duration	Lasing Medium	Wavelength	Treatment Type	Application	Organisation
Excimer	25ns	Excited Dimer	308nm,	Spots, Tracks, Areas	LSM Paint Removal	BAE Systems ATC
TEA-CO_2	3μs	CO_2	10.6μm	Spots	Paint Removal	BAE Systems ATC
Nd:YAG	80-150ns	Nd:$Y_3Al_5O_{12}$ crystal	1064nm	Tracks, Areas	Paint Removal	Airbus Deutschland
Nd:YAG	0.2-50ms	Nd:$Y_3Al_5O_{12}$ crystal	1064nm	Spots, Areas	LSM	Cranfield University
USP-CO_2	7-100μs	CO_2	10.6μm	Areas	LSM	Heriot-Watt University

3.2.1 Excimer Laser

The excimer laser was a Lambda Physik LPX315i XeCl gas mix laser producing pulses of 25ns duration and 308nm wavelength. The laser variables were the pulse repetition frequency (PRF) of 1-100Hz and pulse energy, although laser processing was generally performed at a 100Hz PRF.

The optical set-up for the excimer laser is in Figure 3.3, which shows that a series of mirrors was used to guide the beam from the laser to the workpiece, passing through a Micro-Lens

Array (MLA) and focussing lens combination. The MLA and focussing lens combination are important as these create a spatially homogenised square spot of 1.5x1.5mm (shown in Figure 3.4) at the workpiece surface.

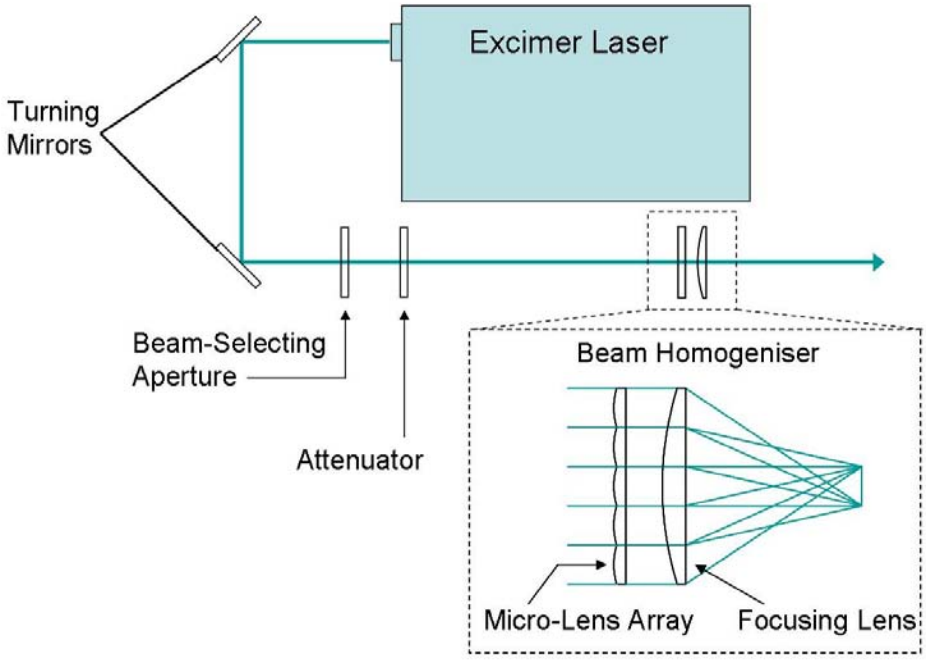

Figure 3.3 Schematic diagram of excimer laser optical set-up.

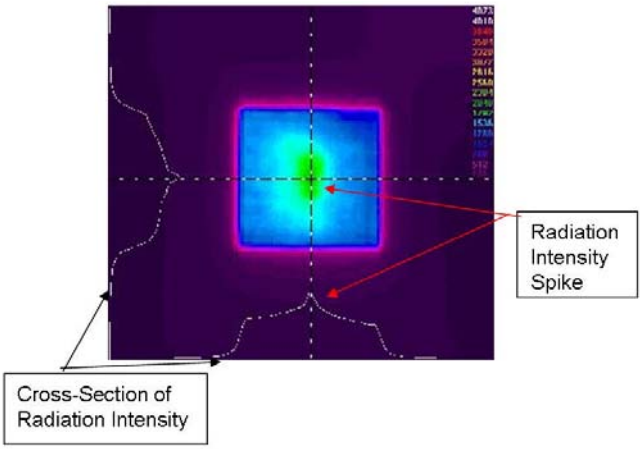

Figure 3.4 Un-calibrated radiation intensity profile of attenuated, MLA and focused excimer laser beam. Measured using a CCD camera with the glass protective aperture removed to provide a high intensity for ultra-violet radiation.

MLAs are available commercially but the one used in this project was manufactured at BAE Systems ATC by multilevel photolithography and is specifically designed for operation at the excimer laser wavelength of 308nm and with a large focal length of 100mm. The MLA works as a beam homogeniser as it consists of a square arrangement of individual diffractive 2.5mm square lenses that are etched onto a quartz substrate. These lenses split the incident beam into a number of partial beams that are focused [193]. The final beam size was determined by the focusing parameters at the MLA and the focusing lens using Equation 3-1.

$$Image\ Size = \frac{Focal\ Length\ of\ Focus\ Lens}{Focal\ Length\ of\ MLA} . Lens\ Size\ of\ MLA \qquad (3\text{-}1)$$

Figure 3.4 shows a radiation intensity profile of the excimer laser spot using the MLA and focusing lens optical set-up shown in Figure 3.3. The radiation intensity was measured using a CCD camera (Charge Coupled Device, which converts optical brightness to electrical signal) which was made sensitive to ultra-violet radiation with the removal of the protective glass lens. Figure 3.4 provides an un-calibrated measure of the radiation intensity across the beam area; it shows that the intensity of the beam is relatively uniform except for a small radiation spike in the centre (shown as green on the image).

The uniform beam profile ensures that the laser treatment is consistent and that the processing energy density fluence (J/cm^2) can be monitored by measurement of the laser energy after the final optical element (using an Ophir model DGX-RP with Optilas Ophir DGG display) and before the laser interaction area on the workpiece.

A MLA was used in preference to an imaging arrangement in this work in order to utilise the entire laser beam. Figure 3.5 is a comparison of a MLA and imaging optic arrangements and shows that when using a MLA the whole beam is captured, but with an imaging arrangement only a portion of the beam is used and a significant portion of the beam energy is lost.

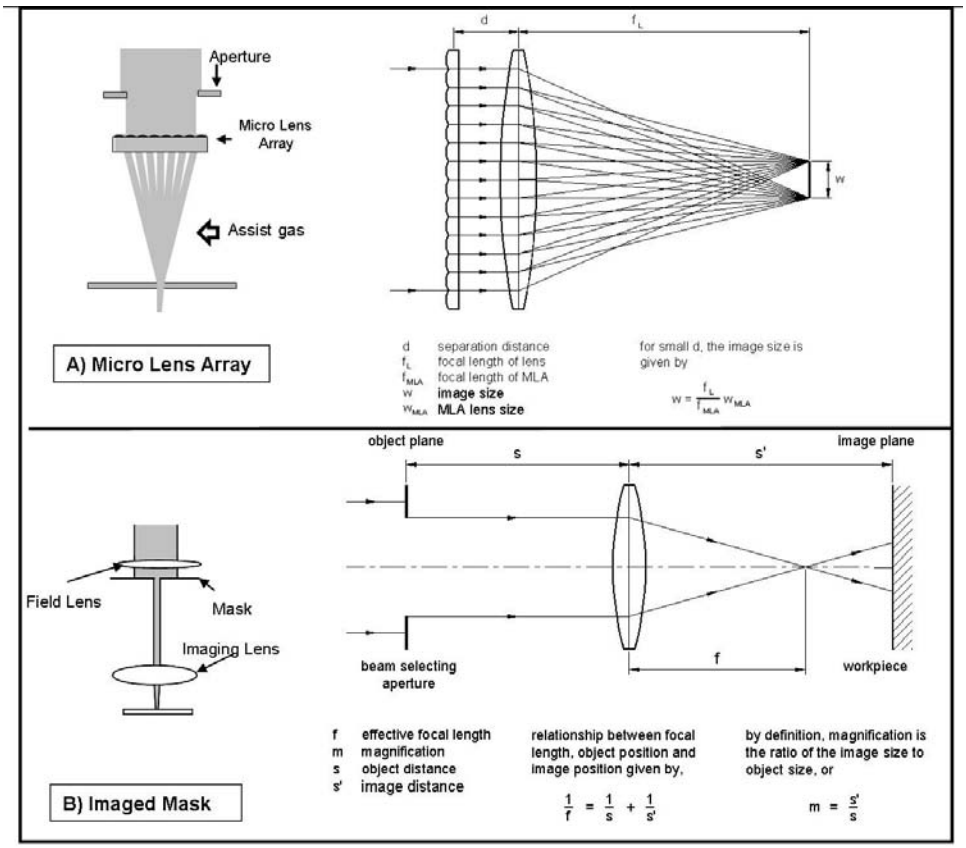

Figure 3.5 Schematic representation of the optical arrangements used for excimer laser processing using A) Micro Lens Array and B) Imaged Mask

The use of a MLA in the optics allowed for complete utilisation of the laser beam energy. To vary the laser energy density or fluence at the workpiece, two methods were used: changing the beam output by altering the laser excitation voltage, (within the operation limits) or placing a variable attenuator (OPTET AT4020) into the beam path which portioned the beam.

Both of these methods were used as it has been shown in previous work, in the development of MLAs, that an attenuator has minimal affect on the beam uniformity [194, 195].

Even with using these two methods to vary the fluence, it was necessary also to employ two variations in the optical set-up to achieve either high fluence (for LSM) or process large areas (for laser paint removal). These were a desk-top arrangement and a gantry arrangement.

In the desk-top arrangement, the samples were mounted perpendicular to the beam path on translation stages for x and y movement. In the gantry arrangement, the sample was stationary and the beam was moved. In both cases however the sample was always normal to incident beam.

For the treatment of areas larger than the focused laser spot size it was necessary to translate the sample in the desk-top arrangement and the laser in the gantry arrangement and overlap the laser interaction area.

There are a number of different overlapping patterns possible for area treatments and each can provide a variable number of pulses per unit area. In this investigation, two patterns were used: a step and repeat pattern and a raster pattern.

A step and repeat pattern, shown in Figure 3.6, is a basic pattern as each unit area of the surface was treated with the required number of pulses before the beam was indexed to the next position with a small amount of overlap (10%) and the treatment repeated.

Raster scanning shown in Figure 3.7 uses continuous movement at a constant speed (dependent on the PRF) in both the x and y directions between every laser pulse e.g. nine pulses per unit area was achieved by movement of a third of the beam in the x direction after each pulse and by a third of the beam in the y direction between laser rows.

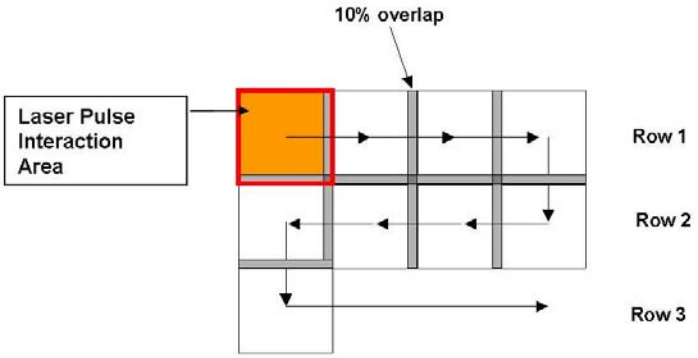

Figure 3.6 Schematic representation of step and repeat laser scanning pattern.

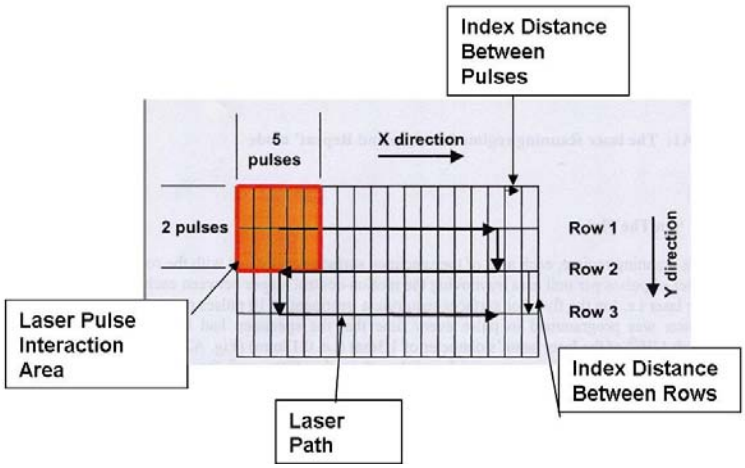

Figure 3.7 Schematic representation of raster laser scanning mode.

3.2.2 TEA-CO_2 Laser

A Transversely Excited Atmospheric (TEA) CO_2 laser MT1000, Platinum Series, was used for the laser paint removal trials as a comparison for the excimer laser. The TEA-CO_2 laser

set-up used a lens to focus the beam onto a stationary sample. This laser set up was only capable of single spot treatments as the sample and beam were both stationary.

3.2.3 Nd:YAG Airbus Deutschland

The Nd:YAG used for laser paint removal trials for comparison to the excimer laser was owned by Airbus Deutschland. The exact details of the set-up were unknown.

The samples were produced at maximum laser power while the PRF and sample feed rate were varied. This parameter variation altered the number of pulses per unit area in treatment as the number of pulses can be indicated by the PRF divided by the feed rate. Further details of the processing parameter variation are provided with the results in Section 4.3.1.1 in Table 4.2 and Table 4.3.

3.2.4 Nd:YAG Cranfield University

The Nd:YAG laser system available from Cranfield University was a Rofin laser En60825 and was used as part of the LSM trials. The laser provided processing parameter variation of pulse duration, energy and the number of pulses per unit area. The laser and the optics were a closed system with the translation of the sample achieved by hand movement.

The Nd:YAG laser parameters were;

- Beam diameter 2mm.
- Variable Pulse Duration between 0.2 and 50ms.
- Variable PRF, with usual operation at 10Hz.
- Operating wavelength of 1064nm.

3.2.5 USP-CO_2 Laser Heriot-Watt

The USP-CO_2 laser from Heriot-Watt University was a planar waveguide laser and was used as part of the LSM investigations. The laser parameters of the USP-CO_2 laser were;

- Pulse duration, 10-100μs.
- Peak power 3kW.
- PRF Variable up to 10kHz.
- Spot size approximately 100μm.

In LSM investigations there was variation in the laser energy, pulse duration and the number of pulses per unit area.

The set-up for the USP-CO_2 laser is that used in previous LSM work by M.G. Tsagkarakis and is shown in Figure 3.8 [98]. The resultant beam profile from this set-up is in Figure 3.9, which shows that there is a variation in radiation intensity across the beam which may be a problem for treatment consistency [98].

In the LSM treatments, energy was varied by changes to the laser excitation and pulse duration was varied by RF pulse generators. The pulse duration value was measured from the start point of the pulse to the peak power shown in Figure 3.10 [98].

Variation in the number of pulses per unit area was achieved by using a stationary beam and moving the sample on x-y translation tables that were synchronised to the laser pulses by two external RF generators. The positioning system was used to translate the sample and the stepper motor output signal was then used to trigger the laser pulse. The output signal could

also be altered by the RF pulse generators to allow a variation in the pulse duration and PRF as shown in Figure 3.11 [98].

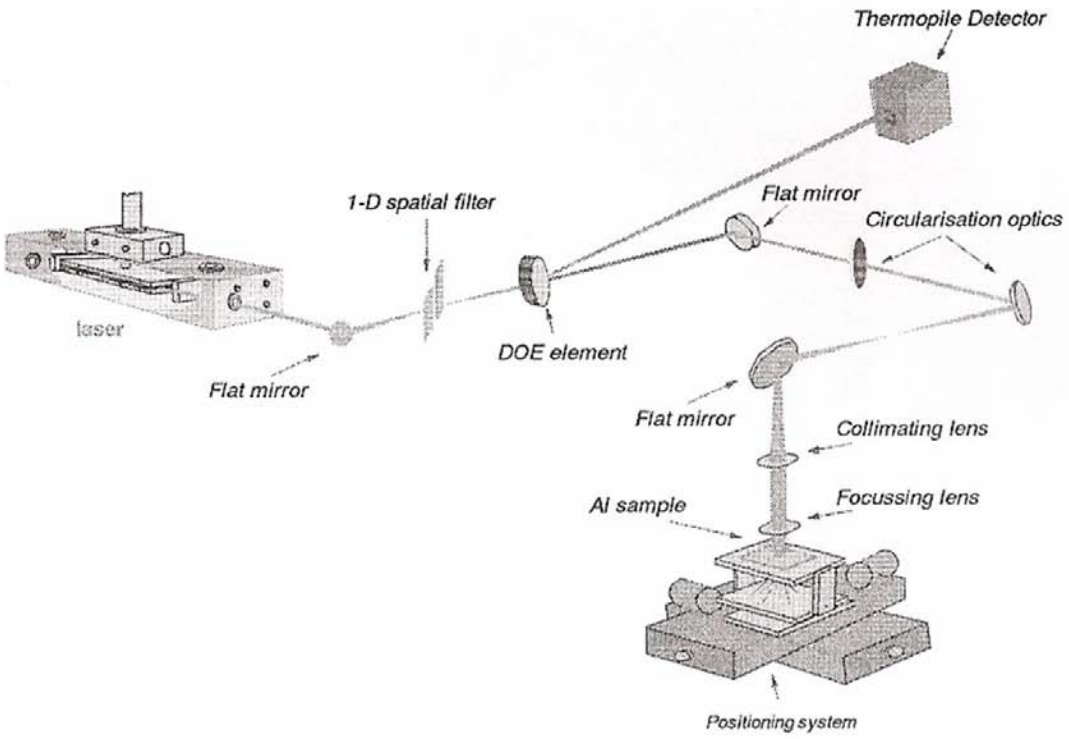

Figure 3.8 Schematic of USP-CO_2 laser optical set up [98].

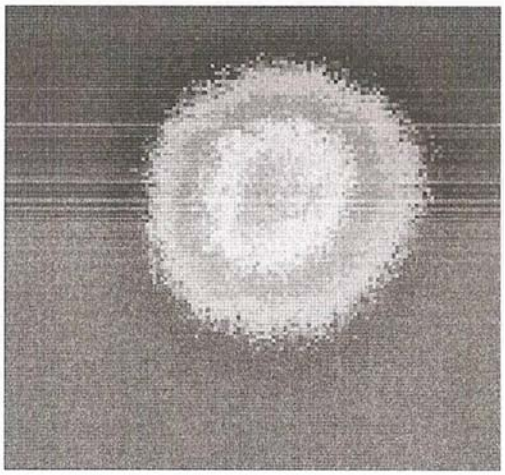

Figure 3.9 Far-field image of the USP-CO_2 laser beam shape [98].

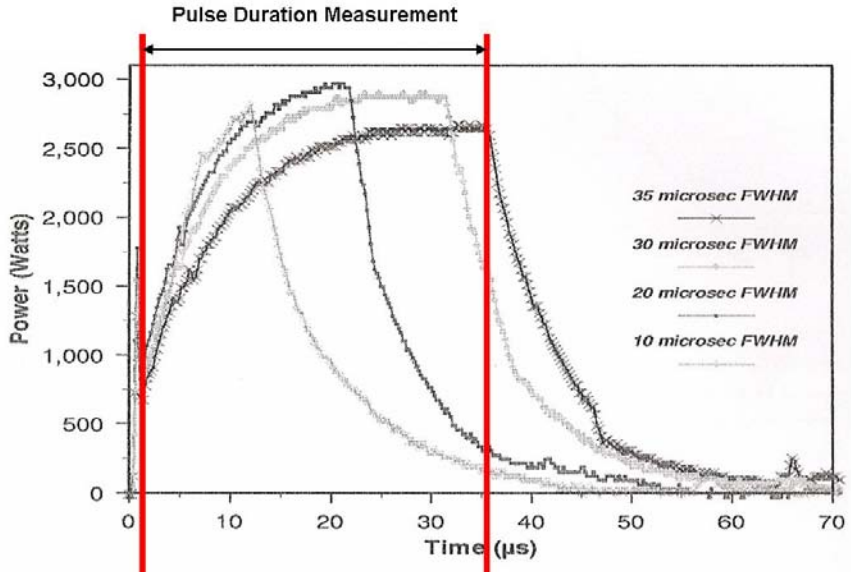

Figure 3.10 Diagram for USP-CO_2 laser pulse shape and pulse duration measurement [98].

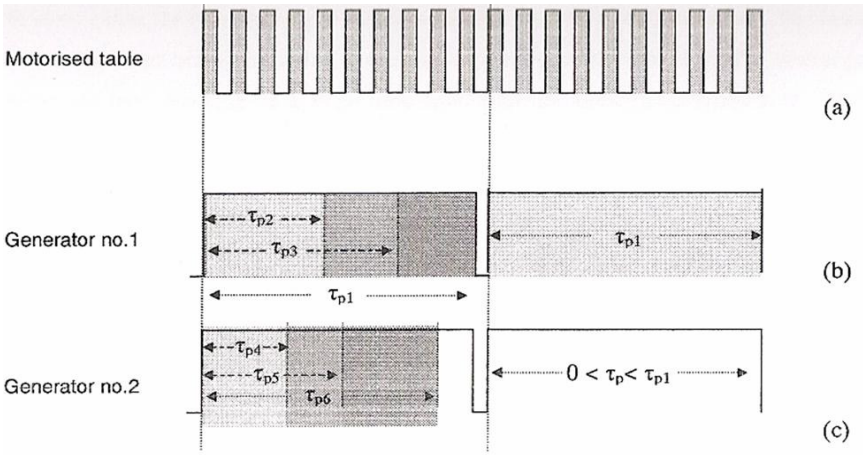

(a) The standard pulses originating from the motorised table.

(b) These pulses trigger a pulse in the pulse generator no.1. Varying the length of this pulse sub-multiplies the initial frequency of the pulses, in this case of τ_{p1} by a factor of 10.

(c) Each of the pulses of the generator no.1 (b) triggers a new pulse of adjustable duration τ_p at the pulse generator no.2 (e.g. τ_{p4}, τ_{p5}, τ_{p6}).

Figure 3.11 Diagram of the laser-motorised stage synchronisation or the USP-CO_2 laser pulse generation [98].

3.2.6 Laser Paint Removal

Three lasers were used to study the removal of surface layers: an excimer, a TEA-CO_2 and an Nd:YAG (Airbus Deutschland). The set-ups for these lasers varied and are described in sections 3.2.1, 3.2.2 and 3.2.3 respectively. The material used is described in Section 3.1.1.

3.2.6.1 Processing Parameter Variation

A processing parameter investigation of energy and number of pulses per unit area was carried out using the three lasers. To aid the parameter investigation, by identification of the maximum removal fluences, etch rate curves (the depth of material removed by one laser pulse) were generated for the excimer and TEA-CO_2 lasers. These investigations identified the parameters that were required to remove specific surface layers and this generated a multiple stage treatment suitable to prepare surfaces for FSW.

3.2.6.2 Generation of Etch Rate Curves

The etch rate curves were generated by a series of spot treatments (1.5x1.5mm) with a progressive increase in laser parameters. Primarily a low fluence was used and spot treatments were performed with an increasing number of pulses until a shiny metal surface was observed in the treated area. The fluence was then increased (between 2 and 10J/cm^2) and the process repeated. This created a series of single pulse treatments of varying energy and number of pulses per unit area: this is shown in Figure 3.12. The amount of material removed in each set of treatment parameters could then be measured and the amount of material removed per pulse calculated.

To calculate the amount of material removed, depth measurements were performed using an optical microscope to measure the difference in the height of the microscope lenses between the untreated material and the single spot treated area. Previous work has established the reasonable accuracy of this method [36].

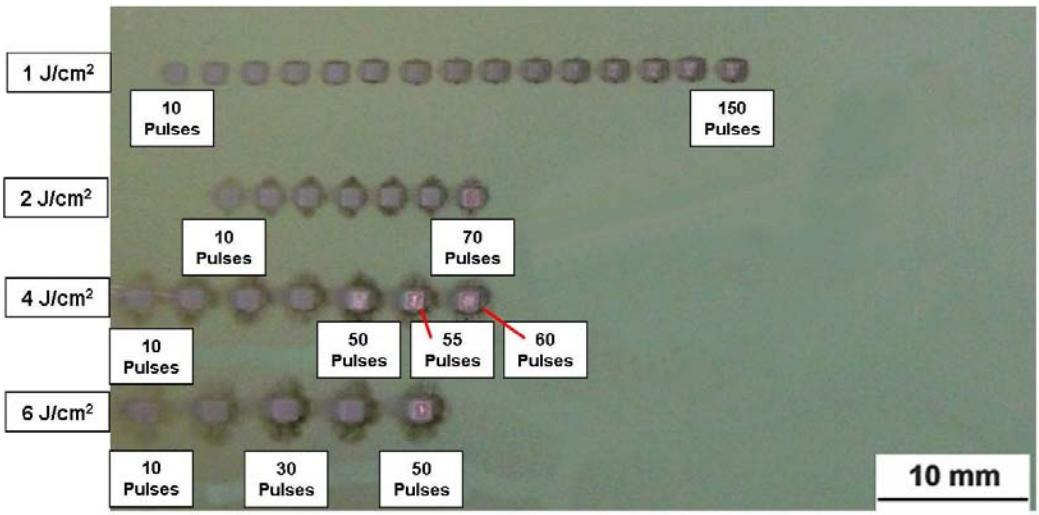

Figure 3.12 Picture of excimer laser spot treatments used to generate etch rate curves. Spot treatments were performed at increasing energy and number of pulses per unit area.

3.2.6.3 Friction Stir Welding

The processing parameter investigation generated a multiple stage treatment that was used to prepare samples for FSW by removing layers from the upper, lower and edge surfaces of the plates to be welded as shown in Figure 3.2.

As a comparison to the laser removal process, machining was also used to prepare samples for FSW. The machining removal process utilised a milling machine to skim off the upper, lower

and edge surfaces. The material removal was to a minimum depth to expose the substrate material.

Another concern for the laser paint removal process, as a preparation technique, was over-treatment of the surface with production of a LSM surface layer. To investigate the effect of welding an LSM surface, a sample was prepared with LSM of 64 pulses per unit area and 6J/cm^2.

The friction stir welds were produced at BAE Systems ATC using a Huron NU5 vertical milling machine adapted for friction stir welding. The Huron NU5 is more conventionally used for heavy duty milling operations and has operating parameters of 30-2066rpm spindle speeds and 1.6-820mm/min table feed rates. The welds were produced at a 195mm/min travel speed and 468 revolutions per minute rotation speed.

3.2.6.4 Destructive Bend Tests

The quality of the welds produced were evaluated by using destructive bend testing as specified in European Standard EN 910:1996 [196]. The principle of the test was to subject samples from a welded joint to plastic deformation by bending. Any weld imperfections (generally root defects) would cause premature weld failure and this would signify that the surface preparation was inadequate.

The bend tests were performed by clamping one end of the sample and continuously applying gradual loading of the sample by rotation of the outer roller through an arc centred on the axis of the former roller as shown in Figure 3.13. The test was completed when the bending angle

reached the standard value depicted by the arc. After testing, both the external and sides of the samples were examined visually. Failure of the test occurred when imperfections in the weld were greater then 3mm or fracture of the weld [196].

Samples were prepared as specified in the standard as "face bend test samples of butt weld" and "root bend test samples of butt weld". A "face bend test sample of butt weld" is a sample for which the surface in tension is the side which contains the larger width of the weld. A "root bend test sample of butt weld" is a sample for which the surface in tension is in the side opposite to the "face bend test sample of butt weld". Figure 3.14 shows tested samples of both weld sample types. The sample dimensions were; width 21mm, length 125mm and thickness 4mm and were prepared by guillotine cutting which meant that no heat treatment was applied between welding and testing [196].

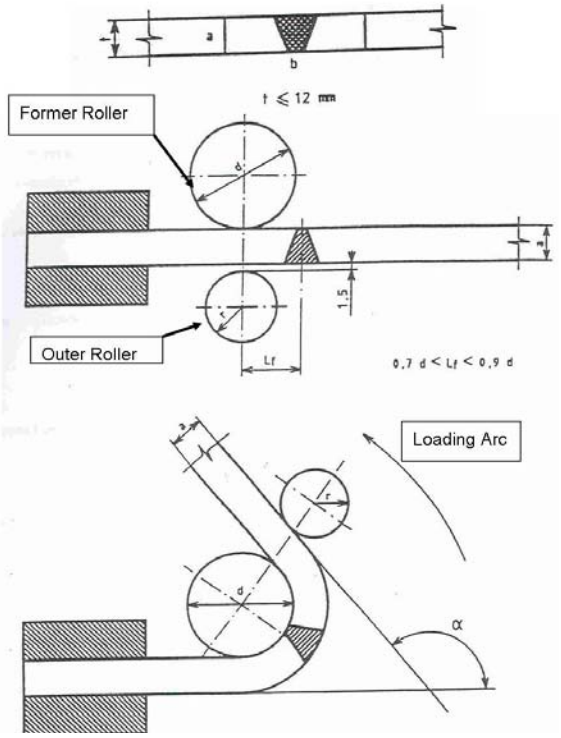

Figure 3.13 Schematic diagram of the destructive bend tests specified in EN 910:1996 using a roller experimental set-up to evaluate FSW and FSW surface preparation processes.

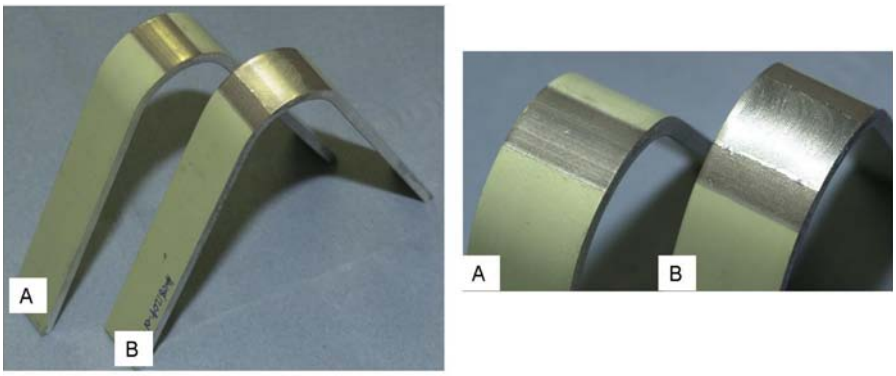

Figure 3.14 Photographs of sample types specified in EN 910:1996. A) Root bend test of butt weld and B) Face bend of butt weld.

3.2.7 Laser Surface Melting

To investigate the effect of radiation pulse duration on the LSM layer depth and properties, a range of lasers were used. These lasers were an Excimer, Nd:YAG and USP-CO_2. The Nd:YAG laser used in the current studies was based at Cranfield University and the USP-CO_2 lasers was sited at Heriot-Watt University. The experimental set-up and treatments performed varied with the laser used so each are described separately. The LSM samples produced were characterised in terms of their microstructure (described in Section 3.5) and corrosion resistance (described in Section 3.6).

3.2.7.1 Excimer Laser

The experimental set-up for the excimer laser is described in Section 3.2.1. Initial trials were performed into the experimental set-up which included beam delivery, shield gas and scanning pattern. It was found that a MLA, air atmosphere and raster scanning gave the most

consistent LSM treatment. Surface preparation of material for excimer LSM was machining and cleaning with iso-propanol.

With this set-up the LSM processing parameters of fluence (1J/cm^2 to 10J/cm^2) and number of pulses per unit area (3-25 pulses) were varied to identify the optimum treatment in terms of microstructure and corrosion resistance.

3.2.7.2 Nd:YAG Laser

The set-up for this laser is described in Section 3.2.4. The surface preparation used with LSM of this laser was the same as that in previous work, by A. Vaugh, which was machined and then wire brushed, which created a reflective surface [197]. In some tests an absorbent carbon (Graphit 33 Agar Scientific) coating was applied to the surface in order to increase the absorption of laser energy.

LSM investigations were into the variation of the pulse duration (10ms and 50ms) and number of pulses per unit area (1-10 pulses). It was noted that any change in pulse duration altered the laser excitation voltage and unavoidably this led to changes in the radiation energy (2.5-70.7J).

3.2.7.3 USP-CO_2 Laser

In investigations using this laser (set-up described in Section 3.2.5) the LSM treatment was performed on AA2024 and AA7150 with variation in the number of pulses per unit area and the pulse duration. The pulse duration was varied between 7 and 30μs and the number of

pulses per unit area varied between 1 and 10. For every parameter variation a sample area of 10mm by 50mm was produced. Surface preparation of material for LSM was machining and cleaning with iso-propanol.

3.3 Electron Beam Surface Melting

The electron beam system developed at BAE Systems was designed to be a simple system with easy operation and was introduced in Section 2.7.2. The capabilities of the BAE systems EBSM system were;

- Pulse duration of a few microseconds (7μs to 100μs).
- Pulse energies of up to 12J.
- PRF 1Hz.
- Normal operating pressure 300mTorr.

A diagram of the processing set-up for EBSM is shown in Figure 3.15, this shows how the cathode separation can be easily changed by mounting the sample at an angle and moving with a translation stage. Movement was possible in the x, y and z directions, but only the x direction was motorised.

To generate the electron beam for processing, a number of commercially available products were used and their details are in Table 3.5. The components of the electron beam detailed in Table 3.5 are shown in Figure 3.16 and the circuitry is shown in Figure 3.17. The circuitry could be adapted to produce a wider range of processing parameters then those stated above.

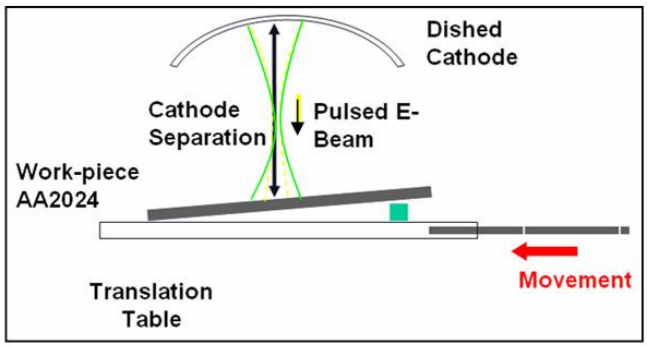

Figure 3.15 Schematic of electron beam surface melting system experimental set-up

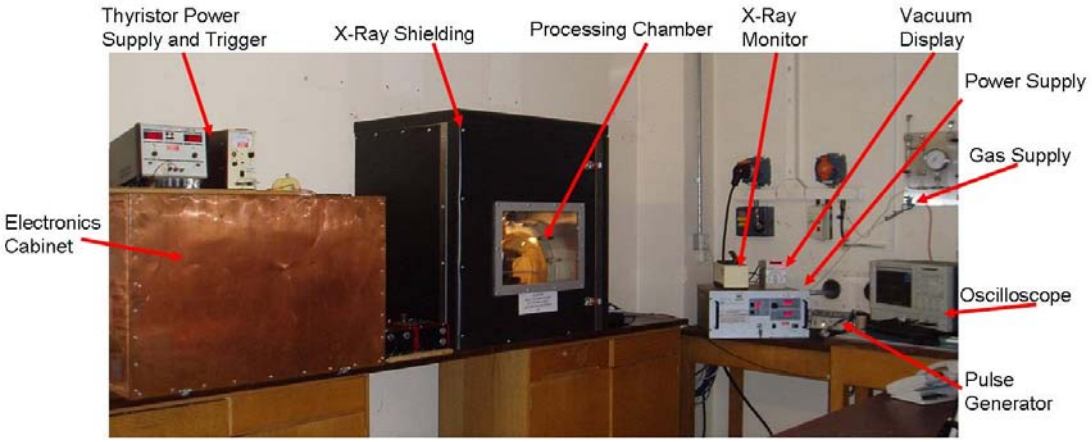

Figure 3.16 BAE Systems ATC electron beam processing facility

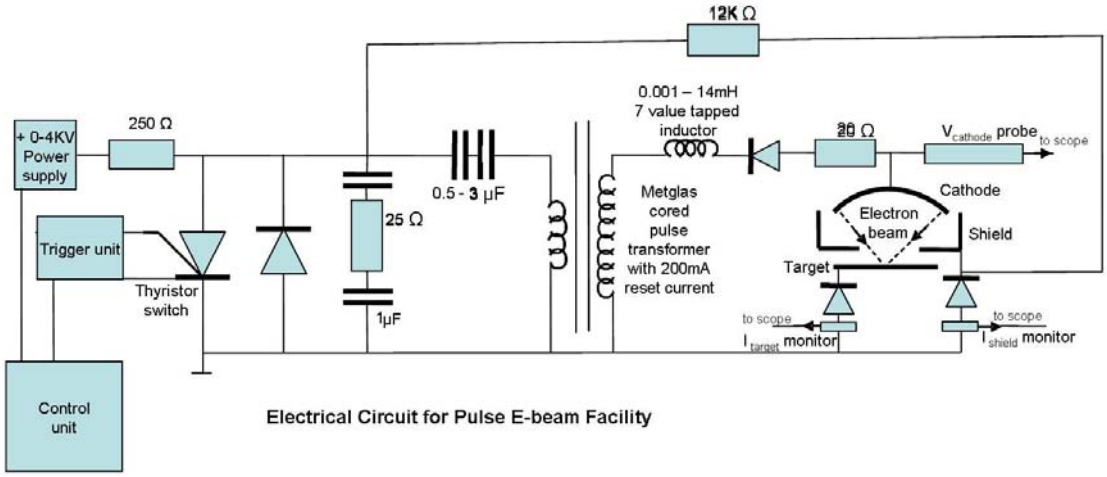

Figure 3.17 Schematic of circuitry used in BAE Systems ATC electron beam facility

Table 3.5 BAE Systems ATC electron beam facility equipment details.

Instrument	Details
Oscilloscope	Tektronic TDS 5054B, Digital Phosphor Oscilloscope, 500MHz, 5GS/s
Power Supply	Model 802L, A.L.E. Systems, 20kV supply
Vacuum Pump	Rotary Pump, Edwards 81/8, A654-01-903
Pirani Vacuum Gauge	Edwards 502
Digital Vacuum Display	Chell Instruments CCD100
Pulse Generator	Lyons Instrument, PG73N, Bipolar
Thyristor Trigger	Regulated DC Supply, LC-6011, 10.5GHz
Thyristor Power Supply	Rest I
Farnell Power Supply	G50-14

3.3.1 Variation in Processing Parameters

The capabilities of the electron beam system were explored by varying the pulse energy (1.5-6J), duration (5-40μs) and number of pulses per unit area (1-80).

The energy of the beam was measured using a simplified faraday cup that was translated through the beam, which meant that beam characterisation was limited by the translation speed [198]. The knowledge gained from the faraday cup measurements allowed the beam energy to be controlled using the cathode charging voltage and the beam focus to be identified at each set of processing parameters.

The beam pulse duration was varied by two methods. The first is a variation in the chamber pressure as a higher pressure leads to a decrease in the pulse duration, shown in Figure 3.18. The second method was variation in the inductance of the electronic circuit, shown in Figure 3.19, where an increase in circuit inductance increases the pulse duration, which is due to a decrease in the discharge speed in the circuit.

The number of pulses per unit area was varied by either single spot treatments or tracks. For the tracks the number of pulses was varied by changing the speed of the translation stage through the electron beam. The spot size produced varied with the processing parameters and this was taken into account when calculating the number of pulses per unit area.

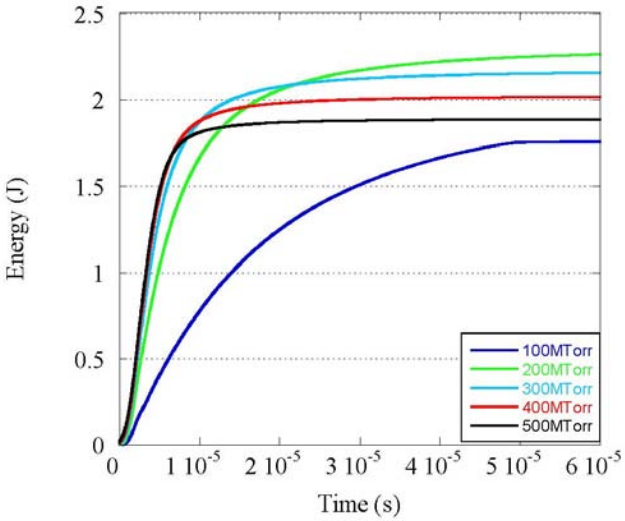

Figure 3.18 Variation in pulse characteristics of electron beam with variation in system pressure.

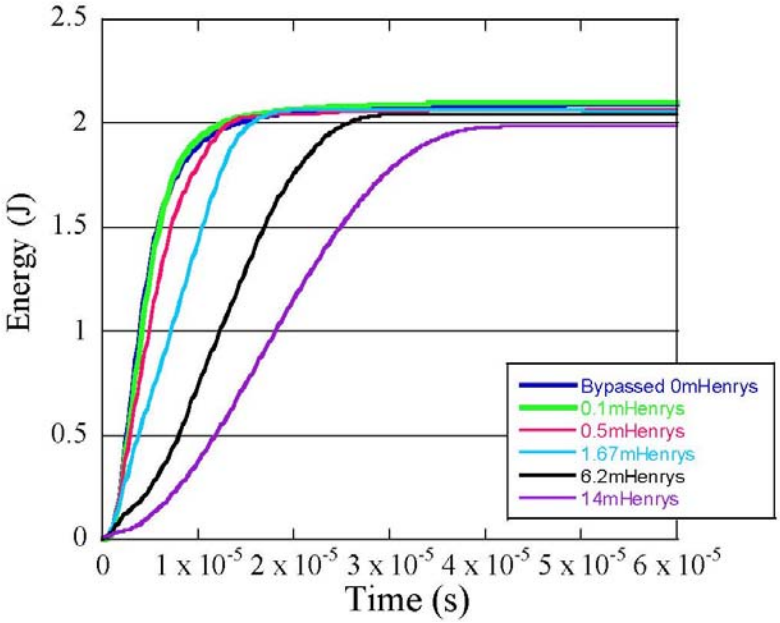

Figure 3.19 Variation in pulse characteristics of electron beam with variation in the electrical circuit inductance.

3.3.2 Surface Preparation

In the initial trials, samples were prepared for EBSM by cleaning with iso-propanol. In later tests the surfaces were polished to 4000 SiC grit paper and cleaned with iso-propanol: this was to increase the reproducibility of results and for a comparison to the LSM work.

3.3.3 Electron Beam System Preparation

Other preparatory work for EBSM included stabilisation of the vacuum and the cathode discharge. The vacuum was maintained by controlling the gas flow of a helium 5% oxygen mixture. The vacuum varied slightly during processing but this was minimised by monitoring the pressure and allowing the system to stabilise for an hour after being opened up to the atmosphere, after this hour the system pressure was slowly increased to the desired value, initially 300mTorr.

Once at 300mTorr, the electron beam was run for 20 minutes to allow for both the pressure and cathode discharge to stabilise. The stabilisation of the discharge was measured by comparing the electron beam traces produced at five minute intervals and traces produced in previous experiments. Once the stable discharge was reached then the electron beam parameters were adjusted to the required value for testing and the system was run for five minutes at these new parameter values to monitor the cathode stability.

Periodic quality checks were performed on the system to ensure consistent operation and these included; safety measurements, monitoring of the translation speeds, cathode discharge

stability, focus position and the surface treatment produced at 2J energy and 300mTorr system pressure.

3.3.4 Electron Beam Generation

The electron beam is generated when a high voltage pulse is transmitted to the cathode in a soft vacuum. The electrical circuit that creates the pulse is shown in Figure 3.17. The electron pulse is initiated by the dual output signal generator which controls the charging of the main capacitor, within a few milliseconds, to a predetermined voltage and then a pulse from a Bournlea generator initiates the spark gap. The capacitor then discharges through an inductor, two 30Ω resistors, a small peaking capacitor and into the cathode feed-through.

A negative high voltage then builds on the cathode and a low pressure glow discharge develops beneath the concave cathode. As a result a concave electric field distribution builds up beneath the cathode with all the applied voltage dropped across it. Thus electrons emerging from the cathode are accelerated to the full applied voltage in a converging high energy electron beam, shown in Figure 3.20.

The discharge, voltage drop across the cathode and the workpiece were monitored by an oscilloscope and manipulated to show instantaneous power and integrated energy. A sample trace showing these is in Figure 3.21.

Figure 3.20 Electron beam discharge in He striking aluminium alloy target

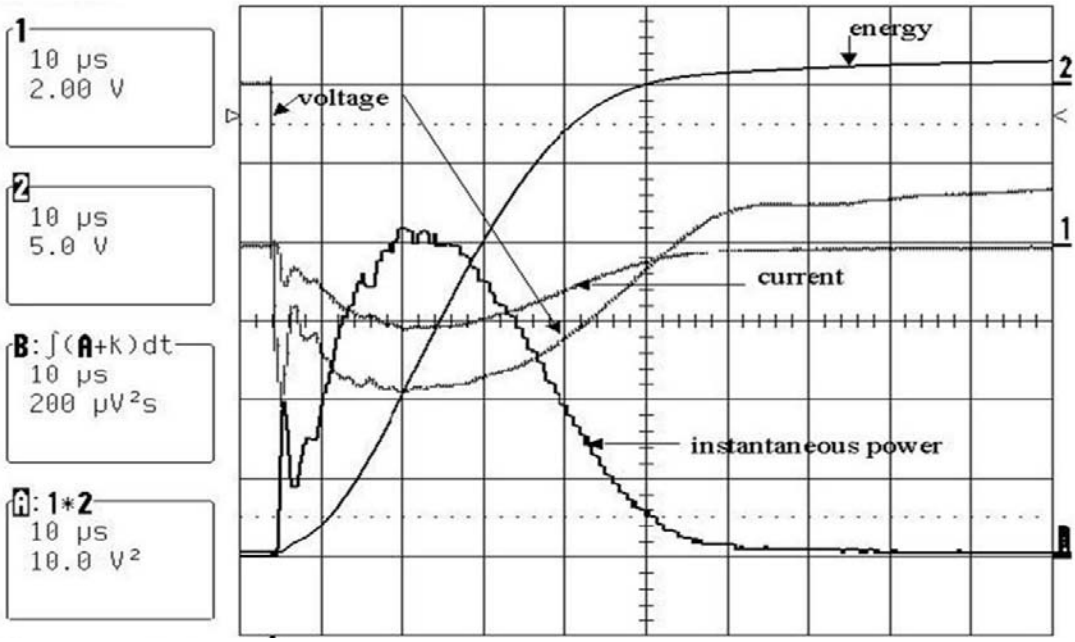

Figure 3.21 Typical electron beam trace of voltage, current, instantaneous power and accumulated energy

3.3.5 Electron Beam Cathode Monitoring

Monitoring of the electron pulses was important as the glow discharge had a tendency under some high energy conditions to show low impedance arcing where the electron beam disappeared.

In order to minimise the arcing, the cathode surface condition was monitored, as a smooth surface with a uniform oxide coating was preferential for stable discharge. The cathodes were periodically removed and re-conditioned to regenerate the surface oxide.

The re-conditioning was achieved by one of two methods: light machining or heat treatment. Out of these two methods it was the heat treatment that was favoured as it was a simple process of prolonged heating of the cathode on a hot plate which was then left to cool in air. Once the surface had been re-generated the stability of discharge was further increased by running the system prior to testing for 15 minutes at 2J and 300mTorr.

3.4 Anodising

HPBSM processes are being assessed in this thesis for their ability to improve the corrosion resistance of aerospace aluminium alloys. It was thought that the application of any HPBSM techniques in the aerospace industry would primarily be in conjunction with the currently used environmental protection treatment of anodising.

There would be concerns about coupling anodising with a HPBSM process, as in anodising part of the surface is removed (further described in Section 2.4). To couple these surface treatments therefore the layers produced by a HPBSM process would have to be thick enough to survive the material removal from anodising.

To investigate this AA2024 and AA7449 alloys were treated with excimer LSM (described in Section 3.2.7.1), 10J/cm^2 9 pulses per unit area, and were then sent to Airbus UK to be

subjected to the standard anodising processes of either chromic acid anodising (CAA) or tartaric sulphuric anodising (TSA). From the initial trials on processing parameter variation (further described in Section 5.4 and 5.1) the initial modified layer depth by this LSM treatment was known to be approximately 5μm.

As a comparison to the excimer LSM process EBSM, (described in Section 3.3.1) of AA2024 was performed, using 4J energy 5μs pulse duration 1 pulse per unit area and varying cathode separation: this created samples of different surface appearance (uniform and non-uniform). Examples of the treatments with different surface appearance were selected and also treated with standard Airbus CAA treatment.

The modified layer depths before treatment of these EBSM samples were estimated by sectioning treatments of similar cathode separation. The non-uniform treatment depth was 20μm compared with a depth of 9μm for the uniform treatment.

3.5 Microstructure Characterisation

Microstructural characterisation was performed throughout investigations. Additional examination of samples used Scanning Electron Microscopy (SEM), Energy Dispersive Analysis of X-rays (EDX) and Electron Backscattered Diffraction (EBSD).

3.5.1 Metallography

Samples were sectioned for metallography using a Discotom-2 with a 34TRE disc and a Struers Accutom-5 with a 357Ca disc. Samples were mounted in Struers Epofix cold

embedding resin by vacuum impregnation, using a Struers Epovac (to less then 200mbar pressure). The samples were left to cure for between 12 and 24 hours.

Grinding of the samples used Struers silicon carbide papers to a 1200 grit finish. Polishing was subsequently performed using Struers DP-P suspensions and Struers polishing cloths to 1μm before a colloidal silica suspension (OP-S Suspension) was used for the final polish. Polishing was performed using Struers Rotopol-22, Rotoforce-4 and Multidoser system. Between polishing stages the samples were; water rinsed, ultrasonically cleaned, rinsed in iso-propanol and then air dried using a Struers DryBox-2.

Once polished, the samples were etched using Keller's Etch (1vol% HF, 1.5vol% HCl, 2.5vol% HNO_3). The samples were rinsed before being submerged into the etch for 10 seconds and then rinsed in water and iso-propanol before being air dried. For all microstructures shown in this thesis only Keller's reagent was used as an etch, except for the cases where non-aqueous polishing was used and in these cases the surfaces were not etched, further details are in Section 3.5.2.

To analyse the centre of single spot EBSM and LSM samples, the Accutom-5 cutting machine was used to mark the sample centre with a notch to be polished back to. Once the notch was reached, the samples were then polished in the standard way.

Examination of samples was performed using two microscopes. Analysis of macrostructure used a Leica MZ75 scope and a Zeiss Axioplan scope was used for microstructure. Both scopes were linked to a Leica DC300 camera and Leica IM50 software.

3.5.2 Non-Aqueous Polishing

A number of samples were prepared for SEM examination by non-aqueous polishing. The surfaces were initially prepared using the metallographic route described in Section 3.5.1 to achieve a flat surface. The surfaces were then prepared by a non-aqueous method. Initially a small amount of the surface was removed by a short dry grinding step using 1200 SiC paper. The surfaces were then polished to a 1µm finish using Struers DP Yellow lubricant and alcohol based DP-A Suspensions. The samples were cleaned with methanol between stages and before carbon coating was applied to the surface for SEM examination.

3.5.3 Scanning Electron Microscopy

More detailed microstructural examination was achieved using SEM in secondary electron and back-scattered electron operating modes. The high resistance of the mounting resin meant that samples had to be prepared for analysis by coating in carbon (Agar SEM carbon coater). The sample was also layered with metallic tape except for the area of interest. The SEMs used were a Cambridge Instruments StereoScan 360 SEM and a Leo 1450 VP SEM. The Leo SEM was used to gain backscattered images. The EDX analysis, used the Cambridge Instruments StereoScan 360 SEM and EDX Oxford instruments Isis Link.

3.5.4 Surface Roughness

Surface roughness measurements were used during initial trials of LSM and primer removal. The measurement showed changes in the surface without destructive testing. The equipment

used was an Alpha Step Tencor which has a resolution of 5nm in the three directions using a 9-11mg stylus weight. A minimum of three surface roughness measurements were taken from random areas of each sample, an average of these results was then taken and used in analysis.

3.6 Corrosion Testing

Two types of corrosion tests were performed; salt spray analysis of large areas and small scale microelectrochemical tests.

3.6.1 Salt Spray

To characterise the corrosion resistance of a material, the aerospace industry generally depends on atmospheric salt spray testing. The corrosion resistance of the excimer LSM layer was tested by this method in three different environments and compared with the corrosion resistance of the un-treated parent material. Materials that were subjected to LSM and salt spray testing were AA2024 and AA7056.

The tests were performed in Ascott S120xp salt spray chambers at 35°C and 100% humidity in accordance to the international standard B117-03. The test parameters are shown in Table 3.6 and Table 3.7 [199]. Three different solutions were used; de-ionised water, Harrison's solution and 5wt% NaCl solution. Harrison's solution contains 0.5wt% ammonium sulphate and 0.35wt% NaCl. To examine the development of corrosion over time five samples were used in each test. The samples were successively removed at exposure times of 1 hour, 2 hours, 4 hours, 8 hours and 24 hours.

After atmospheric testing, the samples were photographed and then chemically treated to remove the corrosion product from the sample surface. Removal of the corrosion product is standard practice for analysis of corrosion particularly pitting. The corrosion product was removed by immersing the sample in a solution of chromic (2.0wt%) and phosphoric (3.5vol%) acid at approximately 60°C for 10minutes. The phosphoric acid made the corrosion oxide soluble for removal into solution and the chromic acid protected the aluminium substrate. The samples were then air dried.

Once the corrosion product had been removed, the samples were examined using an optical microscope. For each sample, six areas (approximately 14mm^2) were selected at random and these were visually inspected and ranked according to the criteria in Table 3.7 which has been used in previous work to assess similar tests [3]. LSM treatment using lasers other then the excimer laser did not produce large enough areas for large scale testing by these methods.

Table 3.6 Summary of the conditions used for the atmospheric salt spray corrosion tests.

Materials	Solution	Surface Condition
AA2024 AA7056	De-ionised water	4000 Grit Polished
AA2024	Harrison's Solution	4000 Grit Polished
AA2024 AA7056	5% NaCl	4000 Grit Polished
AA2024 AA7056	De-ionised water	Standard LSM
AA2024	Harrison's Solution	Standard LSM
AA2024 AA7056	5% NaCl	Standard LSM

Table 3.7 Summary of the ranking criteria used to characterise the samples produced in atmospheric salt spray tests [3].

Ranking	Ranking Description
1	No Visible Pits or 3 very small pits away from edges.
2	Between 3 and 10 small pits away from edges.
3	More then 10 large pits or More numerous small pits
4	Larger number of small to medium pits and some light surface staining
5	Small number of large aggressive pits or numerous smaller pits, extensive staining
6	Aggressive pitting and staining, Substrate visible through one large pit
7	Very, deep pits, staining, Small areas of substrate visible
8	Very deep pits, widespread staining, large areas of substrate visible.

3.6.2 Microelectrochemistry

Microelectrochemistry was used to investigate the corrosion resistance of a material by analysis of the anodic and cathodic electrochemical activity. This analysis technique of microelectrochemistry has been successful in work into FSW and surface modification [18, 33, 45, 107, 128, 131]. The advantage of the test is that only small areas of material are required.

The microelectrochemical set-up is shown in Figure 3.22 and is comparable to a three electrode cell, except that only a small amount of solution is in contact with the sample through the capillary [30, 33, 50]. The system contains an Ag/AgCl reference electrode and a platinum wire counter-electrode. The working electrode is the sample and its active area depends on the size of the capillary, which in this work was approximately 1.2mm^2. The tests were performed with a naturally-aerated 0.1M NaCl solution.

The material's electrochemical activity was measured in open circuit potential (OCP) and polarisation tests using a Gill AC ACM and Field Machine ACM potentiostats. Anodic and cathodic polarisation tests were performed separately starting from the measured OCP and

then polarising the metal to a more positive or negative value. The sweep rate of the polarisation test was 1mV/s.

The sample preparation method involved swabbing the surface in concentrated nitric acid, followed by cleaning in deionised water and ethanol. This preparation increased the reproducibility of measurements and was investigated in the work of C. Padovani, which showed that this surface preparation method did not affect conclusions derived from the comparison between LSM and parent material [18].

Typical anodic and cathodic polarisation curves using this analysis technique of untreated AA2024-T351 parent material and LSM are shown in Figure 3.23. The anodic curve in Figure 3.23a, shows a current increase for potential values higher then the OCP. This current increase is with the onset of localised corrosion and is characterised by the breakdown potential (E_b) value. An improvement in anodic activity is shown by an increase in E_b to a higher potential and the formation of a passive region where there is no electrochemical activity on the material, shown by the LSM curve on Figure 3.23a. The cathodic polarisation curves in Figure 3.23b shows variation of cathodic currents as a function of applied potential. Improvement in cathodic activity is shown by a decrease in the cathodic current and the line lowers on the graph.

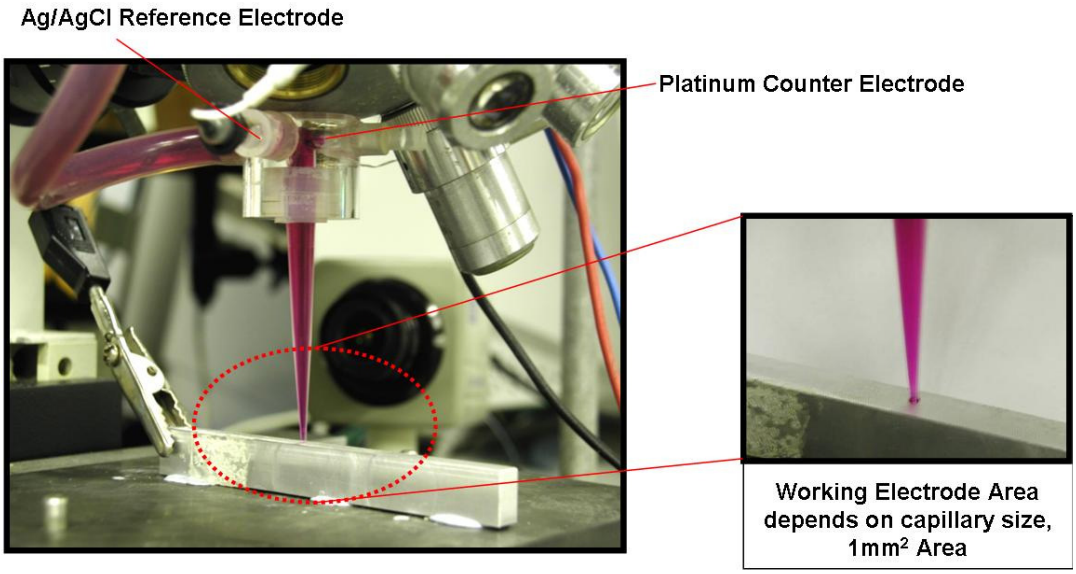

Figure 3.22 The micro-capillary cell used in this work to measure electrochemical activity of untreated, laser treated and electron beam treated samples.

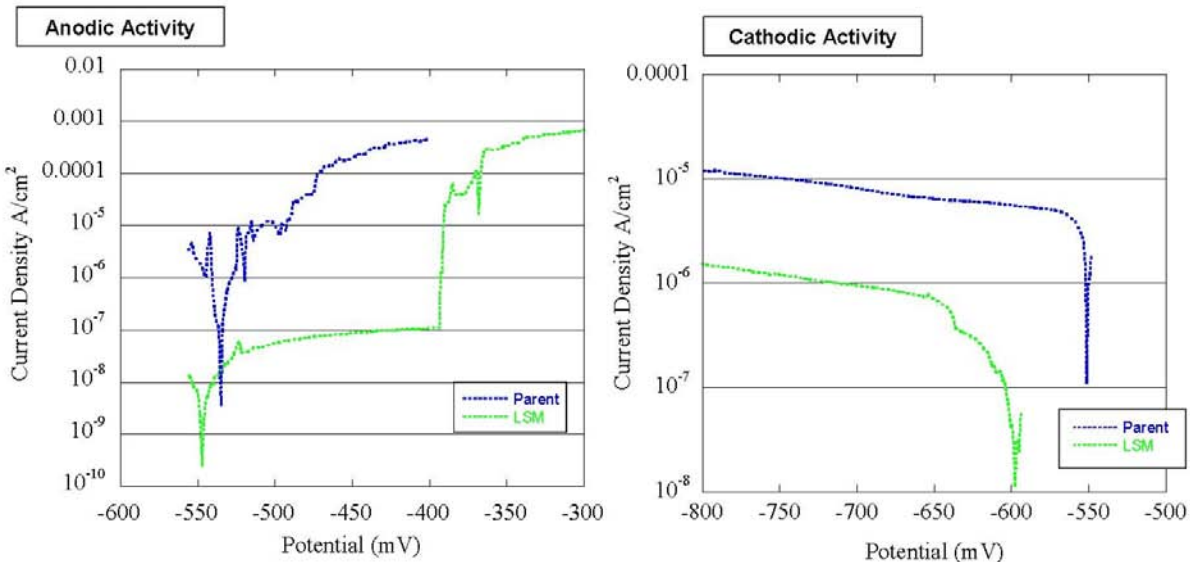

Figure 3.23 Typical electrochemical polarisation measurements performed in the micro-capillary cell (0.1M NaCl, scan rate 1mV/s Ag/AgCl reference electrode) on parent and laser surface melted AA2024 at 10J/cm^2, 9 pulses per unit area. A) anodic polarisation curve B) cathodic polarisation curve.

4 Laser Paint Removal

Friction Stir Welding (FSW) is a joining technique suitable for aluminium alloys. To ensure high quality welds without defects, it is known that the surfaces involved in welding must be free of debris or non-metallic surface layers. Surface preparation for FSW is therefore required when there are environmental protective layers present, as is the case for the FSW of large aerospace structures.

Very large aerospace structures may be too large for the chemical bath used in surface finishing processes such as anodising. It may therefore be necessary to anodise the components and subsequently join them. Anodised layers can become incorporated in the friction stir welds leading to defects that might compromise the mechanical integrity of the weld. It is thus desirable to remove anodised layers at the location where the welding tool will pass.

The aim of this investigation was to use laser treatment to prepare environmentally protected (paint primer and anodised layers) AA2024 material for FSW. The lasers used in this investigation were an excimer laser, a TEA-CO_2 laser and an Nd:YAG laser. The material used is shown in Figure 4.1, with further description of these layers is in Section 3.1.1. The upper surface of the plate has been chromic acid anodised and then painted. The lower surface has only been anodised. Both surfaces have been investigated.

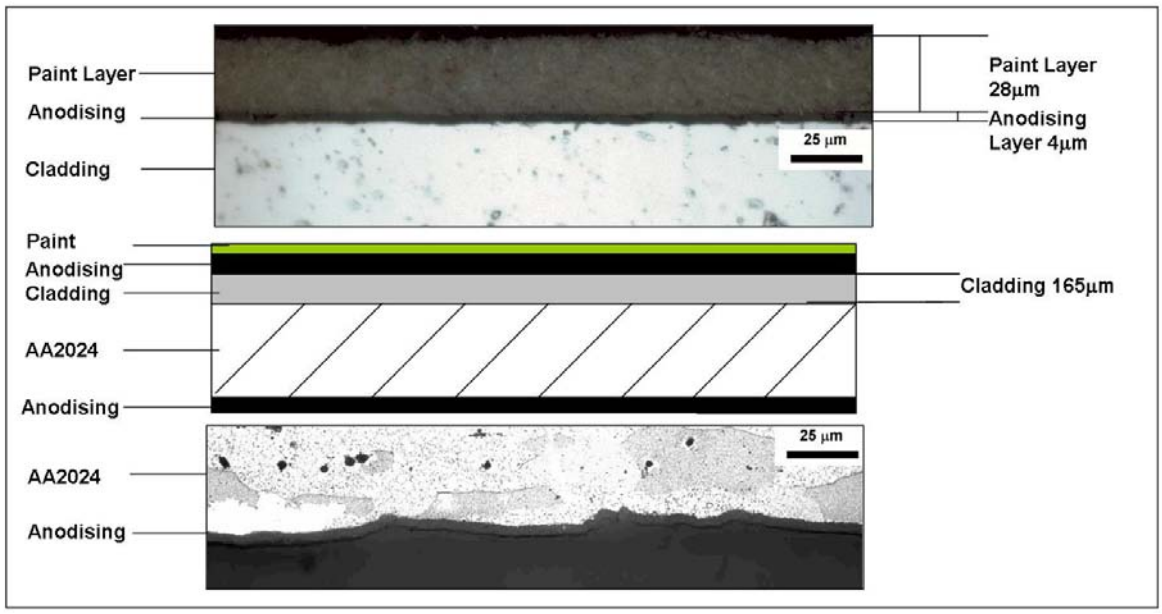

Figure 4.1 Diagram (in the centre of the figure) and cross-sectional micrographs of the upper (top image) and lower surfaces (bottom image) of AA2024 plate used in laser paint removal trials. Both the upper and lower surfaces have been chromic acid anodised and then the upper surface has also been painted.

4.1 Excimer Laser Processing

A processing parameter investigation was performed using the excimer laser with variation in the fluence, number of pulses per unit area and laser scanning pattern (processing parameters are further discussed in Section 3.2.1). The material used is shown in Figure 4.1 and the investigation utilised the different layers present on both sides of the material, with the top side being used to study the removal of both the paint and anodising and the underside being used to study the removal of just the anodising.

The result of this investigation was a three stage treatment designed to remove a specific surface layer in each stage by variation in the processing energy and number of pulses per unit area. The treatment stages were;

1. For primer removal, 2J/cm^2 with 100 pulses per unit area,
2. For anodising removal, 6J/cm^2 with 36 pulses per unit area,
3. For surface oxide removal, 6J/cm^2 with 3 pulses per unit area,

The critical part in optimising each treatment stage was the investigation of the effect of different processing parameters on the removal rate and debris generation. Initial measurements involved single spot treatments with multiple pulses using different fluences.

Initial understanding was achieved with laser spot treatments into the removal of the paint and anodising layers, from the top side of the material shown in Figure 4.1, at different fluence and number of pulses per unit area: these are shown in Figure 4.2. In Figure 4.2 the laser treatment creates a square spot where the surface has been treated and surrounding this square is a black deposit of debris created in processing. These spot treatments provided an etch rate (determination of etch rate curves is described in Section 3.2.6.2) and debris patterns specifically for the excimer laser and surface layer combination of primer and anodising.

Figure 4.3 shows the effect of excimer laser fluence on the etch rate of surface layers of paint and anodising on AA2024. Figure 4.3 shows a maximum etch rate for the removal of these layers between 6 and 8J/cm^2. The fastest removal process would therefore be achieved by using a fluence around these values.

However, visual inspection of Figure 4.2 shows that a fluence of 6J/cm^2 generates a large amount of black debris around the square treatment area. To avoid this widespread of debris a

lower fluence and a higher number of pulses should be used in preference for layer removal. This provided parameters for the first treatment stage of 2J/cm^2 and 100 pulses per unit area.

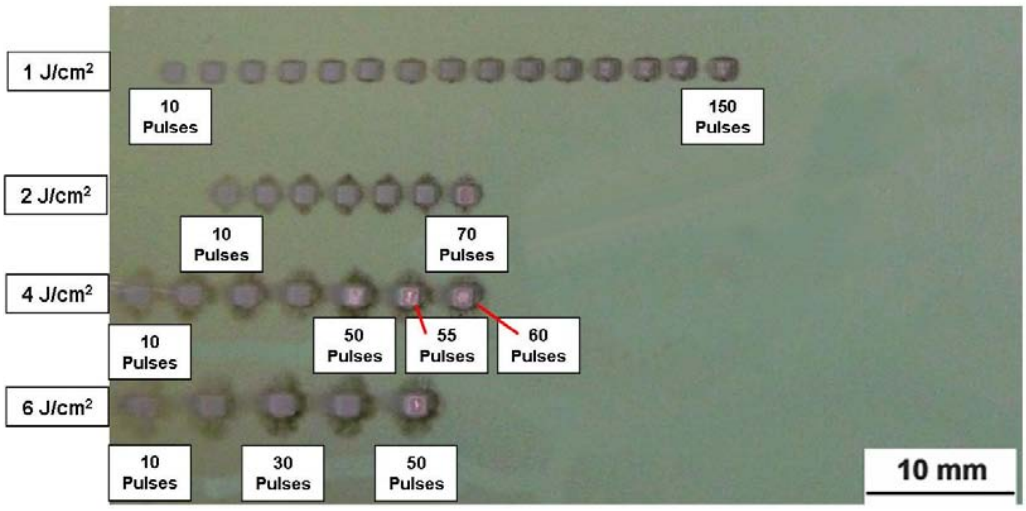

Figure 4.2 Surface picture of excimer laser spot treatments used to generate etch rate curves. Spot treatments were performed at increasing energy and number of pulses per unit area.

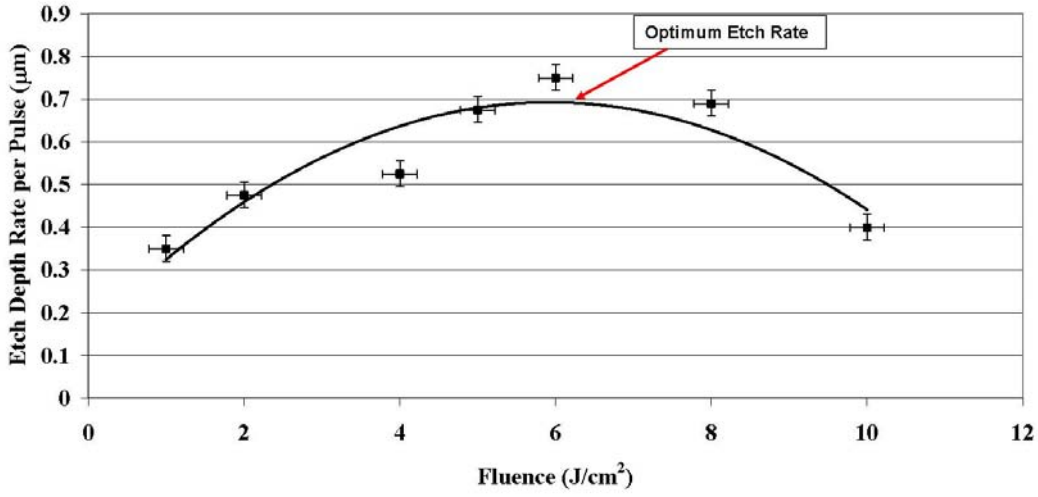

Figure 4.3 Graph of excimer laser fluence versus etch removal rate of material removed per pulse from a surface of primer and anodised aluminium clad AA2024.

The spot treatments allowed for the processing parameters to be identified. However, larger areas of treatment then a single spot size (1.5x1.5mm) were required. Two scanning patterns for the treatment of larger areas were tested, step and repeat and raster scanning (described in Section 3.2.1).

The step and repeat pattern was primarily used as it was closer to the single spot treatments and larger treatment areas were produced with a varying number of pulses per unit area (3 to 200) and 2J/cm^2 laser fluence. Figure 4.4 shows some of these treatments which had different surface appearances and these are referred to as: under-treated, patterned and over-treated.

The under-treated sample in Figure 4.4A has had too few pulses per unit area (3 pulses per unit area) and the primer layer remains as the characteristic green paint can still be observed in the treatment area. Increasing the number of pulses, to approximately 70, in Figure 4.4B shows that the primer was removed but a patterned surface was generated where parts of the treatment were reflective and other parts were blackened. A further increase to a high number of pulses per unit area, approximately 200, in Figure 4.4C shows over-treatment of the surface with the creation a low reflectivity (blackened) surface.

Another observation of Figure 4.4 is that distinct treatment squares were produced and to avoid this and ensure an even treatment over the entire surface the processing pattern was changed from step and repeat to raster scanning (described in Section 3.2.1).

With the processing pattern identified this led to the first proposed treatment stage of 2J/cm^2 and 100 pulses per unit area with raster scanning based on the removal of layers from the top side of the material shown in Figure 4.1.

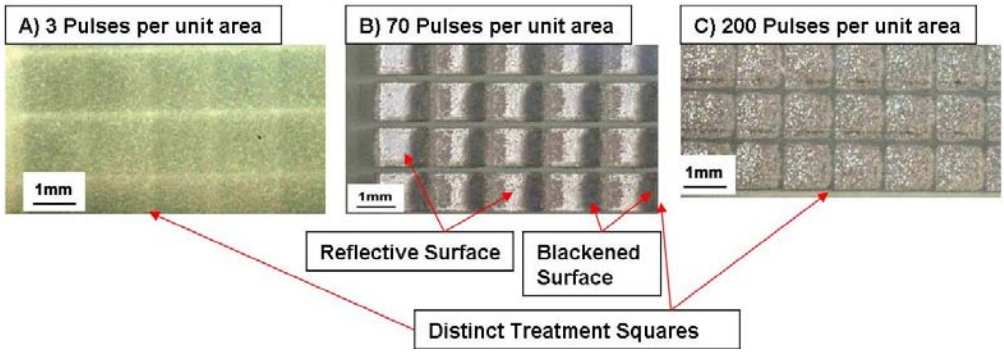

Figure 4.4 Excimer laser processing of step and repeat processing pattern with varying number of pulses per unit area. Different pulses per unit area produced surfaces of different appearances A, is under-treated with 3 pulses per unit area, B, is patterned with 70 pulses per unit area and C, is over-treated with 200 pulses per unit area.

The underside of this material was just an anodising layer and a processing parameter investigation was performed using raster scanning with a range of fluence and number of pulses per unit area to understand the removal of this layer alone.

Figure 4.5 shows micrograph cross-sections of samples produced from this parameter investigation. Figure 4.5A shows that at the fluence of 2J/cm^2 some of the anodising remains after treatment. Increasing the fluence from 2 to 6J/cm^2 however removed the anodising as shown in Figure 4.5B. However, increasing the fluence further to 10J/cm^2 produced a surface oxide layer which is shown in Figure 4.5C.

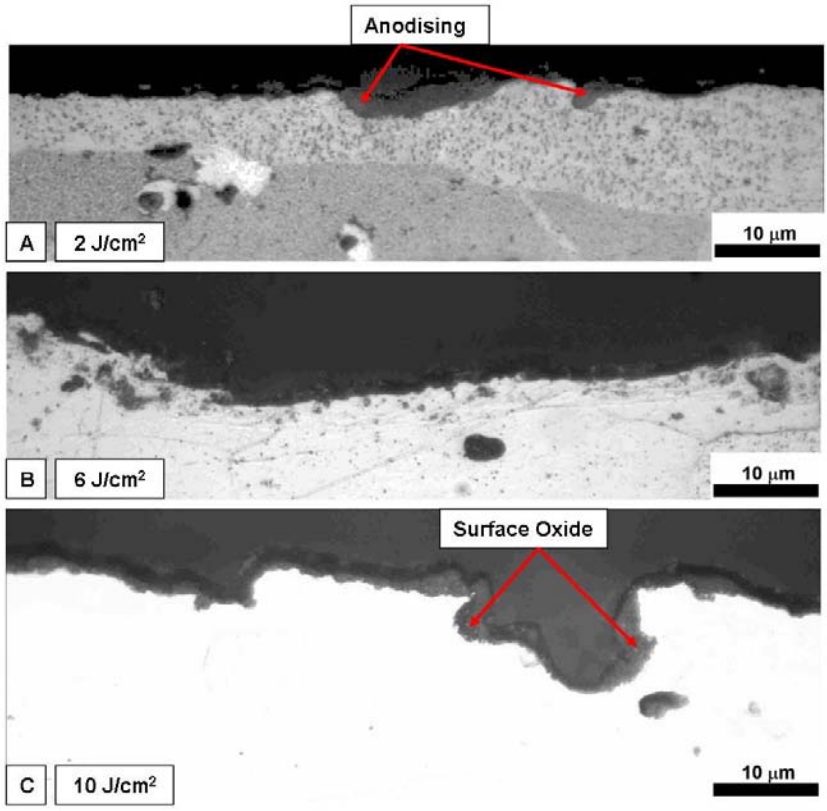

Figure 4.5 Cross-sectional micrographs of excimer laser investigations into anodising layer removal with nine pulses per unit area, raster scanning and varying fluence, A 4J/cm^2, B 6J/cm^2 and C, 10J/cm^2.

Based on the visual inspection of the micrographs produced in these trials, the processing parameters for the second treatment stage of anodising removal were selected to be 6J/cm^2, 36 pulses per unit area and raster scanning.

The raster scanning treatments highlighted some disadvantages of the laser removal process which are shown in Figure 4.6: debris generation (Figure 4.6A) with a black deposit covering the treated surface and incomplete removal of surface layers e.g. paint in Figure 4.6B and anodising in Figure 4.6C.

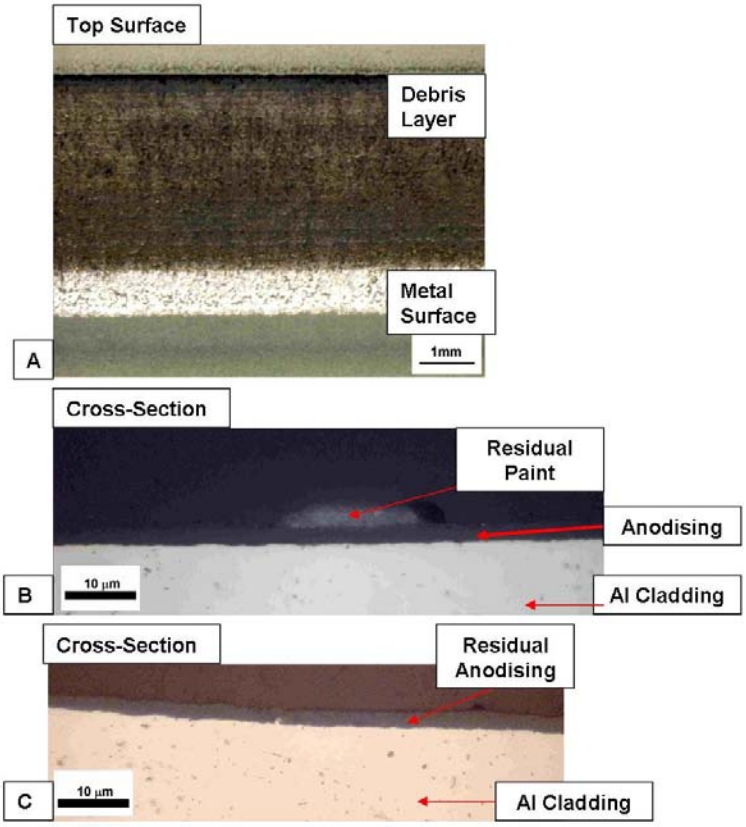

Figure 4.6 Top surface picture and cross-sectional micrographs of typical defects observed with raster scanning excimer laser layer removal A, surface debris remains 6J/cm^2 64 pulses per unit area, B, residual primer laser treatment 2J/cm^2 64 pulses per unit area, C, residual anodising laser treatment 2J/cm^2 64 pulses per unit area.

Figure 4.7 provides a more detailed examination of one of these process disadvantages, the generation of debris from multiple laser passes (as seen in Figure 4.6A). It was observed in raster scanning treatments with a high number of pulses per unit area that there was a difference in appearance between the last and previous laser passes. This is shown in Figure 4.7 with the last pass exhibiting a shiny more reflective metal surface as opposed to the blackened surface from the other passes. The difference in appearance was from the re-deposition of processing debris.

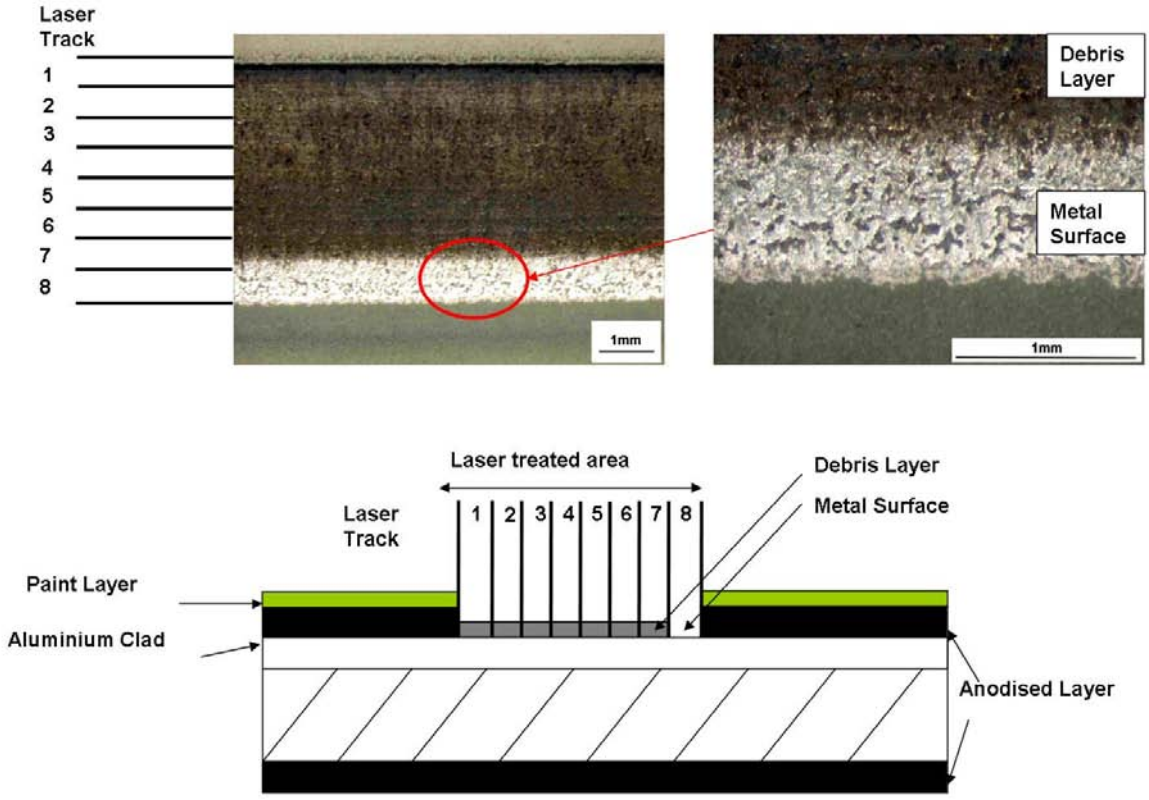

Figure 4.7 Top surface images of excimer laser removal using 6J/cm^2 64 pulses per unit area over 8 laser tracks. Laser tracks 1-7 have a layer of debris deposited where as track 8 has a different surface appearance without debris showing a reflective metal surface.

The large amount of debris generated during processing necessitated a cleaning stage as the final treatment stage. The benefit of a cleaning stage can be seen in Figure 4.8 where a laser treatment has been performed to remove the surface paint and anodising layers (stages 1 and 2 of the excimer laser paint removal process described in Section 4.1) and then an additional cleaning treatment (2J/cm^2 400 pulses per unit area) has been applied to part of the surface. Figure 4.8 shows that there is a distinct difference in surface appearance due to the performance of a cleaning pass.

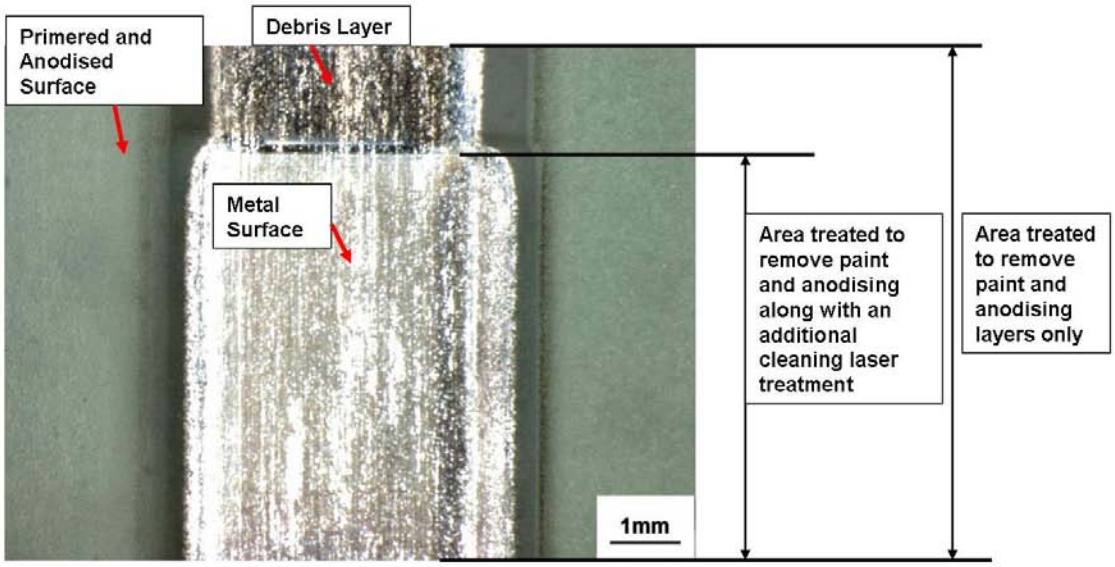

Figure 4.8 Surface appearance before (only stages 1 and 2 of the excimer laser paint removal process described in Section 4.1) and after cleaning stage at 400 pulses per unit area 2J/cm^2 to remove surface debris in excimer laser removal.

Investigations into a cleaning stage found that a variety of different laser processing parameters could have been used as a cleaning stage and some are shown in Figure 4.9. Visual inspection of surfaces produced in these investigations led to the conclusion that a highly reflective surface finish could be achieved with a low fluence and a high number of pulses (Figure 4.9A). However, using a high number of pulses per unit area creates a long processing time and it was thought to be more practical to decrease the processing time by increasing the fluence and decreasing the number of pulses per unit area Figure 4.9B.

The surfaces produced with lower pulses and higher fluence did not produce as good a surface as observed in other treatments but it was thought that the surfaces produced would be adequate for preparation for FSW. The final stage of the treatment was therefore raster scanning at 6J/cm^2 and 3 pulses per unit area.

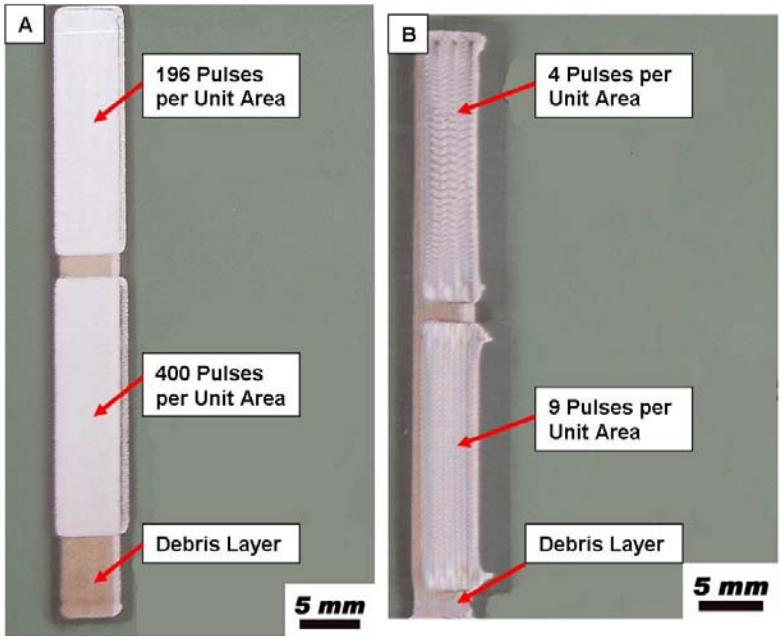

Figure 4.9 Surface appearance of treatments produced with excimer laser surface cleaning at different laser processing parameters: A) 2J/cm^2 high number of pulses per unit area (196 and 400) B) 6J/cm^2 low number of pulses per unit area (4 and 9).

4.1.1.1 EDX Analysis

The proposed treatment was based upon visual inspection of the surfaces produced throughout parameter investigations. EDX analysis was used to provide some quantification of the treatment.

EDX analysis showed that the primer and anodised surface layers initially present contained high levels of chromium compared with bare aluminium cladding, which was the layer being exposed by the treatment. Therefore measuring the chromium concentration of a treated surface should provide an indication as to whether the primer had been removed.

The proposed three stage excimer treatment was examined by EDX analysis and the results are shown in Table 4.1. The proposed paint removal treatment did show a decrease in elements inherent to the primer and anodising layers, indicating that the layers had been removed. However, the high concentration of oxygen suggests the presence of a thick surface oxide.

Table 4.1 EDX elemental weight percent composition analysis of surfaces produced by proposed three stage excimer laser treatment in comparison with the primer and anodised layers that were initially present.

Element (wt%) / Surface	O	Al	Si	Mn	Fe	Cu	Ti	Cr	Mg
Primer	86	1.4	3.7	0.01	0.3	0	4.8	1.6	2.3
Chromic Acid Anodised layer	71	29	0.2	0.05	0.02	0.1	0	0.1	
Proposed Excimer treatment Test 1	49	50	-	-	-	-	0.6	0.4	-
Proposed Excimer treatment Test 2	46	54	-	-	-	-	-	-	-

4.1.2 Friction Stir Welding Laser Preparation

To evaluate the preparation process, laser removal was compared with a machining preparation process and an LSM treated surface. Friction stir welds were then generated and the material used is shown in Figure 3.2.

Examination of the un-welded prepared surfaces established the differences between the laser and machining preparation methods. A closer examination of the machined prepared weld in Figure 4.10 shows that there was an inherent surface roughness imparted by machining. The

laser prepared surface is shown in Figure 4.11 and an oxide layer is observed across the surface.

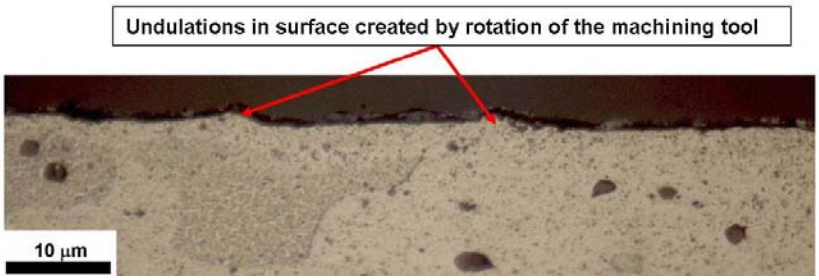

Figure 4.10 Microstructure cross-section of weld produced from machining surface preparation for friction stir welding.

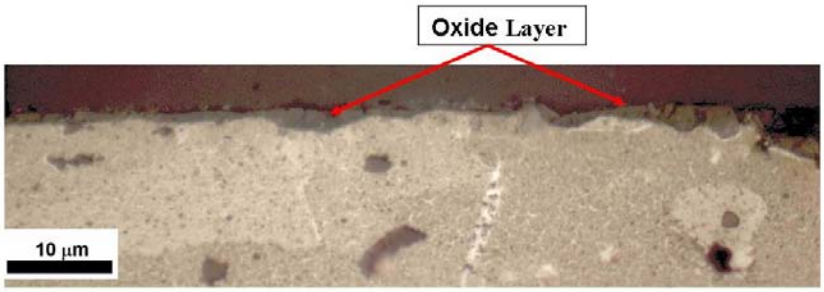

Figure 4.11 Microstructure cross-section of weld produced from proposed three stage excimer laser removal process surface preparation for friction stir welding.

The friction stir welds were produced from the prepared samples at BAE Systems ATC using a Huron NU5 vertical milling machine previously adapted for friction stir welding (further described in Section 3.2.6.3).

The mechanical integrity of the welds was evaluated using destructive bend testing with a roller specified for aluminium alloys in accordance with European Standard EN 910:1996, described in Section 3.2.6.4 and shown in Figure 3.13 and on material shown in Figure 3.2

with paint and anodising layers on all surfaces [196]. A number of destructive bend tests were carried out with no failures for either laser-prepared or machined surfaces. An example of the test for two laser-prepared welds is shown in Figure 4.12. The laser pre-treatment for the welds produced a clean enough surface that did not degrade the weld's plastic properties. Based on these results this surface pre-treatment can be recommended as suitable to use with the welds.

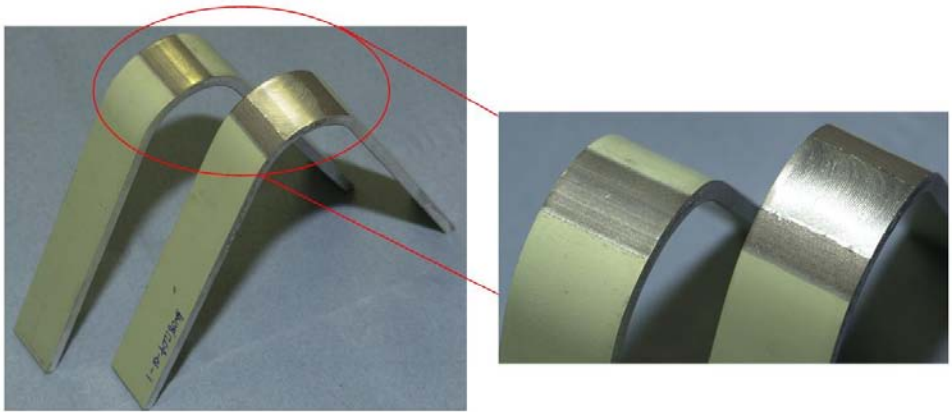

Figure 4.12 Friction Stir Welding samples subjected to the European standard EN 910:1996 of destructive bend tests. Samples were prepared by the three stage excimer laser cleaning process.

The microstructures of the welds produced with laser and machining surface preparation techniques are compared in Figure 4.13. No defects are noticeable on a macroscopic scale for either weld. However the laser prepared surface in Figure 4.14 shows that there is entrapment of the oxide into the weld microstructure. Therefore, the optimised treatment does not produce a clean metal surface but has a surface oxide that becomes entrapped into the weld. No similar defects (entrapped oxide) were observed in the machined weld sample.

The FSW of the LSM prepared surface is shown in Figure 4.15. No obvious oxide or debris was incorporated into this weld and it is thought that if LSM of the surface did occur then there should be no detrimental effect on the weld structure and properties.

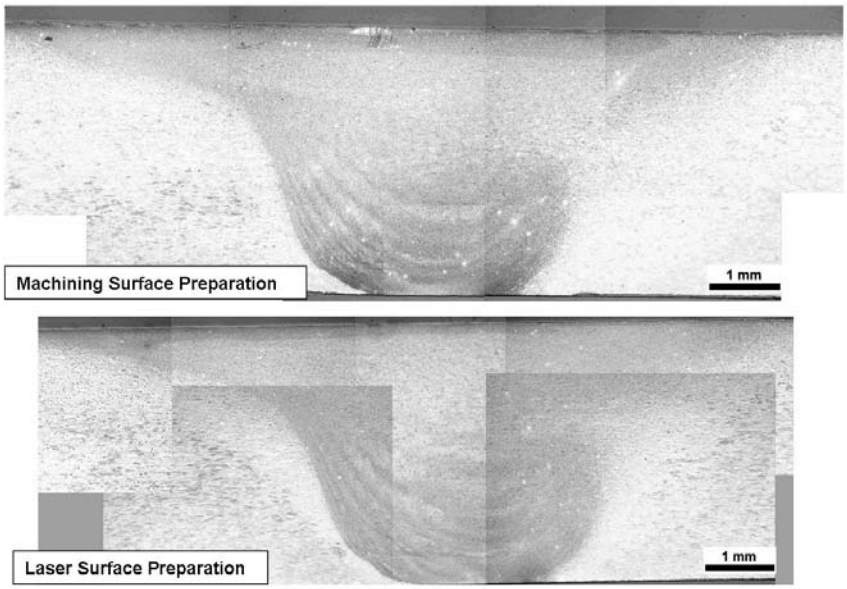

Figure 4.13 Micrograph cross-sections of friction stir welds produced with different surface preparation techniques machining and proposed excimer laser three stage treatment.

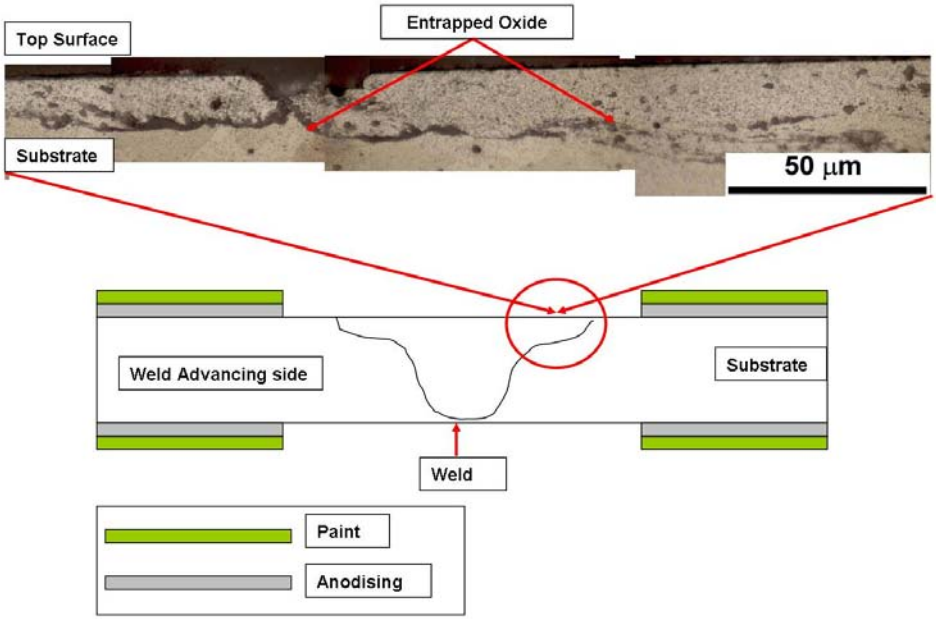

Figure 4.14 Micrograph of cross-section of friction stir weld produced by the proposed three stage excimer laser removal process with oxide entrapment in the weld structure near to the surface.

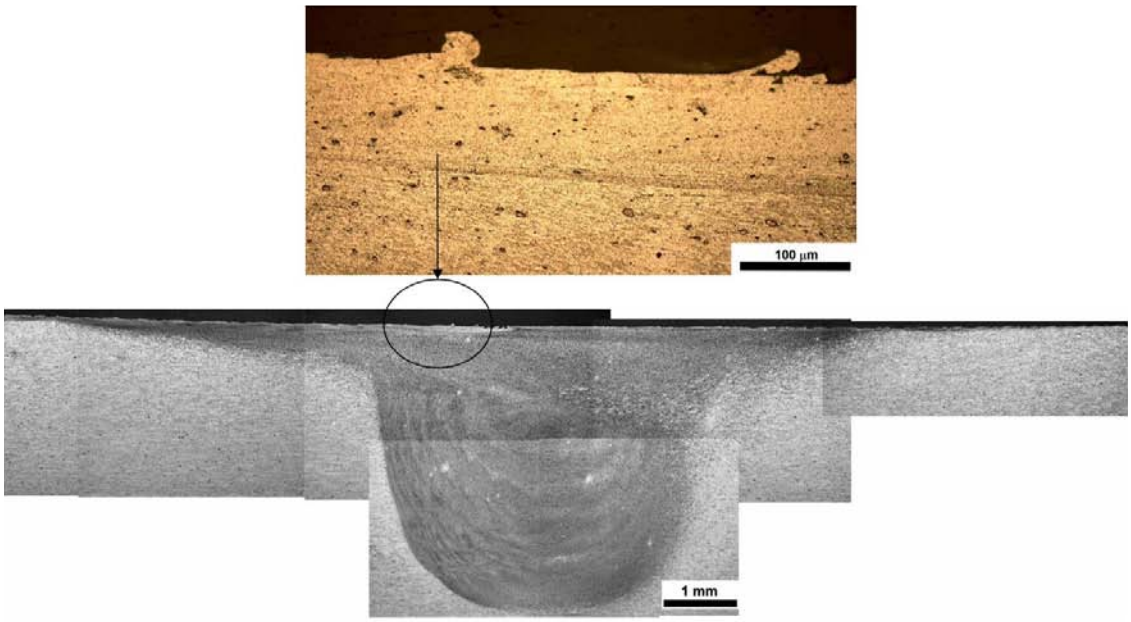

Figure 4.15 Micrograph cross-sections of friction stir weld produced from AA2024 with an excimer laser surface melting treatment of 6J/cm^2, 64 pulses per unit area raster scanning.

4.1.3 Discussion

The excimer laser has been shown to be capable of locally removing anodised layers typical of those used to protect aluminium aerospace alloys. This treatment was used in preparation of surfaces for FSW. The treatment was considered successful as the welds produced survived the specified bend tests. However, examination of the welds showed that there was oxide incorporated into the weld structure across the whole width near to the weld top surface which may have an effect on fatigue properties. It must be considered though that this entrapped oxide did not degrade the weld properties that were tested.

It should be noted that the laser treatment was performed under normal atmospheric conditions. If the oxide on the surface is a concern then it would be beneficial to generate samples in protective atmospheres.

The proposed excimer laser treatment comprised three stages, each of which had processing parameters designed for the removal of a specific surface. The design of this treatment was based around visual inspection of the surfaces produced or a microstructure cross-section. However, it has been shown that the removal of surface layers could be measured more quantitatively by using EDX analysis to monitor the loss of elements that are inherent to the paint and anodising layers such as chromium.

4.2 TEA-CO_2 Laser Processing

The suitability of a TEA-CO_2 for primer removal was tested by the generation of an etch rate curve. This was done because different primers and substrates react differently to the laser type. The samples used were the same as those used with the excimer laser and are shown in Figure 4.1 and discussed in Section 3.1.1. Only single spot treatments were performed as limitations in optics meant that treatment areas could not be created using this laser.

The plot of etch depth versus fluence for the TEA-CO_2 laser is shown in Figure 4.16. The etch rate reached a maximum removal rate with increasing fluence between 6 and 8J/cm^2.

Comparison of the excimer and TEA-CO_2 lasers showed that the amount of material removed per laser pulse was greater for the TEA-CO_2 laser compared with the excimer. At the optimum fluence the excimer laser removed ten times less material per pulse then the TEA-CO_2 laser. Therefore the etch rate for the TEA-CO_2 is higher then that of the excimer. This means that the TEA-CO_2 laser would be capable of removing the primer and anodising layers at a faster rate and fewer number of pulses per unit area then the excimer.

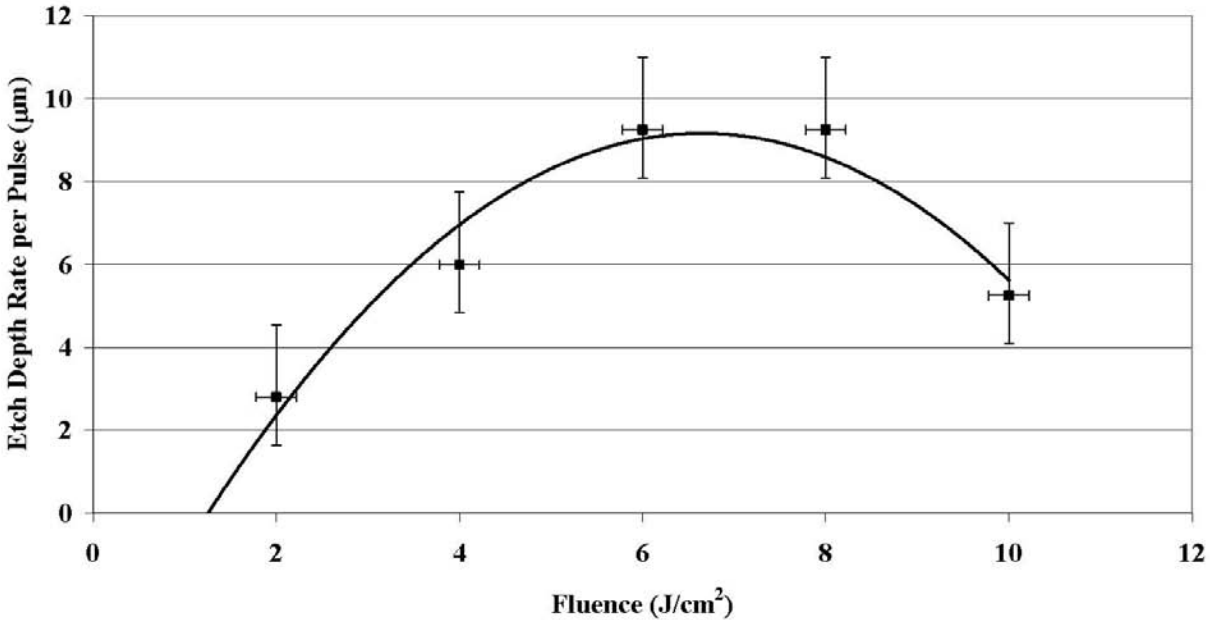

Figure 4.16 Graph of TEA-CO_2 laser fluence versus etch removal rate of material removed per pulse from a surface of primer and anodised aluminium clad AA2024.

4.3 Nd:YAG Laser Processing

The surface layers used for the Nd:YAG tests were same as those employed for the excimer studies in Section 4.1 and the details are given there.

4.3.1 Results

4.3.1.1 Processing Sample Production

Test samples were supplied that had been processed using a range of processing parameters as listed in Table 4.2 [200]. The processing parameters of interest were the sample feed rate and the Pulse Repetition Frequency (PRF) as these were used to infer the number of pulses per unit area. The PRF provides the number of pulses per second and the Feed rate provides the

translation distance per second, so dividing the PRF by the feed rate, referred here to as PRF/FEED, provides an estimate of the number of pulses per unit area. An exact value for the number of pulses per unit area could not be calculated as the beam size was unknown. Table 4.3 show these variables ordered with ascending PRF/FEED, the blue entries are those that were metallographically sectioned.

The samples were not all subjected to metallographic examination, only the samples that had a reflective metal surface were sectioned as they were more likely to be a clean surface as suggested by the excimer laser study. The samples that were sectioned for examination were numbers 1,2 and 8 and surface views of these samples are in Figure 4.17. Figure 4.17 shows that there are different surface appearances produced by the different processing parameters with some surfaces having residual paint, a blackened surface or a reflective metal surface.

Table 4.2 Table of processing parameters used in Nd:YAG laser primer removal trials.

Sample Number	Pulse Repetition Frequency (kHz)	Laser Power (%)	Scan Width (mm)	Feed Rate (mm/min)	Number of Crossings	Scan rate (cm^2/s)
1	20	100	20	1500	3	1.67
2	20	100	20	1000	3	1.11
3	20	100	20	500	3	0.56
4	25	100	20	1500	3	1.67
5	25	100	20	1000	3	1.11
6	25	100	20	500	3	0.56
7	15	100	20	1500	3	1.67
8	15	100	20	1000	3	1.11
9	15	100	20	500	3	0.56
10	17	100	20	650	3	0.72

Table 4.3 Processing parameters of samples used in Nd:YAG laser primer removal trials ordered by pulse repetition rate divided by feed rate (PRF/FEED).

Sample	Feed Rate (mm/min)	Pulse Repetition Frequency (kHz)	Pulse Repetition Frequency / Feed rate (60k.pulses/mm)
7	1500	15	10
1	1500	20	13
8	1000	15	15
4	1500	25	16
2	1000	20	20
5	1000	25	25
10	650	17	26
9	500	15	30
3	500	20	40
6	500	25	50

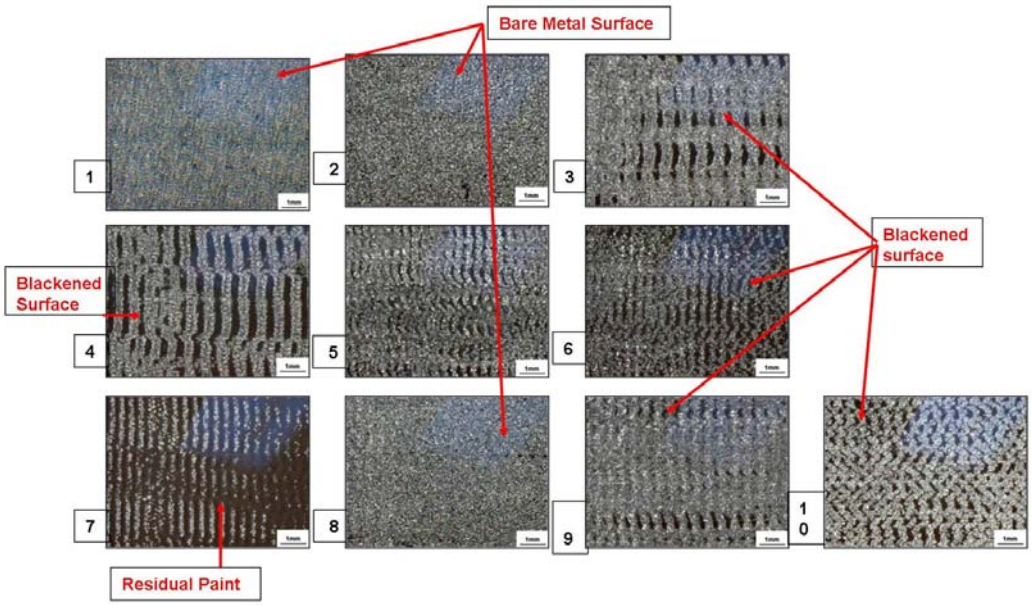

Figure 4.17 Photographs of samples with different surface appearance produced in processing parameter trials for Nd:YAG laser primer removal.

4.3.1.2 Post-Process Characterisation

Figure 4.18 compares the metallographic sections of the untreated surface and the bare metal Nd:YAG samples. From the micrographs it can be seen that there is no oxide or primer on the surfaces after the treatment.

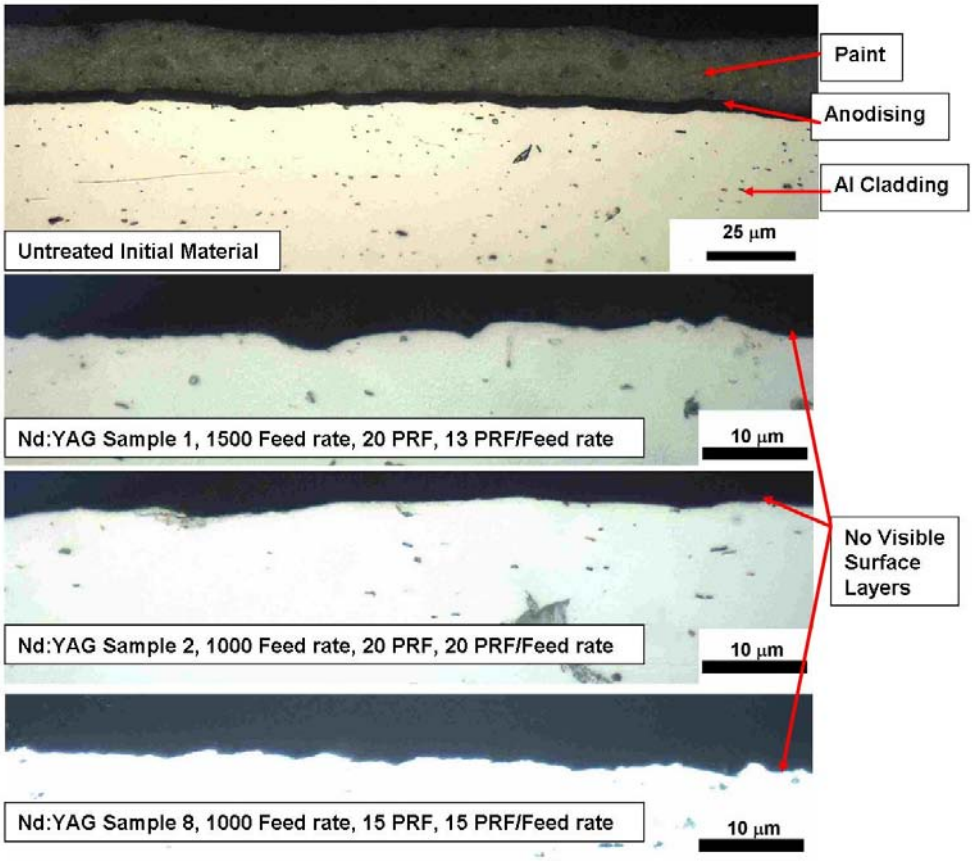

Figure 4.18 Micrograph cross-sections of Nd:YAG laser primer removal samples 1 (1500 Feed rate, 20 PRF, 13 PRF/Feed rate) , 2 (1000 Feed rate, 20 PRF, 20 PRF/Feed rate) and 8 (1000 Feed rate, 15 PRF, 15 PRF/Feed rate) in comparison to initial untreated material.

Surface roughness measurements were also performed, to measure any changes throughout processing and to identify the stages of surface treatment. A comparison of over treated, under treated and bare metal samples was required. The Nd:YAG sample 7 was an under-processed sample as the primer was still visible and an over-treated sample was the excimer laser processed from the Section 4.1. The bare metal Nd:YAG samples were numbers 1,2 and 8. The surface roughness values are summarised in Table 4.4, the values shown are an average of a minimum of three scans performed on random areas across the sample with an error of 0.07μm (one standard deviation of the measurements). The under-treated sample 7

had the highest surface roughness value and a decrease in surface roughness is observed on the other Nd:YAG samples with the production of a bare metal surface.

Table 4.4 Comparison of average surface roughness measurements (from a minimum of three scans taken from different randomly selected areas across the surface with an error of 0.07µm from one standard deviation) from a selection of Nd:YAG laser primer removal and excimer paint removal samples.

Sample	Surface Roughness (Ra - microns)
Nd:YAG – Sample 1	1.1
Nd:YAG – Sample 2	1.0
Nd:YAG – Sample 7	2.7
Nd:YAG – Sample 8	1.4
Excimer Treatment	1.9

SEM images were taken of samples 1,2,7 and 8 and are shown in Figure 4.19. It can be seen that there was minimal variation in the surface appearance of the samples except for the under-treated sample 7. EDX analysis of these areas was also performed and the composition analysis is shown in Table 4.5. The under-treated sample 7 contained elements from the primer as expected, whereas samples 1,2 and 8 all exhibited similar compositions where the only elements present were aluminium and oxygen. The concentrations of aluminium and oxygen were similar to those found in bare AA2024, suggesting a normal oxide composition. The oxygen concentration on the bare metal Nd:YAG samples was a lot lower than that detected on the excimer treated surface which suggests that the proposed excimer treatment was over-treated and oxidised.

Table 4.5 EDX elemental weight percentage composition analysis of surfaces produced by three stage excimer laser treatment (described in Section 4.1) and Nd:YAG laser removal treatments in comparison to primer and anodised layers that were initially present.

Element (wt%) / Surface	O	Al	Si	Mn	Fe	Cu	Ti	Cr	Mg
AA2024 Bare metal	10.2	86.7	1.2	0.2	0.1	1.5	-	-	-
Primer	86.0	1.4	3.7	0.01	0.3	-0.06	4.8	1.6	2.3
Anodised layer Chrome sulphate	70.7	28.8	0.17	0.05	0.02	0.11	-0.01	0.12	
Excimer laser paint removal	49.0	50.0	-	-	-	-	0.62	0.38	-
Nd:YAG 1	13.0	87.0	-	-	-	-	-	-	-
Nd:YAG 2	11.8	88.2	-	-	-	-	-	-	-
Nd:YAG 7	21.8	63.6	7.5	-	0.28	-	5.2	1.2	0.4
Nd:YAG 8	11.8	88.2	-	-	-	-	-	-	-

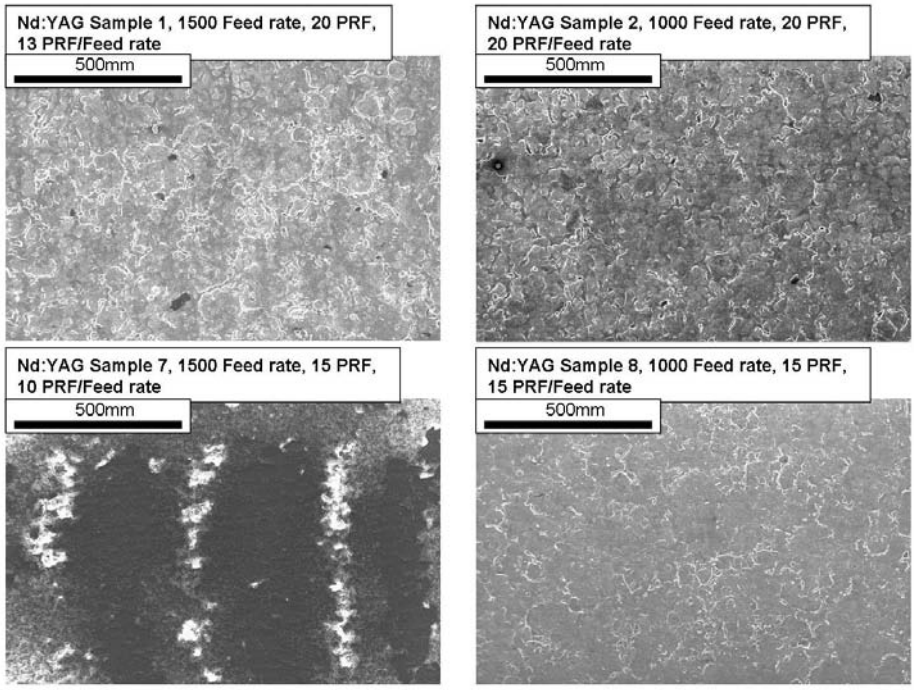

Figure 4.19 SEM images of surfaces with different surface appearances from Nd:YAG laser primer removal samples 1 (1500 feed rate, 20 PRF, 13 PRF/feed rate) , 2 (1000 feed rate, 20 PRF, 20 PRF/feed rate), 7 (1500 feed rate, 15 PRF, 10 PRF/feed rate) and 8 (1000 feed rate, 15 PRF, 15 PRF/feed rate).

4.3.2 Discussion

In Nd:YAG laser paint removal processes the surface condition, in terms of appearance and roughness, can be monitored to ascertain whether the surface layers have been removed. As the surface appearance changed from the colour of the paint to a reflective metallic surface and there was a decrease in surface roughness. If there was over-treatment of the surface this was marked by oxidation which increased the surface roughness and decreased the surface reflectivity.

EDX analysis was used to further investigate the removal of surface layers and it was found that monitoring the oxygen concentration gave a full indication of when a bare metal surface was generated, as the removal of the primer decreased the oxygen concentration to a minimum when a bare metal surface was reached.

Metallographic sectioning of samples was used to confirm the removal of surface layers and it was shown that samples that had PRF/FEED values between 13 and 20 had their surface layers completely removed. The under-treated sample with the surface layers remaining (sample 7) had a lower PRF/FEED value of 10 and samples that were over-treated with surface oxidation had PRF/FEED values higher then 20. From these results it is apparent that there is a narrow processing band for the production of bare metal surfaces which is related to the number of pulses per unit area with PRF/FEED between 11 and 20.

This was found to be true for all samples except for sample 4, which had a PRF/FEED value of 16, this should be in the range to produce a bare metal surface but an oxidised surface was

produced as opposed to a bare metal surface. One possible reason for this is that the PRF for this sample was higher then that of any of the samples that produced a bare metal surface.

4.4 Discussion Laser Removal Processes for Industrial Application of Friction Stir Welding

The current study showed an excimer laser removal process that was capable of removing the primer and anodising layers from aerospace alloy AA2024 in preparation for FSW, however this process also produced a thickened oxide layer on the sample surface. This excimer laser removal process was compared with a standard machining removal process. Machining produced a bare metal surface with no surface oxide present at a faster rate then the laser process.

Given the limitations the laser primer removal process it is only likely to be used when machining processes are considered unsuitable such as for small specific areas in repair, complex component shape or removal from areas which are difficult to access by a machining tool. In these cases laser primer removal process may be suitable as only the region that is irradiated by the laser spot is affected by the process and the treated area can be as small as the beam area.

The application of the excimer laser primer removal process has the concern that laser damage can be caused to the surface as porosity, cracks or other defects, such as over-treatment of surface in oxidation. Other work on the removal of primer from AA2024 using various lasers did observe damage to the substrate in terms of embrittlement, due to hydrogen,

unfortunately the type of laser and processing parameters used in this study were not specified so direct comparisons cannot be drawn [201]. However, in previous work at BAE Systems where the same excimer laser was used to remove primer from aluminium alloy the samples also showed little or no damage to the substrate [36].

After the coating has been removed by the laser treatment, the bare metal substrate is exposed to laser irradiation and this may result in oxidation or melting. In the case of melting it has been shown that an LSM surface can be incorporated into the weld produced by FSW.

There is an optimum fluence for maximum primer removal per pulse as has been observed in previous work on different primers using a carbon dioxide laser [36]. The optimum fluence is due to plasma formation on the surface of the sample from ionisation of ejected sample material. Once formed the plasma absorbs part of the incident laser radiation, which decreases the fluence at the metal surface [36]. The optimum fluence for removal is dependent on the interaction of the laser and the surface, so the rate of removal varies with the laser and the type of surface layers. It was shown in current measurements using single spot treated area, that the TEA-CO_2 laser has a higher optimum fluence and is capable of removing more primer per pulse than the excimer laser.

The highest removal was seen with the TEA-CO_2 laser but this may not be the best laser for industrial application as accuracy in removal may be preferred and this would be achieved with a small amount of material per pulse as in the excimer laser treatment. Other considerations for application of the laser removal process would be; the laser type, commercial availability, consumable costs, operating costs, durability, usability and

processing implications. A Nd:YAG laser system may be more suitable for industrial applications and has been used in primer removal trials at other facilities [11, 39].

The Nd:YAG laser removal tests identified a narrow processing range for the effective removal of surface layers that was related to the number of pulses per unit area. Processing below this range did not remove the surface layers and above this range led to oxidisation. The number of pulses per unit area is therefore the primary processing parameter for material removal as it provides a more accurate control then the laser fluence. This primary parameter was also found in work using both Nd:YAG and excimer lasers on AA5052 [11]. Alternatively it has been argued that the pulse duration may have had an effect on the process as suggested in Nd:YAG paint removal from concrete [130].

Sectioning of welds produced by the excimer laser primer removal process showed that most of the surface layers had been removed but also that the surface had oxidised, fragments of which became trapped in the weld. However, this oxide inclusion did not cause weld failure during bend tests [196]. Further work into the effect of the oxide inclusion on other mechanical (particularly fatigue and tensile) and corrosion properties would be necessary for application of the excimer laser paint removal process. In other primer removal trials damage has occurred to the substrate material such as embrittlement but this improved rather then degraded the fatigue and strength properties [201, 202].

Any technique that will result in lower levels of the surface oxidisation may improve the weld structure. Suitable rapid test methods include: visually monitoring the reflectivity of the surface or measuring for a decrease in the surface roughness. Alternatively EDX analysis

could be used to monitor for a minimum in the oxygen weight percentage of the surface as this gave the best indication for the production of a bare metal surface but this method would not be suitable for in-situ monitoring. The EDX, visual inspection and surface roughness analysis showed that to produce a bare metal surface specific laser parameters have to be used.

The primer removal trails show that there are many factors that influence the laser removal of surface layers. For the ideal removal an etch rate curve needs to be developed for each laser and primer combination. Multiple layer systems cause an increase in the processing time as each layer must be treated separately including the debris layer that can be deposited in processing, this is also shown in other investigations [11, 36].

The main laser primer removal issues are; debris generation, completion time and primer thickness. These issues have been highlighted in other work [10, 36, 37, 39]. The thickness being removed is the critical parameter as it directly controls the processing parameters required by the number of pulses per unit area. Even at optimum fluence a large number of pulses is required to remove a thick layer and this means long and costly processing.

Any variation in primer thickness needs to be at the same level as the amount of primer removed by each pulse to avoid incomplete removal. Problems can occur where primer can build up i.e. on edges and corners as these are the areas used in FSW. This could highlight a need for in-process monitoring of the layer thickness.

4.5 Conclusions

- Laser paint removal is a controllable localised processing technique that can be used to remove anodised layers and primer from AA2024 using excimer, TEA-CO_2 or Nd:YAG lasers. The resulting surfaces have low surface damage but can have thick oxides formed during the treatments.
- Different processing parameters are required to remove different layers of a multilayer structure and to remove surface debris the surface after the main processing.
- The excimer laser is capable of removing the primer coatings and anodised layers on an AA2024 surface for Friction Stir Welding preparation. The resultant weld passed destructive bend tests as described in European Standard EN 910:1996.
- The TEA-CO_2 laser is capable of more rapid removal of the primer coatings with more material removed per pulse compared with the excimer laser.
- The Nd:YAG laser removal tests identified a narrow processing range for effective removal that is related to the number of pulses per unit area.

4.6 Future Work

The following recommendations are made for continuation of this work,

- Application of the proposed excimer treatment to other primer systems, such as glass primers, to test the effectiveness and cross-application of the process.
- Use of a TEA-CO_2 laser for the primer and anodising removal over large areas.
- Application of laser primer stripping process to components.
- Mechanical Testing of friction stir welds with excimer laser surface preparation to ascertain tolerance of oxide inclusion.

- Refinement of excimer laser surface preparation process so that no oxide surface remains after treatment.
- Investigation of the removal of other anodised layers such as Tartaric Sulphuric Acid (TSA) anodising or alternatives to the current Chromate Acid Anodising (CAA).

5 Excimer Laser Surface Melting

The excimer laser was used as the basis for development of Laser Surface Melting (LSM) processes. The excimer laser produced a pulse duration of 25ns and the optical arrangement used is described in Section 3.2.1.

Excimer LSM of AA2024 and AA7150 has been investigated in previous work with The University of Birmingham and The University of Manchester. This work used the excimer laser in an extensive processing parameter investigation varying the fluence, raster pattern, delivery optics, processing atmosphere and number of pulses per unit area. An excimer LSM treatment of 10J/cm^2 and 9 pulses per unit area was found to increase the corrosion resistance (measured by micro-electrochemical tests) of AA2024 through microstructure modification [14, 17, 18, 31, 59, 103, 131, 203].

In this section this excimer LSM treatment will be further evaluated for aerospace technologies using atmospheric salt spray tests and anodising treatments.

A range of 7xxx series alloys and AA2024 were investigated and the parent microstructure was examined for comparison to the modified structures. AA2024 was the primary alloy under investigation and the microstructure of the parent alloy etched is shown by optical and electron microscopy in Figure 5.1. A range of 7xxx series alloys were used: AA7056, AA7150 and AA7449, and their typical etched microstructure is shown in Figure 5.2. The microstructures of these alloys are all similar with an elongated grain structure from rolling and an even distribution of precipitates throughout the alloy.

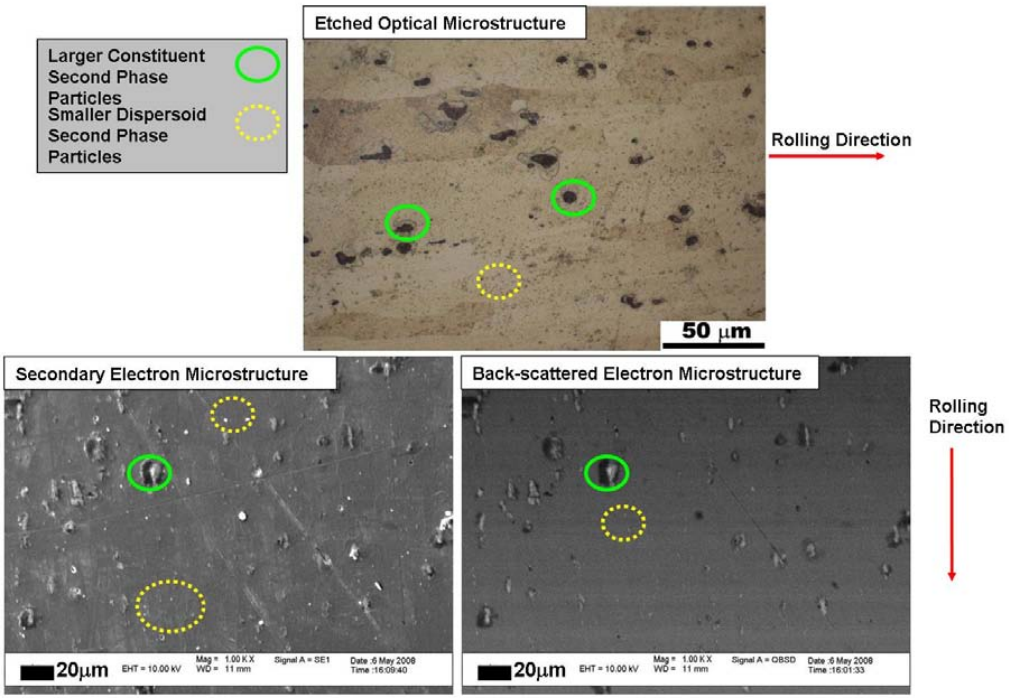

Figure 5.1 Typical SEM and optical microstructure cross-section images of material AA2024.

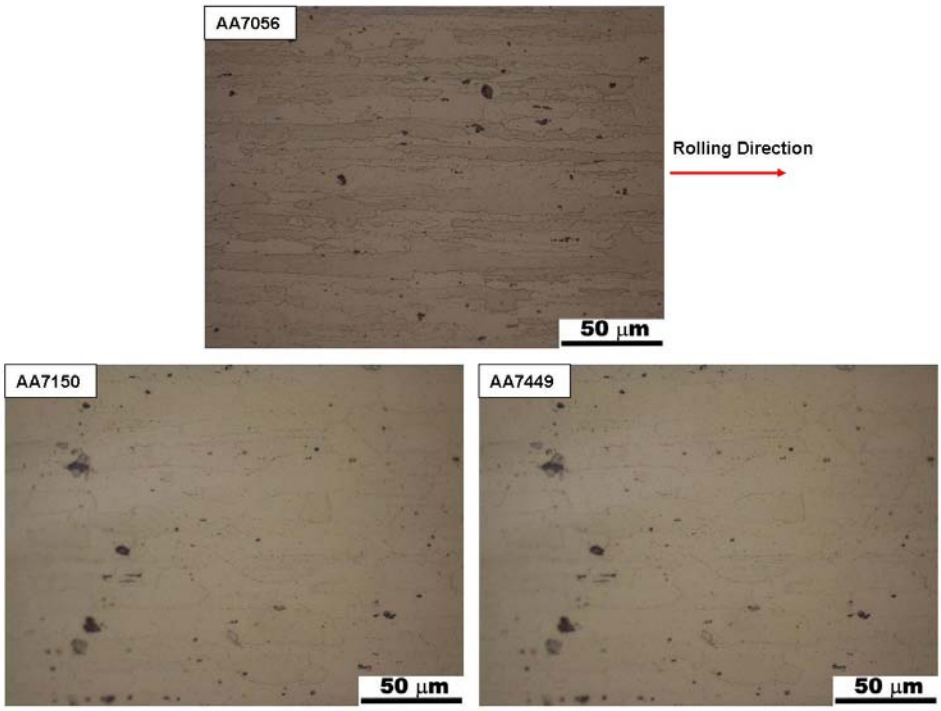

Figure 5.2 Typical etched optical microstructure cross-section images of material AA7056, AA7150 and AA7449.

5.1 Modified Layer Microstructure

The excimer LSM treatment of 10J/cm^2 and 9 pulses per unit area has been shown by previous work to improve the corrosion resistance of AA2024 and in this investigation this excimer LSM treatment was applied to AA2024, AA7150, AA7056 and AA7449 [18].

The surface appearance and etched optical microstructure from the excimer LSM treatment on AA2024 is shown in Figure 5.3. The modified layer appears featureless in terms of porosity or solidification structure whereas grain boundaries and particles can be observed faintly in the substrate material. Over the treated surface, numerous optical measurements of the melted layer thickness were made, yielding values that ranged from 3 to 10μm with an average value of 5μm.

The excimer LSM treatment produced layers of increased homogeneity which has been shown in previous work to increase the corrosion resistance [18, 31]. Figure 5.4 shows the polarisation curves for the parent alloy and material treated with excimer LSM of 10J/cm^2 and 9 pulses per unit area. The polarisation curves were measured in 0.1M NaCl using a microelectrochemical cell, as described in Section 3.6.2. The cathodic polarisation curve shows a plateau at ~10μA/cm^2 for the parent alloy and a plateau at ~1μA/cm^2 for the LSM layer, showing an order of magnitude decrease in cathodic reactivity. The anodic polarisation curve for the parent alloy shows active dissolution throughout, whereas the LSM layer shows a passive region. The LSM layer therefore shows a considerably higher resistance to anodic attack. These curves were typical of the behaviour of the alloy (each measurement was repeated a minimum of three times).

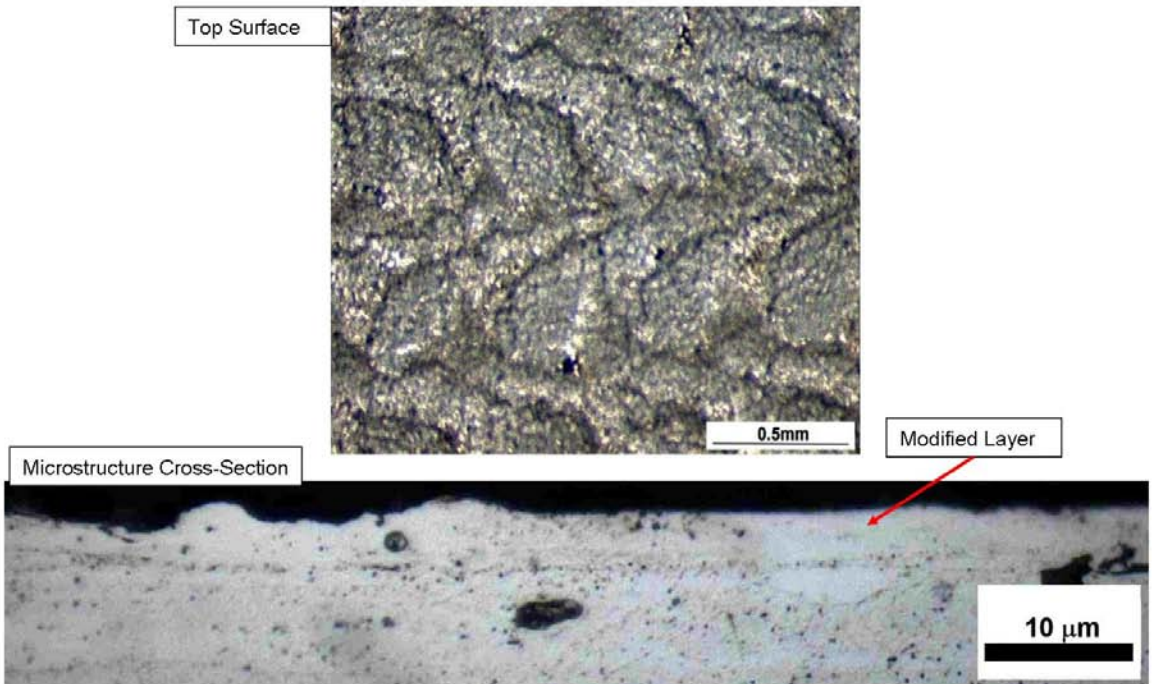

Figure 5.3 Surface appearance and cross-section of excimer laser surface melted AA2024 with treatment parameters of 10J/cm^2, 9 pulses per unit area.

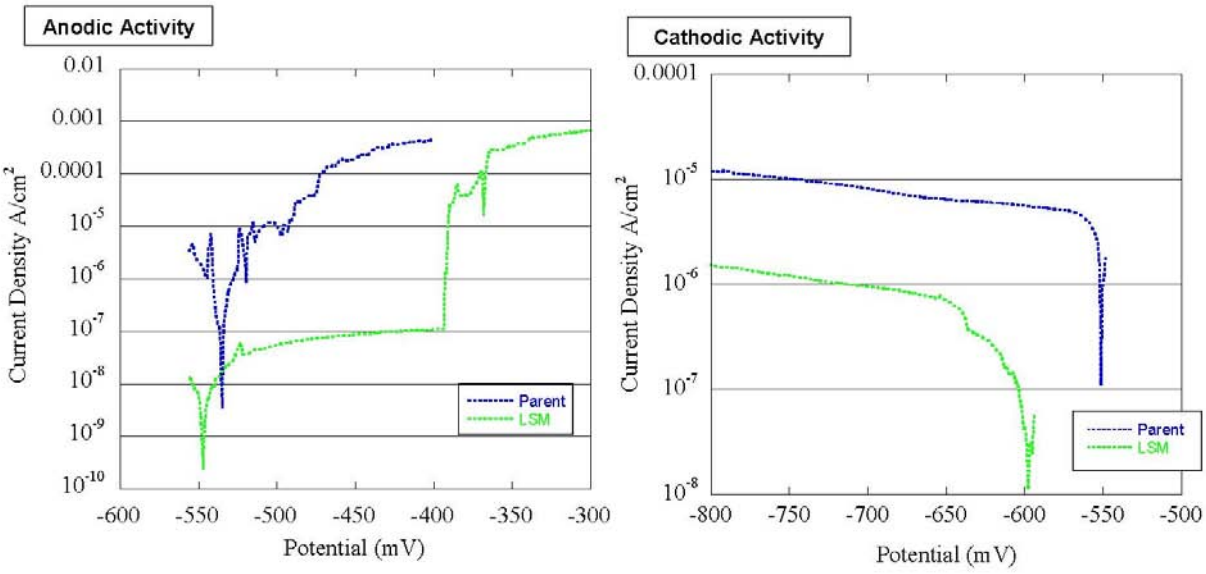

Figure 5.4 Electrochemical reactivity following excimer laser surface melting of AA2024 at 10J/cm^2, 9 pulses per unit area compared with the parent alloy: (a) cathodic polarisation curve and (b) anodic polarisation curves measured with a microelectrochemical cell with 0.1M NaCl solution at a scan rate of 1mV/s scan rate (Ag/AgCl reference electrode).

The excimer LSM treatment of 10J/cm^2 and 9 pulses per unit area was applied to a range of 7xxx series aluminium alloys, AA7056, AA7150 and AA7449, for comparison to AA2024. A comparison of the resulting etched microstructures produced by excimer LSM at 10J/cm^2 9 pulses per unit area for all four alloys are shown in Figure 5.5. For each of the 7xxx series alloys treated, the modified layer had a notable solidification structure of columns perpendicular to the interface between the modified layer and the substrate. Over the treated surface, numerous measurements of the melted layer thickness were taken and these results produced an average modified layer thickness (taken from a minimum of five measurements) of 5μm for AA7150 and of 4μm for both AA7056 and AA7449 (one standard deviation of 0.5μm error in measurements).

In Figure 5.5 there is a noticeable difference between the modified layers produced with the same processing conditions on the alloys treated with the AA2024 modified layer showing the most homogeneity.

5.2 Atmospheric Salt Spray Corrosion Testing

The excimer LSM treatment was developed using microelectrochemical tests to assess the corrosion resistance of AA2024. For application in the aerospace industry, further corrosion testing was required. Atmospheric salt spray testing on both LSM modified 10J/cm^2 and 9 pulses per unit area and parent AA2024 was carried out using three different solutions.

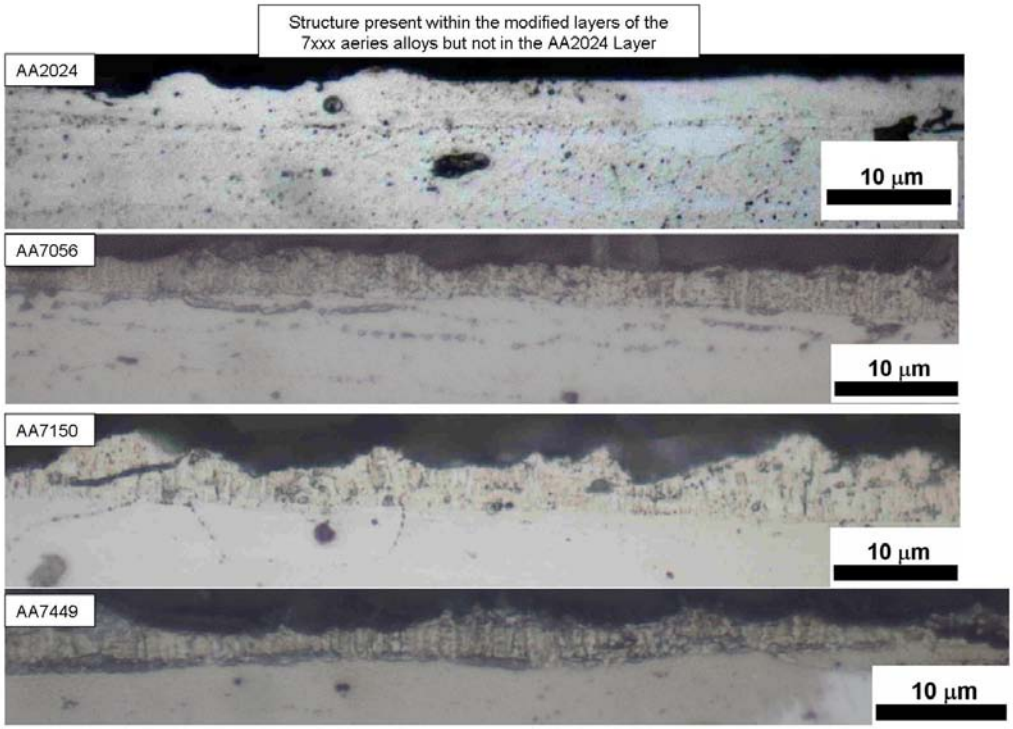

Figure 5.5 Microstructure cross-sections of excimer laser surface melting (10J/cm^2 9 pulses per unit area) of aluminium alloys AA2024, AA7056, AA7150 and AA7449.

The results from de-ionised water exposure, which was likely to contain a small amount of chloride impurities from the chamber, for an exposure over 24 hours are shown in Figure 5.6. The LSM treated samples are on the right in each time period image and it is not until 8 hours exposure that there is any noticeable damage to the LSM surface. In comparison, Figure 5.6 shows that after one hour of exposure to de-ionised water there is a discolouration of the parent material surface.

Two more solutions were used in atmospheric salt spray testing: Harrison's solution (0.5wt% ammonium sulphate and 0.35wt% salt) and a 5wt% salt solution. The sample surfaces over the 24 hours exposure for parent and excimer LSM treated material are shown in Figure 5.7 for Harrison's solution and Figure 5.8 for 5wt% salt solution. Figure 5.7 shows that less

corrosion was observed in the LSM treated samples compared with the parent material for Harrison's solution exposure as there were only notable corrosion sites after 8 hours. The samples treated with LSM and exposure to 5wt% salt solution provided a different result to that from the Harrison's solution with corrosion sites being distinctly noticeable in Figure 5.8 in the LSM treatment after only 2 hours exposure. For all three solutions though the figures show that the LSM modified surface (on right) had fewer corrosion sites than that of the un-treated parent material (on left in the images).

Assessment of the extent of corrosion produced during the atmospheric salt spray tests required the removal of the corrosion product from sample surfaces by a chemical treatment (described in Section 3.6.1). Once the corrosion product had been removed, the samples were analysed by selecting six random areas across the surface and ranking the severity of the corrosion attack observed using the criteria described in Table 3.7 in Section 3.6.1.

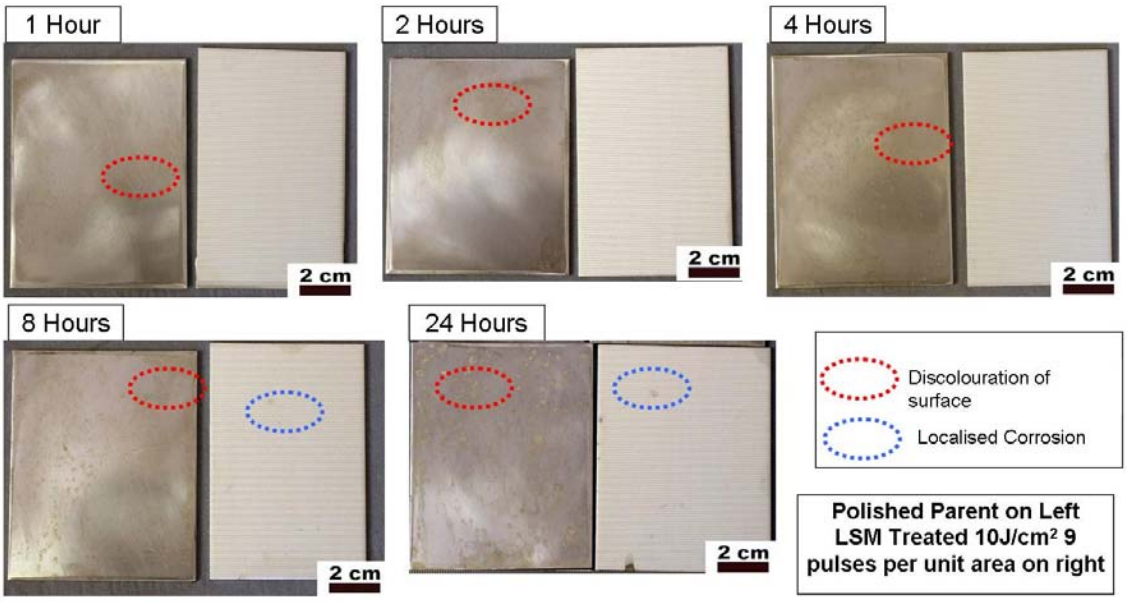

Figure 5.6 Surface appearance of parent (on left) and laser surface melted (on right) AA2024 10J/cm^2, 9 pulses per unit area, samples from atmospheric spray testing over 24 hours in de-ionised water at 35°C.

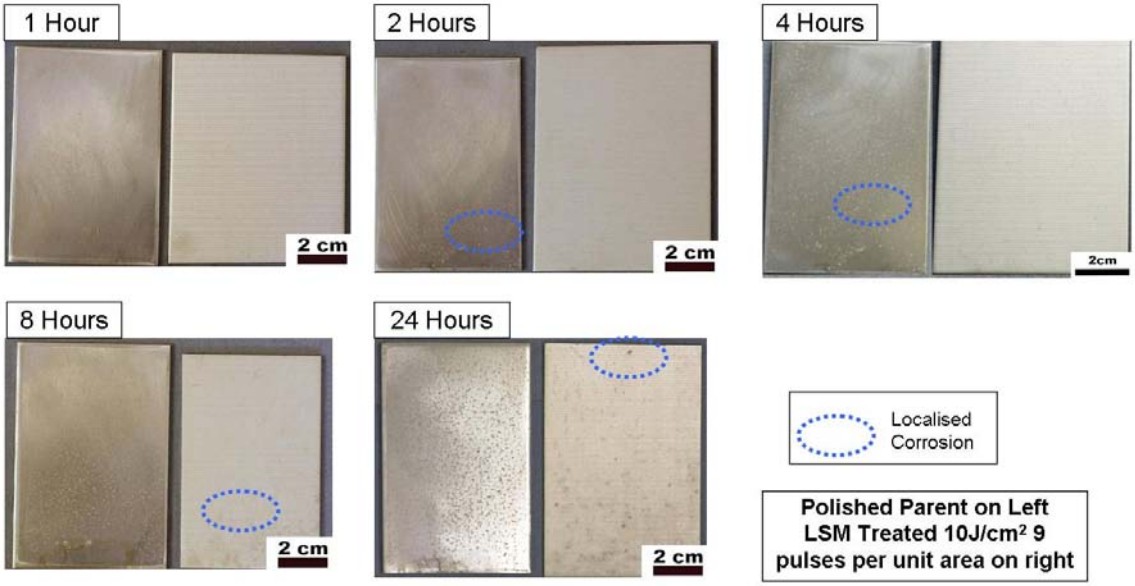

Figure 5.7 Surface appearance of parent (on left) and laser surface melted (on right) AA2024 10J/cm^2, 9 pulses per unit area, samples from atmospheric spray testing over 24 hours in Harrison's solution at 35°C.

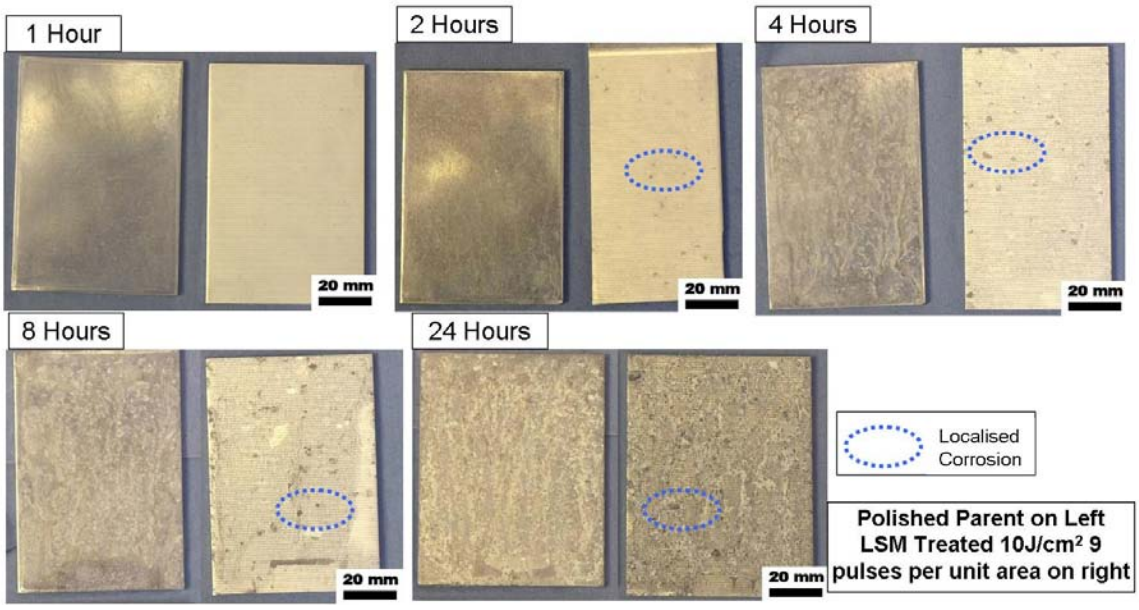

Figure 5.8 Surface appearance of parent (on left) and laser surface melted (on right) AA2024 10J/cm^2, 9 pulses per unit area, samples from atmospheric spray testing over 24 hours in 5wt% NaCl solution at 35°C.

The removal of corrosion product from the surface allowed for examination of the corrosion sites and Figure 5.9 shows a severe case of corrosion causing layer de-lamination that was observed, this figure would have the severest ranking value of 8. The sample in Figure 5.9 was LSM treated after 24 hours exposure in 5wt% salt solution and the LSM treated layer is shown to lift away and expose the underlying substrate.

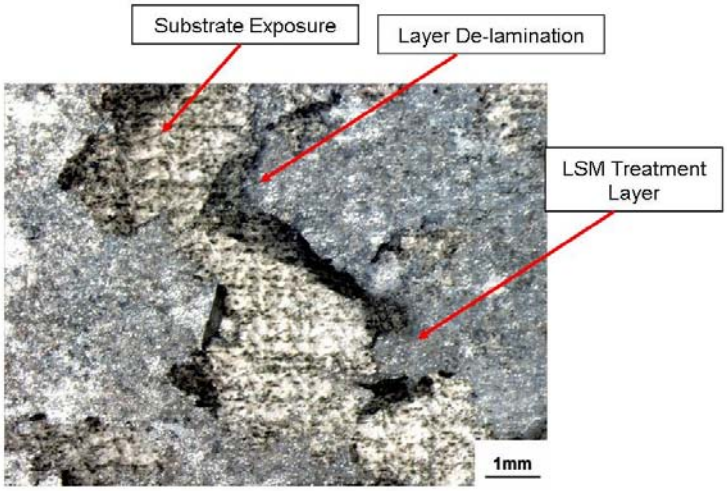

Figure 5.9Surface appearance of LSM layer De-lamination sample excimer laser surface melting AA2024 at 10J/cm^2, 9 pulses per unit area exposed to 24 hours of atmospheric spray tests in 5wt% NaCl solution with corrosion product removed by immersing the sample in a solution of chromic (2.0wt%) and phosphoric (3.5vol%) acid at approximately 60°C for 10 minutes.

The ranking of samples was plotted for de-ionised, Harrison's solution and salt solution over the 24 hour exposure period in Figure 5.10, Figure 5.11 and Figure 5.12, respectively for excimer LSM AA2024 treated at 10J/cm, 9 pulses per unit area compared with parent material polished with the same preparation used for excimer LSM (described in Section 3.6.1).

The graphs show that the severity of the corrosion damage observed increased with the exposure time. Figure 5.10 plots the damage caused by de-ionised water exposure and except for the result at 8 hours exposure the LSM treated samples have lower damage ranking than

the parent material. For the two other solutions, Figure 5.11 and Figure 5.12 show a more scattered result with the parent material having a lower ranking the LSM treated surfaces. There is large amount of scatter in these results and this is not aided by the subjective nature of the ranking procedure.

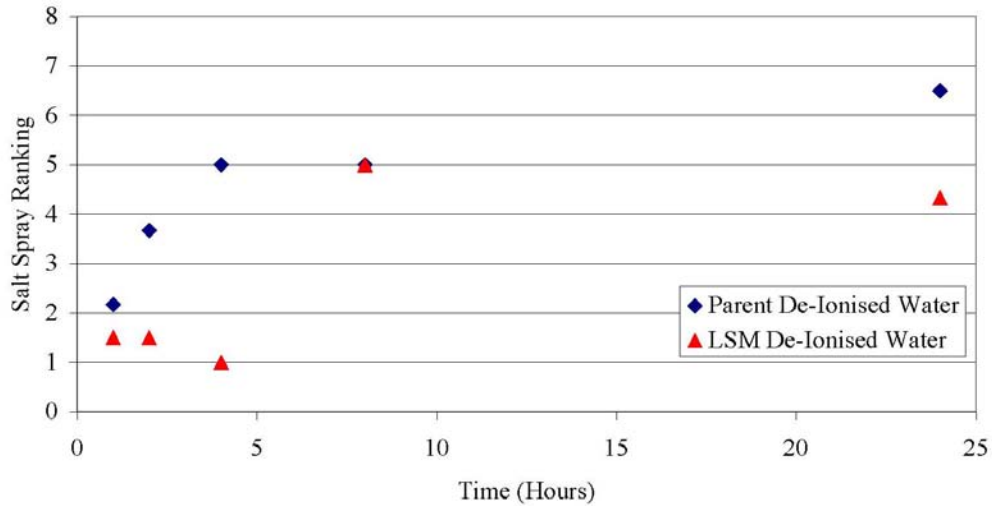

Figure 5.10 Graph of time versus damage ranking from samples of parent material and excimer laser surface melted 10J/cm^2, 9 pulses per unit area exposed to atmospheric spray tests in de-Ionised water over 24 hours at 35°C.

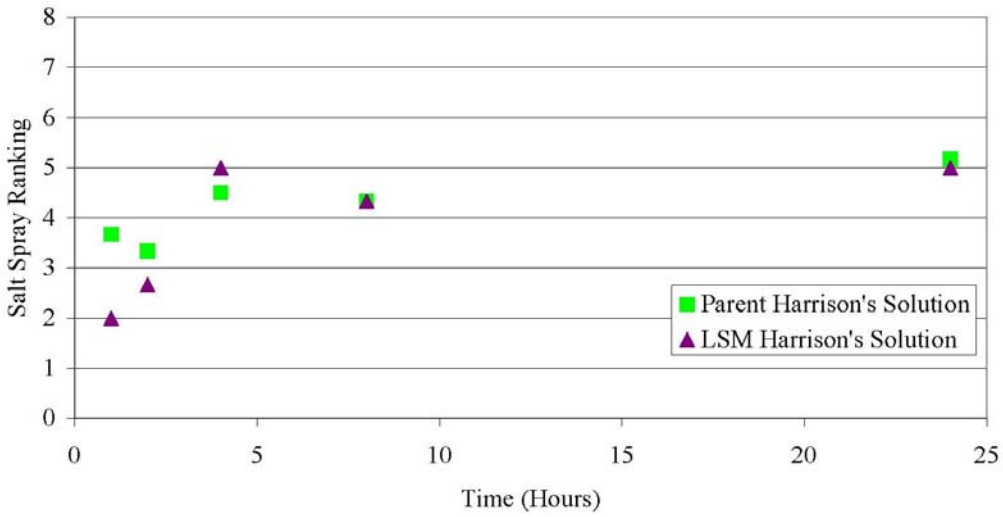

Figure 5.11 Graph of time versus damage ranking from samples of parent material and excimer laser surface melted 10J/cm^2, 9 pulses per unit area exposed to atmospheric spray tests in Harrison's solution over 24 hours at 35°C.

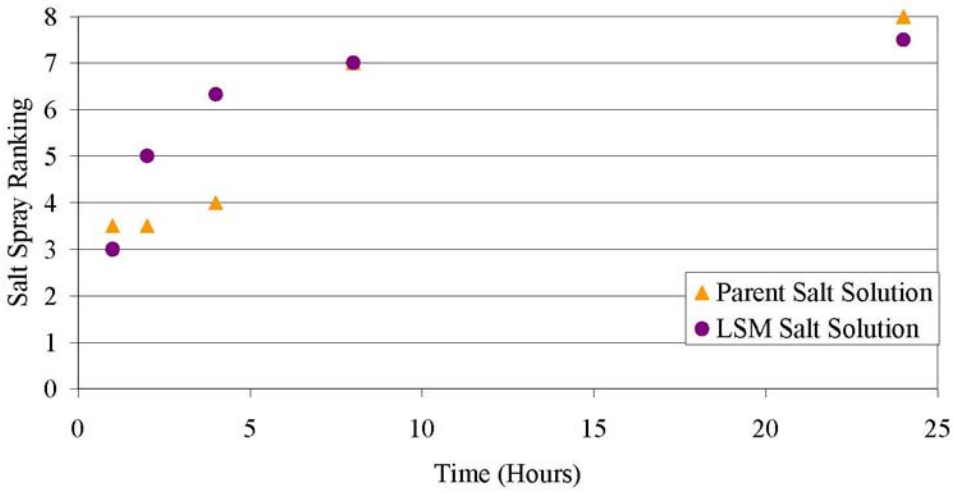

Figure 5.12 Graph of time versus damage ranking from samples of parent material and excimer laser surface melted 10J/cm^2, 9 pulses per unit area exposed to atmospheric spray tests in 5wt% NaCl solution over 24 hours at 35°C.

5.3 Laser Surface Melting and Anodising

The atmospheric salt spray tests showed that de-lamination of the LSM treated layer can occur (Figure 5.9). To avoid this in industrial application of LSM processes it would be necessary to couple LSM with other corrosion protection treatments such as anodising.

To investigate this, AA2024 and AA7449 alloys were treated with the standard excimer LSM treatment (10J/cm^2 9 pulses per unit area) and were then subjected to an anodising process: either the current aerospace standard of chromic acid anodising (CAA) or its possible replacement tartaric sulphuric anodising (TSA).

Figure 5.13 and Figure 5.14 show etched microstructure cross-sections of AA2024 material before and after anodising for CAA and TSA respectively. The microstructure cross-sections

after anodising, in both cases, are over-exposed in one picture to show the presence of the anodising and with normal exposure to examine the microstructure for the presence of the modified layer. The over-exposed images in Figure 5.13 and Figure 5.14 show that an anodising layer is present but the normal exposure images of the microstructure do not show any LSM layer present, which suggests that the entire modified layer was removed by both of the anodising processes.

However, in the case of AA7449 in Figure 5.15 for CAA and for Figure 5.16 for TSA, the etched microstructure cross-sections of anodised samples showed that there was anodising present (in the over exposed images) and also small sections of the LSM layer remaining with microstructure examination. On average, after both anodising processes typically there was 2µm of the LSM layer remaining.

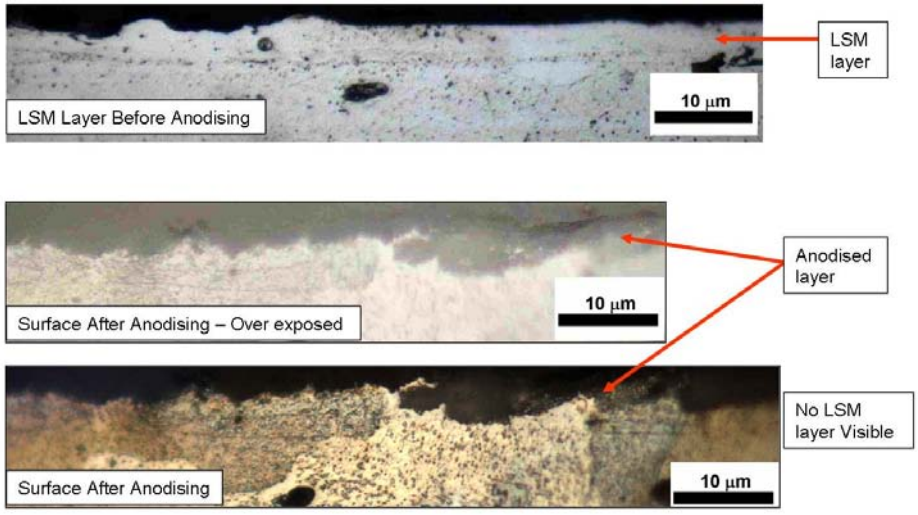

Figure 5.13 Cross-section of AA2024 surface following excimer laser surface melting (10J/cm^2, 9 pulses per unit area) and chromic acid anodising.

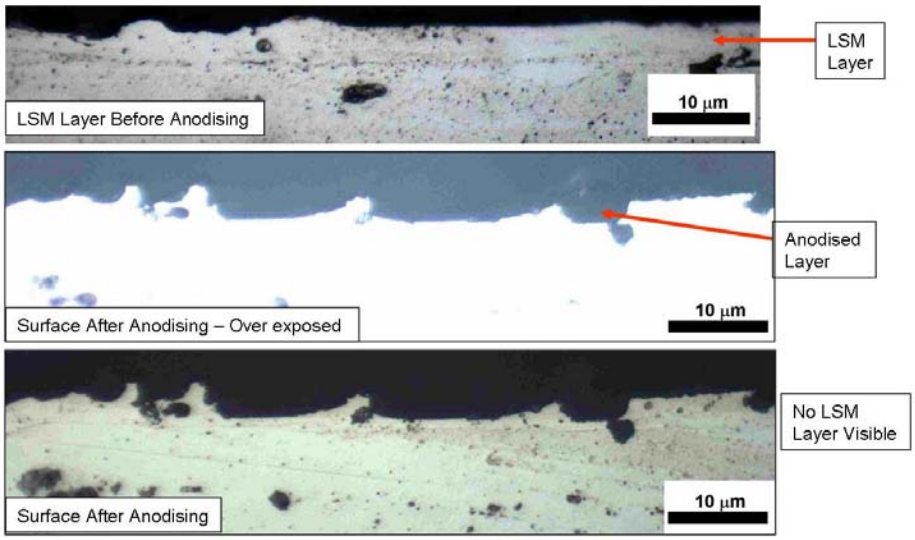

Figure 5.14 Cross-section of AA2024 surface following excimer laser surface melting (10J/cm^2, 9 pulses per unit area) and tartaric sulphuric anodising.

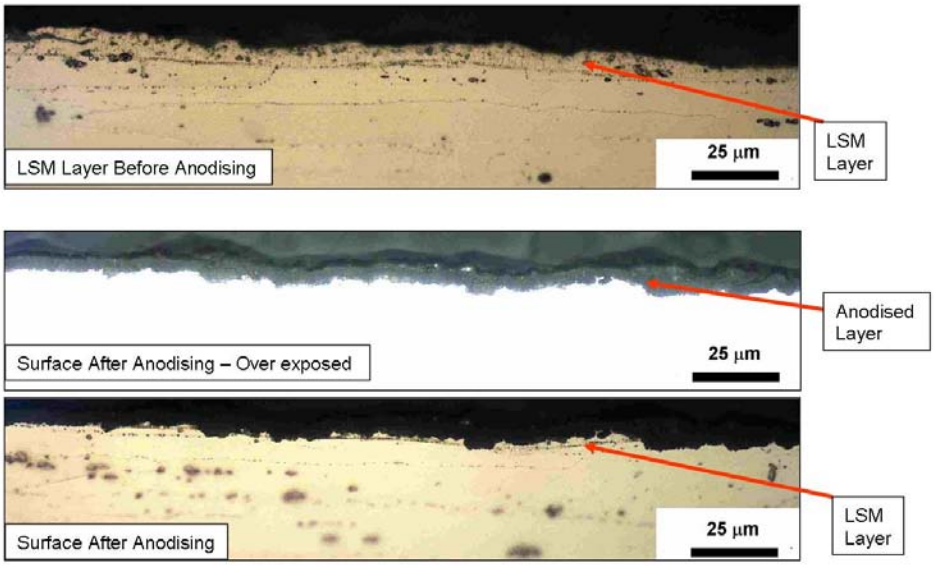

Figure 5.15 Cross-section of AA7449 surface following excimer laser surface melting (10J/cm^2, 9 pulses per unit area) and chromic acid anodising.

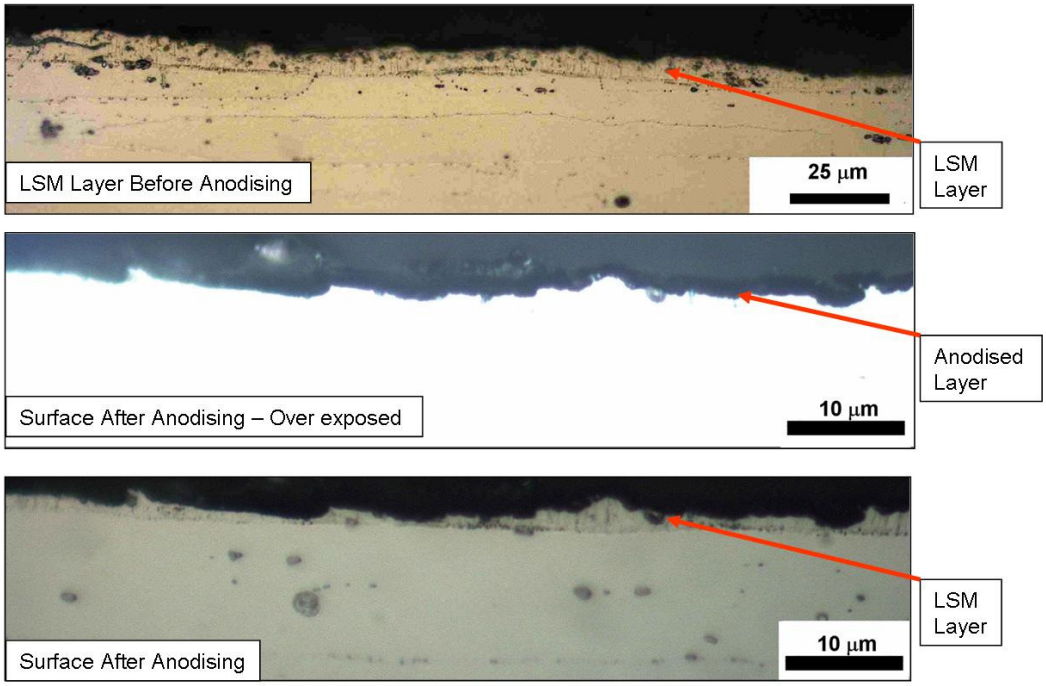

Figure 5.16 Cross-section of AA7449 surface following excimer laser surface melting (10J/cm^2, 9 pulses per unit area) and tartaric sulphuric anodising.

5.4 Processing Parameter Variation

Coupling anodising with excimer LSM treatment (10J/cm^2 and 9 pulses per unit area) was unsuccessful as most if not all of the modified layer was removed. It is therefore necessary to increase the modified layer thickness for coupling the LSM treatment with anodising.

Investigations were then carried out to determine whether the LSM layer could be thickened by increasing the excimer laser fluence for AA2024. The optical arrangement used was a MLA (as described in Section 3.2.1) with raster scanning beam movement in an air atmosphere. Figure 5.17 shows etched microstructure cross-sections of sample treatments produced with increasing fluence between 3 and 10J/cm^2 for AA2024. For AA2024, the laser-treated layer appears featureless and hard to resolve at 3 and 3.5J/cm^2 but the modified

layer is approximately 1-2µm in thickness. Thicker layers, 3-4µm in thickness can be observed though for the higher fluences. These measurements of modified layer thickness for the AA2024 treated with varying fluence are listed in Table 5.1. It can be observed in these figures however that there is very little change in the modified layer thickness with increasing fluence for either of these alloys.

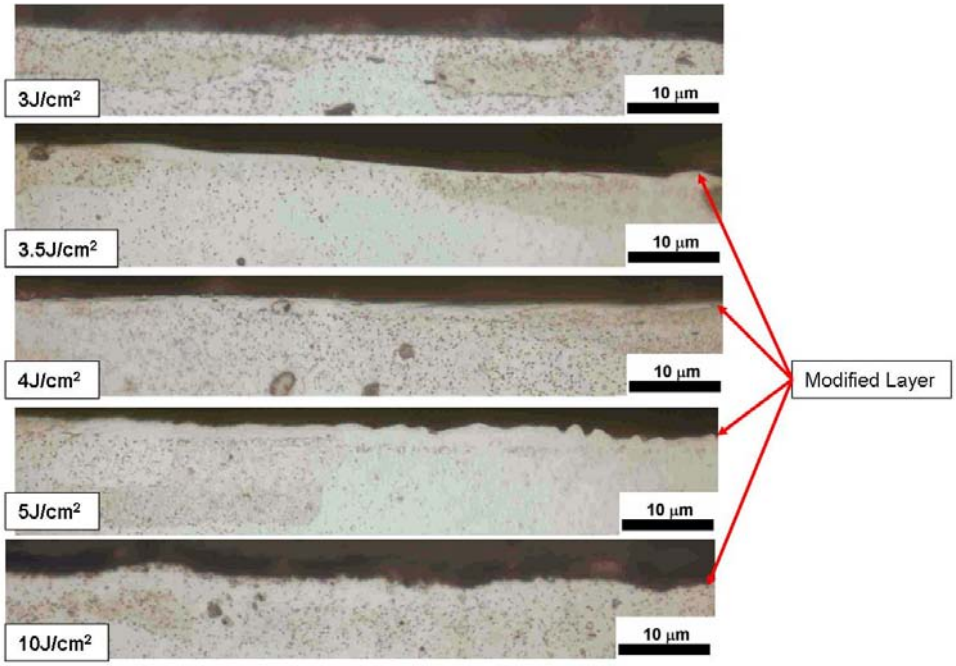

Figure 5.17 Microstructure cross-sections of samples produced by excimer laser surface melting 9 pulses per unit area, with increasing fluence between 3 and 10J/cm^2 on AA2024.

Table 5.1 Excimer laser surface melting of AA2024 with varying fluences modified layer thickness measurements

Fluence (J/cm^2)	Modified depth (µm)
3	2
3.5	1
4	2.5-3.0
5	3
10	3.5-4

5.5 Discussion

Excimer LSM at 10J/cm^2 and 9 pulses per unit area was developed to increase corrosion resistance (Figure 5.4) of AA2024 by production of a homogeneous microstructure (Figure 5.3) [18, 31].

Work performed by C. Padovani [18] and BAE Systems [14, 17, 103] into LSM has shown that an intact LSM layer has a higher corrosion resistance compared with the AA2024 parent material. This improvement was due to homogenisation of the surface which influences the corrosion resistance in a number of possible ways such as modification of the surface oxide [12, 123, 124], microstructure refinement [111], or a decrease in galvanic coupling between precipitates and the matrix reducing the driving force for corrosion [125].

The microstructure produced by the excimer LSM treatment of 10J/cm^2 and 9 pulses per unit area on AA2024 was investigated fully by P. Ryan, who showed that the modified structure had grown epitaxially from the substrate and that the modified surface was more homogeneous compared with the bulk material [31]. Similar conclusions were also found in other LSM work [87, 111, 123, 186].

The 7xxx series alloys all produced similar heterogeneous modified structures which was different to the AA2024 modified structure. P. Ryan investigated the excimer LSM treatment of 10J/cm^2 and 9 pulses per unit area applied to AA7150 in comparison to the treatment on AA2024. The difference in modified microstructure was due to the difference in alloy compositions (Table 3.2) as AA7150 compared with AA2024 has lower copper and manganese levels but higher magnesium, zinc and zirconium concentrations.

Each of these elements has an effect on the microstructure but in particular the changes in manganese and zirconium are significant as they refine the grain structure [21, 31, 76]. Grain refiners act as nuclei for heterogeneous solidification and initiate equiaxed grains that can lead to a columnar structure as opposed to epitaxial growth from the un-melted substrate structure.

Zirconium was identified as the most important alloying element for the formation of the solidification structure in the excimer modified layer of AA7150, as at the base of the melt layer zirconium in β′ phase precipitates (Al_3Zr) initiated an equiaxed zone which was followed by a columnar microstructure [31]. This meant that epitaxial growth from the substrate did not occur.

The influence of zirconium and the formation of an equiaxed grain zone were noted in fusion welding investigations which proposed that heterogeneous nucleation was due to an unmixed colder region. Within an unmixed region (i.e. the base of a melted layer) the composition approximates that of the base metal and precipitates in this zone are isolated from high temperatures and fluid flow meaning that they neither dissolve nor are swept into the melt pool and can act as nucleation sites for solidification [76].

Therefore in the case of the zirconium-containing 7xxx series alloys Al_3Zr precipitates are not dissolved by LSM and remain at the base of the layer to initiate a columnar microstructure, whereas with AA2024 LSM there are no such precipitates at the base of the layer allowing epitaxial growth from the substrate and the production of a homogeneous modified layer with increased corrosion resistance.

In development of the excimer LSM treatment of 10J/cm^2 and 9 pulses per unit area the corrosion performance was assessed using microelectrochemical tests. To further test the corrosion performance for aerospace applications atmospheric salt spray tests were performed.

Initially it appeared that the atmospheric spray tests also showed that LSM increased the corrosion resistance with the occurrence of only a few pitting sites. However a more detailed examination showed that as there was not a wide distribution of small pits but in the case of a few pits the corrosion was concentrated and severe. The initiation of corrosion therefore controlled the corrosion performance and initiation varied with the atmospheric spray solution.

Testing in de-ionised water meant that corrosion was not easily initiated and the corrosion was ranked lower for LSM then the parent material. The testing with de-ionised water must be treated with some caution as the solution would probably have contained a small amount of impurities from contamination in the chamber even though the chamber was rinsed with de-ionised water for 72 hours before testing.

Increasing the severity of the solution increased the likelihood of pit initiation and corrosion in the LSM increased until it was worse than the parent material. The concentration of corrosion in a few large pits suggested that corrosion either propagated into the substrate or along the base of the layer causing de-lamination. It was found that de-lamination of the LSM

layer was observed in samples left for 24 hours in 5wt% salt solution and also in immersion tests performed on excimer LSM by C. Padovani [18].

The corrosion resistance improvement of excimer LSM is limited by the initiation of corrosion and this can be in the form of a few isolated pits. Once a few pits have formed then severe corrosion and layer de-lamination can occur. To ensure a corrosion improvement therefore the layer needs to remain intact which raises concerns about the small thickness of the modified layer and its damage tolerance.

To provide additional protection against corrosion and modified layer de-lamination the excimer LSM layers were exposed to an anodising treatment. Investigations into combining LSM treatment with anodising processes were considered unsuccessful however as the layer was too thin to survive the anodising process. The quality of the anodised layer produced was not part of this investigation however other work has suggested that this may affect the success of combining the LSM with anodising, as ruby laser LSM on aluminium combined with anodising improved the quality of the resultant anodised layer and decreased the pitting resistance even with anodising removing the LSM layer [204].

The anodising processes removed the excimer modified layer from the sample surfaces and any benefit from the laser treatment was assumed lost. To avoid this removal the modified layer thickness needed to be increased.

Increase in fluence did not provide a large increase in the modified layer thickness for AA2024 and this suggested that another laser parameter controlled the modified layer depth.

Laser pulse duration has been identified by modelling (described in Section 2.6.1) to increase the modified layer thickness [19, 82, 126]. However this could not be tested using the excimer laser as the pulse duration is an inherent laser parameter. Investigations into the affect of pulse duration on modified layer thickness would therefore require the use of other laser systems.

5.6 Conclusions

- Excimer LSM of 10J/cm^2 and 9 pulses per unit area on AA2024 increased the corrosion resistance, from microelectrochemical tests.
- Atmospheric salt spray tests of excimer LSM of 10J/cm^2 and 9 pulses per unit area on AA2024 showed that the corrosion resistance improvement was limited by the initiation of corrosion as once corrosion initiates severe corrosion and layer de-lamination can occur.
- Coupling anodising processes with excimer LSM treatment 10J/cm^2 and 9 pulses per unit area on AA2024 to avoid corrosion initiation and layer de-lamination was unsuccessful as the anodising process removed the entire modified layer.
- Increasing the excimer LSM modified layer thickness was not achieved by increasing the laser fluence.

6 USP-CO_2 Laser Surface Melting

The USP-CO_2 laser was used to investigate the effect of varying the laser pulse duration (between 7 and 30μs) and number of pulses per unit area (between 1 and 10) on the properties of the modified LSM layer for AA2024 and AA7150. Etched microstructure cross-sections of initial material for these alloys, highlighting the precipitates present, are shown in Figure 6.1. The optical set-up for these investigations is described in Section 3.2.7.3.

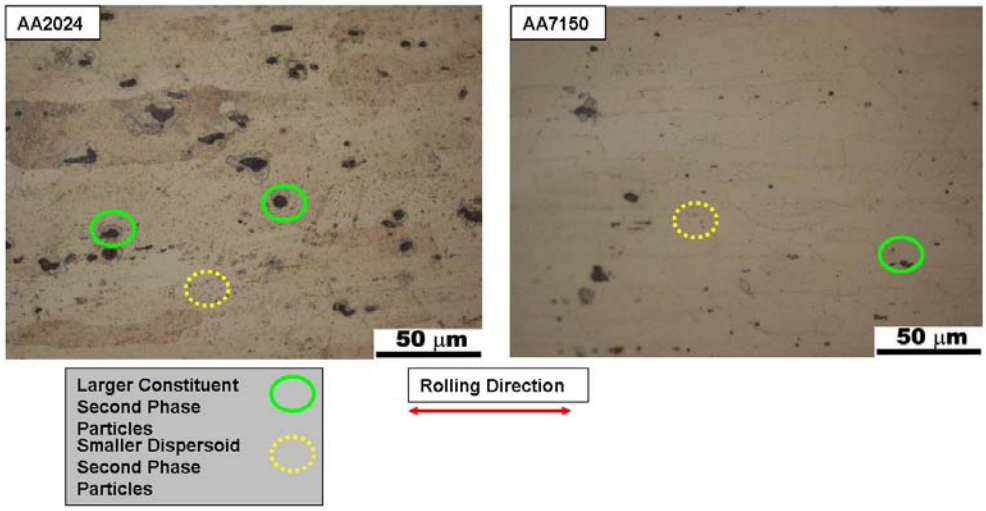

Figure 6.1 Etched microstructure cross-sections of parent material AA2024 and AA7150 used in USP-CO_2 LSM investigations.

6.1 Modified Layer

The typical etched microstructure cross-sections of isolated USP-CO_2 LSM treated spots on AA2024 and AA7150 are shown in Figure 6.2 and Figure 6.3, respectively. These figures both show that the base of the modified layer is curved. In Figure 6.2 an individual treatment spot is shown and in Figure 6.3 two overlapped treatments are shown. However, the parameters used to create both of these treatments were 5 pulses per unit area by the

overlapping of pulses. These figures show that the 5 pulses per unit area were not achieved and this was due to variation in the melt zone size which was smaller than those used in the design of the processing parameters.

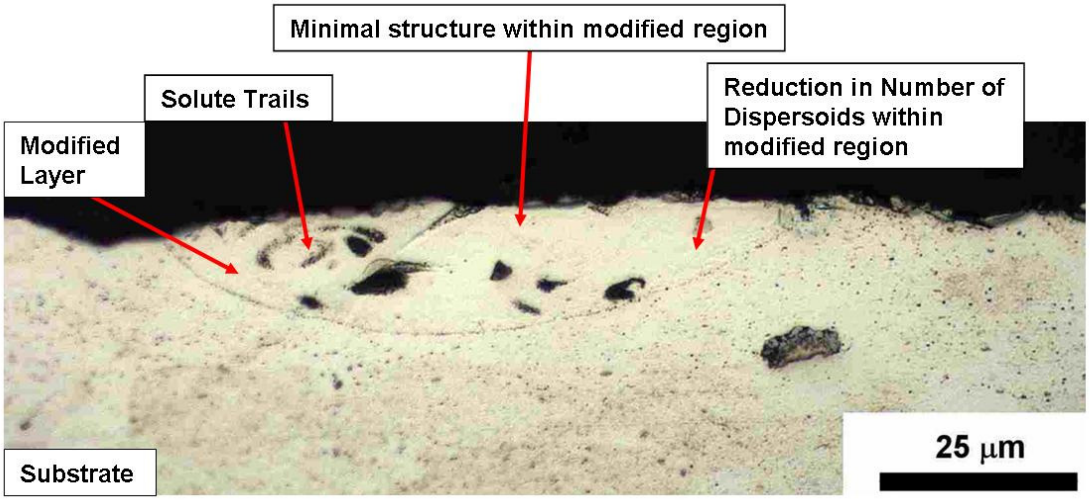

Figure 6.2 Typical etched microstructure cross-section produced by USP-CO_2 laser surface melting on AA2024 with pulse duration 22.4μs and 10 pulses per unit area.

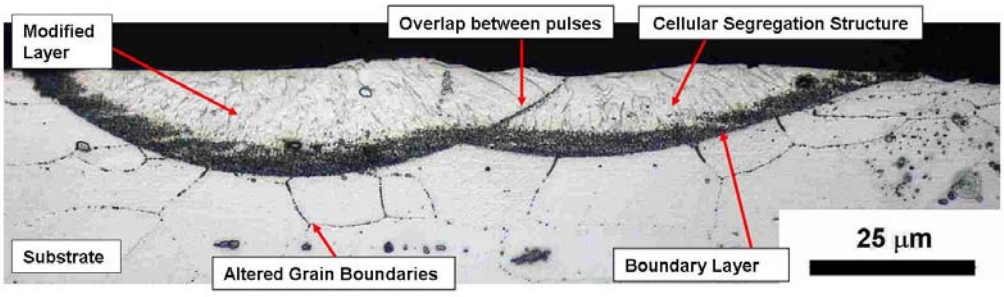

Figure 6.3 Typical microstructure cross-section produced by USP-CO_2 laser surface melting on AA7150 with pulse duration 27.2μs and 5 pulses per unit area.

Comparing the microstructure of these two figures shows a difference in modified structure with the alloy being treated. Figure 6.2 shows the typical etched modified microstructure

produced by USP-CO_2 LSM treatment (using 22.4μs pulse duration and 10 pulses per unit area) on AA2024. This figure shows that in the area of the laser treatment there is a reduction in the number of small precipitates in comparison to the surrounding substrate material. In the case of large precipitates this figure shows that their shape had been altered into solute trails.

The typical etched microstructure of USP-CO_2 LSM treatment of two overlapping laser pulse treatments on AA7150 (in this case 27.2μs pulse duration and 5 pulses per unit area), is shown in Figure 6.3. The modified layer shown in Figure 6.3 is different to that of Figure 6.2. In Figure 6.3 there is an overall segregated solidification structure within the modified layer. Towards the base of the modified layer there is a different solidification structure present in a boundary layer. Beneath this boundary and the modified layer it can also be seen in Figure 6.3 that the substrate grain boundaries have been modified by the process in a type of HAZ.

6.2 Modified Layer Thickness

The USP-CO_2 laser was used to investigate whether the LSM processing parameters of pulse duration and number of pulses per unit area could increase the modified layer thickness on AA2024 and AA7150. Figure 6.4 shows the relationship between the laser pulse duration (12.4-30μs) and the average (minimum of five measurements were taken) modified layer thickness for both of the alloys tested, with error bars for layer thickness measurements at one standard deviation. Figure 6.4 shows that for both alloys, an increase in pulse duration led to an increase in modified layer thickness.

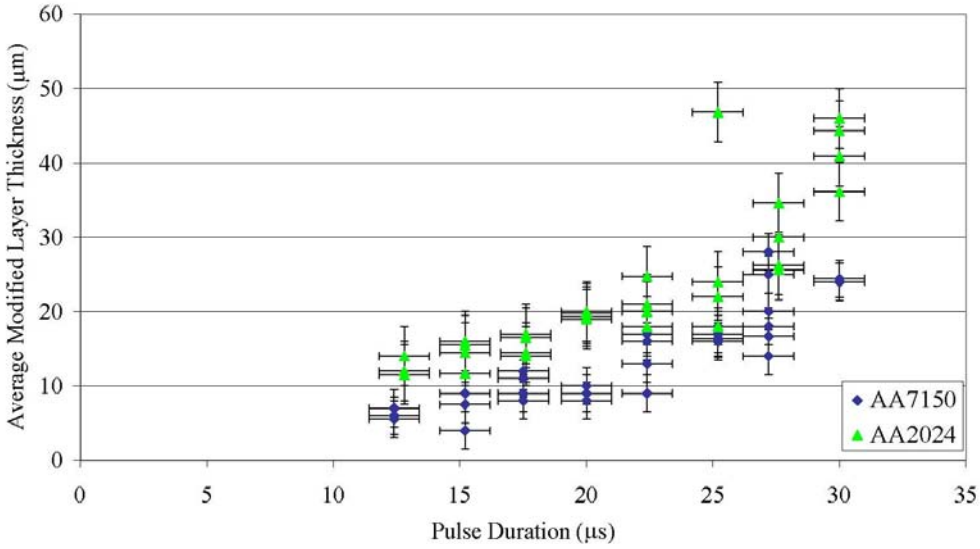

Figure 6.4 Graph of pulse duration (12.5-30µs) versus average (with a minimum of five measurements taken) modified layer thickness for USP-CO_2 laser surface melting on AA2024 and AA7150. Error bars for the modified layer depth measurements and pulse duration are at one standard deviation based on a minimum of 10 measurements.

The other laser processing parameter under investigation was the number of pulses per unit area used in LSM of both alloys. The average modified layer thicknesses produced with variation in the number of pulses per unit area (1-10 pulses) is shown in Figure 6.5 for AA2024 treated at 22.4µs pulse duration and AA7150 treated at 20µs pulse duration respectively. In these figure it is apparent that in the treatment of both of the alloys that there was no relationship between the modified layer thickness and the number of pulses per unit area. This was the case with each of the pulse durations tested.

The error bars in this figure are based on one standard deviation in measurements. The error bars are large due to scatter in measurements from the large curvature at the base of the modified layers over the treatment area.

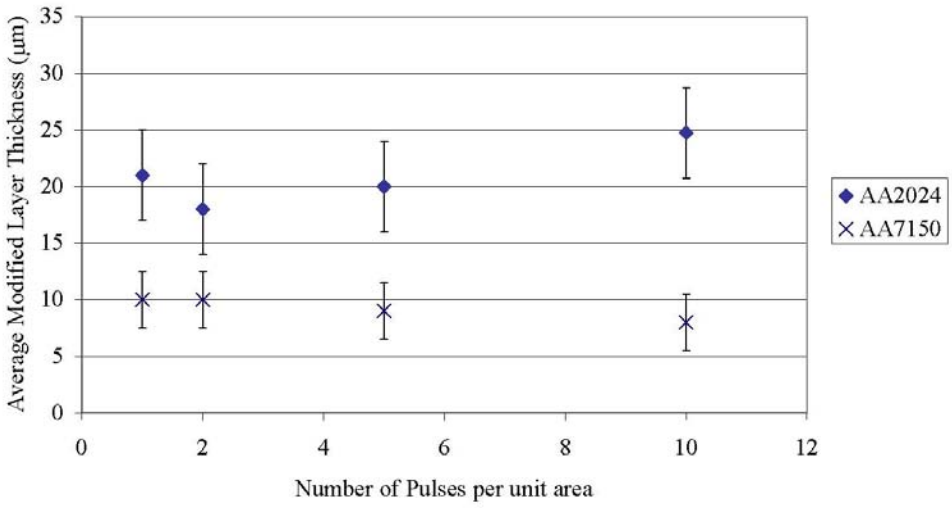

Figure 6.5 Graph of number of pulses per unit area (1-10) versus average layer thickness (minimum of five measurements) for USP-CO_2 laser surface melting 22.4µs pulse duration on AA2024 and 20µs pulse duration on AA7150. Error bars for the modified layer depth measurements are at one standard deviation based on a minimum of 10 measurements of modified layer thickness.

6.3 Solute Dispersion within the Modified Layer

The typical etched microstructure cross-section of the AA2024 LSM modified layer shown in Figure 6.2 did contain some large precipitates that had been modified in shape but the smaller precipitates had been removed by the USP-CO_2 LSM treatment. Further examination of this change in precipitates was performed using backscattered SEM imaging with a non-aqueous polishing sample preparation to 1µm finish.

Figure 6.6 is a backscattered SEM image of a non-aqueous polished microstructure cross-section of USP-CO_2 LSM treated AA2024 at 22.4µs pulse duration and 2 pulses per unit area. The figure shows that large precipitates remain in the modified layer and that these

precipitates had been modified in terms of their shape as their boundaries were ill-defined from the dispersion of solute atoms from the edges of the precipitates.

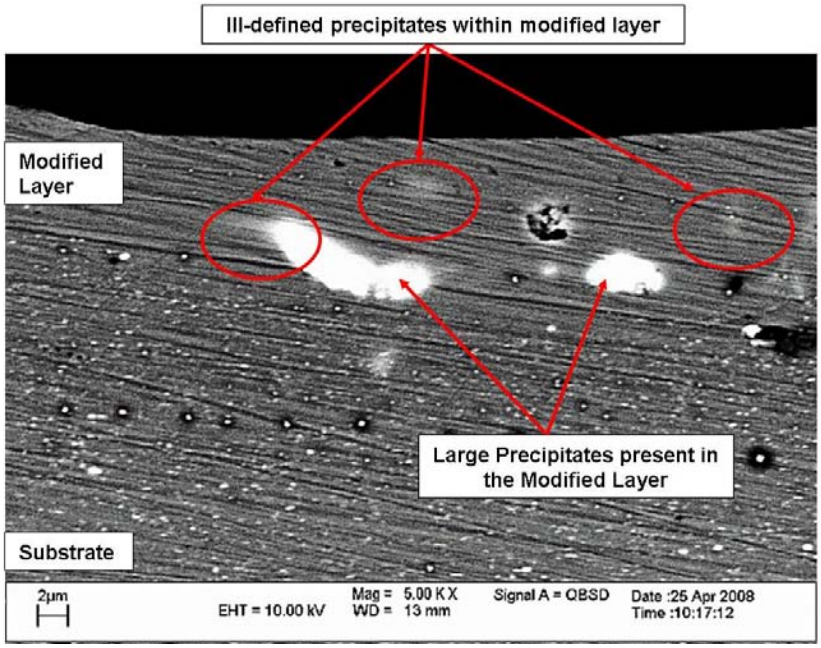

Figure 6.6 Backscattered SEM imaging of microstructure cross-sections showing solute dispersion in USP-CO_2 laser surface melting on AA2024 from pulse duration 22.4µs and 2 pulses per unit area. Surface prepared by non-aqueous polishing to 1µm.

The modification of precipitates from solute dispersion was observed to a greater extent in LSM treatments at other processing parameters as shown in the typical etched microstructure cross-sections of USP-CO_2 LSM treated AA2024 in Figure 6.2 (at 22.4µs pulse duration and 10 pulses per unit area) and AA7150 in Figure 6.7 (at 27.2µs pulse duration and 5 pulses per unit area).

This solute dispersion was further examined using backscattered SEM imaging of microstructure cross-sections prepared by non-aqueous polishing to a 1µm finish for both alloys. Figure 6.8 shows solute trails from USP-CO_2 LSM treatment of AA2024 at 27.2µs

pulse duration and 5 pulses per unit area, where as Figure 6.9 shows the solute trails created from USP-CO_2 LSM treatment of AA7150 at 25.2μs pulse duration and 1 pulse per unit area. These figures suggest that the solute trails observed in the treatment of both alloys were due to mass movement and convection when in the liquid phase.

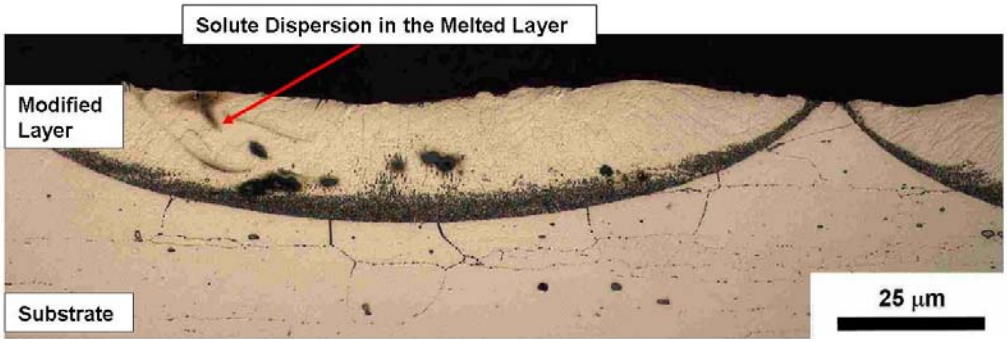

Figure 6.7 Microstructure cross-section showing element mixing in USP-CO_2 laser surface melting on AA7150 with pulse duration 27.2μs and 5 pulses per unit area producing an average modified layer thickness of 20μm.

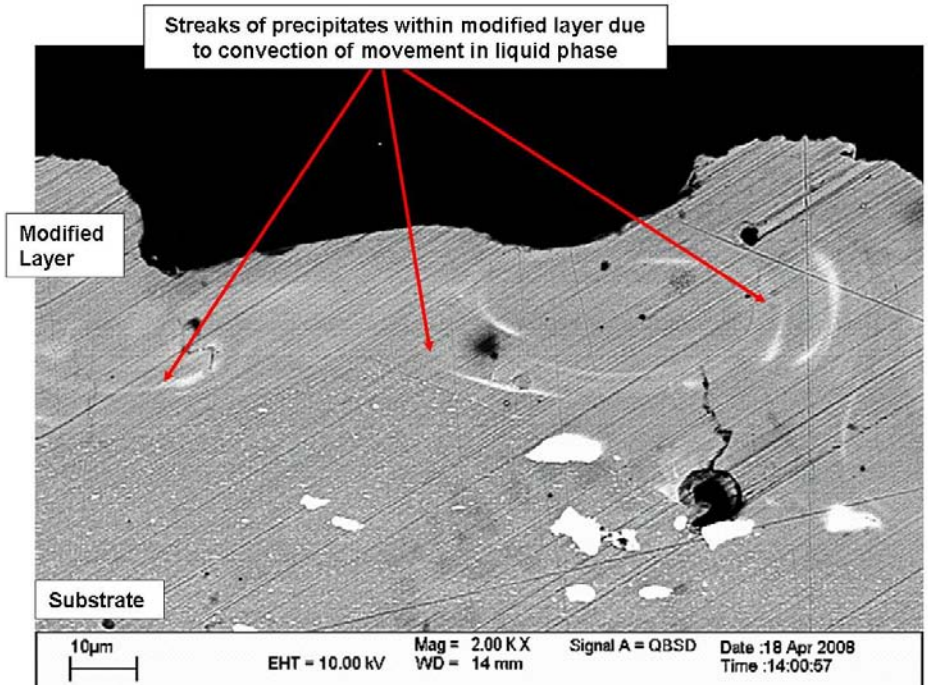

Figure 6.8 Backscattered SEM microstructure cross-section images showing element dispersion mixing by convection in USP-CO_2 laser surface melting on AA2024 from pulse duration 25.2μs and 1 pulse per unit area. Surface prepared by non-aqueous polishing to 1μm.

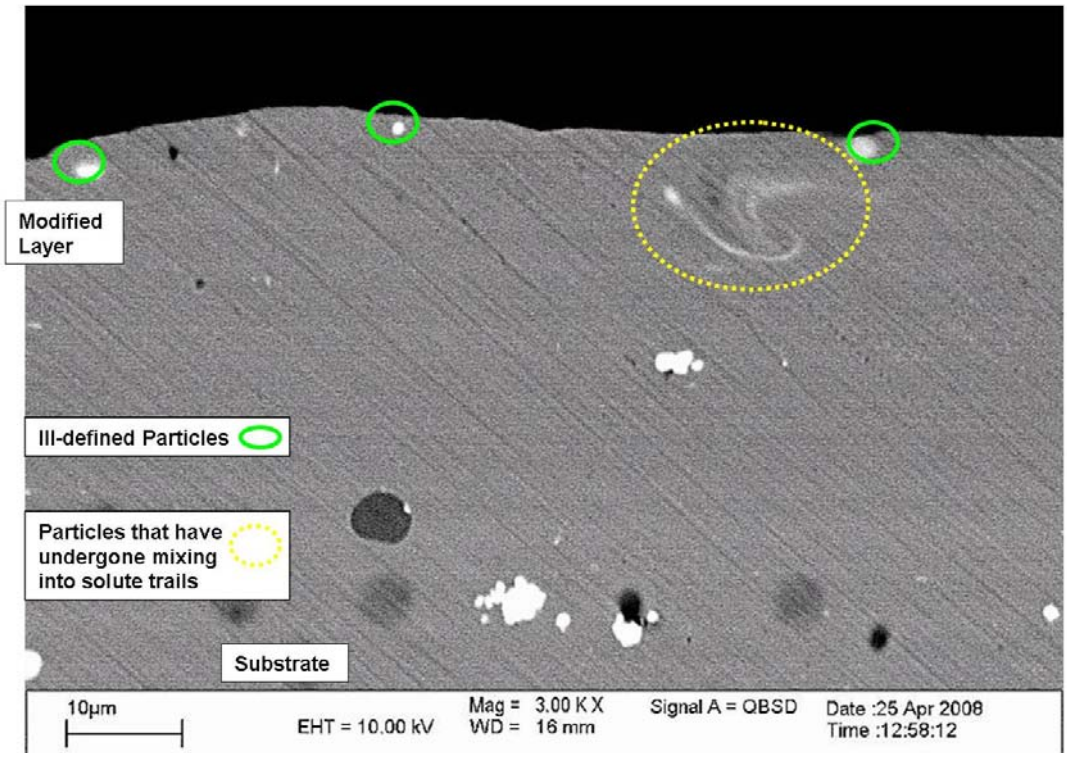

Figure 6.9 Backscattered SEM microstructure cross-section images showing precipitate dispersion by mixing in USP-CO_2 laser surface melting on AA7150 from pulse duration 27.2µs and 1 pulse per unit area. Surface prepared by non-aqueous polishing to 1µm.

The form of solute dispersion observed within the modified layers produced was investigated in terms of the processing parameters used.

Figure 6.10 compares backscattered SEM images of microstructure cross-sections (prepared to 1µm finish with non-aqueous polishing) produced by USP-CO_2 LSM at 1 pulse per unit area and various pulse durations (22.4-30µs). The increase in pulse duration has been shown to increase in the modified layer thickness (Figure 6.4). Figure 6.10 shows the different extent of solute dispersion that can occur in the modified layers produced at different pulse durations. The lowest pulse duration of 22.4µs shows the least solute dispersion where as the cross-sections produced by longer pulse durations show extensive convection mixing.

The cross-section from the 27.6μs pulse duration Figure 6.10C shows solute dispersion at different depths within the modified layer, with the least dispersion at the base and the most near the top.

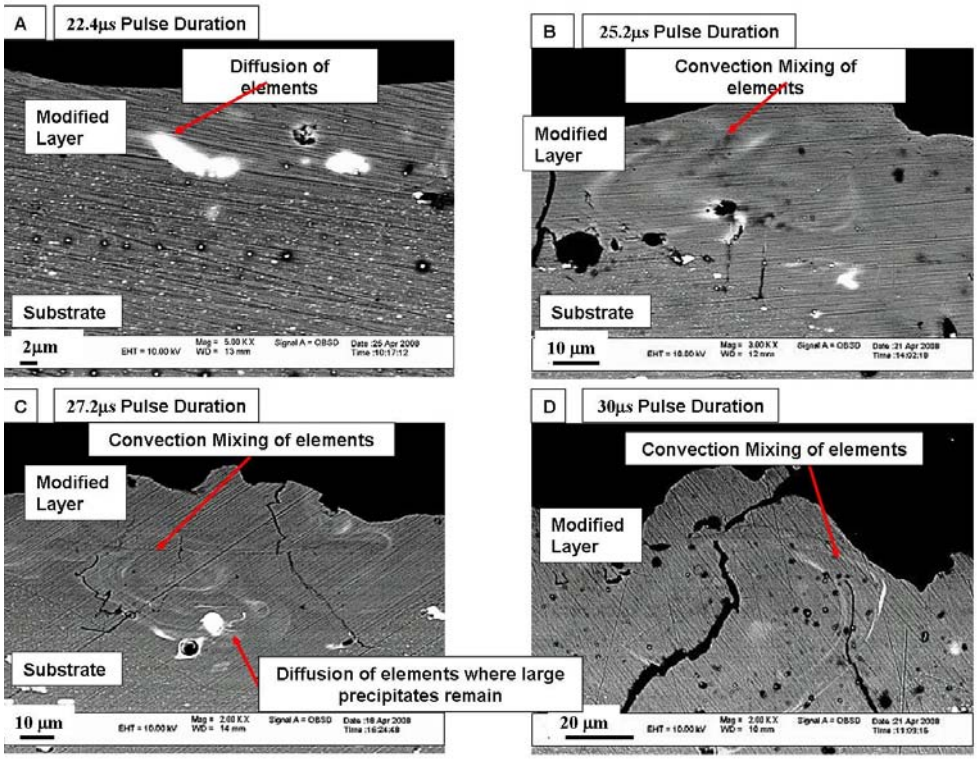

Figure 6.10 Backscattered SEM imaging of different amounts of element dispersion in USP-CO_2 laser surface melting on AA2024 with 1 pulse per unit area and varying pulse duration between 22.4 and 30μs. Surface prepared by non-aqueous polishing to 1μm.

An increase in pulse duration gave an increase in thickness and an increase in the dispersion of solute. Figure 6.11 shows backscattered SEM images of microstructure cross-sections of samples produced by USP-CO_2 LSM at 25.2μs pulse duration and varying number of pulses per unit area between 1 and 10 (prepared by non-aqueous polishing to 1μm finish). The images in Figure 6.11 illustrate the solute dispersion caused by variation in the number of pulses per unit area.

Figure 6.11 shows that solute dispersion by convection mixing occurred at each number of pulses per unit area. There is an increase in solute dispersion with increasing number of pulses. Even, however with the increase in mixing within the layer it can be seen in Figure 6.11 that some large precipitates still remain towards the base of the modified layer.

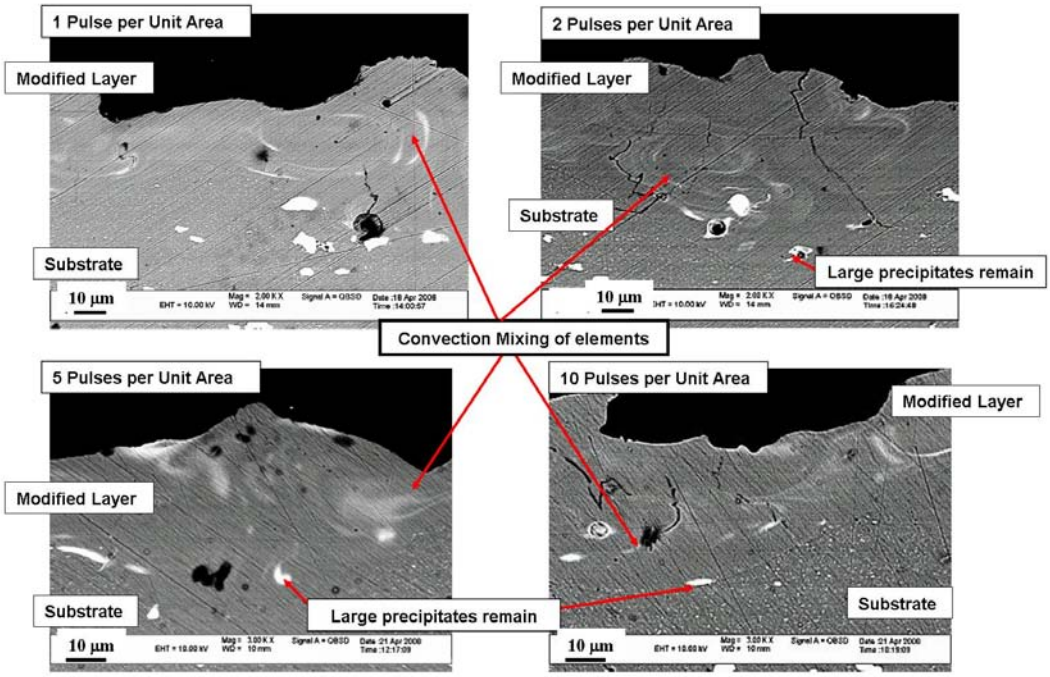

Figure 6.11 Backscattered SEM microstructure cross-section images of convection mixing in USP-CO_2 laser surface melting on AA2024 Pulse Duration 25.2µs with varying number of pulses per unit area (1 and 10). Surface prepared by non-aqueous polishing to 1µm.

6.4 Mixing and Cracking Onset

The amount of solute dispersion within the modified layer depended on the processing parameters. The dispersion of solute is an essential part of LSM as it is required to homogenise the surface and increase the corrosion resistance.

The amount of mixing that would be required to improve the corrosion resistance has not been quantified so the corrosion performance of the modified layers cannot be predicted. Analysis of the modified microstructure can provide some corrosion performance indication, as solute dispersion is needed but cracking needs to be avoided within the modified layer.

The onset of both mixing and cracking within the modified layers varies with the layer depth and also the processing parameters. Examination of the microstructure cross-sections for the modified layers, produced with variable pulse duration, allowed for the identification of the onset of solute dispersion by mixing and cracking as the modified layer thickness increased.

The onset of both cracking and mixing is shown in relation to pulse duration in Figure 6.12 for AA2024 and Figure 6.13 for AA7150 (layer thickness error bars at one standard deviation). These figures show that the onset of solute dispersion by mixing occurred within thinner layers than those that showed cracking, so layers were produced with mixing but no cracking.

6.5 Discussion

The USP-CO_2 was used for LSM treatment of AA2024 and AA7150. The modified layer thickness and structure did however vary with substrate alloy as has been seen in other work with excimer laser modification of these alloys by P. Ryan [31]. In the excimer LSM work the difference in alloy composition in particular zirconium was identified as the case for the solidification structure variation [31].

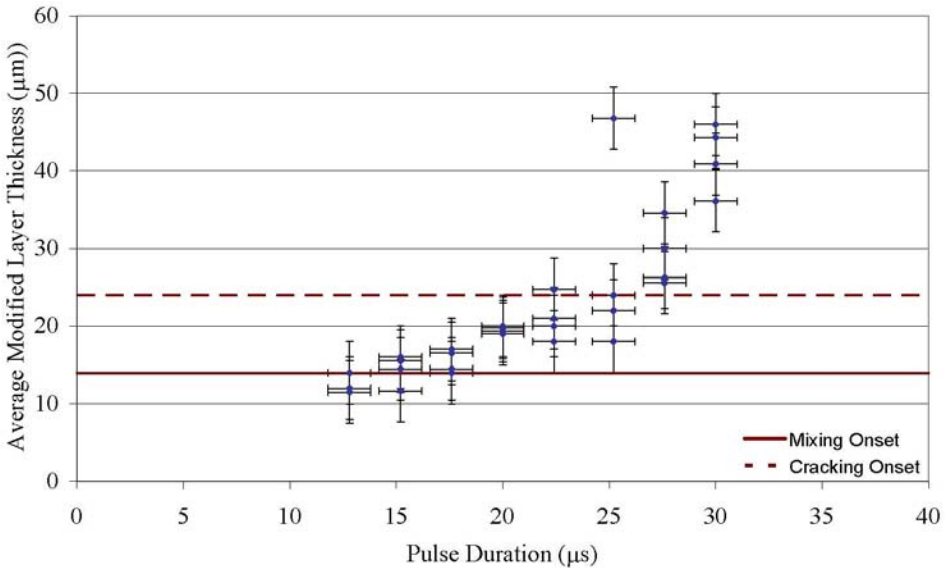

Figure 6.12 Graph of pulse duration versus average modified layer thickness of USP-CO_2 laser surface melting on AA2024, showing the onset of cracking and mixing. Error bars for the modified layer depth measurements are at one standard deviation based on a minimum of 10 measurements of modified layer thickness.

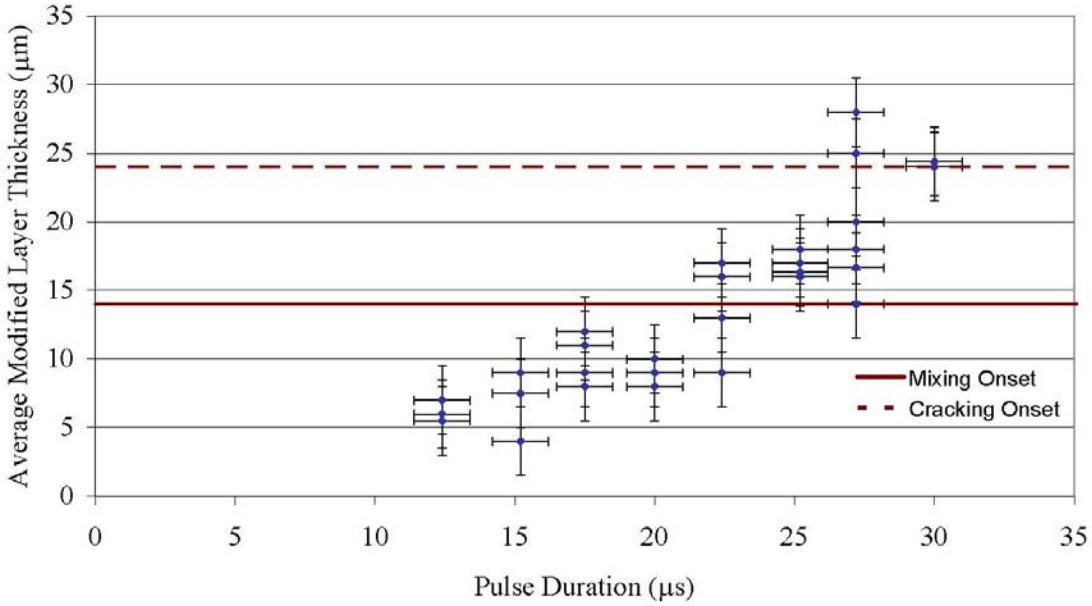

Figure 6.13 Graph of pulse duration versus average layer thickness for USP-CO_2 laser surface melting on AA7150 with the onset of mixing and cracking. Error bars for the modified layer depth measurements are at one standard deviation based on a minimum of 10 measurements of modified layer thickness.

In contrast to the excimer LSM on AA7150, LSM using the USP-CO_2 laser produced more features within the modified layer with a distinct boundary layer at the base of the modified layer. This feature was not clearly identified using electron microscopy but was thought to be related to the initiation of the columnar structure. A similar case was observed by P. Ryan in excimer LSM of AA7150 as at the base of the layer, the solidification front is at its slowest speed and this allowed time for precipitation and segregation which caused a columnar segregation structure throughout the modified layer [96].

In the USP-CO_2 LSM for both alloys treated the modified layer was discontinuous over the surface. The result of this was that spot treatments were produced as opposed to patches.

The discontinuous nature of the layer was due to variation in the laser interaction area between pulses and with processing parameters. In some conditions where the beam size was smaller than predicted this meant that the adjacent beam pulses were not overlapped as much as was calculated for and the treatment became discontinuous. This also means that an accurate number of pulses per unit area cannot be guaranteed.

Even with continuous treatments across the surface there was still a variation in melt depth across a beam interaction zone, due to intensity variation across the beam. This created a curved interface with the substrate. There needs to be further development of the experimental set-up to ensure that there is a more consistent interaction area.

USP-CO_2 LSM was used to treat AA2024 and AA7150 with variation in the pulse duration processing parameters. These investigations provided a correlation between the modified

layer thickness and the laser pulse duration for both alloys being treated. This was as predicted by the modelling described in Section 2.6.3 and found in other LSM work [96, 98].

In the variation of the number of pulses per unit area there were some concerns over the consistency in processing due to the varying overlap between pulses from changes in beam interaction area. The results considering this did not provide an increase in the modified layer thickness with an increase in number of pulses per unit area in the USP-CO_2 LSM treatment of either alloy tested.

Variation in the pulse duration provided a range of modified layer thicknesses for both alloys and in the examination of microstructure cross-sections solute dispersion was observed for both alloys.

The solute dispersion observed generally resulted in the dispersion of the smaller precipitates into solid solution and alteration in the shape of the larger precipitates into solute trails. There may also have been some dissolution and fragmentation of particles.

The extent of solute dispersion varied with modified layer depth, as larger precipitates were seen to remain at the base of the modified layers. The variation in which precipitates remained after LSM was due to differences in the precipitate properties in terms of solubility as well as size.

The time that the layer is molten for controls the amount of mixing and circulation that can occur. This was seen in Nd:YAG LSM of AA2024 and AA6061 where a decrease in

interaction time caused a decrease in the mixing that occurred within the modified layers [96]. Time is thought to be a factor as it was noted that precipitates remained at the base of the modified layer and this part of the layer was molten for the shortest amount of time. In comparison, solute at the top of the layer was more dispersed as these were molten for a longer period of time.

It was the case for both alloys that at a low number of pulses per unit area and a short pulse duration the least solute dispersion occurred. An increase in the processing parameters caused extensive material movement by mixing. The key processing parameter that increased mixing was the number of pulses per unit area.

The degree of movement within the layer is important for the dispersion of phases and an increase in the corrosion resistance. It is also important not to have cracking through the layer.

An increase in pulse duration used in USP-CO_2 LSM processing was found to increase the modified layer thickness. As the modified layer thickness increased mixing and cracking occurred.

At the pulse durations being used with this laser (15-30μs) mixing occurred within a thinner layer than cracking for both alloys. A layer thickness of 14μm for both alloys saw the onset of mixing in the modified layer but this was not a significant degree of mixing. Cracking in the layer occurred at a thickness of 18μm on AA2024. There is therefore a narrow processing band for there to be mixing and not cracking of the layer between 14 and 18μm for AA2024.

This corresponded to pulse durations between 15.2μs and 20μs, depending on the number of pulses per unit area.

Mixing occurred in the AA7150 specimens at layer thickness of 14μm which is consistent with AA2024 and the associated pulse duration was 17.5μs. For AA7150 samples cracking occurred at 24μm and this corresponded to a pulse duration of 27μs. In the case of the AA7150 the modified layer thickness range was between 14 and 24μm and this was associated with pulse duration of 17.5μs and 27.2μs. It was noted however, that at a low number of pulses there was no mixing with the layer even as the pulse duration increased. Overall these results suggest a larger processing range for the AA7150 than for the AA2024 concentrations.

6.6 Conclusions

- Increase in pulse duration increases layer thickness on laser treatment of both AA7150 and AA2024 alloys.
- Increasing the number of pulses per unit area increased the amount of convection mixing in the liquid phase within the modified layer, particularly for AA2024. This increased the solute dispersion within the modified layer.
- With increasing modified layer thickness convection mixing in the liquid phase occurred within the modified layer before cracking for both alloys. This provides a processing range to produce modified layers which experience convection mixing and solute dispersion before the layer becomes cracked.

7 Nd:YAG Laser Surface Melting

The Nd:YAG laser was used to investigate the effect of varying the laser pulse duration (between 10 and 50ms) and number of pulses per unit area (between 1 and 10) on the properties of the modified LSM layer for AA2024. The initial material etched microstructure cross-sections for AA2024, highlighting the precipitates present, is shown in Figure 7.1. The optical set-up for this laser (described in Section 3.2.7.2) produced a circular spot which was overlapped by manual translation of the sample.

7.1 Modified Layer

Typical etched microstructure cross-sections of the Nd:YAG LSM treatments using 1 pulse per unit area, 10ms and 50ms pulse durations are shown in Figure 7.2 and Figure 7.3, respectively. In both of these figures it can be seen that the modified layers are thick, 300-550µm, with micro-segregation and cracking.

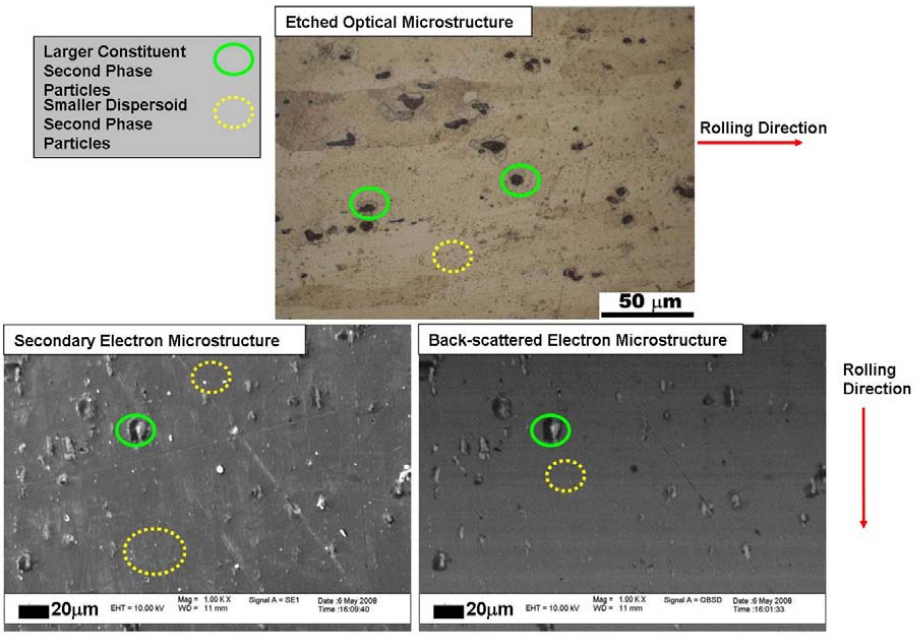

Figure 7.1 Microstructure cross-section of parent material AA2024 and AA7150.

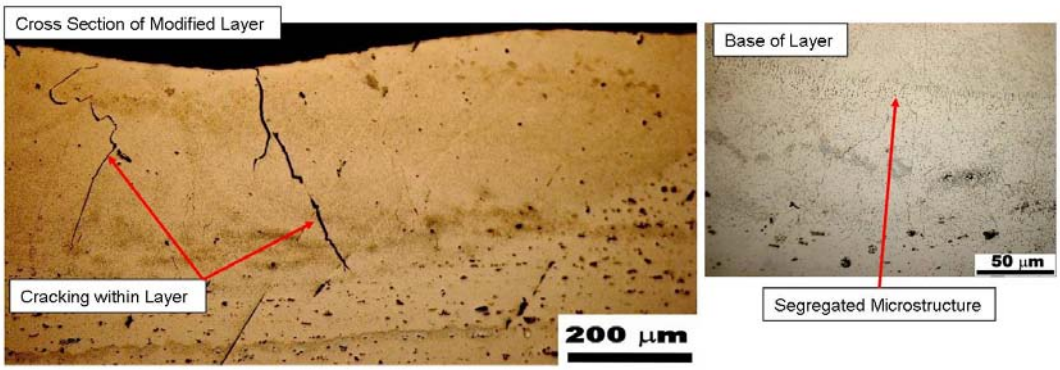

Figure 7.2 Typical etched microstructure cross-sections of Nd:YAG laser surface melting on AA2024, at 10ms pulse duration, 41.9J, 1 pulse per unit area.

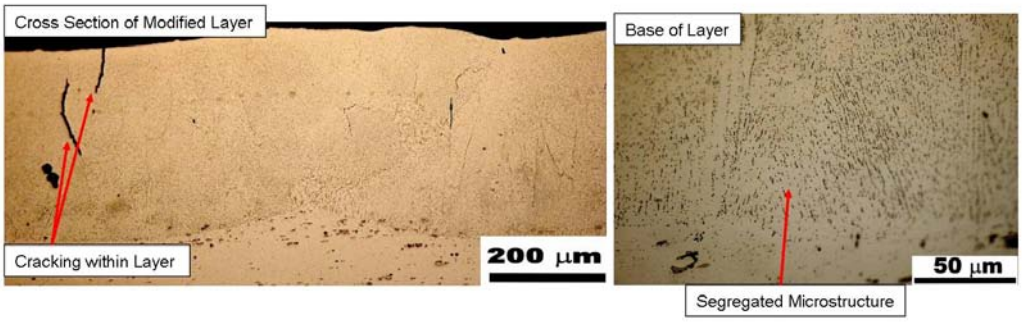

Figure 7.3 Typical etched microstructure cross-sections of Nd:YAG laser surface melting on AA2024, 50ms pulse duration, 70.7J, 1 pulse per unit area.

The micro-segregation present within the modified layer was examined by preparing cross-sections by non-aqueous polishing to 1µm surface finish and using backscattered SEM imaging. A typical example of the backscattered SEM Nd:YAG LSM modified layer using, 50ms pulse duration and 1 pulse per unit area, microstructure cross-section is shown in Figure 7.4. The contrast in this figure shows the composition differences across the modified layer with segregation of solute shown as white.

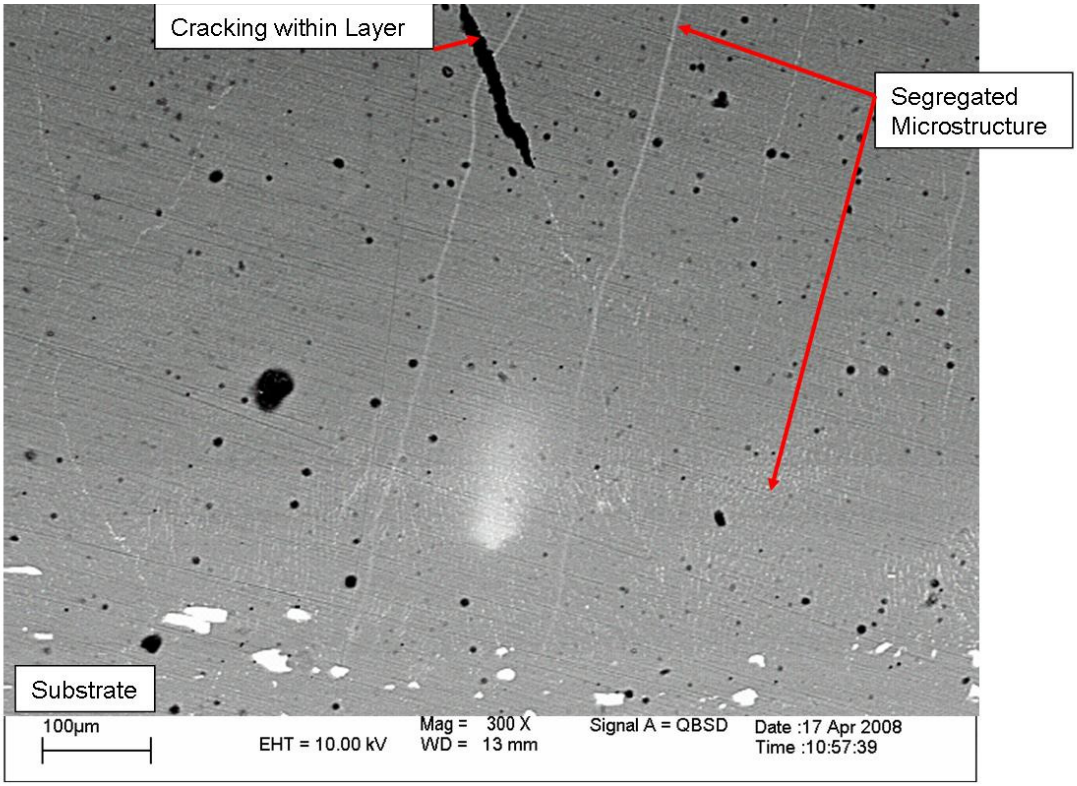

Figure 7.4 Backscattered SEM images of segregation in microstructure of Nd:YAG laser surface melted AA2024 at 50ms pulse duration, 59.2J, 1 pulse per unit area.

7.2 Modified Layer Thickness

The Nd:YAG laser was utilised for LSM investigations into the modified layer thickness as the pulse duration can be varied and two values of 10 and 50ms were used. Unfortunately it was not possible to vary the pulse duration without an associated change in the processing energy, which is illustrated graphically in Figure 7.5 with a plot of energy versus modified layer depth with different pulse durations. The error bars in Figure 7.5 for modified depth are at one standard deviation.

Figure 7.5 suggests that at 50ms pulse duration an increase in energy causes an increase in modified layer depth, but there were a limited number of samples with increasing energy and

this apparent increase in modified layer thickness could just be due to experimental scatter. Comparing the modified layer thicknesses produced from the different pulse durations in Figure 7.5 shows that between the two pulse durations tested there was not an increase in the modified layer depth. Due to this variation in energy therefore no definite conclusions can be drawn about the relationship between pulse duration and the modified layer thickness.

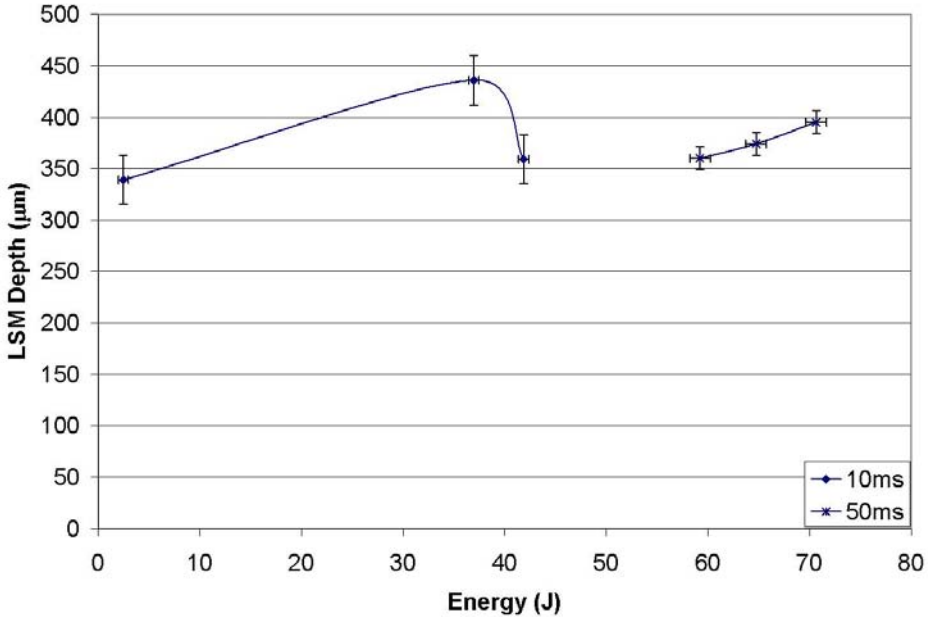

Figure 7.5 Graph of energy versus modified depth of Nd:YAG laser surface melting on AA2024. Error bars for the modified layer depth measurements are at one standard deviation based on a minimum of 10 measurements of modified layer thickness.

The number of pulses per unit area was the other laser parameter under investigation. Figure 7.6 shows typical etched microstructure cross-sections of modified layers produced with varying number of pulses per unit area (1-10) and a 50ms pulse duration. Figure 7.6 shows that increasing the number of pulses per unit area causes an increase in the porosity present within the modified layer.

Figure 7.7 plots LSM modified depth against the number of pulses per unit area for the two different pulse durations with error bars for melt depth at one standard deviation. This large degree of porosity increased the modified layer thickness with increasing number of pulses per unit area.

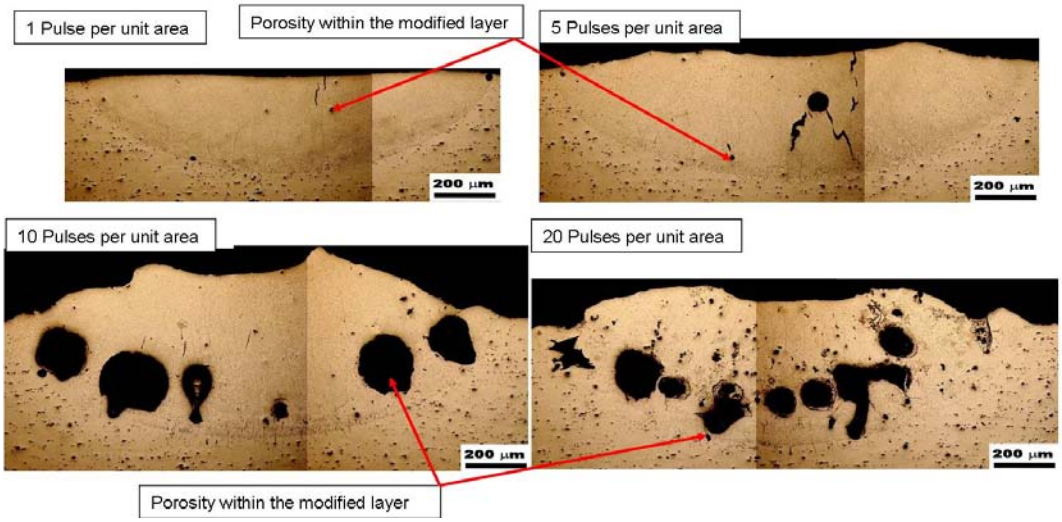

Figure 7.6 Microstructure cross-sections of porosity in Nd:YAG laser surface melting on AA2024, at 50ms Pulse Duration, 70.7J, with a variable number of pulses per unit area (1-10).

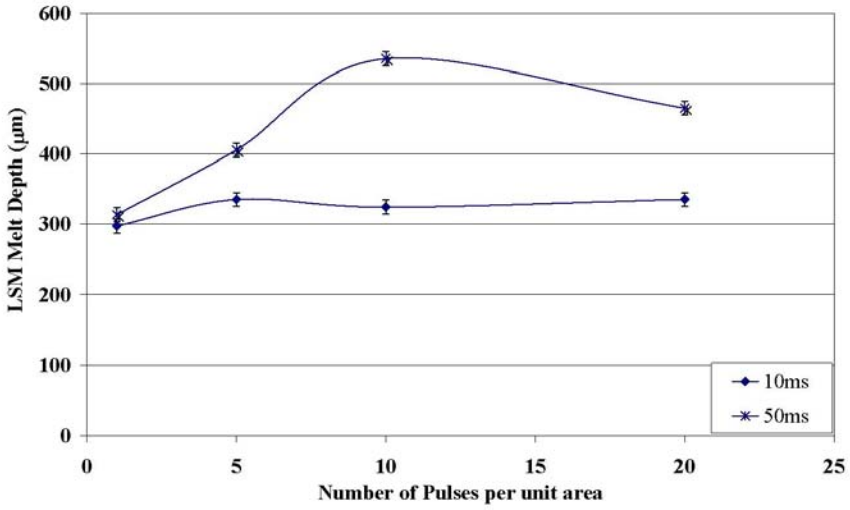

Figure 7.7 Graph of number of pulses per unit area versus modified depth in Nd:YAG laser surface melting on AA2024. Error bars for the modified layer depth measurements are at one standard deviation based on a minimum of 10 measurements of modified layer thickness.

7.3 Modified Layer Segregation

Figure 7.2 and Figure 7.3 show the typical etched microstructure cross-sections of the LSM modified layer produced by the different pulse durations at one pulse per unit area. These figures and the backscattered SEM image in Figure 7.4 show that there is segregation present within the modified layer. Further examination of the segregation within the modified layer was carried out using optical and backscattered SEM microscopy.

Examination of modified layers showed that there was a distinct boundary caused by segregation at the pulse overlap region. Figure 7.8 uses backscattered SEM imaging of Nd:YAG LSM at 50ms pulse duration and 1 pulse per unit area microstructure cross-sections, (prepared by non-aqueous polishing to 1μm) showing an overlap region where there is segregation and a change in segregation directionality.

The base of the modified layer was another area in which to examine the segregation. Typical microstructure cross-sections of the modified layer base from Nd:YAG LSM at 50ms pulse duration and 1 pulse per unit area are shown with optical microscopy in Figure 7.9. This figure shows that the segregation structure was not all aligned at the base of the modified layer but that there were different regions of orientation.

Examination of the segregation within the modified layer shows that there is a variation in segregation structure with depth. For a pulse duration of 50ms, 70.7J energy with layer depth 395μm, at the base of the layer segregated solute was at an average distance of 4μm where as at the top of the layer the separation had reduced to 1μm (average taken from a minimum of five measurements).

The degree of segregation was compared between the modified layers produced with different pulse durations. Figure 7.10 shows microstructure cross-sections using backscattered SEM imaging of modified layers produced using different pulse durations. Figure 7.10 shows that there is a difference between the segregation scale produced with different pulse durations, with the longer pulse duration producing a coarser segregation.

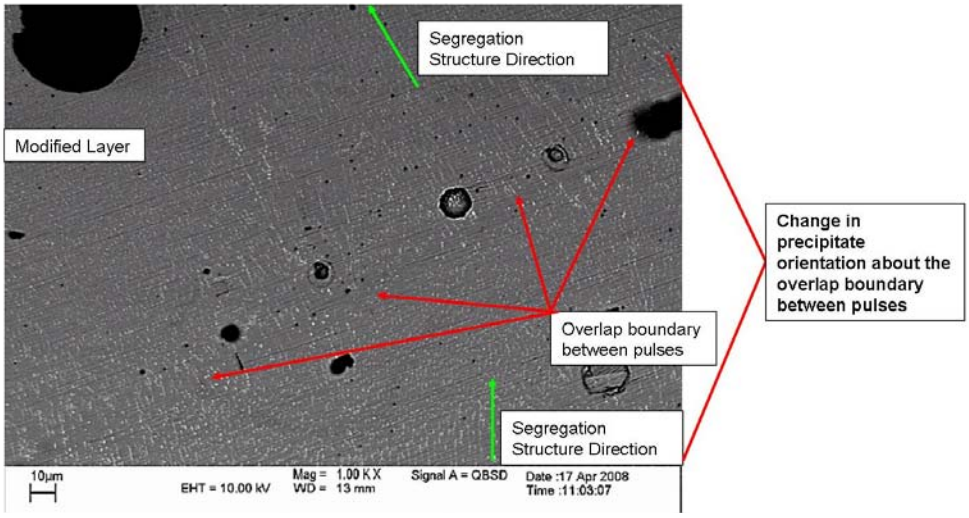

Figure 7.8 Backscattered SEM images at pulse overlap in Nd:YAG laser surface melting on AA2024, at 50ms pulse duration, 70.7J, 1 pulse per unit area.

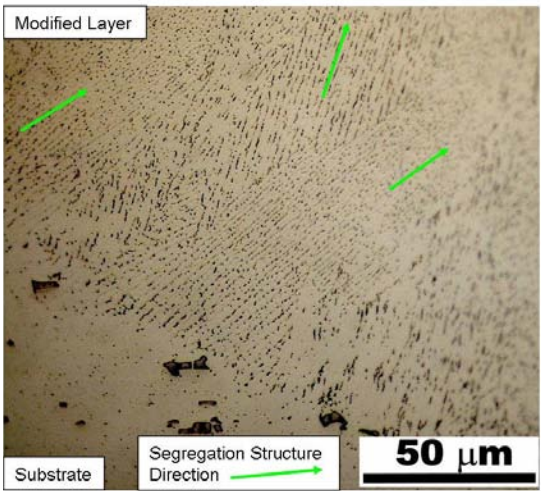

Figure 7.9 Microstructure cross-section of precipitate alignment at the modified layer base from Nd:YAG laser surface melting on AA2024, at 50ms pulse duration, 64.7J, 1 pulse per unit area.

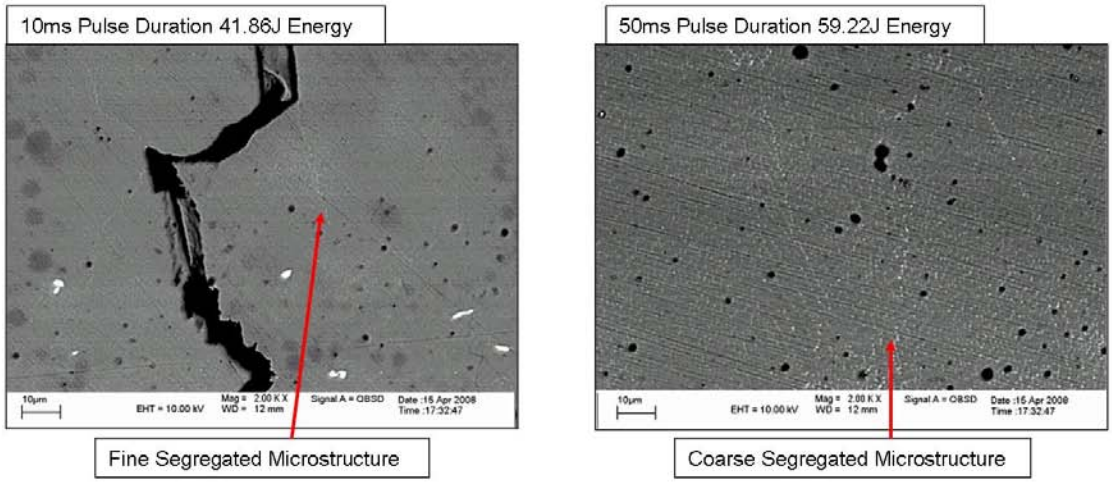

Figure 7.10 Backscattered SEM images of microstructure segregation at 10 and 50ms pulse duration in Nd:YAG laser surface melting on AA2024.

7.4 Corrosion Testing

A limited number of microelectrochemical corrosion resistance tests (described in Section 3.6.2) were performed on the Nd:YAG LSM samples using 0.1M NaCl solution, a scan rate of 1mV/s and an Ag/AgCl reference electrode.

These tests compared the cathodic and anodic activity of LSM and untreated parent material. The results of the anodic and cathodic polarisation tests are shown in Figure 7.11 and Figure 7.12 respectively. Both of these figures show that the LSM treatment produced a lower corrosion resistance compared to the parent material as the LSM surfaces had increased current density, which increases the rate of corrosion (described further in Sections 2.3 and 3.6.2).

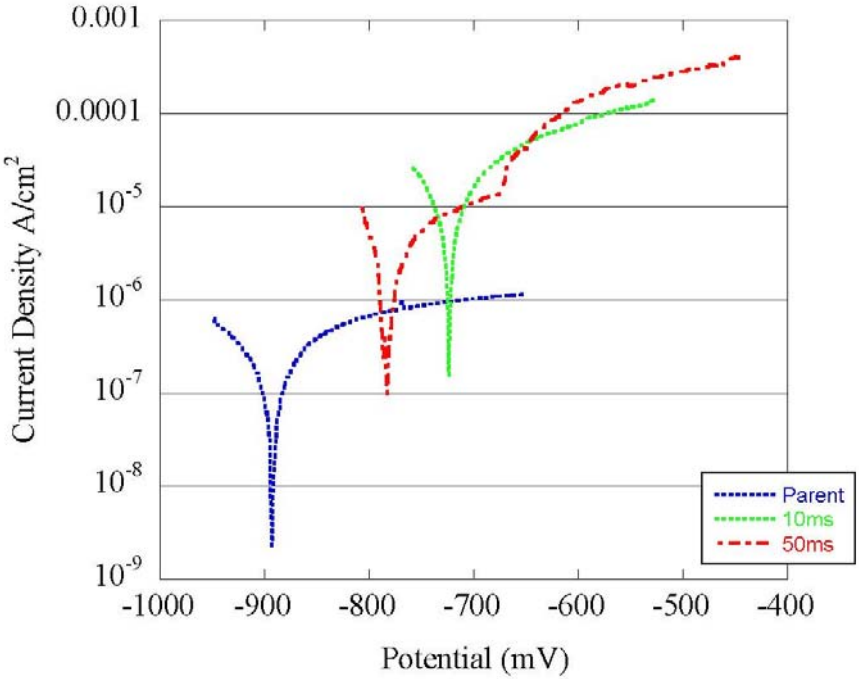

Figure 7.11 Electrochemical anodic polarisation following Nd:YAG laser surface melting of AA2024 at 10 and 50ms pulse duration compared with the parent alloy measured using a micro-electrochemical cell with 0.1M NaCl solution 1mV/s scan rate, Ag/AgCl reference electrode.

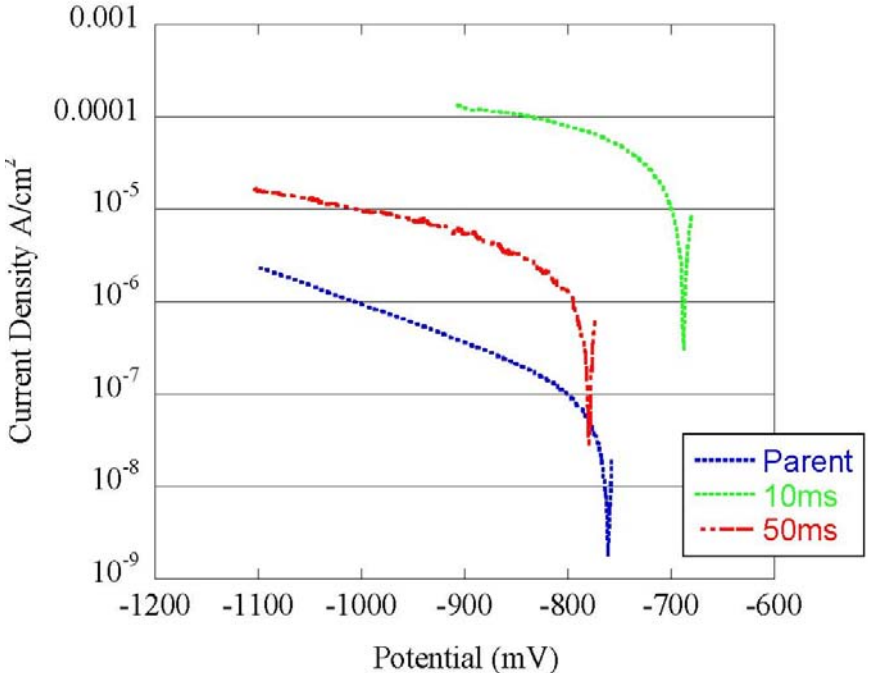

Figure 7.12 Electrochemical cathodic polarisation following Nd:YAG laser surface melting of AA2024 at 10 and 50ms pulse duration compared with the parent alloy measured using a micro-electrochemical cell with 0.1M NaCl solution 1mV/s scan rate, Ag/AgCl reference electrode.

7.5 Discussion

The Nd:YAG laser was used to investigate the effect of pulse duration on the thickness and microstructure of the LSM modified layer on AA2024.

The Nd:YAG LSM treatments of AA2024 produced large modified layers (~350μm) which had long solidification times. This meant that there was sufficient time for segregation to occur within the Nd:YAG LSM modified layer. Such segregation with the large melt layer depth was predicted in a detailed microstructure study of AA2024 excimer LSM at The University of Manchester [31] and this was also observed in LSM on AA2024-T651 at The University of Liverpool using a CO_2 laser [109].

The Nd:YAG laser treatments were performed using variable pulse duration, of 10 and 50ms and this was a six orders of magnitude increase in the pulse duration compared with the excimer laser pulse duration of 25ns. This large increase in pulse duration was predicted by modelling to increase the modified layer thickness (Section 2.6.3). The observations were consistent with the predictions as thicker layers were produced with the Nd:YAG (average modified layer thickness ~350μm) compared with those from excimer LSM laser (average modified layer thickness 5μm).

The increase in pulse duration between the excimer and the Nd:YAG laser produced a significant increase in modified layer thickness. However, the increase in pulse duration between the two tests performed with the Nd:YAG laser (10 and 50ms) did not result in an increase in the modified layer thickness, which was a five fold increase compared with the

increase of six orders of magnitude from the excimer laser. It may have been that the increase in pulse duration between 10 and 50ms may not have been large enough to observe an increase in the layer thickness.

It must also be noted that the energy of the laser was not kept constant with the change in pulse duration and that at 50ms pulse duration an energy increase gave an increase in the modified layer thickness, but further investigations would be required to confirm this.

The increase in pulse duration between 10 and 50ms may not have exhibited conclusive effects on the modified layer thickness, but the microstructures between the two tests did show significant differences in terms of segregation. It was observed that the segregation varied with depth within the modified layer with finer segregation towards the modified layer surface. This change in segregation spacing was due to acceleration of the solidification front from stationary at the base of the layer to a maximum speed at the surface, this has been observed in other work with cw-Nd:YAG laser [82] and pulsed lasers [31, 74].

The solidification front moves from the base of the melt pool towards the surface as the substrate acts as the heat sink to remove energy from the melted surface material. The heat is therefore always removed from the base of the melt pool. The base of the melt pool is always the coolest point of the modified layer and solidification is nucleated heterogeneously on the substrate surface.

The speed of the solidification front depends on the thermal gradient (and therefore the melt depth) and depicts which solidification microstructure is produced. The faster the

solidification front the less time there is for segregation and a more homogenous microstructure results. A slower solidification time allows for segregation, which was observed in the Nd:YAG LSM samples. This effect of solidification parameters on the LSM microstructure was investigated in work from The University of Manchester [31, 71, 78].

The segregation within the modified microstructure also exhibited directionality with there being distinct regions of alignment, particularly at the laser pulse overlap and the base of the layer. It was thought that this directionality was due to the direction of heat dissipation and therefore segregation within the modified layers signified changes in the solidification conditions. However, it should also be considered that the directionality would also be influenced by crystallography variations within the modified layer.

The aim of LSM treatments was to improve the corrosion resistance of the surface which is related to the segregation and heterogeneity of the microstructure [18]. A surface with high corrosion resistance requires minimal heterogeneity and segregation [47]. The segregation formed from Nd:YAG LSM decreased the corrosion resistance of the surface in comparison to the parent material.

The Nd:YAG LSM modified layers that exhibited less segregation, i.e. finer precipitates and less heterogeneity, were the layers produced by a shorter pulse duration. These modified layers from the shorter pulse durations should have shown an increase in the corrosion resistance compared with the longer pulse duration however this was not seen consistently in the limited number of tests that were possible.

The Nd:YAG laser produced thick modified layers that were heterogeneous due to segregation and this meant that the surface had poor corrosion resistance compared with the parent material.

7.6 Conclusions

- The LSM layers produced with the Nd:YAG laser were thicker than those produced with the excimer laser, which was attributed to the increase in pulse duration.
- The high layer thickness meant that segregation was present in the LSM layer owing to a lower cooling rate.
- The corrosion resistance of the Nd:YAG LSM layer was found to be less then that of the parent material.

8 Electron Beam Surface Melting

An electron beam system was developed at BAE Systems ATC to investigate Electron Beam Surface Melting (EBSM) for comparison with Laser Surface Melting (LSM) of AA2024. Etched microstructure cross-sections of the initial AA2024 material, highlighting the precipitates present, are shown in Figure 8.1. The electron beam system (described in Section 3.3) processing parameters are variable pulse duration (5-40μs), energy (1.5-6J) and number of pulses per unit area (1-80).

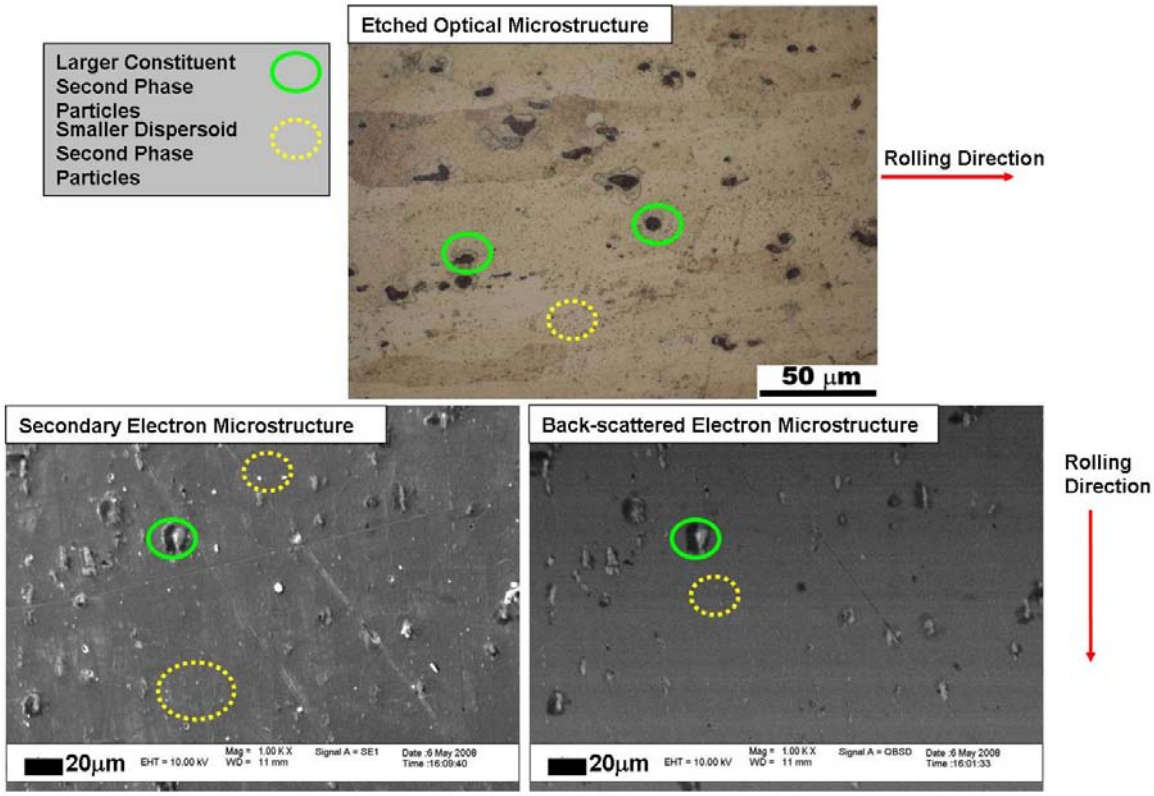

Figure 8.1 Etched microstructure cross-section of parent material AA2024.

8.1 Surface Modification

EBSM on AA2024 was performed to ascertain the effect of each of the variable processing parameters on the microstructure modification. The EBSM treatments were performed at and around the beam focus, by changing the cathode separation.

Figure 8.2 shows the variation in beam energy with changes in cathode separation and that there is a peak in the energy when the beam focuses (error bars at one standard deviation of measurements). The degree of beam focus depicts the energy density available for processing and in EBSM this alters the modified layer thickness, shown in Figure 8.3, and the melt zone surface appearance, shown in Figure 8.4. Figure 8.3 shows that with varying cathode separation the modified layer thickness increases towards the focus, but at the focus the modified layer thickness is reduced. Figure 8.4 shows that variation in the cathode separation changes the EBSM melt zone size and appearance from uniform to non-uniform with a highly reflective centre.

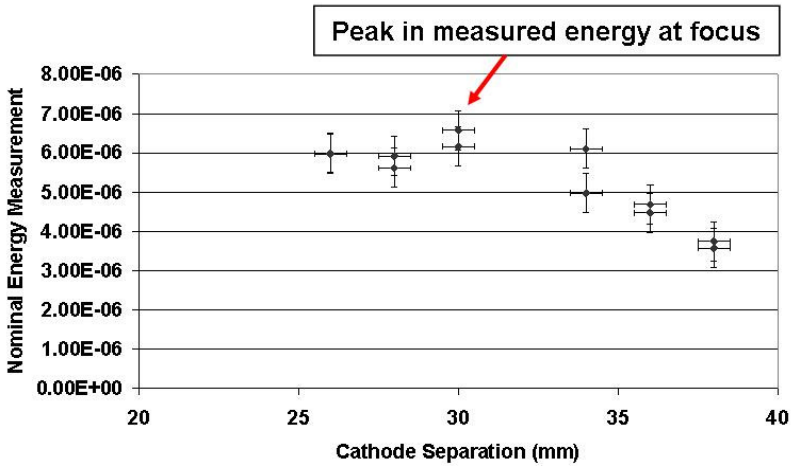

Figure 8.2 Graph of cathode separation versus nominal energy measurement for 20µs pulse duration, 3J and 1 pulse per unit area. Error bars are at one standard deviation based on a minimum of 3 measurements.

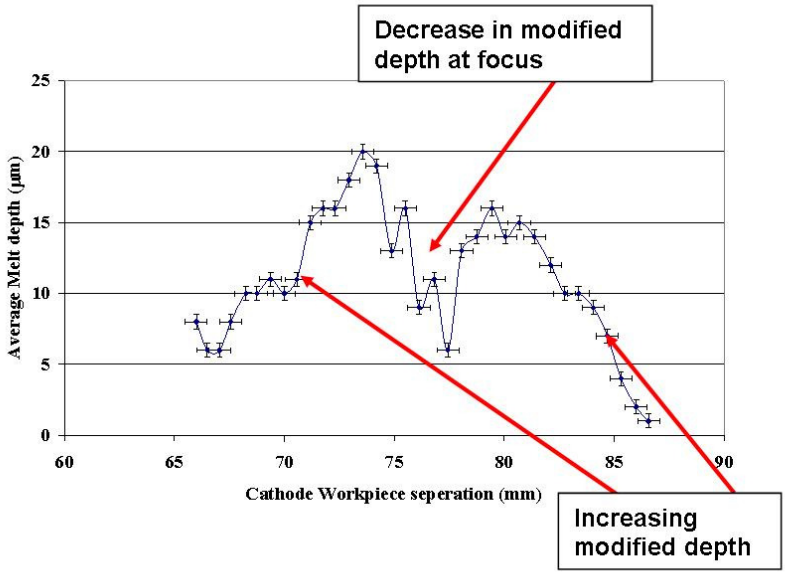

Figure 8.3 Graph of cathode separation versus modified depth for 5µs pulse duration, 5.3J and 1 pulse per unit area. Error bars for the modified layer depth measurements are at one standard deviation based on a minimum of 10 measurements of modified layer thickness.

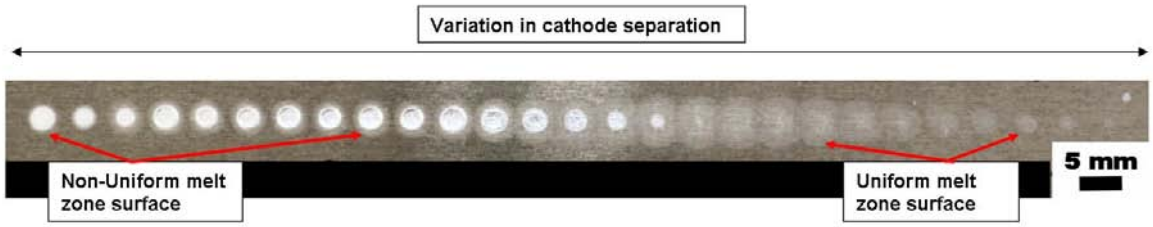

Figure 8.4 Image of varying surface appearance for 20µs pulse duration, 1 pulse per unit area, 6J from changing cathode separation.

The characteristic melt zone surface appearances, uniform and non-uniform, produced in EBSM are shown in Figure 8.5 along with their associated typical etched microstructure cross-sections. Figure 8.5 shows that the non-uniform melt zone microstructure has more cracking compared with the uniform melt zone.

Another feature of the non-uniform melt zone of Figure 8.5 was shown by EDX analysis with results presented in Figure 8.6. Figure 8.6 shows that the non-uniform melt-zone has a variation in composition across the melt zone and in the central reflective region there is a change in element concentrations, particularly a decrease in magnesium, which suggests vaporisation. The changes in the other element concentrations may not be statistically significant.

EBSM at set processing parameters produced a range of melt zone appearances depending on the beam focus. Investigations into EBSM at different processing parameters required comparisons of samples that had similar melt zone appearances.

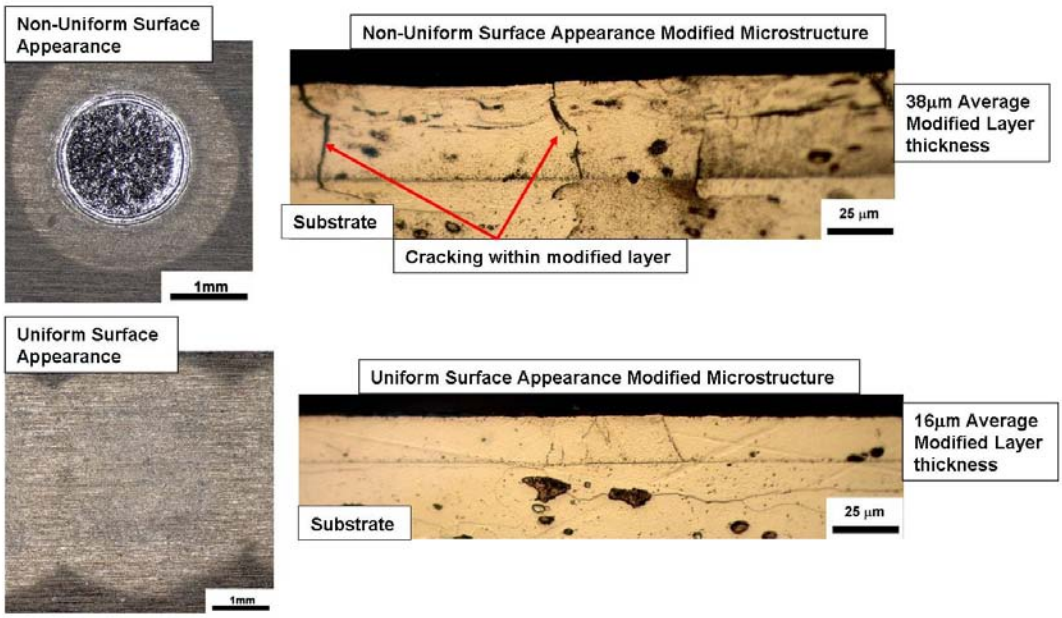

Figure 8.5 Examples of uniform and non-uniform melt zone surface appearances and their associated etched microstructure cross-sections produced in electron beam surface melting of AA2024 at 20µs pulse duration, 6J, 1 pulse per unit area.

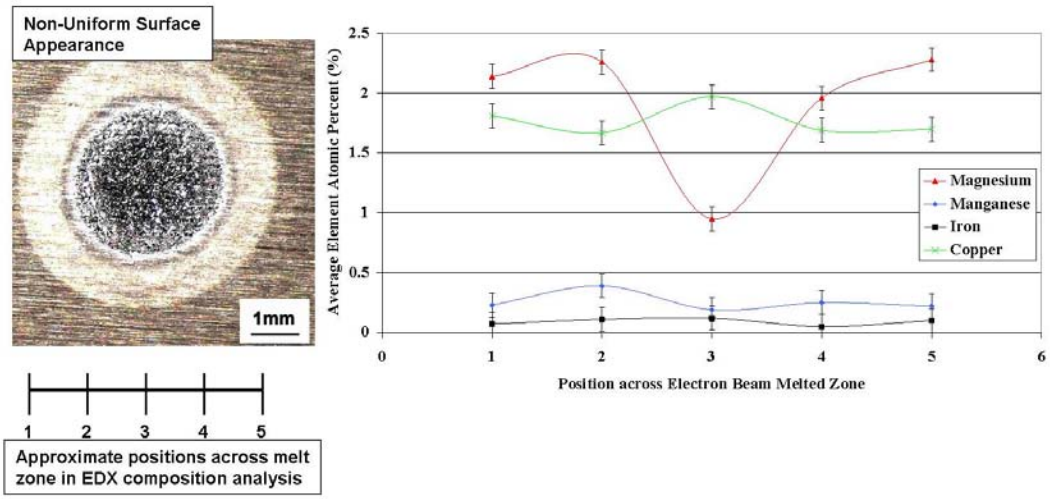

Figure 8.6 Image of the surface appearance of a non-uniform surface electron beam melt zone (6J, 20μs pulse duration, 1 pulse per unit area) with graph of EDX compositional analysis showing variation in composition across the melt zone. The error bars are those produced in EDX quantification process.

8.2 Modified Layer Microstructure

In EBSM there are common microstructure features for both melt zone surface appearances: precipitate dissolution, solute dispersion, minimal precipitation, epitaxial growth from the substrate and cracking.

Figure 8.7 is an etched EBSM microstructure cross-section (4 pulses per unit area, 8J, 20μs pulse duration) showing typical precipitate dissolution and solute dispersion observed in EBSM. Comparing the modified layer precipitate content with that of the substrate in Figure 8.7 shows that in the modified layer there are fewer small precipitates (complete dissolution) and the larger constituent precipitates have changed shape forming trails (partial dissolution). Solute dispersion is also apparent in Figure 8.7 as the small precipitates have not reformed and the larger precipitates are distorted.

Figure 8.8 further illustrates the change in precipitate content in the EBSM modified layers (40µs pulse duration, 4J and 10 pulses per unit area) using SEM imaging and EDX composition mapping analysis. This figure shows that within the modified layer the elements inherent to precipitates, for example copper, are still concentrated in some regions but there is also a distribution of these elements between these localised points. EBSM has therefore caused precipitate dissolution and solute dispersion which increased the surface homogeneity.

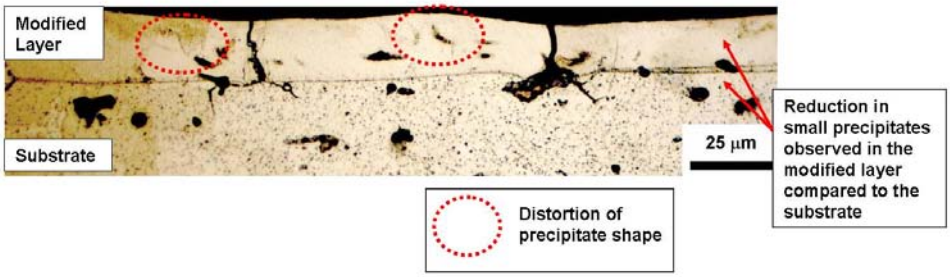

Figure 8.7 Typical etched microstructure cross-sections with precipitate trails within the modified layer from electron beam surface melting on AA2024 at 20µs pulse duration,2.5J and 4 pulses per unit area.

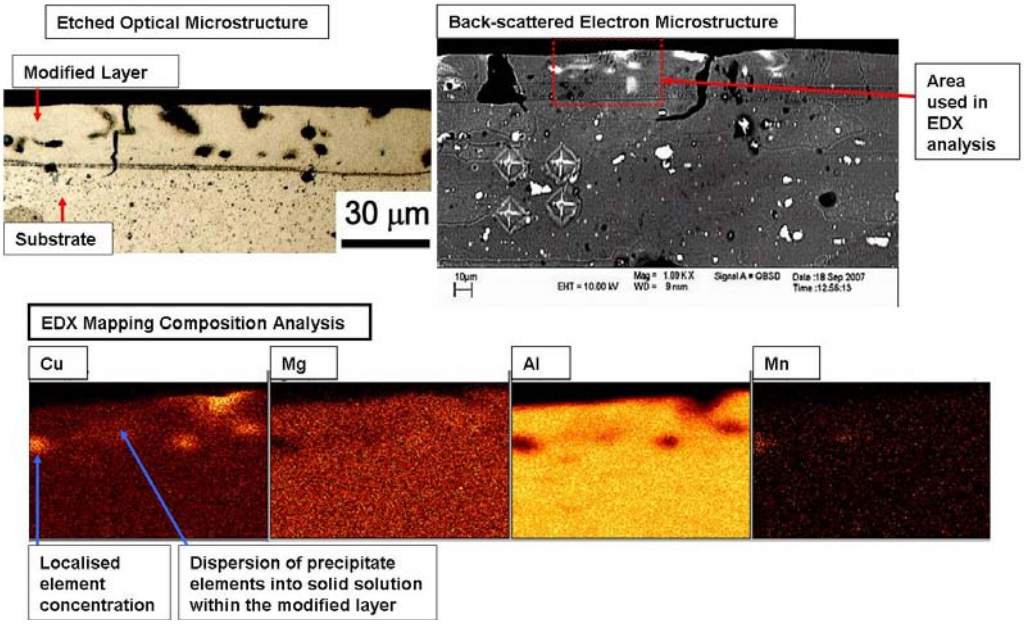

Figure 8.8 Optical and backscattered SEM images of element mixing with EDX composition analysis of electron beam surface melting on AA2024 at 40µs pulse duration, 4J and 10 pulses per unit area.

Other common microstructure features are highlighted in the etched EBSM microstructure cross-sections of Figure 8.9 and are related to solidification: formation of grain structure from epitaxial solidification (Figure 8.9A), precipitation parallel to the surface (Figure 8.9A and B) and precipitation perpendicular to the surface (Figure 8.9B).

Epitaxial solidification that occurs in EBSM is shown in Figure 8.9A where the grain structure within the modified layer is continued from the substrate. The boundary between the modified layer and the substrate is marked by the fine line of precipitates that generally form parallel to the surface in the centre of the melt zone. Curvature in these lines of precipitates occurs towards the edges of the melt zone and when there has been large scale movement within the modified layer causing undulations across the surface.

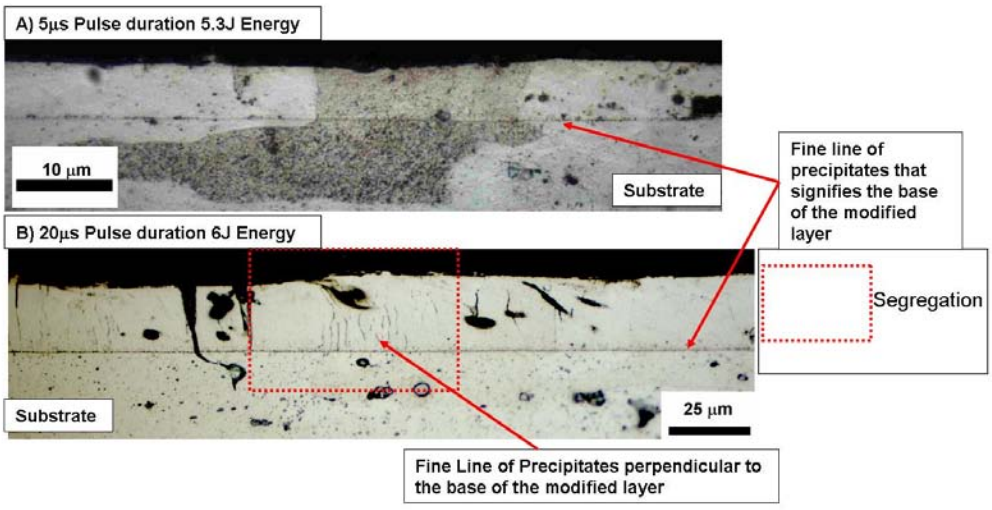

Figure 8.9 Etched microstructure cross-sections showing influence of the substrate on solidification structure and segregation in modified layer produced by electron beam surface melting on AA2024 1 pulse per unit area, variable pulse duration (5-20μs) and variable energy (5.3-6J).

Figure 8.9B shows lines of precipitates parallel and perpendicular to the surface. Measurements from the line of precipitates parallel to the surface provided an average (minimum of five measurements) modified layer thickness of 25μm for this treatment.

In most EBSM treatments the base of the modified layer is clearly defined by lines of precipitates. However, Figure 8.10 shows that there are EBSM treatment (20μs pulse duration, 2.5J and 80 pulses per unit area) where this is not the case. The EBSM modified microstructure shown in Figure 8.10 using backscattered SEM imaging (prepared by non-aqueous polishing to 1μm surface finish) showed a curved surface and the lines of precipitates towards the base of the modified layer formed over a range of depths. This separation of precipitate lines was found in EBSM treatments with a high number of pulses per unit area but the lines of precipitates did not have a one to one correlation with the number of pulses used in treatment.

Another feature of the line of precipitates at the base of the layer is shown in the etched EBSM (20μs pulse duration, 2J energy and 1 pulse per unit area) microstructure cross-section in Figure 8.11 where there is a deviation in the line of precipitates due to the influence of nearby large constituent particles.

The final common feature in the EBSM microstructures is cracking and this has been observed to occur around solidification features: precipitates and grain boundaries. Figure 8.12 shows etched microstructure cross-sections of EBSM treatments (20μs pulse duration, 2.5-3J and 1-20 pulses per unit area) which are typical examples of cracking observed: within

the layer at grain boundaries which continue into the substrate and along the base of the modified layer.

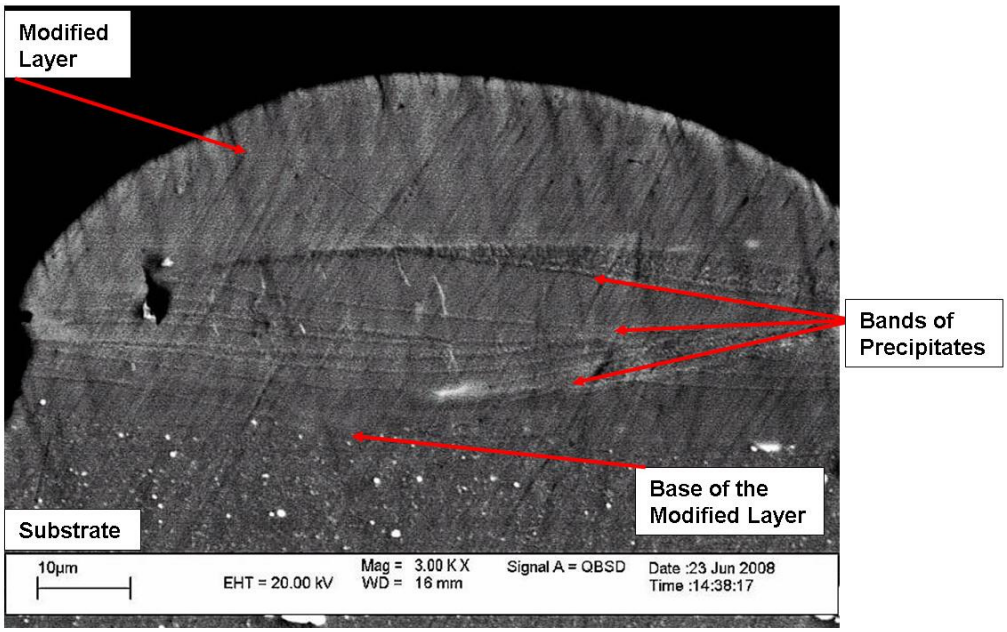

Figure 8.10 Typical un-etched (surface preparation was non-aqueous polishing to 1µm finish) microstructure cross-sections of precipitate banding throughout the modified layer using backscattered SEM imaging of electron beam surface melting of AA2024 at 20µs pulse duration, 80 pulses per unit area and 2.5J.

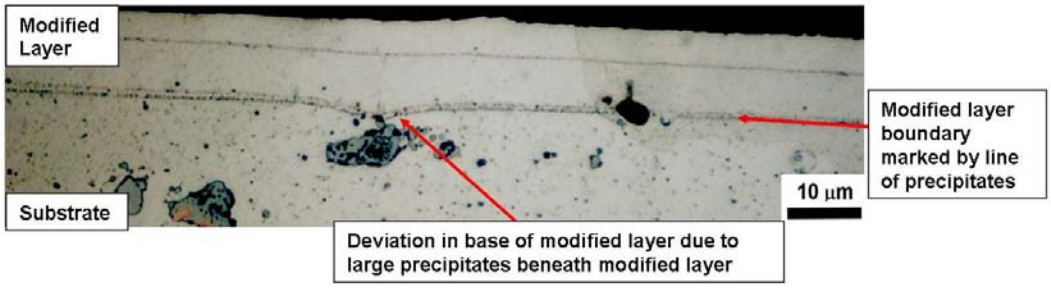

Figure 8.11 Etched microstructure cross-sections of precipitate line marking the base of the modified layer which deviates due to large precipitates in the substrate in electron beam surface melting on AA2024 at various processing parameters (20µs pulse duration, 1 pulse per unit area and 2J energy).

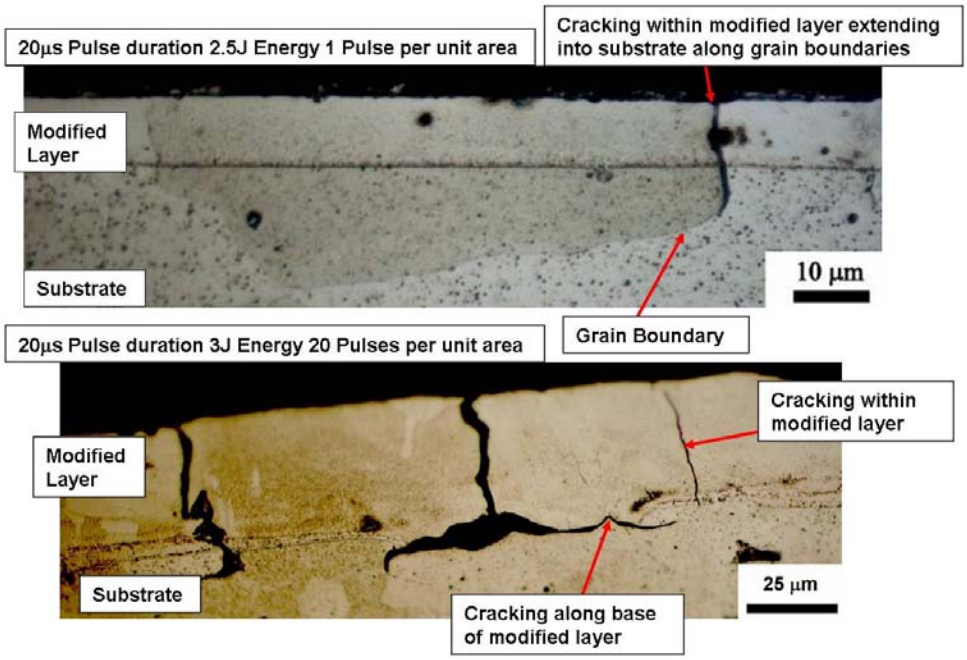

Figure 8.12 Etched microstructure cross-sections of cracking along grain boundaries, within the modified layer and at the base of the modified layer in electron beam surface melting on AA2024 at 1 and 20 pulses per unit area, 20µs pulse duration, 2.5 and 3J.

8.3 Modified Layer Thickness

The aim of EBSM was to produce a layer that was homogeneous and of adequate thickness to survive anodising. Variation in EBSM processing parameters was used to alter microstructure modification in terms of the microstructure features (described in previous section) and particularly the modified layer thickness.

Figure 8.13 shows the relationship between cathode separation and the average modified layer thickness for EBSM at variable pulse durations (10 and 20µs), 6J and 1 pulse per unit area, with error bars set at one standard deviation. The results in Figure 8.13 are offset for the different pulse durations due to the change in electron beam focus with processing

parameters. Comparison can be performed between these two pulse durations as both were performed around the focus. The treatment at 20μs produced more results as there was greater cathode stability.

Figure 8.13 shows that increasing pulse duration from 10 to 20μs increased the modified layer thickness.

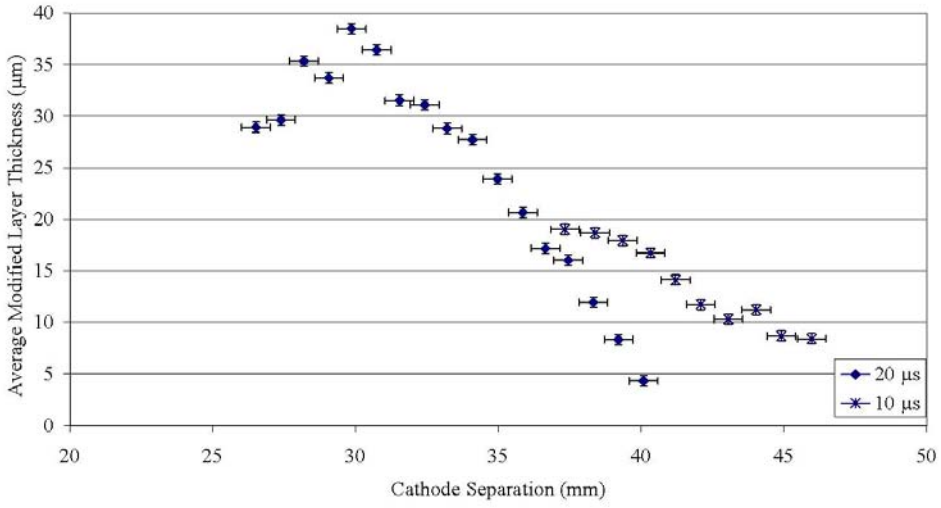

Figure 8.13 Graph of cathode separation versus modified layer thickness for electron beam surface melting at 6J, 1 pulse per unit area, and variable pulse duration, 10 and 20μs. Error bars for the modified layer depth measurements are at one standard deviation based on a minimum of 10 measurements of modified layer thickness.

To compare EBSM treatments performed at different processing energy it was necessary to compare melt zones of similar appearance. The uniform melt zones appearances were used as they provided more consistent microstructure modification. Figure 8.14 shows that for uniform surface appearance melt zones an increase in EBSM energy (3-8J) at 20μs pulse

duration and 1 pulse per unit area, increased the average modified layer thickness (error bars set at one standard deviation).

The other processing variable under investigation was the number of pulses per unit area and Figure 8.15 shows the influence of this variable on the average modified layer thickness with error bars at one standard deviation, 20μs pulse duration and variable energy (2-3J). Figure 8.15 shows that increasing the number of pulses per unit area at a constant energy did not greatly change the modified layer thickness, but there is a larger influence on modified layer thickness from the energy variation.

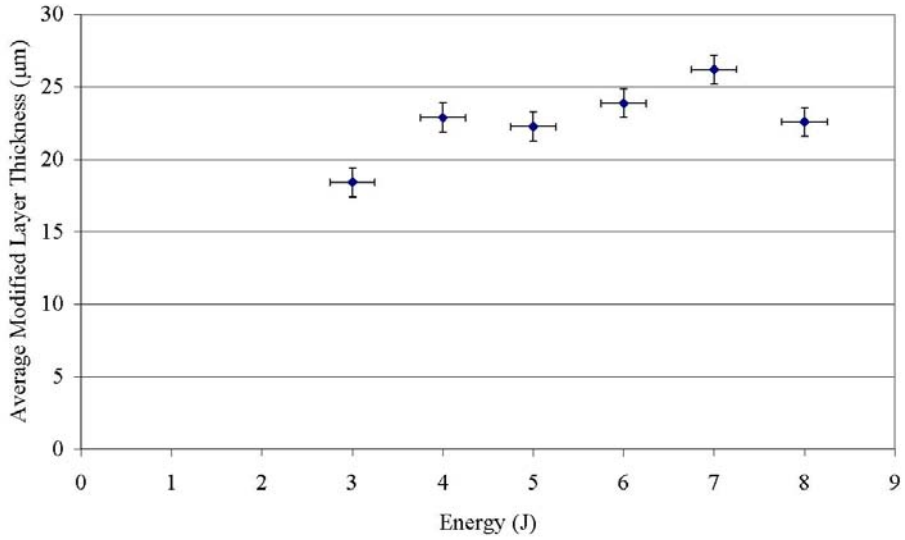

Figure 8.14 Graph of energy versus average modified layer thickness for electron beam surface melting of AA024 at 20μs pulse duration and 1 pulse per unit area. Error bars for the modified layer depth measurements are at one standard deviation based on a minimum of 10 measurements of modified layer thickness.

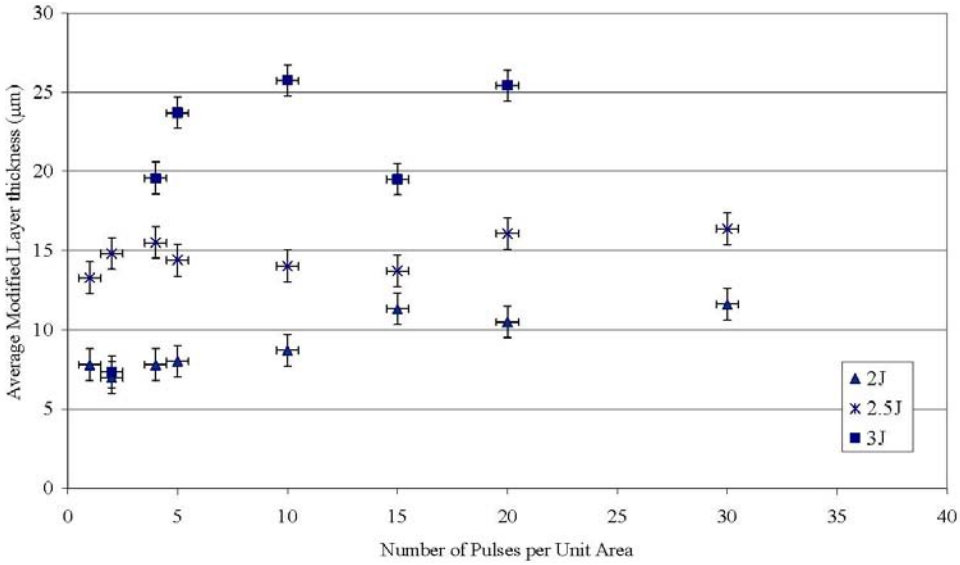

Figure 8.15 Graph of number of pulses per unit area versus average modified layer thickness with energy between 2 and 3J for electron beam surface melting at 20µs pulse duration. Error bars for the modified layer depth measurements are at one standard deviation based on a minimum of 10 measurements of modified layer thickness.

8.4 Modified Layer Thickness and Anodising

Figure 8.13 and Figure 8.14 show that an increase in modified layer thickness can be produced by an increase in either the processing energy or the pulse duration. Generally all EBSM treatments performed produced modified layers of reasonable thickness. It was necessary to investigate whether these modified layer's thicknesses were adequate to survive a chromic acid anodising (CAA) process.

EBSM at set processing parameters (4J, 5µs pulse duration and 1 pulse per unit area) with varying cathode separation was used to produce a range of modified layer thicknesses that were then treated with CAA. Figure 8.16 and Figure 8.17 show typical etched microstructure cross-sections of non-uniform and uniform EBSM melt zones that were anodised. The EBSM

layer on the non-uniform melt zone sample (20μm) was thicker than on the uniform sample (9μm). Both of these figures show that the EBSM layers were thick enough to survive anodising for both the melt zone appearances.

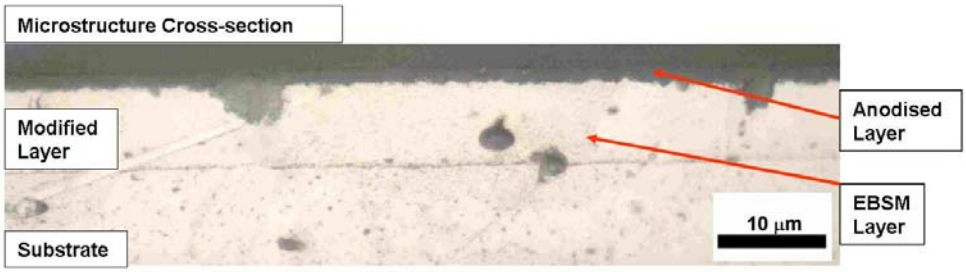

Figure 8.16 Non-uniform melt zone etched microstructure cross-section electron beam surface melted AA2024 at 4J, 5μs pulse duration and 1 pulse per unit area, coupled with chromic acid anodising.

Figure 8.17 Uniform melt zone etched microstructure cross-section electron beam surface melted AA2024 at 4J, 5μs pulse duration and 1 pulse per unit area, coupled with chromic acid anodising.

8.5 Increase in Modified Layer Homogeneity by Solute Dispersion

The typical EBSM modified layer thickness was large enough to survive anodising and could be controlled by variation in the energy and pulse duration. The other key feature for HPBSM to increase the corrosion resistance of the surface was an increase in the surface homogeneity

by the removal of precipitates through: dissolution, solute dispersion and planar solidification to retain the dispersion.

EBSM has been observed to cause solute dispersion within the modified layer (Figure 8.8). Figure 8.18 uses backscattered SEM imaging (prepared by non-aqueous polishing to 1µm surface finish) to show typical microstructure cross-sections with different degrees of solute dispersion that were observed in EBSM treatments (40µs pulse duration, 10 pulses per unit area and varying energy 4-6J). This solute dispersion has been observed in some EBSM to a large scale shown in the EBSM microstructure cross-section in Figure 8.19, using backscattered SEM imaging (prepared by non-aqueous polishing).

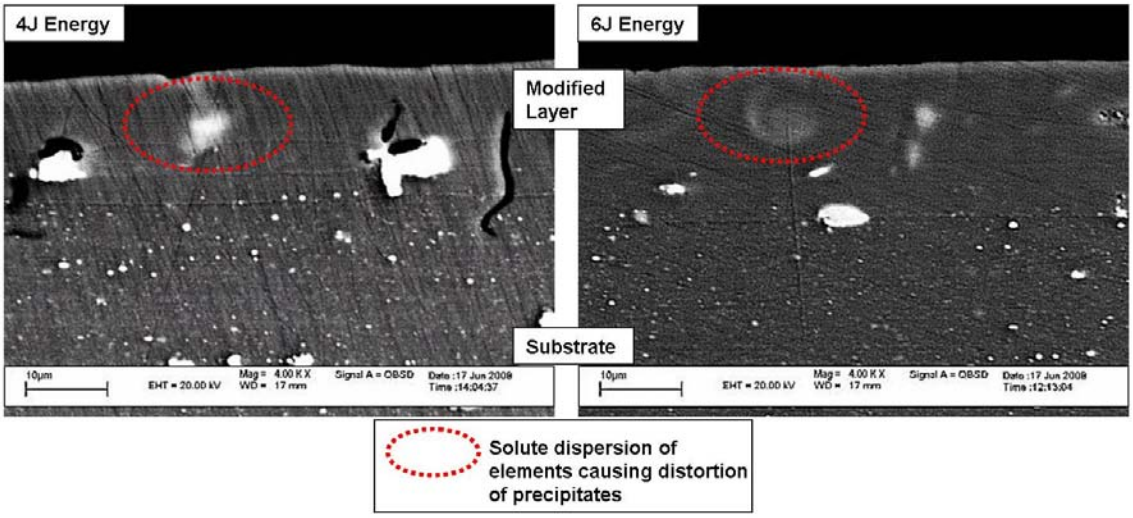

Figure 8.18 Backscattered SEM images (prepared by non-aqueous polishing to 1µm surface finish) of solute dispersion in electron beam surface melting of AA2024 at 40µs pulse duration 10 pulses per unit area and variable energy (4 and 6J).

Although large scale dispersion of the precipitates from EBSM has been observed in Figure 8.19, this does not always achieve a complete homogenisation of the modified layer. Figure

8.20 uses backscattered SEM imaging (sample prepared by non-aqueous polishing to 1µm surface finish) of EBSM microstructure cross-section to show that although solute dispersion is present within the modified layer produced that large precipitates can still remain at the base of the modified layer.

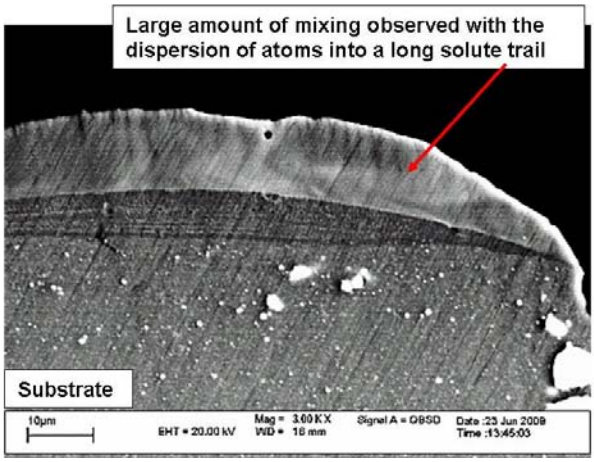

Figure 8.19 Backscattered SEM images (prepared by non-aqueous polishing to 1µm surface finish) of microstructural cross-section of solute dispersion by convection mixing from electron beam surface melting on AA2024 with a high number of pulses per unit area (40) at 20µs pulse duration 2.5J.

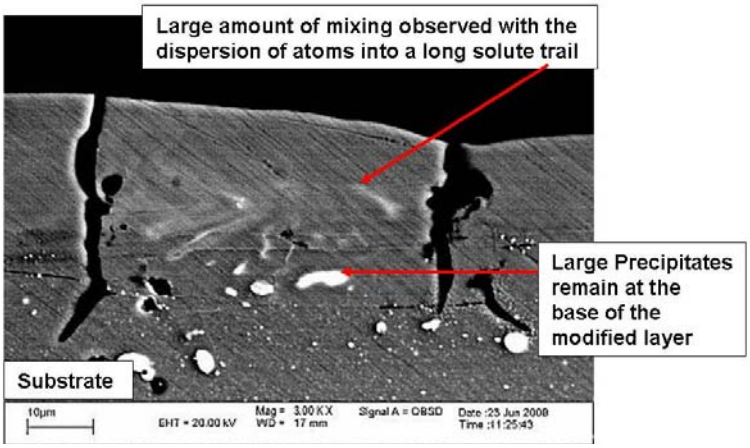

Figure 8.20 Backscattered SEM images (prepared by non-aqueous polishing to 1µm surface finish) of microstructural cross-sections of solute dispersion by convection mixing and precipitates remaining at the base of the modified layer from electron beam surface melting on AA2024 with a high number of pulses per unit area (40) at 20µs pulse duration and 2.5J.

8.6 Solute Dispersion Increase by Processing Parameter Variation

Investigations into the EBSM modified layers showed that large amounts of solute dispersion can occur and to ensure an improvement in the corrosion resistance it is desirable to have a homogeneous layer with the maximum amount of solute dispersion. EBSM at the different processing parameters (energy, pulse duration and number of pulses per unit area) were performed to identify which variable increased solute dispersion.

Figure 8.21 shows typical etched microstructure cross-sections produced at 20μs pulse duration, 1 pulse per unit area and varying energy, between 3 and 8J. These microstructures show that the amount of mixing within a modified layer varies with the processing energy, as increasing the energy causes longer solute trails.

Figure 8.22 shows the affect of pulse duration variation between 10 and 20μs at 6J energy and 1 pulse per unit area on etched modified layer microstructure cross-sections of similar thicknesses. Figure 8.22 shows that the longer pulse duration exhibited more solute dispersion by mixing within the modified layer. This pulse duration increase was achieved by an increase in the system pressure (discussed in Section 3.3.1).

A further increase in pulse duration to 40μs was achieved by an increase in the circuit inductance (discussed in Section 3.3.1). Figure 8.23 shows typical etched microstructure cross-sections of EBSM layers at 20 and 40μs pulse duration, 4J energy and 10 pulses per unit area. The increase in pulse duration to 40μs increased the convection mixing observed within the modified layer.

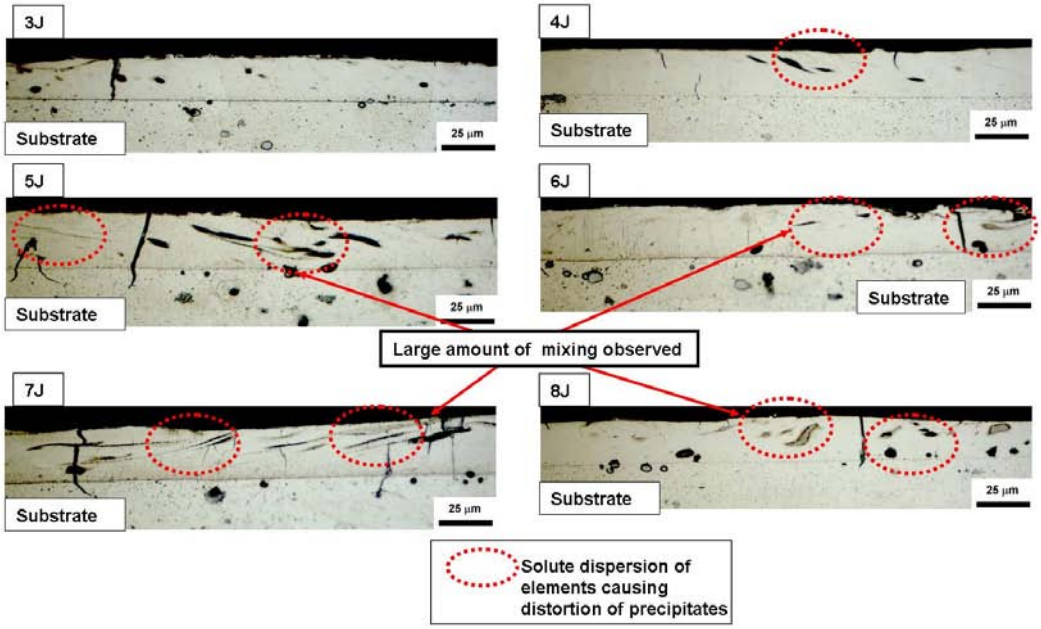

Figure 8.21 Typical etched microstructure cross-sections of modified layers produced with varying energy between 3 and 8J in electron beam surface melting at 20µs pulse duration and 1 pulse per unit area.

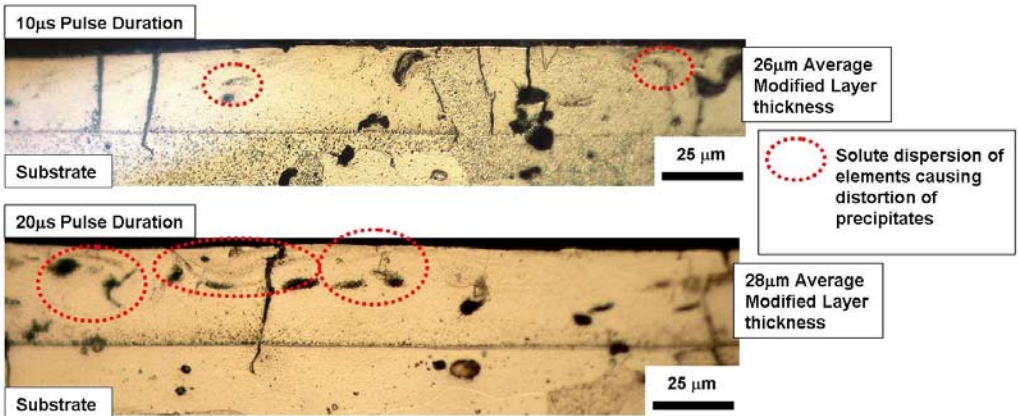

Figure 8.22 Etched microstructure cross-sections of modified layers produced by electron beam surface melting by 6J, 1 pulse per unit area and variable pulse duration of 10µs and 20µs by alteration in the electron beam system pressure.

Another observation from Figure 8.23 is that a high number of pulses per unit area (10) were used and this altered the modified layer microstructure that formed at the two pulse durations,

as the modified layer at 20μs was discontinuous or "globular" whereas at 40μs the layer was continuous.

The effect of multiple pulses per unit area (1-10) on solute dispersion is shown in the etched microstructure cross-sections in Figure 8.24. Figure 8.24 shows that an increase in mixing within the modified layer occurred with an increase in the number of pulses per unit area between 1 and 10, as at 10 pulses there are solute trails but this is not observed in the 1 pulse per unit area treatment.

The extent of solute dispersion observed within EBSM modified layers has been shown to increase with the three processing parameters used.

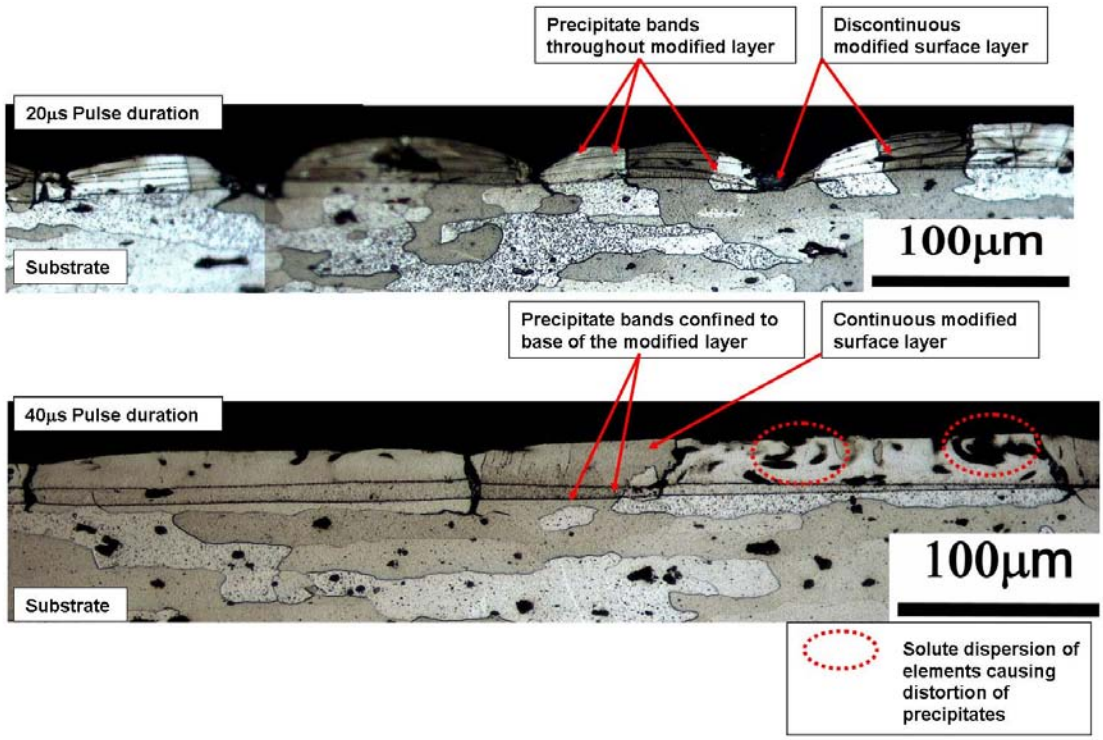

Figure 8.23 Etched microstructure cross-sections of modified layers produced by electron beam surface melting by 4J, 10 pulses per unit area and variable pulse duration of 20μs and 40μs by alteration in the electron beam circuit inductance.

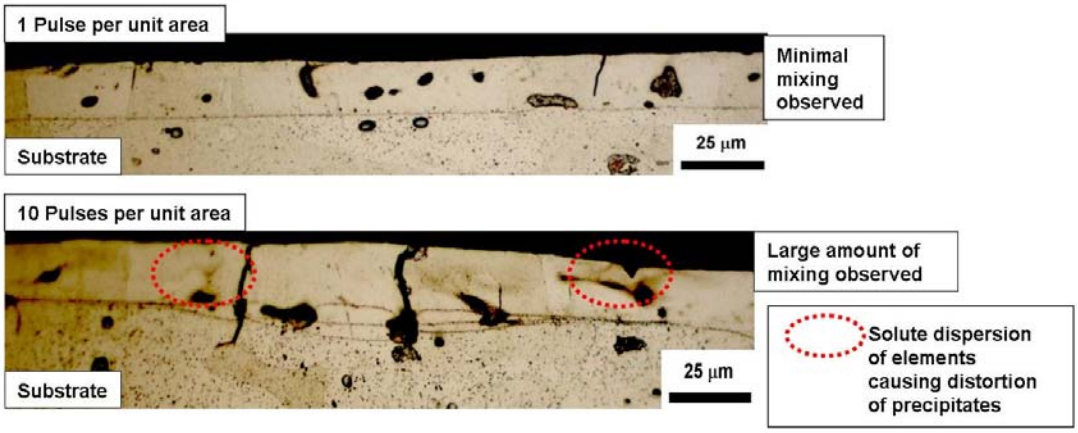

Figure 8.24 Typical etched microstructure cross-sections with electron beam surface melting at variable number of pulses per unit area (1 and 10), 20μs pulse duration and 2J.

8.7 Issues with Increasing Solute Dispersion

To provide an improvement in the corrosion resistance solute dispersion needs to be maximised in EBSM. It has been shown that increasing the processing parameters of energy, pulse duration or number of pulses per unit area increased the solute dispersion.

Increasing either the pulse duration or energy to increase the solute dispersion has the added effect that increasing these processing parameters will also increase the modified layer thickness (Section 8.3). To compare similar thickness modified layers produced by EBSM treatments with different energy and pulse duration, for each set of processing parameters the cathode separation was varied to produce a range of modified layer thicknesses.

The production of a range of modified layer thicknesses provided the added benefit that for a set of processing parameters the modified layer thickness could be identified where the onset of solute dispersion by mixing and the onset of cracking occurred.

Figure 8.25 shows the average modified layer thickness (from a minimum of three measurements) produced from EBSM treatment at 6J, 1 pulse per unit area and 10μs pulse duration over a range of cathode separation with error bars at one standard deviation. Figure 8.25 shows that cracking occurs within a thinner modified layer (9μm) compared with mixing (16μm).

A similar test over a range of cathode separations but increasing the pulse duration to 20μs and keeping 6J and 1 pulse per unit area produced similar results as shown in Figure 8.26 (error bars at one standard deviation) where cracking occurred in thinner average modified layers (13μm) compared with those of mixing (15μm).

The results from increasing the pulse duration further to 40μs but keeping the energy at 6J and 1 pulse per unit area (by circuit inductance variation) is shown in Figure 8.27 (error bars at one standard deviation). Figure 8.27 also showed the onset of cracking to occur at 9μm layer thickness and mixing still to occur within thicker modified layers at approximately 15μm.

It was apparent from Figure 8.25 to Figure 8.27 for all of the pulse durations investigated that mixing required a deeper modified layer, of approximately 15μm, than that for cracking, at less then 10μm.

Figure 8.27 also shows the effect of energy variation (4-6J) at 40μs pulse duration and 1 pulse per unit area on the onsets of cracking and mixing. For each of these energies the onset of cracking occurred in thinner layers compared with that of mixing. For 4J cracking onset was at 7μm modified layer thickness and mixing at approximately 18μm. At 5J the onset of cracking was at 5μm and mixing at 17μm.

With variation in the pulse duration and energy to increase the solute dispersion there was no solute dispersion by mixing observed within the modified layers without some degree of cracking also being present. In this HPBSM process there is therefore a limit to the amount of solute dispersion that can be induced to increase the homogeneity by using these processing parameters.

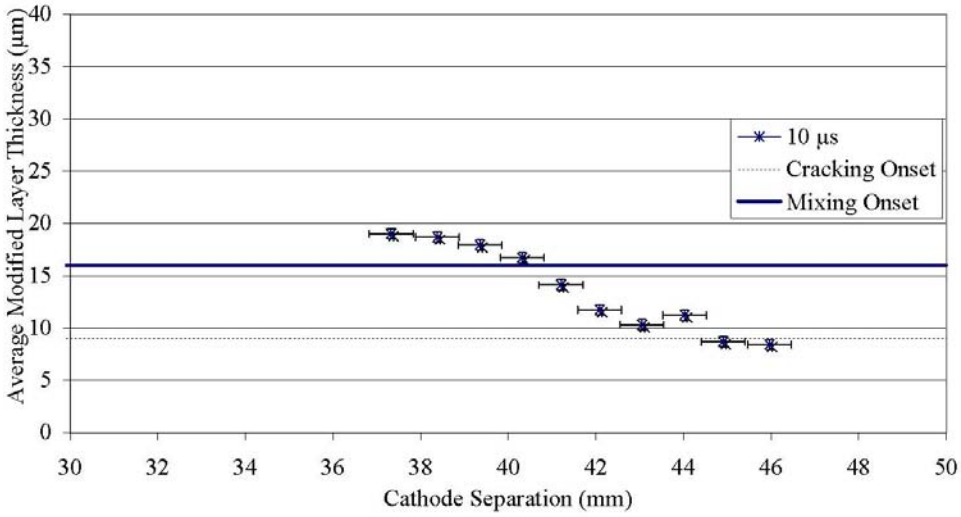

Figure 8.25 Graph of cathode separation versus modified layer thickness with the onset of mixing at 16μm modified layer thickness and onset of cracking at 9μm modified layer thickness for electron beam surface melting at 10μs pulse duration, 6J and 1 pulse per unit area. Error bars for the modified layer depth measurements are at one standard deviation based on a minimum of 10 measurements of modified layer thickness.

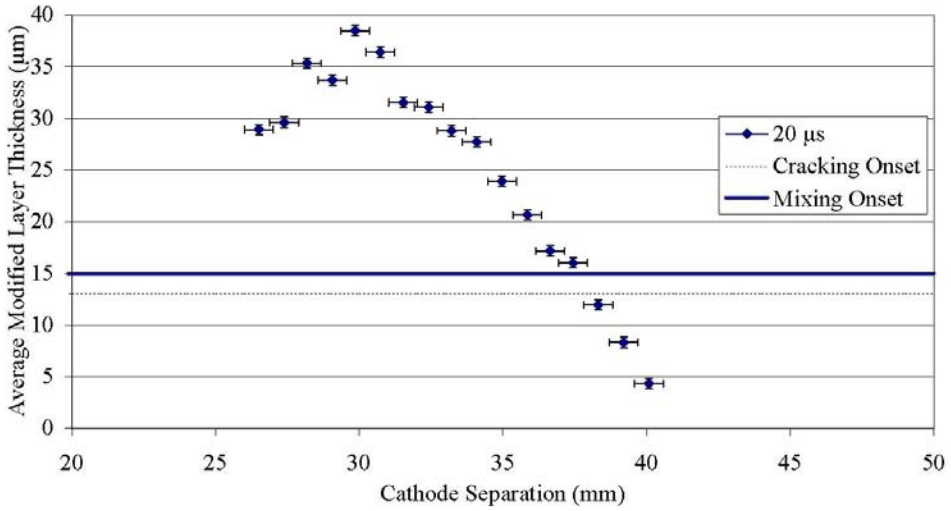

Figure 8.26 Graph of cathode separation versus modified layer thickness with the onset of mixing at 15µm modified layer thickness and onset of cracking at 13µm modified layer thickness for electron beam surface melting at 20µs pulse duration, 6J and 1 pulse per unit area. Error bars for the modified layer depth measurements are at one standard deviation based on a minimum of 10 measurements of modified layer thickness.

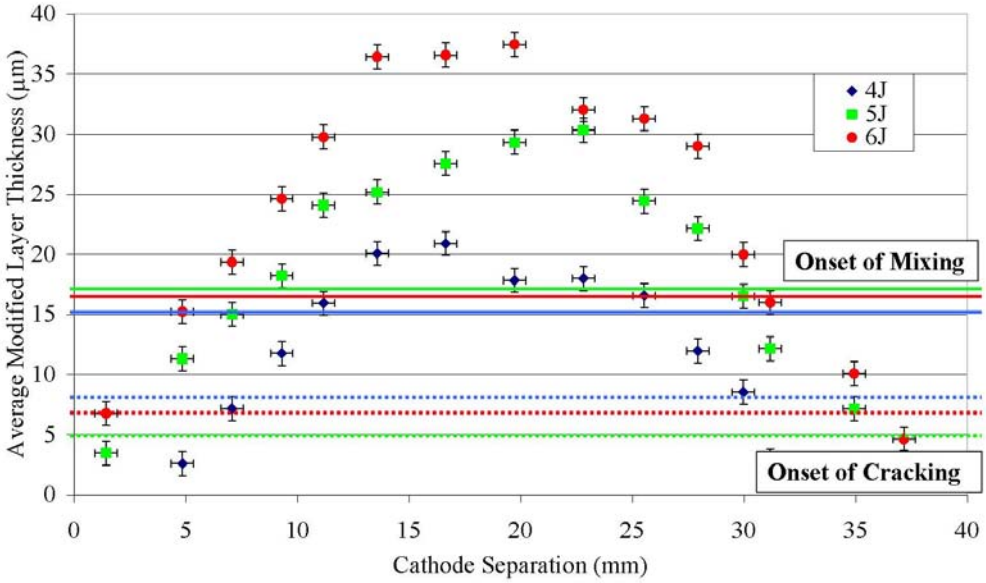

Figure 8.27 Graph of cathode separation versus modified layer thickness with the onset of mixing cracking for electron beam surface melting at 40µs pulse duration, variable energy (4J, 5J and 6J) and 1 pulse per unit area. Error bars for the modified layer depth measurements are at one standard deviation based on a minimum of 10 measurements of modified layer thickness.

Variation in the number of pulses per unit area has also been identified as being able to increase solute dispersion by mixing within the modified layer (Section 8.6).

Figure 8.28 shows typical etched microstructure cross-sections produced by EBSM at a range of number of pulses per unit area 1-15, 20μs pulse duration and 2.5J. Figure 8.28 shows that increasing the number of pulses per unit area between 10 and 15 pulses per unit area caused a significant change in the modified layer from continuous covering to "globular" and discontinuous (previously shown in Figure 8.23).

Figure 8.29 also shows typical etched microstructure cross-sections with increasing number of pulses per unit area (2-20), 2J and 20μs pulse duration. The onset of a "globular" surface from these treatments was at 20 pulses per unit area.

Comparing the microstructures in Figure 8.28 and Figure 8.29 shows that the formation of a "globular" surface occurred at different number of pulses per unit area depending upon the processing energy, as at 2J the onset is at 20 pulses whereas at 2.5J the onset was at 15 pulses.

The formation of a discontinuous surface with increasing number of pulses per unit area creates a limit to the amount of solute dispersion that can be achieved by increasing the number of pulses per unit area.

There are limitations to the amount of solute dispersion that can be achieved by increasing any of the processing parameters investigated, as cracking before mixing occurs with an

increase in pulse duration or energy and an increase in the number of pulses per unit area creates a discontinuous surface.

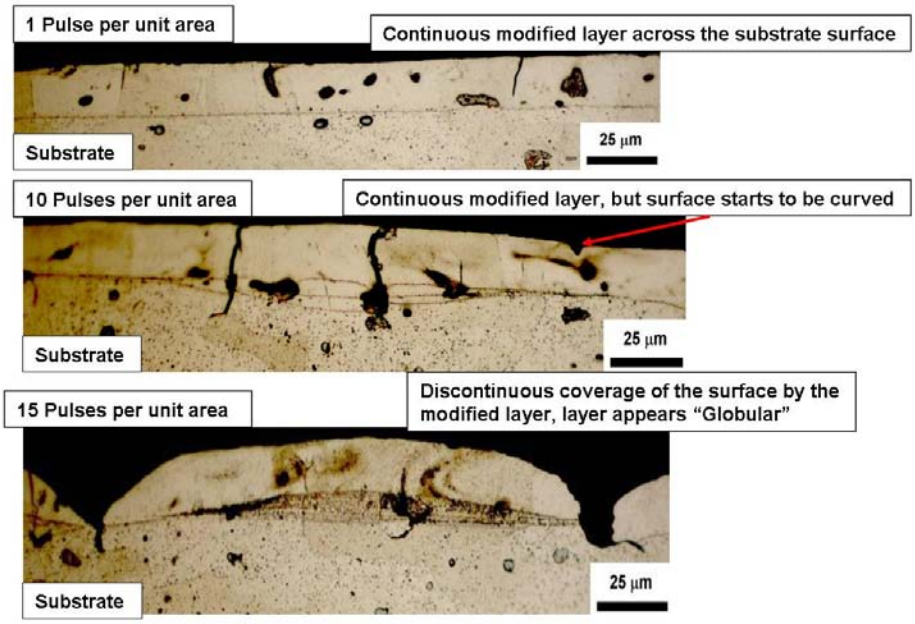

Figure 8.28 Typical etched microstructure cross-sections of the change in modified layer continuity with increasing number of pulses per unit area (1 to 15) at 2.5J energy for electron beam surface melting of AA2024 at 20µs pulse duration.

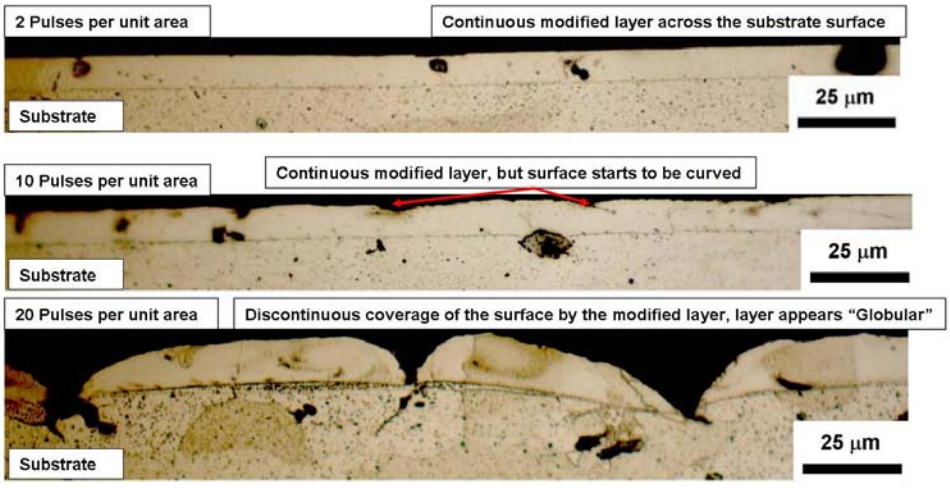

Figure 8.29 Typical etched microstructure cross of the change in modified layer continuity with increasing number of pulses per unit area (2 to 20) at 2J energy for electron beam surface melting of AA2024 at 20µs pulse duration.

8.8 Solute Dispersion and Corrosion Resistance

The EBSM layers that were produced did have an increase in homogeneity compared with the underlying substrate (example shown in Figure 8.7) and microelectrochemical tests were used to assess whether the level of homogeneity produced improved the corrosion resistance compared with the parent material.

Microelectrochemical tests (with 0.1M NaCl solution, 1mV/s scan rate, Ag/AgCl reference electrode) were used to test the anodic and cathodic activity of EBSM treatments by the method described in Section 3.6.2 and the results were compared with similar tests performed on parent material and excimer LSM treatments (10J/cm^2 9 pulses per unit area).

Figure 8.30 shows that the anodic activity results from microelectrochemical tests on the EBSM surfaces at 2.5J, 20μs pulse duration and variable number of pulses per unit area. This figure shows that the results were inconsistent but generally they had a lower breakdown potential compared with the parent and there was no passive region, as has been observed with excimer LSM results. It could be argued from Figure 8.30 that a low number of pulses per unit area (1-4) produced better corrosion resistance with a higher breakdown potential compared to the treatments from a higher number of pulses (5-20), but this was not consistently observed. Figure 8.31 shows the corresponding cathodic activity and generally the cathodic current density was higher then that produced from excimer LSM.

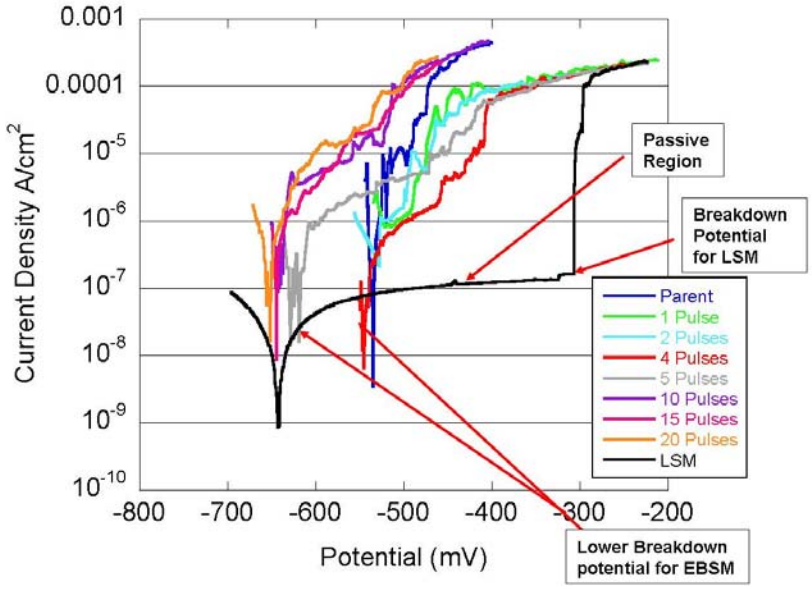

Figure 8.30 Anodic polarisation of electron beam surface melting at 20µs pulse duration, 2.5J, and variable number of pulses per unit area and excimer laser surface melting 25ns pulse duration, 10J/cm^2, 9 pulses per unit area, by microelectrochemical tests 0.1M NaCl solution 1mV/s scan rate, Ag/AgCl reference electrode.

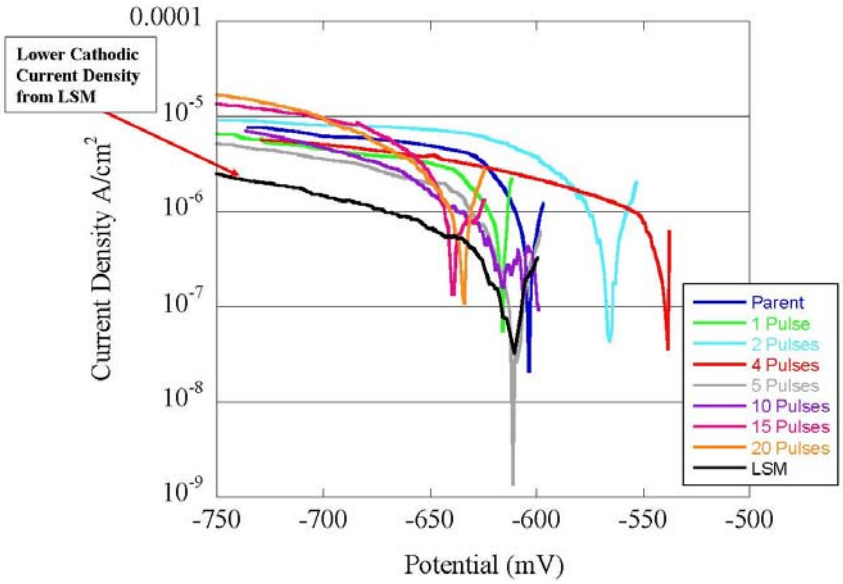

Figure 8.31 Cathodic polarisation of electron beam surface melting at 20µs pulse duration, 2.5J, and variable number of pulses per unit area and excimer laser surface melting 25ns pulse duration, 10J/cm^2, 9 pulses per unit area, by microelectrochemical tests 0.1M NaCl solution 1mV/s scan rate, Ag/AgCl reference electrode.

Figure 8.32 is a typical graph of cathodic activity measurements of a single EBSM treated surface, 25μs pulse duration, 2J and 1 pulse per unit are and shows the main problem of inconsistency of results from the microelectrochemical tests of the EBSM treatments.

The electrochemical results did however became more consistent with the testing of an EBSM treatment of uniform appearance melt zones at 2J energy, 25μs pulse duration and 4 pulses per unit area. Figure 8.33 shows the cathodic activity measurements of this EBSM treated surface and more consistently there was a decrease in cathodic current density with respect to the parent, but this decrease in cathodic activity for EBSM was not as large as that from excimer LSM.

However unlike the cathodic activity, Figure 8.34 shows the anodic activity measurements from the uniform surface appearance EBSM treatment at 2J, 25μs pulse duration and 4 pulses per unit area showing result inconsistency and no improvement in the corrosion resistance as there is no passive region formed and there is a lower breakdown potential compared with the parent material.

Figure 8.34 also shows the anodic activity measurements from the non-uniform surface appearance EBSM treatment at 2J, 25μs pulse duration and 4 pulses per unit area in these results the consistency has increased but again there is no improvement in the corrosion resistance compared with the parent material.

Overall it was found that the EBSM treatments provided no improvement in corrosion resistance compared with the parent material.

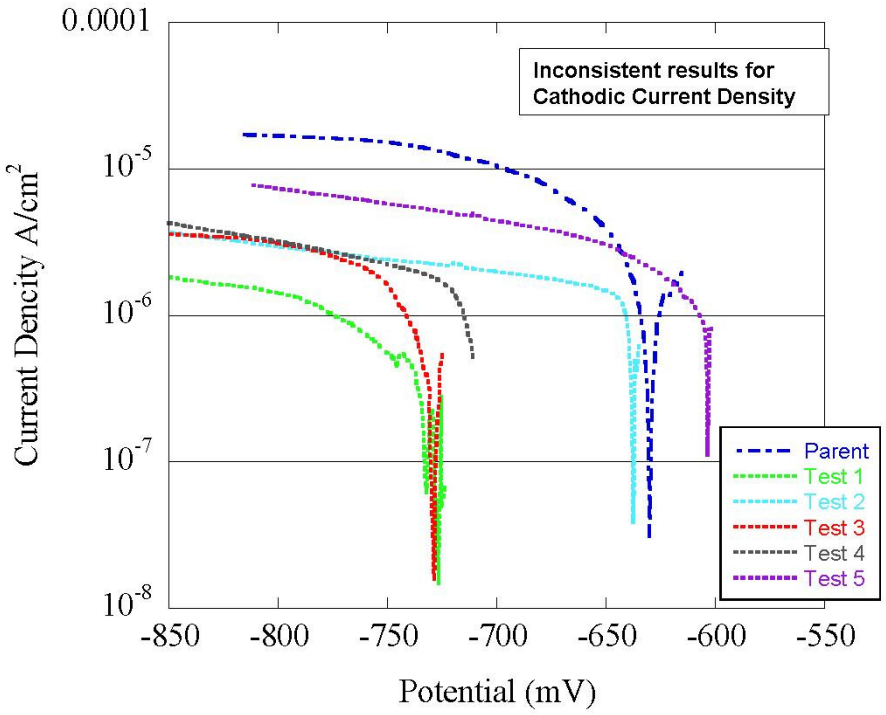

Figure 8.32 Scattered cathodic polarisation results from multiple tests of electron beam surface melting at 25µs pulse duration, 2J 1 pulse per unit area by microelectrochemical tests 0.1M NaCl solution 1mV/s scan rate, Ag/AgCl reference electrode.

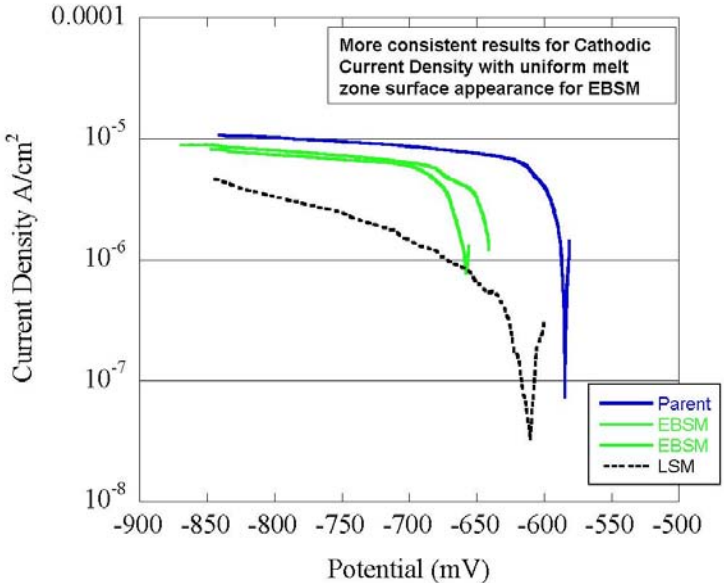

Figure 8.33 Cathodic polarisation of uniform melt zone appearance of electron beam surface melting at 20µs pulse duration, 2J, and 4 pulses per unit area and excimer laser surface melting 25ns pulse duration, 10J/cm^2, 9 pulses per unit area, by microelectrochemical tests 0.1M NaCl solution 1mV/s scan rate, Ag/AgCl reference electrode.

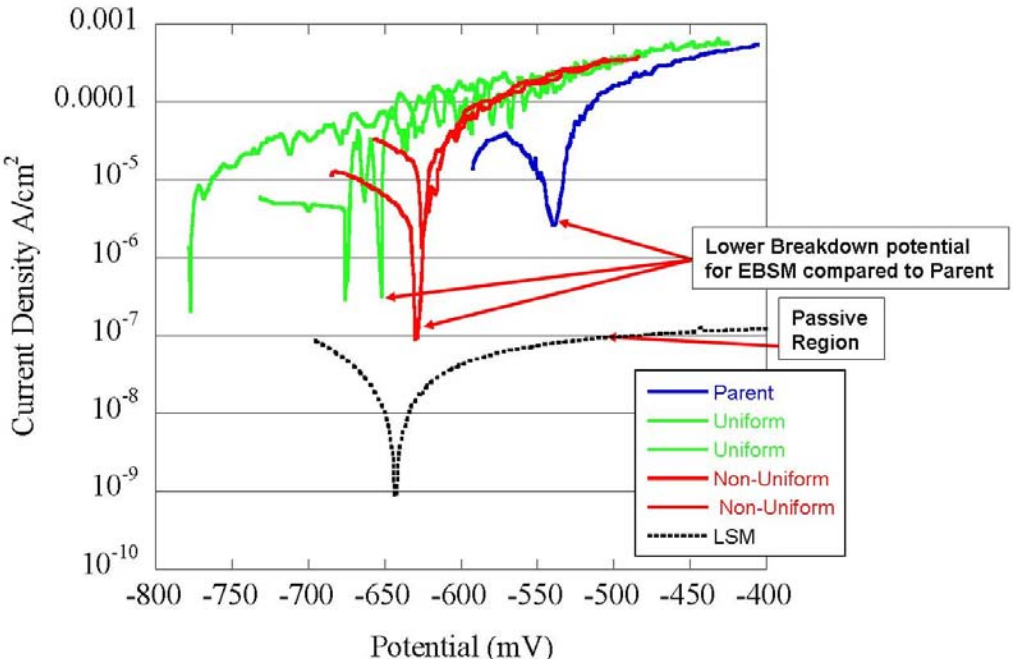

Figure 8.34 Anodic polarisation of uniform and non-uniform melt zone appearances of electron beam surface melting at 20µs pulse duration, 2J, and 4 pulses per unit area and excimer laser surface melting 25ns pulse duration, 10J/cm^2, 9 pulses per unit area, by microelectrochemical tests 0.1M NaCl solution 1mV/s scan rate, Ag/AgCl reference electrode.

8.9 Electron Beam Surface Melting and Laser Surface Melting

EBSM was found to produce modified layers that were thick enough to survive anodising, (Section 8.4) exhibit solute dispersion (Section 8.5) but did not provide an increase in the corrosion resistance (Section 8.8). The excimer LSM process produced modified layers that increased the corrosion resistance by solute dispersion but were too thin to survive anodising. Examination of the EBSM and LSM treatments is required to understand the differences between the modified layers produced so that a corrosion resistance improvement can be gained in HPBSM.

The pulse durations, modified layer thicknesses, cracking and mixing onsets for the LSM and EBSM processes used throughout this thesis are summarised in Table 8.1. However, due to experimental constraints not all of the processes could provide the required information. In the case of the excimer LSM as there was no variation in the modified layer thickness the onset of cracking was not observed and similarly the onset of mixing was not observed due to segregation within the Nd:YAG LSM layers. The EBSM process is compared with each of the LSM processes in the following section.

Table 8.1 Comparison of modified layer properties and pulse duration for high power beam surface modification processes used in this thesis.

AA2024	Pulse Duration	Modified Layer Thickness	Modified Thickness for Cracking Onset	Modified Thickness for Mixing Onset	Type of Mixing Observed
Excimer LSM	25ns	3-5μm	-	3-5μm	Convection
USP-CO_2 LSM	7-30μs	12-45μm	24μm	14μm	Convection
EBSM	5-40μs	5-40μm	5-10μm	15μm	Diffusion and Convection
Nd:YAG LSM	10-50ms	300-550μm	300μm	-	-

8.9.1 Excimer Laser

Figure 8.35 compares typical etched microstructure cross-sections of the EBSM layers (20μs pulse duration, 6J, 1 pulse per unit area, average modified layer thickness 24μm, non-uniform melt zone) and excimer LSM (25ns pulse duration 10J/cm^2 fluence, 9 pulses per unit area, layer thickness 3-6μm) layers. These microstructures show that the EBSM modified layers were thicker than the excimer LSM modified layers. This difference in modified layer thickness meant that when the excimer LSM and EBSM modified layers were coupled with

anodising treatment (CAA) that for EBSM most of the modified layer survived but for excimer LSM the entire layer was removed.

Figure 8.35 also shows that the microstructure varied between these two treatments, as the EBSM layer microstructure was continued from the substrate microstructure and exhibited segregated regions with fine lines of precipitates perpendicular to the substrate interface. The difference in microstructure accounts for the different corrosion resistance performance produced by these two treatments as excimer LSM treatment has been shown to improve corrosion resistance compared with the parent material (Section 5.2 and [18]) but EBSM has not (Figure 8.30 to Figure 8.34).

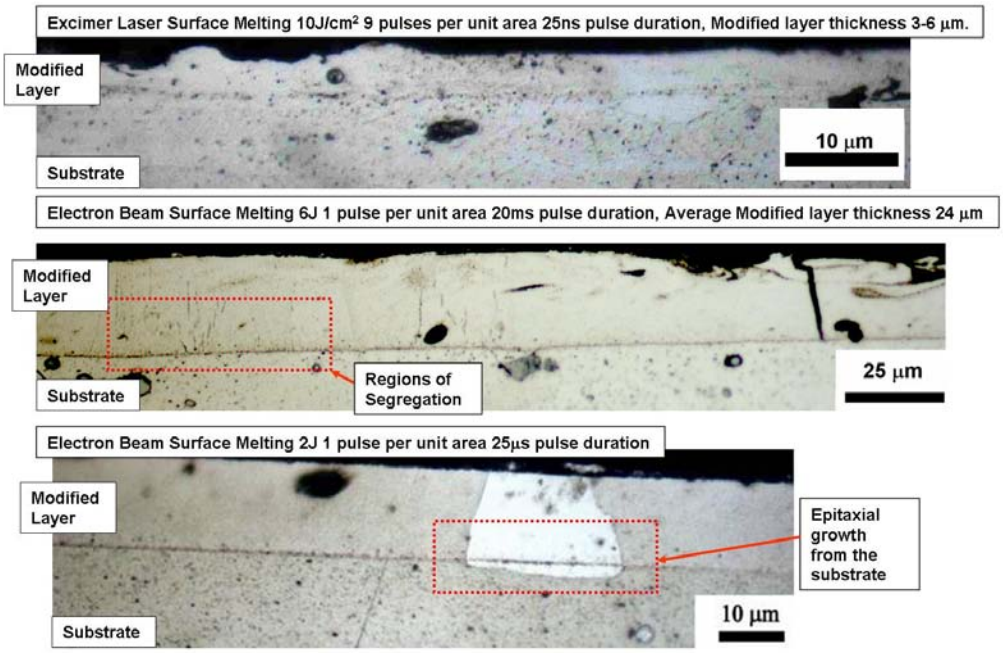

Figure 8.35 Typical etched microstructure cross-sections of electron beam surface melting 20µs pulse duration, 6J, 1 pulse per unit area, average modified layer thickness 24µm, non-uniform melt zone, electron beam surface melting 25µs pulse duration, 2J, 1 pulse per unit area and excimer laser surface melting 25ns pulse duration 10J/cm^2 fluence, 9 pulses per unit area, layer thickness 3-6µm.

8.9.2 USP-CO_2 Laser

Figure 8.36 compares typical etched microstructure cross-sections produced by EBSM (6J, 20μs pulse duration and 1 pulse per unit area) and USP-CO_2 LSM (22.4μs pulse duration and 10 pulses per unit area). Notable differences between the modified layer microstructures are that the EBSM modified layer was continuous over the surface with a flat base where as the USP-CO_2 LSM modified layer was scalloped due to the smaller beam area. The EBSM layer also showed some segregation which was not apparent in the USP-CO_2 LSM modified layer. Both treatments did however exhibit precipitate trails from material movement and also lines of precipitates at the modified layer base.

Figure 8.37 further compares these treatments using backscattered SEM imaging of microstructure cross-sections prepared by non-aqueous polishing to a 1μm surface finish. Figure 8.37 shows that in both EBSM and USP-CO_2 LSM that there is large scale solute dispersion by convection mixing.

The EBSM and the USP-CO_2 laser both had similar pulse durations (Table 8.1) and both processes produced similar average modified layer thicknesses (5-40μm for EBSM and 12-45μm for USP-CO_2 LSM). Although the modified layers produced were of similar thickness the onset of cracking varied with the modification process and occurred in thinner layers for EBSM (5-10μm) than in LSM (24μm). Mixing within the layer however occurred at similar modified depths regardless of treatment (15μm for EBSM and 14μm for USP-CO_2 LSM).

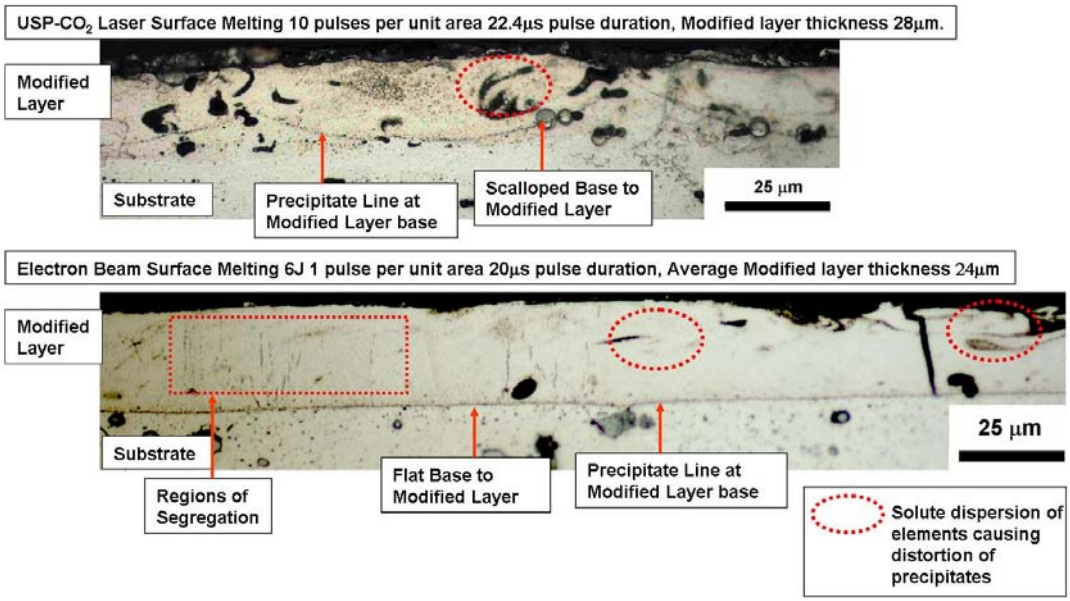

Figure 8.36 Typical etched microstructure cross-sections of electron beam surface melting 20μs pulse duration, 6J, 1 pulse per unit area and laser surface melting and USP-CO_2 laser surface melting 22.4μs pulse duration, 10 pulses per unit area.

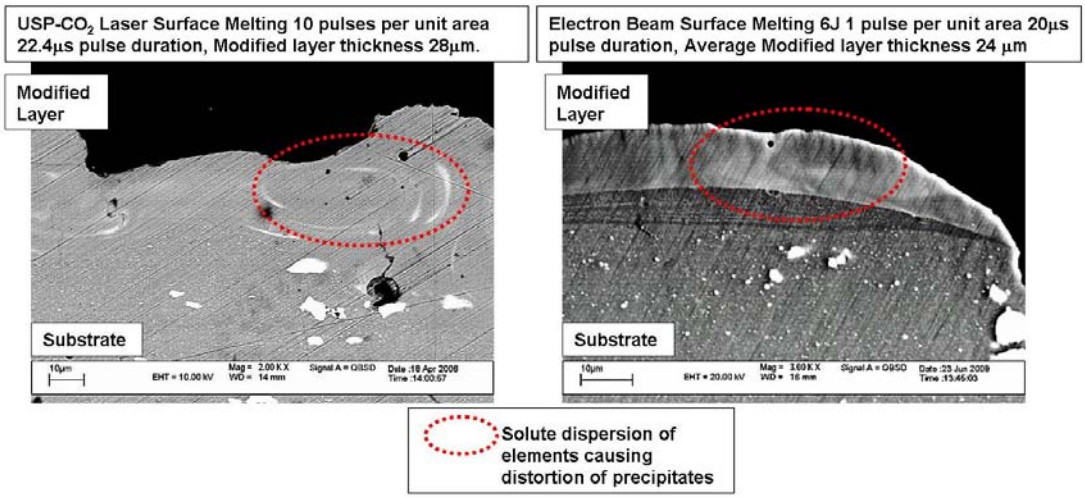

Figure 8.37 Typical backscattered SEM images of etched microstructure cross-sections showing convection mixing in USP-CO_2 laser surface melting pulse duration 25.2μs 1 pulse per unit area, and electron beam surface melting 20μs pulse duration, 2.5J, 40 pulses per unit area.

8.9.3 Nd:YAG laser

The Nd:YAG laser had a much longer pulse duration (10ms) than the electron beam system (20μs). Figure 8.38 compares the typical etched microstructure cross-sections of EBSM (6J, 20μs pulse duration and 1 pulse per unit area) and Nd:YAG LSM (70.6J, 50ms pulse duration and 1 pulse per unit area). Figure 8.38 shows that the Nd:YAG LSM layers were much thicker (300-550μm) and had a greater degree of segregation throughout the entire modified layer than the EBSM layers (24μm) with only segregated regions at the base of the modified layer.

Figure 8.39 compares etched microstructure cross-sections from the base of the modified layer for these EBSM and Nd:YAG LSM treatments. Figure 8.39 shows that the EBSM layer was strongly influenced by the substrate with epitaxial growth where as the Nd:YAG LSM layer had an influence from the substrate with the alignment of segregation.

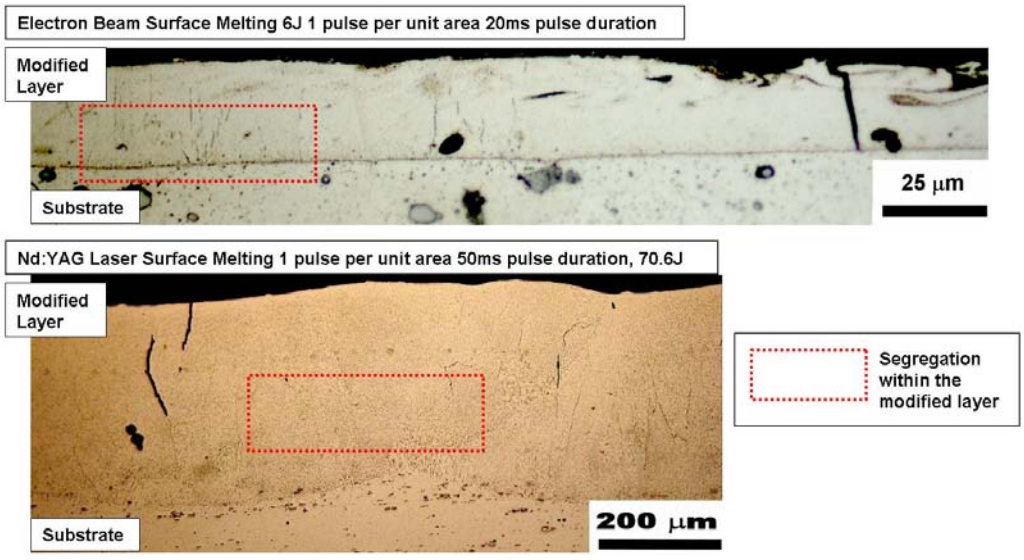

Figure 8.38 Typical etched microstructure cross-sections of electron beam surface melting 20μs pulse duration, 6J, 1 pulse per unit area, and Nd:YAG laser surface melting 50ms pulse duration, Energy 70.7J, 1 pulse per unit area.

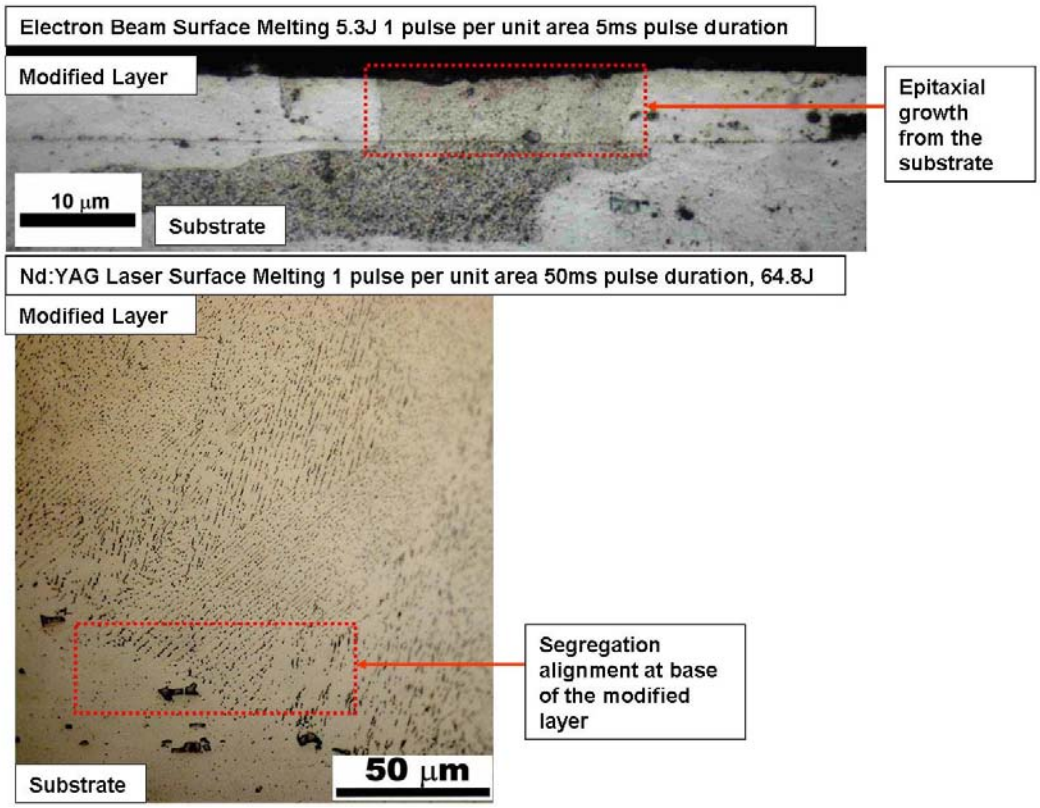

Figure 8.39 Typical etched microstructure cross-sections showing the influence of the substrate on the modified layer in electron beam surface melting 5μs pulse duration, 5.3J, 1 pulses per unit area, and Nd:YAG laser surface melting 50ms pulse duration, Energy 64.8J, 1 pulse per unit area.

8.10 Discussion

EBSM produced layers of various microstructures, depths and surface appearances depending on the processing parameters; pulse duration, energy and number of pulses per unit area.

The EBSM microstructure was observed to vary with depth, with regions of segregated structure generally forming at the base of modified layers that had an average thickness larger then 25μm. The formation of a segregated structure signified where the solidification rate

was below the speed required for ultimate stability and planar growth, which generally was observed throughout the majority of the EBSM modified layer. The solidification structure in EBSM was therefore highly sensitive to solidification rate as in a 25μm modified layer the rate was near that for ultimate stability for planar growth.

Other EBSM work on AA2024 and stainless steel have also shown microstructure sensitivity to solidification rate [165]. EBSM of stainless steel showed the change in structure with an acceleration of solidification from the layer base, where there was a planar growth region of a few microns beneath a cellular structure before dendrites formed nearer the surface. EBSM on AA2024 showed a similar trend of an accelerating growth front from the layer base as, although there was generally epitaxial growth from the substrate, there were also segregated microstructure regions of cells nearer the layer base. Solidification for both these materials was slower then observed in this current work, as the ultimate stability criteria was not reached for the second onset of planar solidification [165].

EBSM has shown in this and other work [165] that the solidification rate increases from the base of the modified layer creating a transient region of slow growth. This transient region has created in some LSM and EBSM work a line of precipitates at the base of the layer [31, 74, 88]. The LSM treatments showed a one to one correlation between the precipitate lines and the number of treatment pulses [31, 74] however, this was not found in EBSM treatments. The precipitate lines in EBSM were also observed over a range of melt depths.

This suggested that as precipitates were dissolved into solution the electron conduction of the layer changed causing variation in the melt depth between pulses. The influence of second

phase precipitates (carbides) on the modified layer thickness has also been shown in other EBSM work on D2 tool steels [171]. This means that an increase in melt depth between pulses would remove the precipitate lines formed from the previous pulses. However, the last pulse would have to produce the thinnest layer to be able to observe a range of precipitate bands. This was supported as in EBSM the presence of large constituent particles near the maximum melt depth locally increased the melt depth suggesting that electron conduction was deeper in this area.

An increase in the number of pulses per unit area did not increase the modified layer thickness. It is possible, as mentioned above, that small changes in the modified depth were related to multiple pulses per unit area as the precipitate lines at the layer base varied in depth. However, multiple pulses did not have such a strong influence on the modified depth as pulse duration or energy. EBSM of tool steels similarly found that increasing the number of pulses increased both the layer homogenisation and the melted layer thickness. The influence of multiple pulses on the melt depth in tool steels was due to the fact melting was initiated at the second phase carbide particles and as each pulse dissolved the carbides, the thermal properties of the layer changed [171].

The precipitate lines present at the base of the modified layers were a concern as they were a susceptible path for crack propagation which would lead to layer de-lamination. Cracking was frequently observed in EBSM layers and was associated with grain boundaries which as the layers solidified with epitaxial growth copying the substrate microstructure continued from the substrate into the modified layer. If cracks formed at grain boundaries within the layer these were continued down into the substrate which could lead to layer de-lamination.

Cracking along the transition region has also been observed in LSM (cw-CO_2 laser) of AA7075 when scanning speeds were above 70mm/s. Cracking was first observed along the transition region as this was where the highest stresses were found [143, 169]. The microstructure produced in the LSM of AA7075 had a columnar structure [83, 173], which was different to the structure observed in these EBSM investigations of AA2024. The occurrence of epitaxial solidification in EBSM of AA2024 produced grain boundaries within the modified layer which were weak points for cracking to occur. If these grain boundaries were removed then the transition region could be the next region of weakness for cracking to occur.

This is assuming that no other weak points are present within the modified structure. EBSM of titanium (6Al4V) alloy work highlighted the fact that cracking can occur within the modified structure when brittle phases are present, such as in a highly alloyed material. To avoid cracking in EBSM it was suggested to reduce the alloy constituents [83].

Cracking within the layer varied with EBSM treatment processing parameters. In particular more cracking was observed with processing parameters which created an EBSM treatment with a non-uniform surface appearance at high energy density.

The modified layer thickness was also increased by increasing either the pulse energy or the pulse duration as has also been shown in other AA2024 EBSM [31]. Similarly EBSM, with a continuous electron beam, of titanium alloys and nickel aluminium bronzes found that a scan speed increase (decrease in interaction time) or decrease in power caused a decrease in the

modified depth [109]. The increase in scan speed (decrease in interaction time) was shown to have a greater effect on the modified depth than the power [109].

The EBSM modified layers had fewer precipitates present in comparison to the substrate. The surface was not completely homogenised however as the smaller particles were dispersed into solid solution, but the larger particles remained, although their shape had altered into trails. This was because the EBSM treatment only initiated enough movement within the layer to disperse the smaller precipitates and to partially disperse the larger precipitates.

Solute dispersion was observed by diffusion and convection movement within the modified layers. Previous examination of AA2024 EBSM treatment by P. Ryan have only observed diffusion processes, which made EBSM unsuitable to homogenise the surface and improve the corrosion resistance, this is shown using backscattered imaging of microstructure cross-sections of excimer LSM and EBSM in Figure 8.40 [31].

However P. Ryan's conclusions were based on a limited number of EBSM samples and in contrast this work has shown that mixing by movement can occur within EBSM layers with the production of precipitate trails Figure 8.7 and Figure 8.8. Although movement was induced in EBSM layers this was to a smaller extent than observed in excimer LSM as shown in Figure 8.35 and therefore LSM produced a higher degree of precipitate dispersion which was favourable to improve the corrosion resistance.

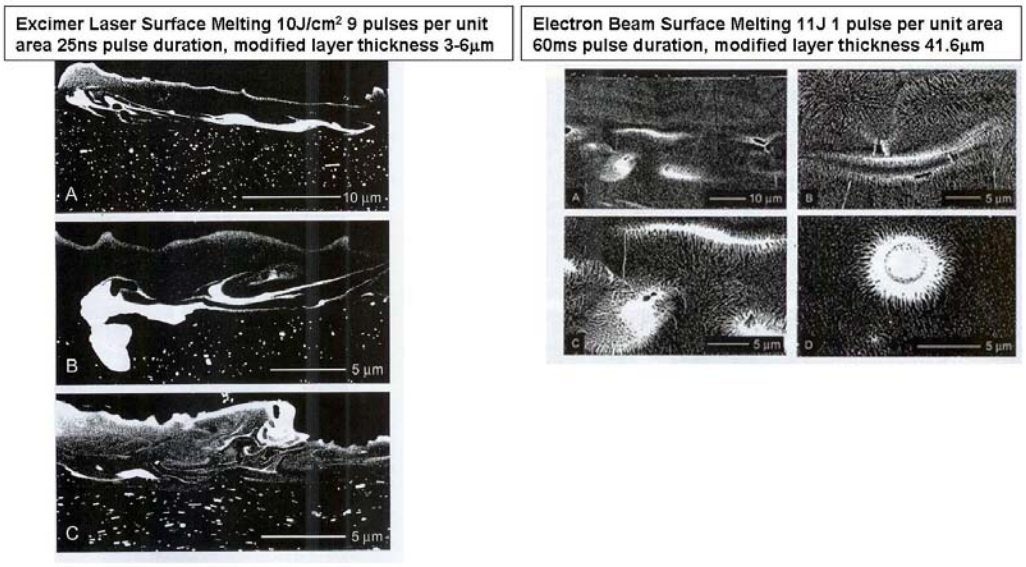

Figure 8.40 Microstructural cross-section SEM images showing solute trails from constituent particles within the modified layer from excimer laser surface melting 25ns pulse duration 10J/cm^2 Fluence, 9 pulses per unit area and diffusion of solute around constituent particles in electron beam surface melting at 60µs pulse duration, 11J, 1 pulse per unit area [31].

The influence of precipitate size on dispersion within an EBSM layer has also been observed in earlier work on AA2024. This work concluded that particles of less than 1µm were removed (completely dissolved) by EBSM treatment and particles above 1µm were only reduced (partially dissolved). This conclusion was modified in later work which took into account the position of precipitates within the layer, as complete dissolution only occurred in the top 0.4µm of a 7µm layer [143, 169]. This was also found in this work where large precipitates were observed to remain at the base of the modified layer where there was too short a liquid time.

Variation in processing parameters has been shown to increase the extent of solute dispersion within the modified layer in EBSM although limitations were identified with increasing the solute dispersion by processing parameter variation. These limitations were cracking

occurring within modified layers before solute dispersion by mixing could occur and the formation of a discontinuous modified layer.

The onset of mixing always occurring within a thicker layer than cracking meant that it was not possible using the current processing parameters to produce modified layers that had adequate mixing to disperse precipitates and were also crack free.

The change in microstructure from a uniform layer to a discontinuous "globular" layer would also not be suitable to provide an improvement in the corrosion resistance as the substrate would be exposed to the environment. The change in structure with multiple pulses has been observed in EBSM work on stainless steels and tool steels, where EBSM using a low fluence and high number of pulses was used to induce movement to smooth the steel surfaces [168, 179]. Although further increase in the number of pulses caused surface "cratering" as lower melting point second phase precipitates vaporised [168].

EBSM work on titanium alloy (6Al4V) also highlighted problems of the poor surface finish induced by EBSM due to rippling of the surface. The rippling was caused due to vapour pressure on the surface and differences in surface tension. The rippling could be minimised by using a low power or interaction time. The problem with minimising the vapour pressure and surface tension gradients is that these factors also induce mixing which means that they are essential for the homogenisation of modified layers. The vapour pressure and surface tension gradients therefore need to be carefully controlled to avoid excessive rippling of the surface, or the formation of a "globular" surface whilst still inducing the required amount of solute dispersion.

Solute dispersion is critical in EBSM to increase homogeneity and the factors which control mixing need to be further investigated, although numerous modelling work has tried to predict it [31, 77, 122]. The limitations from increasing solute dispersion by processing parameter variation means that the EBSM layers produced using this system have not provided an improvement in the corrosion resistance with respect to the parent material.

Excimer LSM layers have been shown to improve the corrosion resistance of AA2024. However the excimer LSM layers were too thin to survive the CAA anodising process. The EBSM layers were thicker than the excimer LSM layers and did survive CAA anodising but did not provide a corrosion resistance increase.

The corrosion resistance of AA2024 was improved in excimer LSM by the dispersion of precipitates from a large degree of mixing. Mixing was also observed in EBSM treatments but not to the same extent as shown in excimer LSM.

It is thought that mixing in LSM layers was induced by vaporisation of elements [31, 77, 122]. Vaporisation in EBSM occurred with the formation of the non-uniform melt zones which also contained cracks so even if there was large scale mixing there would be no observed improvement in the corrosion resistance due to the cracks acting as localised corrosion sites. Uniform appearance EBSM treatments did not undergo large scale vaporisation so there was less solute dispersion by convection mixing and diffusion would be the main mechanism for homogenisation.

EBSM and USP-CO_2 LSM had similar pulse durations and produced similar modified depths. EBSM provided a more consistent treatment due to having a larger beam interaction area but contained some segregation and grain boundaries from epitaxial solidification from the substrate. By comparison USP-CO_2 LSM showed no solidification structure suggesting faster solidification even though the layers were of similar modified depth. Both treatments though did exhibit precipitate lines at the modified layer base where solidification was at its slowest.

The similar modified layer depths produced by EBSM and USP-CO_2 LSM did have similar modified layer thicknesses (15μm) for the onset of solute dispersion by convection mixing but cracking occurred in thinner modified layers for EBSM than in USP-CO_2 LSM. This difference in the onset of cracking within layer could be related to uniformity of the treatment or the difference between laser and electron interaction with the surface, which is further discussed in Section 9.

The Nd:YAG laser LSM had a much larger melt depth compared with EBSM. The deeper modified layer meant that solidification was much slower so produced a segregated solidification structure that contained no signs of mixing or precipitate lines at the modified layer base.

8.11 Conclusions

- Electron beam surface melting increased the homogeneity of the surface by dissolving fine precipitates and partial dissolution of larger constituent particles.
- An increase in modified layer thickness was achieved by increasing either the energy or the pulse duration.

- Electron beam surface melting produced modified layers that were thick enough to survive a chromic acid anodising process.
- Mixing of material is desirable in EBSM to increase the homogeneity of the modified layer. This can be achieved by increase in the energy, pulse duration or the number of pulses per unit area. However, there are limitations to increasing mixing from varying the processing parameters as such treatments incurred cracking or formed a discontinuous modified layer, which are detrimental to the corrosion resistance.
- The modified layers that were produced by electron beam surface melting had increased homogeneity but this did not provide a consistent increase in the corrosion resistance with respect to the parent material.

9 Discussion

It was identified that the successful application of FSW in aerospace structures would require a pre-weld treatment of surface preparation with the removal of surface layers, such as on aerospace materials anodising and paint, and a post-weld treatment that increased the weld's corrosion resistance. Investigations in this thesis have identified high power beam processes of laser paint removal and LSM that meet requirements for the FSW application. Table 9.1 lists the high power beam treatments that were investigated in this thesis for their applicability to the FSW process.

Table 9.1 Summary of high power beam systems and materials used throughout thesis

	Pulse Duration	Lasing Medium	Application	Material
Excimer Laser	25ns	Excited Dimer	LSM Paint Removal	AA2024, AA7056, AA7150, AA7449,
TEA-CO_2 Laser	3µs	CO_2	Paint Removal	AA2024
Nd:YAG Laser	80-150ns	Nd:$Y_3Al_5O_{12}$ crystal	Paint Removal	AA2024
Nd:YAG Laser	0.2-50ms	Nd:$Y_3Al_5O_{12}$ crystal	LSM	AA2024
USP-CO_2 Laser	7-100µs	CO_2	LSM	AA2024, AA7150
Electron Beam	7-40µs	-	EBSM	AA2024

The pre-weld treatment for FSW was the preparation of surfaces by the removal of contaminants or surface layers from the material to be welded. A multiple staged excimer laser paint removal process was developed to remove the anodising and paint from aerospace materials (Section 4.1). The resultant surfaces from this treatment had an oxidised surface with no damage to the substrate. The prepared surfaces were then welded together and the welds produced passed destructive bend tests, indicating that they had adequate mechanical properties and that the laser paint removal process was successful (shown in Figure 4.12).

Although the laser removal process was capable of producing surfaces that welded successfully, there were some concerns with the process: the production of an oxidised surface (Figure 4.14), production and deposition of debris (Figure 4.2), a long processing time from the high number of pulses required and "over-treatment" of the surface with excessive oxidation (Figure 4.11).

The laser removal process created an oxidised surface which was unavoidable, as metal oxidation occurs instantaneously on exposure to the atmosphere. However, if the laser treatment continued beyond the initial metal exposure then there was further oxidation and over-treatment. It is important to avoid over-treatment of the surface as the oxide produced was incorporated into the weld microstructure and although this did not hinder the weld mechanical properties tested in the bend tests there may be a reduction in other properties. Other work into laser paint removal processes has observed a reduction in ductility and an increase in fatigue life, but this was due to compressive residual stresses in the surface and oxide incorporation was not noted [202].

To limit oxide incorporation into the welds surface over-treatment needed to be minimised. To achieve this each surface region must receive the exact number of pulses required to remove the surface layers at that point. To achieve this over an area the surface layer thickness (for example paint) would have to be measured and then the appropriate number of pulses applied, which adds complexity to the process. If processing does not take into account the thickness variation and the same number of pulses per unit area was applied over the whole surface, then there would be regions of under-treatment and over-treatment.

Therefore to ensure complete removal without over-treatment thickness variation of the layer must be taken into account in processing. For example if it were a paint layer being removed there is variation at the edges of the samples with paint build up.

The excimer laser paint removal treatment was designed in stages to minimise over-treatment as at each stage the processing parameters, energy and number of pulses per unit area, were designed to remove a specific layer. This was required as each layer (anodising, paint and debris) had different properties, chemistry and laser interaction [10, 41]. The problem with a multiple stage treatment is that it adds cost and complexity to the process.

In the current work careful selection of processing parameters in a staged treatment created a laser paint removal process that was suitable for the surface preparation of FSW. An alternative process to laser paint removal is machining which can be quicker and still provide the necessary accuracy of removal.

Machining is an acceptable process for the pre-treatment of FSW components as it can easily be used to treat areas that are long and continuous. However, there are drawbacks to using machining processes as FSW preparation, including substrate damage, generation of a large amount of swarf and high labour intensity. In general, machining will also have problems where access is restricted, but these restrictions are likely to be the same as those of a FSW machine and therefore where a FSW machine is being used then the access will also be suitable for machining. Machining is also capable of material removal at fast rates on an adapted milling machine which could also perform FSW (further description of the milling machine adaptation into a FSW machine is in Section 3.2.6.3 and [17]). The machining and

FSW processes would use the same machine but different tool heads would be interchanged automatically in an industrial process. The high processing speed of machining and FSW on one machine would not be achievable with laser paint removal as the process involves multiple stages and is much slower than FSW [11, 36-38]. Machining is the preferred method for FSW preparation as even with the disadvantages the process is capable of producing suitable treatment areas at high speeds.

The laser paint removal process has been shown to be capable of preparation of surfaces for FSW. However, it may not be the most suitable process for this task, but as the process is highly specific and controllable there are other applications where access is restricted or small localised removal is required, such as repair.

The post-weld treatment for FSW was required to increase the weld corrosion resistance. HPBSM with lasers (LSM) and electron beams (EBSM) can achieve this by altering material surface microstructure through rapid solidification. Table 9.2 summarises the results from the LSM and EBSM processes by the modified layer characteristics that were produced and Table 9.3 summarises the affects on the modified layer from each of the processing parameters investigated; energy, pulse duration and number of pulses per unit area.

The most successful high power beam post-weld treatment in terms of increasing the corrosion resistance of AA2024 material in both the parent and FSW states was excimer LSM [15, 16, 18, 33, 45, 58, 59, 109, 127, 130, 131, 203, 205]. This improvement in corrosion resistance was due to the formation of a homogeneous surface layer in terms of microstructure and composition, by the dissolution of precipitates into solution and then solute dispersion through convection mixing within the liquid phase. The solute dispersion is maintained in the solidified surface

layer through planar solidification from high cooling rates characteristic of rapid solidification [31].

Table 9.2 Comparison of modified layer properties and pulse duration for high power beam surface modification processes used in this thesis.

Property / High Power Beam	Pulse Duration	Modified Layer Thickness	Modified Thickness for Cracking Onset	Modified Thickness for Solute Dispersion by Mixing Onset	Type of Solute Dispersion Observed
Excimer LSM	25ns	3-5μm	-	3-5μm	Convection
USP-CO_2 LSM	7-30μs	12-45μm	24μm	14μm	Convection
EBSM	5-40μs	5-40μm	5-10μm	15μm	Convection
Nd:YAG LSM	10-50ms	300-550μm	300μm	-	-

Table 9.3 Summary of the influence of laser surface melting processing parameter on the properties of the resultant modified layer.

Processing Parameter	Properties of Modified Layer Influenced
Energy	Maximum Temperature Precipitate Dissolution Degree of Vaporisation Modified Layer Thickness Cooling Rate Solidification Structure Degree of Mixing Degree of Cracking
Pulse duration	Maximum Temperature Precipitate Dissolution Time material in Liquid State Modified Layer Thickness Cooling Rate Solidification Structure Precipitate Dispersion Degree of Cracking
Number of pulses per unit area	Degree of Mixing Precipitate Dispersion Layer Homogeneity Accumulation of any property that is changed in a single laser pulse

The corrosion resistance improvement was dependent on the removal of precipitates and this removal process can be separated into stages: dissolution of precipitates, solute dispersion and maintaining precipitate removal through planar solidification.

For the complete dissolution of all precipitates present in a surface the temperature must be raised above that of the highest precipitate melting point. However, such high temperatures may also be enough to initiate vaporisation and loss of elements.

The solute dispersion within the modified layer has been observed to occur in EBSM processes by two mechanisms diffusion and convection mixing, as listed in Table 9.2 and shown by P. Ryan in Figure 8.40. The solute dispersion is important as the solute concentration needs to be as homogeneous as possible to minimise the risk of precipitation on solidification. From the two mechanisms a greater extent of solute dispersion was observed with convection mixing which makes this the preferred mechanism to induce in HPBSM, although diffusion will occur also.

Once solute dispersion has occurred the homogeneity needs to be maintained and solidification needs to be rapid to trap the solute in solid solution by planar solidification. If the cooling rates are below the ultimate limit for planar solidification then segregated microstructures of dendrites and columns can form as was observed in Nd:YAG LSM. These segregated microstructures are unfavourable in HPBSM processes, as in previous studies corrosion has been observed within segregated structures in LSM material [110].

Excimer LSM provided a corrosion resistance improvement through the dissolution, solute dispersion and planar solidification however, the modified layer was not completely homogeneous. This suggests that some degree of heterogeneity can be present in the modified layers and still provide a corrosion resistance improvement. In excimer LSM the segregation was; distorted precipitates, solute trails and precipitate bands at the base of the modified layer in the transient region [31, 74].

The maximum amount of segregation that can be present within a modified layer and still provide a corrosion resistance improvement is unknown, but a corrosion resistance increase is more likely to be achieved if segregation is minimised.

To minimise segregation there needs to be dissolution, solute dispersion and planar solidification. Dissolution is achieved readily in HPBSM, but the other two stages of solute dispersion and planar solidification vary with the processing parameters used, as listed in Table 9.3. Planar solidification varies with the cooling rate induced and is only beneficial if there has been a large amount of solute dispersion.

Solute dispersion has been observed in HPBSM by diffusion and mixing by convection [31, 74, 88]. If there is not a large amount of solute dispersion then the precipitates reform on solidification as was the case in the EBSM layers investigated by P. Ryan where there was only solute dispersion by diffusion (shown in Figure 8.40) [31]. P. Ryan also investigated the solute dispersion that provided the corrosion resistance improvement in excimer LSM and this showed large scale solute dispersion to occur by convection mixing. A greater degree of

solute dispersion occurs by convection mixing, making it the preferred solute dispersion method in HPBSM processes [31, 74].

The initiation of solute dispersion by convection movement in a liquid can occur by a number of different mechanisms, with the most influential being vaporisation and surface tension gradients [72, 77, 121, 145, 191]. Both of these mechanisms are dependant on the modified layer surface temperature, as vaporisation requires high temperatures and surface tension gradients depend on temperature differences [17, 31, 94]. The onset of vaporisation is observed in HPBSM by a change in the surface appearance, with it becoming more reflective, as observed in some EBSM and all of the LSM treatments. It is unclear which of these two initiation mechanisms is preferred in HPBSM although if convection mixing initiated by vaporisation could be avoided then there would be no loss of elements.

Another concern with using vaporisation to induce solute dispersion by convection mixing is that on vaporisation the surface is at the vaporisation temperature and modified layer thickness is at a maximum for that processing energy (Section 2.6.3.3) and large thermal stresses are present, which may be sufficient to initiate cracking within the modified layer. If the modified thickness is large enough to initiate cracking then there will be no improvement in the corrosion resistance, as was the case in non-uniform melt zones in EBSM (Figure 8.34). To avoid cracking within the layer, the modified layer thickness should be reduced and vaporisation avoided which means that surface tension gradients are then relied upon to achieve the required solute dispersion.

The initiation mechanisms for solute dispersion were dependant on temperature and therefore the processing parameters, Table 9.3 summarises that the number of pulses per unit area and energy have the greatest influence on the degree of convection mixing observed in all of the HPBSM processes investigated. It should also be noted that for EBSM, it was observed that there is an influence of pulse duration on the degree of convection mixing. Variation in these processing parameters can therefore be used to maximise the solute dispersion by convection mixing and the corrosion resistance increase.

In excimer LSM there was adequate solute dispersion to increase the corrosion resistance but the layers were too thin to be coupled with anodising processes (Figure 5.13 to Figure 5.16). The application of anodising to LSM surfaces was considered to be a requirement for using LSM in aerospace applications. To design a HPBSM treatment suitable for aerospace applications, the minimum modified layer thickness required to survive the anodising process needs to be identified and designed for. Table 9.3 shows which processing parameters can be used to increase the modified layer thickness and meet the minimum modified layer thickness requirement set by anodising processes.

The modified layer thickness is increased by raising the temperature increase further into the surface this is achieved through variation in the processing parameters by increasing either the energy or the pulse duration (Table 9.3) [89, 96, 99, 105, 108]. In excimer LSM the surface is at the vaporisation temperature and the maximum melt depth has been reached for this pulse duration, so an energy increase does not increase the modified layer depth. Therefore, to increase the modified layer thickness of the layers produced by the excimer laser means an increase in the pulse duration, but this requires the use of different lasers or an electron beam.

There is a limit to the increase in modified layer thickness that can be induced by an increase in pulse duration because as the modified layer thickness increases, the cooling rate and solidification front velocity decrease, which can allow precipitation and segregation to occur. The reduction in solidification front velocity can be a particular problem if it is reduced below the limit for planar solidification as this causes a segregation solidification microstructure to form.

Another concern is that an increase in the modified layer thickness also increases the thermal stresses that can cause cracking within the modified layer. The location of cracking in HPBSM processed samples can be related to a number of different microstructure features: precipitates (e.g. at the interface), grain boundaries and the transient region microstructure. The removal of these microstructure features from the modified layer would reduce the amount of cracking observed.

An increase in modified layer thickness can lead to cracking and segregation within the modified layers, which are both detrimental to the corrosion resistance. Ideally, processing parameters are required that produce the largest possible modified layer thickness with a large amount of solute dispersion by convection mixing but also avoids segregation and cracking within the modified layer.

Such a processing parameter window was observed in USP-CO_2 LSM (Figure 6.12 and Figure 6.13) but not in EBSM (Figure 8.25 to Figure 8.27) which have similar pulse durations

and modified layer thicknesses. USP-CO_2 LSM, produced layers that had solute dispersion by convection mixing but not cracking (Figure 6.2).

The difference in the occurrence of mixing and cracking within similar thickness modified layers produced by EBSM and USP-CO_2 LSM, is due the difference in surface interaction from the different radiation forms of lasers and electron beams as shown in Figure 9.1.

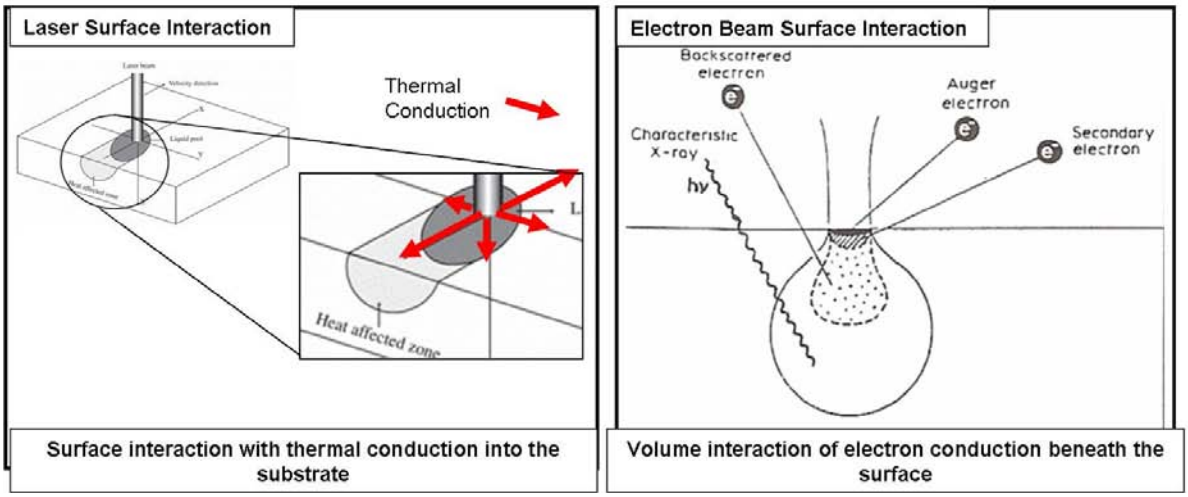

Figure 9.1 Diagrams comparing the surface interaction of lasers and electron beams [93, 149].

Figure 9.1 shows that the electron beam interacts with a volume of material beneath the surface and this is due to the scattering of electrons from collisions with nuclei, which transfers the electron energy into the material [99]. In EBSM therefore, the temperature gradient follows the electron energy loss profile. The magnitude of the electron interaction volume depends on the electron conduction and therefore also the material composition.

In comparison, Figure 9.1 shows that the laser radiation interacts with the surface and the radiation is absorbed through the excitation of surface electrons which increases atomic motion and heats the material. Once the laser radiation is absorbed by the surface, Figure 9.1

shows that heat propagates into the material in all directions through thermal conduction. The maximum energy intensity is therefore at the surface. The depth of heat propagation can be much greater than the depth of radiation absorption and this means that temperature gradients depend on the heat conduction [99].

The different surface interaction of lasers and electron beams (shown in Figure 9.1) can influence the modified layer in HPBSM in a number of ways. An important example is the difference in the volume of deposition as this is smaller with lasers compared with electron beams. The smaller deposition volume means that in LSM, higher temperatures and larger thermal gradients can be reached [99]. These large temperature gradients in LSM are beneficial as they create large surface tension gradients for the initiation of convective mixing and also high cooling rates which are likely to be sufficient for planar solidification.

To provide the corrosion resistance improvement regardless of the type of beam used in HPBSM, the solidification front velocity must be above the critical value required for planar solidification to retain the solute dispersion and avoid a segregated solidification structure. In HPBSM, the solidification is always heterogeneously nucleated as the liquid is in contact with the solid substrate. This means that the solidification front moves from the solid substrate up to the surface following the thermal gradient. The solidification front moves from the substrate and accelerates from stationary towards the surface (Figure 2.12 [74]).

As the solidification front accelerates from stationary this means that there is always a region of slow growth at the base of the modified layer, which has been referred to as the transient region. The solidification front velocity in this transient region can be below the limit for

planar solidification and therefore there can be precipitation, segregation and a different solidification microstructure [31, 74, 88].

Precipitation occurs preferentially in the transient region as bands of precipitates. The number of precipitate bands has been correlated to the number of pulses per unit area in LSM, but not in EBSM. This correlation in LSM was due to each pulse creating a separate solidification front and precipitate band. This also occurred in EBSM, but the variation in the modified depth between pulses meant that precipitate bands formed over a variety of depths and precipitate bands from earlier pulses were dissolved by subsequent pulses. This meant that there were fewer precipitate bands than pulses per unit area (Figure 8.10). This occurred in EBSM as each pulse altered by a small amount the properties that affected electron conduction which meant a change in both the electron interaction depth and modified layer thickness. The property change from one radiation pulse is therefore cumulatively increased by using multiple pulses.

The different microstructure that forms in the transient region makes the region susceptible to corrosion and can lead to de-lamination of the modified layer as was observed in corrosion tests of excimer LSM [18, 127].

As the properties of the transient region are inherent to HPBSM processes, the de-lamination of the modified layer could be unavoidable once the modified layer is breached. Therefore the modified layer thickness must be large enough to prevent this region being exposed to the environment.

These investigations into LSM and EBSM have identified the key processing parameters for HPBSM along with the fundamental differences that can occur with the type of beam used. To apply HPBSM to increase the corrosion resistance of aerospace alloys, the current investigations have identified the necessary modified layer requirements: a large layer thickness to survive anodising, a large enough layer to protect the transient region from exposure to the environment, a thin enough layer thickness to avoid cracking, initiation of solute dispersion through convection mixing to increase homogeneity within the layer and planar solidification to maintain the gained homogeneity.

This ideal surface modification has not been achieved but further work into HPBSM would result in the ideal surface layer for aerospace applications.

To increase material corrosion resistance using EBSM treatments, there needs to be careful control of the processing parameters that control the modified layer thickness i.e. energy and pulse duration. As thinner modified layers have lower thermal stresses, this could mean cracking can be avoided but the surface tension gradients would still be present to induce convection mixing. A reduction in pulse duration would require acceleration of the cathode discharge by modification of the electron beam system electronics. The energy can be more easily changed by performing treatment away from the beam focus. The removal of cracking from a modified surface would allow for a more detailed study on solute dispersion by convection mixing within the modified layer and what extent of solute dispersion would be required for a corrosion resistance improvement to parent and FSW surfaces.

In the LSM treatments, the USP-CO_2 laser produced layers with reasonable thickness with solute dispersion by convection mixing occurring before cracking and the excimer laser

produced layers of increased corrosion resistance. The layers produced from USP-CO_2 LSM had less convective mixing compared with those of excimer LSM [18, 31, 45]. The convection mixing observed in excimer LSM was enough to increase the corrosion resistance although some heterogeneity remained within the layer, but at this point in time it is unclear as to whether this level of solute dispersion was the minimum amount required for such an improvement. To utilise any solute dispersion from multiple pulses in USP-CO_2 LSM, the process needs to be developed to create a uniform treatment with controlled beam overlap and scanning.

Successful application of FSW in aerospace structures requires both pre- and post-weld treatments. High power beams can be used for both treatments with laser paint removal as the pre-weld treatment and HPBSM as the post-weld treatment (LSM and EBSM). Investigations identified both laser paint removal and HPBSM processes that achieved the requirements for FSW application. Although the ideal modified layer has not been achieved (as described previously) in this work future work into the development of the USP-CO_2 laser and electron beam system could achieve this.

Whilst laser paint removal and HPBSM meet the FSW application requirements they may not be suitable at present as industrial production processes due to the long processing times required in laser paint removal (compared to machining) and in HPBSM a consistent corrosion resistance improvement has only been achieved with thin modified layers that do not survive an anodising process. At present a more likely application of laser paint removal and HPBSM is where localised treatment is required such as in repair. More applications however may arise in the future with the phasing out of chromate acid anodising and alternative corrosion protection treatments are being sought.

10 Conclusions

For Friction Stir Welding (FSW) of aerospace materials pre- and post-weld treatments are required and can be performed using high power beams.

A laser paint removal process was designed for FSW surface preparation. The process was successful as the resultant welds had adequate mechanical properties. However, laser paint removal may not be the most suitable process for FSW preparation as only a small amount of material is removed per pulse and the process it is more suited to localised material removal or situations where there is restricted tool access.

Excimer Laser Surface Melting (LSM) was used as the FSW post-weld treatment to increase corrosion resistance by precipitate removal through dissolution and dispersion. To provide adequate solute dispersion, convection movement within the modified layer was critical. Once the dispersion had increased the surface homogeneity it was maintained on cooling through planar solidification.

The HPBSM processing parameters controlled the modified layer characteristics in terms of solute dispersion, solidification structure and modified layer thickness. Excimer LSM layers were thin and were consequently completely consumed by the standard corrosion protection treatment of anodising. Thicker modified layers could not be formed using the excimer laser as the layer thickness was under pulse duration control and this parameter could not be modified, which meant that other lasers and electron beams that could vary the pulse duration were required. A thicker modified layer thickness produced by other high power beams

provided greater protection to the substrate and transient region of the modified layer as once the modified layer is breached there can be accelerated corrosion of the substrate or along the modified layer transient region causing layer de-lamination. The transient region is susceptible to corrosion due to fine line of precipitates which forms there and variation in the solidification structure but it is an inherent part of the modified layer due to heterogeneous solidification and varying growth front speed.

For the ideal application of HPBSM to fiction stir welds to increase the corrosion resistance requires that the treatment processing parameters induce solute dispersion by convection mixing, planar solidification and produce an adequate modified layer thickness that avoids exposure of the transient region.

11 Future Work

To use laser paint removal processes for FSW preparation or more localised removal applications there needs to be further investigation into the affect of the process on the material mechanical properties such as fatigue.

For the development of HPBSM there are many recommendations for further work:

- Identification of the substrate factors on material removal in anodising.
- Investigate the affect of pulse repetition frequency on the modified layer properties.
- Investigate the different HPBSM solidification structures to understand their relationship to composition and identify at what modified layer thickness they change
- Investigate segregation in HPBSM to quantify what degree of segregation and grain boundaries can be tolerated and still improve the corrosion resistance.
- Investigate convection mixing in HPBSM to quantify the amount of solute dispersion required to increase corrosion resistance and understand the influences from surface tension or vaporisation.
- Investigate the relationship between modified layer thickness and the initiation of cracking to identify the maximum layer thickness for convection mixing to occur before cracking.
- Investigate the effect of vaporisation and the loss of elements on the modified layer corrosion resistance.
- Develop USP-CO_2 LSM into a uniform treatment and investigate the effect of using a helium atmosphere.

- Develop EBSM with a decrease in the modified layer thickness and investigate how modified layer depth changes with surface composition or electrical properties through EBSM of a range of alloys.

12 Appendix 1 – Summary of Laser Surface Melting Treatments, Review of the Literature

Reference	First Author	Laser	Modified Layer Thickness	Number of pulses and Pulse Duration	Power or Fluence	Material
[12]	T.M. Yue	Excimer	8μm	25ns 2mm/s	10.3J/cm^2	AA7075
[13]	G. Abbas	Cw-CO_2	1mm	160mm/s	1.5kW	AZ31, AZ61, WE43, Mg alloy
[14]	S.W. Williams	Excimer	5-10μm	9 at 25ns	10J/cm^2	AA2024-T351 AA7010-T7651
[15]	P.C. Morgan	Excimer	-	20 at 120ns	5J/cm^2	AA8090-T8171
[16]	P.C. Morgan	Excimer	-	10 pulses	5J/cm^2	AA8090
[29]	R. Li	CO_2 2kW	> 100μm	-	-	AA2024-T351
[31]	P. Ryan	Excimer Nd:YAG CO_2	5-10μm,	9 at 25ns	10J/cm^2	AA2024 AA7010
[74]	P. Ryan	Excimer	10μm	25ns	10J/cm^2	AA2024 and AA7150
[79]	M. Zimmermann	CO_2	-	0.2-8m/s	1000-1500W	-
[80]	S.C. Gill	-	-	0.01-2m/s	-	Al-Cu
[81]	S.C. Gill	Cw-CO_2 laser	150μm	0.01-10m/s	1200 1750W	Al-Cu
[82]	P.H. Chong	Cw-Nd:YAG	20μm	0.75-2m/min	-	AA2014
[88]	P. Ryan	Excimer Nd:YAG CO_2	Range	Range	Range	AA2024, AA7xxx
[90]	T.H. Sarnet	Excimer	-	>300ns	0.3-120J/cm^2	AA2017
[18]	C. Padovani	Excimer	5-10μm	9 at 25ns	10J/cm^2	AA2024 AA7010
[93]	M.A. Pinto	1kW cw-CO_2	-	500 - 800mm/min	-	Al-15wt% Cu
[95]	F. Audebert	CO_2	20-40μm	> 2m/s	2.8x10^{6}J/cm^2	Zirconium, Magnesium and Aluminium Alloys
[96]	P. Kadolkar	Nd:YAG	433-767μm	100-200cm/min	1714-3429J/cm^2	AA2024 AA6061
[98]	M. Tagarsakis	CO_2	8-30μm	15-20μs	70-150J/cm^2	Al-alloys AA2xxx, AA2024
[102]	G.N. Haidemenopoulos	Excimer	-	29ns	Range	Al-7Si Al-4Mg-1.3Li

[103]	S.W. Williams	TEA-CO_2, cw-CO_2 Excimer	Range	Range	Range	AA8090 AA2024
[104]	P.L. Bonora	Ruby	-	15ns	1-5J/cm^2	Pure Aluminium
[106]	Z. Liu	CO_2, Nd:YAG	5-20µm 10-15µm	5-50mm/s	1.6-3kW	AA2014, AA2024, AISI304L, 3CR12
[108]	R. Bujte	Excimer	-	10Hz,	4mJ	Ti6V4Al
[109]	M.A. Mahon	CO_2 Nd:YAG	Range	Range	Range	AA2014-T651 AA7075-T6
[110]	Z. Liu	Excimer 2kW cw-CO_2	-	20ns, 0.5-180mm/s	140mJ/pulse 2.4-3.2 x10^5W/cm^2	AA2014, Cr LSA
[111]	J. Noorduis	Cw-CO_2	-	1/8-25cm/s	-	AA2024-T3
[112]	H.J. Hegge	CO_2	Range	1-40cm/s	1300W	Al-Si
[113]	J.L. de Mol van Otterloo	Cw-CO_2 laser	-	0.0125-0.125m/s	1300W	AA2024 Al-Cu
[114]	T.M. Yue	Excimer	8µm	25ns	3.6 and 9.9J/cm^2	AA8090
[115]	T.M. Yue	Excimer	-	-	2.5J/cm^2	Ti-6Al-4V
[116]	D. Dube	Nd:YAG	100-200µm	1, 6ms 3 -20mm/s	100 and 300W	Mg Alloy AZ91D, AM60B
[117]	E. McCafferty	CO_2	10µm	150ns – 1/3 energy, 1.8µs 2/3 energy,	60J	1.2%Mn, 3003
[118]	H. Badekas	Excimer KrF	-	-	250mJ	Al-Cu
[119]	W.L. Xu	Excimer	5-10µm	2mm/s	5.5J/cm^2	AA6013
[121]	O. Kachurina	Excimer	-	15ns 20-1000 pulses	0.02-5J/cm^2	AA2024-T3
[123]	K.G. Watkins	CO_2	-	-	3.2x10^5 W/cm^2	AA2014
[124]	T.T. Wong	CO_2	1.2mm	-	-	Al-Si
[125]	Z. Liu	CO_2	-	15-180mm/s	1.6kW	AA2014 AA2024
[126]	S. Tosto	Excimer, XeCl	<20µms,	-	120ns	Fe, Ti, Ti64, AA2219, Cu, 316SS, Al
[129]	C. Spadaro	Nd:YAG	-	4ns	0.5-10J/cm^2	AA2024-T3

[130]	P. Mazzoldi	Ruby	1μm	15ns	1J/cm^2	Aluminium
[132]	L.F. Guo	Excimer	1.5-2μm	25ns, 2-10mm/s,	6J/cm^2	WE43 Mg alloy
[144]	M. Autric	KrF Excimer	Al-Alloys <10μm, 35NCD16 <3μm	20ns, <50shots per unit area	1.7-4.1J/cm^2	Al-Alloys, AA2xxx, AA2017 AA6xxx, AA6056 Steels, 35NCD16304, 434LSS Cr coated mild steels
[145]	C.P. Chan	KrF Excimer	5μm	25ns	9.3J/cm^2	AA6013
[146]	C. Padovani	Excimer	5-10μm	9 at 25ns	10J/cm^2	AA2024 AA7010
[203]	C. Padovani	Excimer	5-10μm	9 at 25ns	10J/cm^2	AA7449
[204]	P.L. Bonora	Ruby	-	15ns	3.5J/cm^2	Pure Al
[206]	T.M. Yue	Excimer	8μm	25ns	8J/cm^2	AA7075
[207]	E. Sicard	Excimer	5μm	28ns, 100-2000 pulses	1-3J/cm^2	AlSi7Mg
[208]	N.H. Prasad	Nd:YAG	Range	2.5ns 10 pulses	650mJ	Al-Li-Cu
[209]	D. Dube	Nd:YAG	100-200μm	1, 6ms 3 -20mm/s	100 and 300W	Mg Alloy AZ91D, AM60B
[210]	S. Tosto	Excimer, XeCl	<20μms,	-	120ns	Fe, Ti, Ti64, AA2219, Cu, 316SS, Al
[211]	C. Spadaro	Nd:YAG	-	4ns	0.5-10J/cm^2	AA2024-T3
[212]	P. Mazzoldi	Ruby	1μm	15ns	1J/cm^2	Aluminium

13 Appendix 2 – Summary of Electron Beam Surface Melting Treatments, Review of the Literature

Reference	First Author	Layer Thickness	Pulse Duration	Power or Fluence	Material
[121]	T.R. Anthony	0.3cm	2cm/s	-	304SS
[144]	Y. Qin	-	0.8μs	2.25, 3.7, 5J/cm^2	Aluminium
[145]	J. Zou	2-3μm	0.5-5μs, 1.5μs	1-6J/cm^2,	Aluminium, Mould steel D2H13, steel GCr15
[146]	S.Z. Hao	-	5μs	10^4 beam current	Al
[151]	D.I Proskurovsky	-	1μs	10-45keV	Iron
[163]	T. Grosdidier	-	1.5μs	3J/cm^2	Treatment below melting threshold Fe-Al alloy
[164]	V.P. Rotshtein	100μm Iron 200μm steel 7μm AA2024	0.02-300μs	1-2000J/cm^2	Iron, Copper, Iron-carbon alloy aluminium alloy
[165]	R.G. Song	-	1.8m/min	-	AISI 321 Al-Alloy AA2024
[166]	M. Ahmad	-	600mm/min	40kV, 20μA	Ni alloy single crystal
[167]	A. La Barbera	2mm	20cm/min	60kW	316 on Plain carbon steel
[168]	V.P. Rotshtein	0.5μm	2.5μs	2-10J/cm^2	304l and 316L
[169]	D.I Proskurovsky	5μmIron, 25μmAA2024	0.5-5μs	0.5-40J/cm^2	Iron, Ti alloys, steels, hard materials, al-alloys AA2024, 6061
[170]	Y. Ivanov	0.1-1μm	2.5μs	3-18J/cm^2	High speed steel
[171]	J. Zou	5 pulses 3.1μm 25 pulses 4.4μm	1μs	10^9-10^{12}W/cm^2	AISId2 cold worked die steel
[172]	N. Mingolo	100μm	20μs	-	MgZn alloys
[175]	S. Tosto	Tens of microns	150-200ms	500-600kW/cm^2	Pure Al, 5Si,3Cu, Mg Al-alloy
[177]	D.A. Price	-	100μs	12J	NAB
[178]	T. Bell	-	5mm/s	-	Ti alloys
[179]	Y. Uno	-	2-3μs	1.4-10.7J/cm^2	NAK80 Daido steel
[180]	V.P. Rotshtein	0.5μm	2-3μs	1-40J/cm^2	High speed steel
[181]	D.I Proskurovsky	7μm AA2024	0.5-5μs	0.5-40J/cm^2	Steels, Al-alloys, Ti-alloys,

[182]	D.S. Nazarov	7-10μm	Microsecond	2-5J/cm^2	AA2024, 6061
[183]	S.H. Choo	-	2.45cm/s	5.2-7.7kW	AISI 4140
[184]	A. Zecca	6μm	0.75μs	2.3-5.2J/cm^2	α-Fe
[185]	V.P. Rotshtein	0.5-1μm	2-3μs	2.4-8.4J/cm^2	Copper sputtered 316L
[186]	K. Zhang	-			316L SS
[187]	M. Ahmad	-	600mm/min	40kV, 20μA	Zircaloy 4 and SiC
[188]	B. Gao	2μm discontinuous	1μs	2.5J/cm^2	Mg alloy AZ31
[189]	C. Dong	1μm	5μs	10^8-10^9W/cm^2	Pure AL, Mold Steel
[191]	B. Gao	8-10μm	1μs	3J/cm^2	Mg alloy AZ91HP
[192]	S. Hao	5μm steels, 10μm Mg-alloy α	1μs	2.2J/cm^2	Carbon steel, Mould steel Mg alloy AZ91HP
[213]	P. Petrov	-	0.5-2.5cm/s	-	Al-Si
[214]	W. Biller	<1μm	10ms	0.01-2J/cm^2	Aluminium, Al-Mg-Si

14 References

1. G.S. Frankel, *Pitting corrosion of metals.* Journal of electrochemical society 1998. 145(6).
2. E.A. Starke and J.T. Stanley, *Application of modern aluminium alloys to aircraft.* Progress in aerospace science, 1996. 32: p. 131-172.
3. S. Church, J. Bailey, S. Childs, C. Figgures and S. Harris, *Chromate free conversion coatings: A surface analytical study of Alodine 1200, 2600 and Sanchem 3400,* 2000, BAE Systems. JS14467.
4. C.M. Rangel, T.I. Paiva and P.P. daLuz, *Conversion coating growth on AA2024-T3. The effect of pre-treatments.* Surface and Coating Technology, 2008. 202: p. 3396-3402.
5. P.B. Pragnall and A.F. Norman, *Cost effective manufacturing of welding aerospace materials,* 2000, University of Manchester Institute of Science and Technology.
6. M. Ericsson and R. Sandstrom, *Influence of welding speed on the fatigue of friction stir welds, and comparison with MIG and TIG.* International Journal of Fatigue, 2003. 25(12): p. 1379-1387.
7. W.M. Thomas, E.D. Nicholas and J.C. Needham, 1995, Improvements relating to Friction welding. European 92923926.6.
8. W.M. Thomas, E.D. Nicholas, J.C. Needham, M.G. Murch, P. Temple-Smith and C.J. Davies, 1995, Improvements related to Friction Welding. United States US005246317A.
9. R.S. Mishra and Z.Y. Ma, *Friction stir welding and processing.* Materials Science and Engineering R, 2005(50): p. 1-78.
10. P.W. Feesik and F.A. Lancaster, *Laser based paint decoating process.* Metal Finishing, 2000: p. 10-14.
11. C.T. Walters, B.E. Campbell and R.J. Hull. *Laser cleaning of metal surfaces*. *SPIE* 1998 3343. Santa Fe, New Mexico.
12. T.M. Yue, L.J. Yan, C.P. Chan, C.F. Dong, H.C. Man and G.K.H. Pang, *Excimer laser surface treatment of aluminium alloy AA7075 to improve corrosion resistance.* Surface and Coatings technology, 2004. 179(2-3): p. 158-164.
13. G. Abbas, Z. Liu and P. Skeldon, *Corrosion behaviour of laser melted magnesium alloys.* Applied surface science, 2005. 247: p. 347-353.
14. S.W. Williams, D.A. Price and A. Wescott, *The use of laser surface melting treatments to improve corrosion resistance of friction stir welds,* March 2003, Internal report BAE Systems JS14981.
15. P.C. Morgan and P.L. Salter, *The effect of pulse length on the corrosion of Excimer laser surface treated 8090-T8171 Al-Alloy,* 1993, BAE SYSTEMS Report JS 12404.
16. P.C. Morgan and G. Scott, *The corrosion of Excimer laser surface treated Al-alloys,* 1993, BAE SYSTEMS Report JS 11645.
17. S.W. Williams, *DUWALP Special Technical Report* 1993, BAE SYSTEMS Report JS 12541.
18. C. Padovani, *Corrosion protection of friction stir welds in aerospace aluminium alloys,* 2007, University of Birmingham, Metallurgy and Materials, PhD.
19. S.W. Williams, *Laser Surface Melting Modelling Discussion*, May 2004, E. Siggs.

20. D.A. Price, *Pulsed high power electron beam materials processing* 2004, BAE Systems Advanced Technology Centre Internal Report.
21. I.J. Polmear, *Light alloys, Metallurgy of light metals*. 1981: Edward Arnold.
22. *The Aluminium Association International Alloy Designation and Chemical Composition Limits for Wrought Aluminium and Aluminium Alloys*. 1998.
23. C. Blanc, B. Lavelle and G. Mankowski, *The role of precipitates enriched with copper on the susceptibility to pitting corrosion of the 2024 aluminium alloy.* Corrosion science, 1997. 39(3): p. 495-510.
24. P.C. Morgan and P. Nichols, *Localised corrosion 2014-T4 alloy,* 1998, Internal report, JS13808, Issue 1, BAE Systems, Sowerby research centre.
25. J.R. Davis, ed. *Aluminium and Aluminum Alloys*. ASM Speciality Handbook. 1994, The Materials Information Society. 394-395.
26. V. Guillaumin and G. Mankowski, *Localized corrosion of 2024-T351 aluminium alloy in chloride media.* Corrosion Science, 1999. 41: p. 421-438.
27. A.E. Hughes, R.J. Taylor, K.J.H. Nelson and L. Wilson, Materials science and technology, 1996. 12: p. 928-936.
28. S.C. Wang and M.J. Starink, *The assessment of GPB2/S'' structures in Al-Cu-Mg alloys.* Materials Science and engineering A, 2004. 386: p. 156-163.
29. R. Li, M.G.S. Ferreira, A. Almeida, R. Vilar, K.G. Watkins, M.A. McMahon and W.M. Steen, *Localized corrosion of laser surface melted 2024-T351 Aluminium Alloy.* Surface and Coatings technology, 1996. 81: p. 290-296.
30. P. Campestrini, E.P.M. van-Westing, H.W. van-Rooijen and J.H.W. de-Wit, *Relation between microstructural aspects of 2024 and its corrosion behaviour investigated using AFM scanning potential techniques.* Corrosion science, 2000. 42: p. 1853-1861.
31. P.J. Ryan, *Surface treatment of aluminium aerospace alloys using pulsed laser and electron beam systems,* 2007, The University of Manchester, School of Materials, PhD.
32. A. Squillace, A.D. Fenzo, G. Giorleo and F. Bellucci, *A comparison between FSW and TIG welding techniques: modifications of microstructure and pitting corrosion resistance in AA 2024-T3 butt joints.* Journal of Materials Processing Technology, 2004. 152(1): p. 97-105.
33. R. Ambat, M. Jariyaboon, A.J. Davenport, S.W. Williams, D.A. Price and A. Wescott. *Micro-electrochemical investigations of friction stir welds in aluminium aerospace alloy 2024. 15th International corrosion congress*. 2002. Granada, Spain.
34. W.M. Thomas and E.D. Nicholas, *Friction stir welding for the transportation industries.* Materials and Design, 1997. 18(14/16): p. 269-273.
35. C. Goodfellow, *Friction Stir Welding of Aluminium Alloys*, 21/11/05, E. Siggs. EngD Conference presentation.
36. G. Scott, *Assessment of laser paint stripping,* 1991, Bae Systems Report JS 11643.
37. J. Workman, *Scale up tests for laser paint stripping,* 1993, BAE Systems Report JS 12599.
38. J. Sidhu and A. Wescott, *Development of the laser cleaning process,* 2003, BAE Systems Sowerby Research Centre. JS14325.
39. K.X. Liu, E. Garmie and C. Phipps. *Conference on high power laser ablation, Predicting laser coating removal rates. SPIE* 1998 3343 805-813.
40. M.J.J. Schmidt, L. Li and J.T. Spencer, *An investigation into the feasibility and characteristics of using a 2.5KW high power diode laser for paint stripping.* Journal of materials processing technology 2003. 138: p. 109-115.

41. F. Brygoa, C. Dutouquet, F. LeGuern, R. Oltra, A. Semerok and J.M. Weulersse, *Laser fluence, repetition rate and pulse duration effects on paint ablation.* Applied Surface Science, 2005. 252(6): p. 2131-2138.
42. P.B. Pragnall, A.F. Norman, A.A. Hassan, S.W. Williams and D.A. Price, *Effect of welding parameters on nugget zone microstructure and properties in high strength aluminium alloys friction stir welds.* Science and technology of welding and joining, 2003. 8(4): p. 257-268.
43. P.B. Pragnall, A.F. Norman, A.A. Hassan and D.A. Price, *Stability of nugget zone grain structures in high strength al-alloys friction stir welds during solution treatment.* Acta Materialia, 2003. 51(7): p. 1923-1936.
44. M.A. Sutton, B. Yang, A.P. Reynolds and R. Taylor, *Microstrucural studies of friction stir welds in 2024-T3 aluminium.* Materials Science and Engineering A, 2002. 323 p. 160-166.
45. M. Jariyaboon, *Corrosion of friction stir welds in high strength aluminium alloys,* 2006, University of Birmingham, Metallurgy and Materials, School of Engineering, PhD.
46. R.N. Parkins, *Corrosion processes*. 1982: Applied Science publishers.
47. M. Stratmann, *Reprint from encyclopedia of electrochemistry: Intergranular corrosion, corrosion and oxide films*. 2003: Wiley-VCH. Chapter 4.3.
48. E. Mattsson, *Basic Corrosion technology for scientists and engineers*. 1996.
49. E. McCafferty, *Sequence of steps in the pitting of aluminium by chloride ions.* Corrosion science 2003. 45 p. 1421-1438.
50. K.R. Trethewey and J. Chamberlain, *Corrosion*. 1988: Longman Scientific and technical.
51. J.R. Galvele and S.M.d. Micheli, *Mechanism of intergranular corrosion of Al-Cu alloys.* Corrosion Science, 1970. 10: p. 795-807.
52. R. Winsley, A.J. Davenport and B. Connolly, *Corrosion resistance of AA2024-T351 laser surface alloyed with manganese and vanadium,* 2004, University of Birmingham Department Metallurgy and Materials Student Report.
53. I.L. Mueller and J.R. Galvele, *Pitting potential of high purity binary aluminium alloys-I. Al-Cu Alloys. Pitting and Intergranular Corrosion.* Corrosion Science, 1977. 17: p. 179-193.
54. J. M.West, *Basic Corrosion and Oxidation*. 1986: John Wiley and Sons. Chapters 1-9, 10.5.
55. R.G. Bucheit, R.P. Grant, P.F. Hlava, B. McKenzie and G.L. Zender, *Local dissolution phenomena associated with S phase (Al2CuMg) particles in aluminium alloy 2024-T3.* Journal of electrochemical society, 1997. 144(8): p. 2621-2628.
56. F. Andretta, M.M. Lohrengel, H. Terryn and J.H.W. deWit, *Electrochemical characterisation of aluminium AA7075-T6 and solution heat treated AA7075 using a micro-capillary cell.* Electrochemica Acta, 2003. 48(20-22): p. 3239-3247.
57. A.J. Davenport and S.W. Williams, *Laser surface alloying of friction stir welds in high strength Aluminium alloys*. Apirl-May 2004, University of Birmingham presentation.
58. R. Ambat, M. Jariyaboon, A.J. Davenport, S.W. Williams, D.A. Price and A. Wescott, *Laser treatment method for improvement of the corrosion resistance of friction stir welds.* Materials science forum, 2006. 519-521: p. 699-704.
59. A.J. Davenport, R. Ambat, M. Jariyaboon, B.J. Connolly, S.W. Williams, D.A. Price, A.Wescott and P.C. Morgan. *Corrosion of Friction stir welds in aerospace alloys*.

International Conference on Corrosion in the 21st Century. 2003. UMIST, Manchester, UK.
60. M. Jariyaboon, A.J. Davenport, R. Ambat, B.J. Connolly, S.W. Williams and D.A. Price, *The effect of welding parameters on the corrosion behaviour of friction stir welded AA2024-T351* Corrosion science, 2007. 49(2): p. 877-909.
61. J. Corral, E.A. Trillo, Y. Li and L.E. Murr, *Cororsion of friction stir welded aluminium alloys 2024 and 2195* Journal of materials science letters 2000. 19: p. 2117- 2122.
62. R. Ambat, M. Jariyaboon, A.J. Davenport, S.W. Williams, D.A. Price and A. Wescott, *The effect of welding parameters on corrosion behaviour of friction stir welds 2024-T351 Al-alloy,* University of Birmingham Department Metallurgy and Materials.
63. C. Goodfellow, *The corrosion of friction stir welding of Aluminium alloys used in aerospace applications,* 2007, The University of Birmingham, Metallurgy and Materials, PhD.
64. A.d. Frutos, M.A. Arenas, Y. Liu, P. Skeldon, G.E. Thompson, J. de-Damborenea and A. Conde, *Influence of pre-treatments in cerium conversion treatment of AA2024-T3 and AA7075-T6.* Surface and Coating Technology, 2008. 202(16): p. 3797-3807.
65. S.A. Kulinich, A.S. Akhtar, P.C. Wong, K.C. Wong and K.A.R. Mitchell, *Growth of permanganate conversion coating on 2024 Al-alloy.* Thin solid films, 2007. 515 p. 8396-8392.
66. L. Domingues, C. Oliveira, J.C.S. Fernandes, M.G.S. Ferreira and I.T.E. Finseca, *Corrosion behaviour of environmentally friendly treatments for aluminium alloys.* Key engineering materials, 2002. 230/232(193): p. 392-295.
67. R.L. Twite and G.P. Bierwagen, *Review of alternatives to chromate for corrosion protection of aluminium aerospace alloys.* Progress in organic coatings, 1998. 33: p. 91-100.
68. Y. Xingwen, C. Chunan, Y. Zhiming, Z. Derui and Y. Zhongda, *Corrosion behaviour of rare earth metal (REM) conversion coatings on aluminium alloy LY12.* Materials science and engineering A, 2000. 284: p. 56-63.
69. H. Guan and R.G. Bucheit, *Corrosion protection of aluminium alloy 2024-T3 by vanadate conversion coatings, corrosion science section.* Corrosion, 2004: p. 284-296.
70. C. Purry, A. Fien and K. Shankar, *The effect of corrosion preventative compound on fatigue crack growth properties of 2024-T351 Aluminium alloys.* International Journal of Fatigue 2003. 25: p. 1175-1180.
71. W. Kurz, B. Giovanola and T. Trovedi, *Theory of microstructural development during rapid solidification.* Acta Metallurgica materialla, 1986. 34(5): p. 823-830.
72. S.A. David and J.M. Vitek, *Correlation between solidification parameters and weld structures.* International materials reviews 1989. 34 (5): p. 213-245.
73. D.A. Porter and K.E. Easterling, *Phase Transformations in Metals and Alloys*. 2001: Nelson Thornes.
74. P. Ryan and P.B. Pragnell, *Grain structure and homogeneity of pulsed laser treated surfaces on Al-aerospace alloys and FSWs.* Materials Science and Engineering A, 2008. 479: p. 65-75.
75. D.R. Askeland, *The science and engineering of materials*. 1990: Chapman and Hall.
76. D.C. Lin, G.X. Wang and T.S. Strivatsan, *A mechanism for formation of eqiaxed grains in welds of aluminium-lithium alloy 2090.* Materials Science and engineering A, 2003. 351: p. 304-309.

77. J. Mazumder, *Overview of melt dynamics in laser processing.* Optical engineering 1991 30(8): p. 1208-1219.
78. R. Trivedi and W. Kurz, *Morphological stablilty of a planar interface under rapid solidification conditions.* Acta Metallurgica, 1986. 34(8): p. 1663-1670.
79. M. Zimmermann, M. Carrard and W. Kurz, *Rapid Solidification of Al-Cu eutectic alloy by laser remelting.* Acta Metallurgica, 1989. 37(12): p. 3305-3313.
80. S.C. Gill and W. Kurz, *Rapid solidification Al-Cu alloys-II, Calculation of the microstructure selection map.* Acta metallurgica materialla, 1995. 43(1): p. 139-151.
81. S.C. Gill and W. Kurz, *Rapid solidification Al-Cu alloys-I, Experimental determination of the microstructure selection map* Acta metallurgica materialla, 1993. 41(12): p. 3563-3573.
82. P.H. Chong, Z. Liu, P. Skeldon and G.E. Thompson, *Corrosion behaviour of laser surface melted 2014 aluminuim alloy in T6 and T451 tempers.* The journal of corrosion science and engineering, 2003. 16(12).
83. Z. Shi and T. Bell, *Electron beam surface engineering of Al-Bronzes,* 1995, University of Birmingham, School of Metallurgy and Materials, PhD.
84. P.H. Chong, Z. Liu, P. Skeldon and G.E. Thompson, *Large area laser surface treatment of aluminium alloys for pitting corrosion protection.* Applied surface science, 2003. 281-286: p. 399-404.
85. E. Schubert and H.W. Bergmann, *Modification of metallic surfaces by means of Excimer lasers; fundamentals and applications.* Lasers in Engineering 1993. Vol 2 p. 111-155.
86. F. Sanchette, T.H. Loi and C. Frantz, *Deposition of metastable aluminium-chromium alloys by r.f.magnetron sputtering from mixed powder targets.* Surface and coatings technology, 1993. 57: p. 179-182.
87. W.M. Steen, *Laser material processing*. 1991: Springer-Verlag.
88. P. Ryan, *Laser surface melting of aerospace aluminium aerospace alloys,* 2004, University of Manchester, First Year Transfer Report.
89. M.I. Cohen, *Material Processing*. 1972: North-Holland. 1577-1647.
90. T.H. Sarnet, and J.E. Montagne, *Characterisation of metal surfaces irradiated by a long pulse KrF Excimer laser.* Journal of Laser applications, 1994. 6: p. 149-152.
91. K. Burt and G. Scott, *Continuous wave and TEA-CO_2 laser surface processing of Aluminium alloys,* 1995, Issue 1 BAE Systems Sowerby Research Centre Report JS 13298.
92. H.W. Bergmann, B. Juckenath, S.Z. Lee and E. Geissler. *Comparison of surface treatments of different lasers (excimer, Nd:YAG, CO_2). Proceedings 5th international conference lasers in manufacturing*. 1988 327-340.
93. M.A. Pinto, N. Cheung, M.C.F. Ierardi and A. Garcia, *Microstructural and hardness investigation of an aluminium-copper alloy processed by laser surface melting.* Materials Characterisation, 2003. 50 p. 249-253.
94. S.W. Williams, *Drilling*. 2004: Institute of Physics. 1633-1652.
95. F. Audebert, R. Colaco, R. Vilar and H. Sirkin, *Production of glassy metallic layers by laser surface treatment.* Scripta Materialia 2003. 48: p. 281-286.
96. P. Kadolkar and N.B. Dahorte, *Variation of structure with input energy during laser surface engineering of ceramic coatings on aluminium alloys.* Applied surface science, 2002. 199: p. 222-233.

97. C.P. Chan, T.M. Yue and H.C. Man, *The effect of Excimer laser surface treatment on the pitting corrosion fatigue behaviour of AA 7075.* Journal of Materials Science, 2003. 38 p. 2689-2702.
98. M.G. Tsagkarakis, *Laser surface melting of an Al-Cu-Mg alloy for enhanced corrosion resistance,* 2005, Heriot-Watt, Laser and Applied Photonics, PhD.
99. J.M. Poate, G. Foti and D.C. Jacobson. *Surface modification and alloying by laser, ion and electron beams*. *Proceedings of a NATO Advanced study institute on surface modification and alloying* 1983. New York: Plenum press.
100. A.M. Prokhorov, V.I. Konov, I. Ursu and I.N. Mihailescu, *Laser heating of metals*. 1990: Adam Hilger.
101. E. Schubert, H.W. Bergmann, S. Rosiwal and G. Barton, *Aspects of surface treatments with excimer lasers.* Opto elektronik magazine, 1989. 5(7/8): p. 651-661.
102. G.N. Haidemenopoulos, A. Zervaki, K. Papadimitriou, D.N. Tsipas, J. McIntosh, G. Zergoti, A. Manousaki and E. Hontzopoulos, *Surface treatment of metals with excimer and CO_2 lasers.* 9th International symposium on gas flow and chemical lasers, SPIE 1993. 1810: p. 712-715.
103. S.W. Williams, *Special Technical report STR6.3 - Surface treatment of aluminium alloys,* 1995, Project 030091, JS 13169, Issue 1, BAE Systems Internal Report Advanced Technology Centre.
104. P.L. Bonora, M. Bassoli, P.L. DeAnna, G. Battagliu, G. Dellamea and P. Mazzoldi, *Electrochemical and corrosion behaviour of laser modified aluminium surfaces.* Electrochemica Acta, 1980. 125: p. 1497-1499.
105. S. Morgan, *Laser Surface Melting Discussion*, 2008, E. Siggs.
106. Z. Liu, P.H. Chong, P. Skeldon, P.A. Hilton, J.T. Spencer and B. Quayle, *Fundamental understanding of the corrosion performance of laser-melted metallic alloys.* Surface and Coatings Technology, 2006. 200(18-19): p. 5514-5525.
107. S. Fox, A.J. Davenport and B. Connolly, *Corrosion resistance of AA2024-T351 laser surface alloyed with cerium and cobalt,* 2004, University of Birmingham Department Metallurgy and Materials Student Report.
108. R. Butje, *Excimer laser processing of metals considering the effect of pulse duration and geometrical aspects.* SPIE, High power gas lasers, 1990. 1225.
109. M.A. McMahon, *The microstructure and corrosion properties of laser processed aluminium alloys,* 1994, University of Liverpool, PhD.
110. Z. Liu, M.A. McMahon, K.G. Watkins, W.M. Steen, M.G.S. Ferreira and R.M. Vilar. *Pitting behaviour of laser surface melted and alloyed 2014 aluminium alloy*. *ISLOE International Symposium Laser and Optoelectronics Technology and Applications*. 1993 60-65.
111. J. Noorduis and J.T.M.D. Hosson, *Microstructure and mechanical properties of laser treated aluminium alloys.* Acta Matallurgical Materials, 1993. 47(7): p. 1989-1998.
112. H.J. Hegge and J.T.M. DeHosson, *Microstructure of laser treated Aluminium alloys.* Acta Metallurgica Materialla, 1990. 38(12): p. 2471-2477.
113. J.L.d. Otterloo and J.T.M. Dehosson, *Laser treatment of aluminium aopper alloys: a mechanical enhancement.* Scripta metallurgica et materiallia, 1994. 30: p. 493-498.
114. T.M. Yue, C.P. Chan, L.Y. Yan and H.C. Man, *Effect of excimer laser surface melting on intergranular corrosion cracking of aluminium-lithium alloy 8090.* Journal of laser applications, 2004. 10(1): p. 31-39.

115. T.M.Yue, J.K. Yu, Z. Mei and H.C. Man, *Excimer laser surface treatment of Ti-6Al-4V alloy for corrosion resistance enhancement.* Materials Letters, 2002. 52: p. 206-212.
116. E. McCafferty, E.G. Shafrin and J.A. McKay, *Microstructural and surface modification of an aluminium alloy by rapid solidification with a pulsed laser.* Surface technology 1981. 14: p. 219-223.
117. H. Badekas, A. Koutsomichalis and C. Panagopoulos, *The influence of excimer laser treatment on an aluminium alloy surface.* Surface and coatings technology, 1988. 34: p. 365-371.
118. W.L. Xu, T.M. Yue, H.C. Man and C.P. Chan, *Laser surface melting of aluminium alloy 6013 for improving pitting corrosion fatigue resistance.* Surface and coatings technology 2006. 200: p. 5077-5086.
119. O. Kachurina, T.L. Metroke and K. Dou, *Laser induced electrochemical characteristics of aluminium alloy 2024-T3.* Journal of Laser Applications, 2004. 16(1): p. 46-51.
120. K.G. Watkins, M.A. McMahon and W.M. Steen, *Microstructure and corrosion properties of laser surface processed aluminium alloys: a review.* Materials Science and engineering A, 1997. A231: p. 55-61.
121. T.R. Anthony and H.E. Cline, *Surface rippling by surface tension gradients during laser surface melting and alloying.* Journal of Applied Physics, 1977. 148(9): p. 3888-3894.
122. C. Xie, *Evaluation of alloy element redistribution within laser-melted layer.* Surface and Coatings Technology, 1999. 113 p. 1-4.
123. K.G. Watkins, Z. Liu, M. McMahon, R.Vilar and M.G.S. Ferreira, *Influence of the overlapped area on the corrosion behaviour of laser treated aluminium alloys.* Materials Science and engineering A, 1998. 252: p. 292-300.
124. T.T. Wong and G.Y. Liang, *Effect of laser melting treatment on structure and corrosion behaviour of Aluminium and Al-Si alloys.* Journal of materials processing technology, 1997. 63: p. 930-934
125. Z. Liu, P.H. Chong, A.N. Butt, P. Skeldon and G.E. Thompson, *Corrosion Mechanism of laser melted AA2014 and AA2024 alloys.* Applied surface science 2005. 247: p. 294-299
126. L.F. Guo, T.M. Yue and H.C. Man, *Excimer laser surface treatment of magnesium alloy WE43 for corrosion resistance improvement.* Journal of Materials Science 2005. 40: p. 3531-3533.
127. N. Tareelap, *Laser Surface Alloying of Aluminium alloys,* 2009, The University of Birmingham, Metallurgy and Materials, PhD.
128. R. Doyle, B. Connolly and P. Bowen, *Effects of Laser surface melting technique used for corrosion resistance on the fatigue properties of friction stir welded Al-alloys,* 2004, University of Birmingham Department Metallurgy and Materials Student Report.
129. M. Autric, J. Perrais and G. Barreau, *Corrosion resistance improvement of metals by excimer laser surface treatment.* High power lasers in manufacturing, proceedings of SPIE, 2000. 3888: p. 742-749.
130. C.P. Chan, T.M. Yue and H.C. Man, *Effect of excimer laser surface treatment on corrosion behaviour of aluminium alloy 6014.* Materials science and technology, 2002. 18: p. 575-580.

131. A.J. Davenport, M. Jariyaboon, C. Padovani, N. Tareelap, B.J. Connolly, S.W. Williams and E. Siggs, *Corrosion and protection of friction stir welds* Materials science forum 2006. 519-521: p. 699-704.
132. C. Padovani, A.J. Davenport and B. Connolly, *Atmospheric exposure of 2024 and 7010 after laser surface melting*. 2004, University of Birmingham Metallurgy and Materials Student Report.
133. J.M. Ranalli, A.J. Davenport and B. Connolly, *Corrosion resistance of AA2024-T351 laser surface alloyed with manganese and tungsten,* 2003, University of Birmingham Department Metallurgy and Materials Student Report.
134. R. Bell, A.J. Davenport and B. Connolly, *Corrosion resistance of AA2024-T351 laser surface alloyed with manganese and molybdenum,* 2004, University of Birmingham Department Metallurgy and Materials Student Report.
135. Z. Szklarska-Smialowska, *Insight into the pitting corrosion behaviour of aluminium alloys.* Corrosion Science, 1992. 33(8): p. 1193-1202.
136. G.S. Frankel, R.C. Newman, C.V. Jahnes and M.A. Russak, *On the pitting resistance of sputter-deposited aluminium alloys.* Journal of Electrochemistry Society, 1993. 140(8): p. 2192-2197
137. R.B. Inturi and S. Szklarska-Smialouwska, *Structure, composition and pitting behaviour of sputtered Al Al-Cr and Al-Ta films.* Corrosion science, 1993. 34(8): p. 1201-1212
138. A.J. Davenport, B. Connolly, M. Jariyaboon, R. Ambat, C. Padiovani, J.M. Ranalli, S. Fox, R. Winsley and R. Bell, *Laser surface modification of 2024: Summary of Undergraduate projects.* 2004.
139. H. Yoshika, H. Habazaki, A. Kawashima, K. Asami and K. Hasimoto, *An XPS study of corrrosion behaviour of sputter-deposited amorphous Al-W alloys in 1M HCl.* Corrosion science, 1991. 32(3): p. 313-325.
140. G.D. Davis, W.C. Mosher, T.L. Fritz and G.O. Cote, *Evolution of chemistry of passive films of sputter deposited supersaturated aluminium alloys.* Journal of Electrochemistry Society, 1990. 137(2): p. 422-427
141. H. Schafer and H.R. Stock, *Improving the corrosion protection of aluminium alloys using reactive magnetron sputtering.* Corrosion Science, 2005. 47: p. 953-964
142. F. Mansfield and Y. Wang, *Develpoment of "stainless" aluminium alloys by surface modification.* Materials science and engineering A, 1995. 198 p. 51-61.
143. V.P. Rohshtein. *Metallic materials processing with intense pulsed e-beams*. *12th International Conference High-Power Particle Beams*. 1998 1 105-110: IEEE.
144. Y. Qin, J. Zou, C. Dong, X. Wang, A. Wu, Y. Liu, S.Z. Hao and Q.F. Guan, *Temperature-stress fields and related phenomena induced by a high current pulsed electron beam.* Nuclear instruments and methods in Physics research B, 2004. 225: p. 544-554.
145. J. Zou, Y. Qin, C. Dong, X. Wang, A. Wu and S. Hao, *Numerical simulation of the thermal-mechanical process of high current pulsed electron beam treatment.* Journal of vacuum science technology A, 2004. 22(3): p. 545-552.
146. S.Z. Hao, Y. Qin, X.X. Mei, B. Gao, J.X. Zou, Q.F. Guan, C. Dong and Q.Y. Zhang, *Fundamentals and applications of material modification by intense pulsed beams.* Surface and coatings technology, 2007(19-20): p. 8588-8595.
147. E. Dewald, K. Frank, D.H.H. Hoffman, R. Stark, M. Ganciu, B.N. Mandache, M.G. Nistor, A.M. Pointu and I.I. Popescu, *Pulsed intense electron beams generated in*

transient hollow cathode discharges: fundamentals and applications. IEEE transactions on plasma science 1997. 25(2): p. 272-278.
148. E. Dewald, K. Frank, D.H.H. Hoffmann, M. Ganciu, N.B. Mandache, M. Nistor, A.M. Pointu and I.L. Popescu, *Intense electron beams produced in pseudospark and PCOHC for beam-plasma interaction experiments.* Nuclear instruments and methods in Physics Research A 1998 415 p. 614-620.
149. P.E.J. Flewitt and R.K. Wild, *Physical Methods for Materials Characterisation*. 1994: Institute of Physics Publishing.
150. P.M. Belcaguy, N. Mingolo and O.E. Martinez, *Measurement of the current density profile of a pulsed electron beam for surface treatment.* IEEE transactions on plasma science, 2003. 31(4): p. 788-792.
151. D.I. Proskurovsky, V.P. Rotshtein and G.E. Ozur, *Use of low energy, high current electron beams for surface treatment of materials.* Surface and Coatings Technology, 1997. 96: p. 117-122.
152. V. Engelko, B. Yatsenko, G. Mueller and H. Bluhm, *Pulsed electron beam facility (GESA) for surface treatment of materials.* Vacuum 2001. 62 p. 211-216.
153. H. Gotkas, H. Kirkice, G. Oke and M.V. Udrea, *Microprocessing by intense pulsed electron beam.* IEEE transactions on plasma science, 2002. 30(5).
154. R.A. Dugdale, *Review soft vacuum processing of materials with electron beams.* Journal of materials science, 1975. 10: p. 896-904.
155. C. Schulthesis, V. Engelko, G. Kraft, G. Schumacher and G. Muler, 2000, Pulsed electron beam sources and its use. US 6049162.
156. G. Mueller, H. Bluhm, A. Heinzel, G. Schumacher, D. Strauss, V. Engelko, V. Shulov, N. Notchovnaia, A. Weisenburger and F. Zimmermann. *Application of pulsed electron beams for improvement of material surface properties*. *25th IEEE International Pulsed Power* 2002 154-157.
157. H. Goktas, H. Kirkici, G. Oke and M.V. Udrea, *Microprocessing by intense pulsed electron beam.* IEEE transactions on plasma science, 2002. 30(5): p. 1837-1841.
158. N. Mingolo, Y. Cesam, O.E. Martinez, J.I. Etcheverry and J.J. Rocca, *Enhanced energy deposition efficiency of glow discharge electron beams for metal surface treatment.* IEEE transactions on plasma science 2000. 28(2): p. 386-393.
159. J.I. Etcheverry, O.E. Martinez and N. Mingolo, *Numerical modelling of materials processing applications of a pulsed cold cathode electron gun.* Journal of Applied Physics, 1998. 82(8): p. 3856-3864.
160. J.J. Rocca, C.R. González, O.E. Martinez and N. Mingolo, *Stabilization of a cold cathode electron beam glow discharge for surface treatment.* Journal of Applied Physics 1997 82(8): p. 4118-4120.
161. D.A. Price, *Characterisation of electron beam samples*, 2004, E. Siggs.
162. R. Stark, *Pseudospark produced electron beam for material processing.* IEEE Transactions on plasma science, 1995. 23(3): p. 258-264.
163. T. Grosdidier, J.X. Zou, N. Stein, C. Boulanger, S.Z. Hao and C. Dong, *Texture modification, grain refinement and improved hardness/corrosion balance of a FeAl alloy by pulsed electron beam surface treatment in the "heating mode"*. Scripta Materialia, 2008. 58(12): p. 1058-1061.
164. V.P. Rotshtein. *Metallic materials processing with intense pulsed electron beams*. *12th International High Power Particle Beams*. 1998 1 105-110. Israel: IEEE.

165. R.G. Song, K. Zhang and G.N. Chen, *Electron beam surface treatment. Part 2 microstructure evolution of stainless steel and aluminium alloy during electron beam rapid solidification.* Vacuum 2003. 69: p. 517-520.
166. M. Ahmad, J.I. Akhter and M.A. Shaikh, *Microstructure evolution in the electron beam treated surface of a Ni-base single crystal.* Journal of alloys and compounds, 2006. 422(28, 1-2): p. 97-101
167. A.L. Barbera, A. Mignone, S. Tosto and C. Vigaud, *Electron beam cladding and alloying of AISI 316 on plain carbon steel: microstructure and electrochemical corrosion behaviour.* Surface and coatings technology 1991. 46 p. 317-329.
168. V.P. Rotshtein, D.I. Proskurovsky, G.E. Ozur, K.V. Karlik, Y.F. Ivanov and A.B. Markov, *Microstructure of near surface layers of austenic stainless steels irradiated with low energy high current electron beams.* Surface and Coating Technology, 2004. 180-181 p. 382-386.
169. D.I. Proskurovsky, V.P. Rotshtein, G.E. Ozur, Y.F. Ivanov and A.B. Markov, *Physical foundations for surface treatment of materials with low energy, high current electron beams.* Surface and Coatings Technology, 2000. 125: p. 49-56.
170. Y. Ivanov, W. Matz, V.P. Rotshtein, R. Gunzel and N. Shevchenko, *Pulsed electron beam melting of high speed steel: structural phase transformations and wear resistance.* Surface and Coatings Technology, 2002. 150: p. 188-198.
171. J. Zou, T. Grosdidier, K. Zhang and C. Dong, *Mechanism of nanostructures and metastable phase formations in the surface melted layers of a HCPEB-treated D2 steel.* Acta Materialia 2006. 54: p. 5409-5419.
172. N. Mingolo and J.J. Rocca, *Production of amorphous metallic surfaces by means of a pulsed glow discharge electron beam.* Journal of Materials research 1992. 7(5): p. 1096-1098.
173. H.M.W. Hailu and T. Bell, *Electron beam surface alloying of Titanium alloy Ti6Al4V towards improved tribological properties,* 1997, University of Birmingham School of Metallurgy and Materials, PhD.
174. R.G. Song, K. Zhang and G.N. Chen, *Electron beam surface treatment. Part 1 surface hardening of AISID3 tool steel.* Vacuum 2003. 69: p. 513-516.
175. S. Tosto, P. Vanhille and C. Vignaud, *Ti cladding and Ni alloying on pure aluminium and aluminium alloys by an electron beam technique.* Surface and coatings technology, 1993. 58: p. 137-142.
176. J.P. Sargent, S. Jenkins, S.J. Harris, C.C. Figgures and D.G. Dixon, *Adapting crawler Robot Crawler for NDT,* 2003, BAE Systems JS15114.
177. D.A. Price and S. Scott, *Surface melting of NAB using a pulsed e-beam source*, 2004, E. Siggs. BAE systems presentation.
178. T. Bell, M.H. Sohi, J.R. Betz and A. Bloyce, *Energy beams in second generation surface engineering of aluminium and titatnium alloys.* Scandinavian Journal of Metallurgy, 1990. 19: p. 218-226.
179. Y. Uno, A. Okada, K. Uenura, A. Raharjo, T. Furukawa and K. Karato, *High efficiency finishing process for metal mold by large area electron beam irradiation.* Precision Engineering, 2005. 29(4): p. 449-455.
180. V.P. Rotshtein, D.I. Proskurovsky, G.E. Ozur, Y.F. Ivanov and A.B. Markov, *Surface Modification and alloying of metallic materials with low energy high current electron beams.* Surface and Coating Technology, 2004. 180-181: p. 377-381.
181. D.I. Proskurovsky, V.P. Rotshtein, G.E. Ozur, A.B. Markov, D.S. Nazarov, V.A. Shulov, Y.F. Ivanov and R.G. Buchheit, *Pulsed electron beam technology for surface*

modification of metallic materials Journal vacuum science and technology A 1998. 16(4): p. 2480-2488.
182. D.S. Nazarov, A.B. Markov, G.E. Ozur, D.I. Proskurovsky, I.M. Goncharenko, V.P. Rotshtein, L.S. Bushnev, R.G. Buchheit, E.F. Dudarev and G.P. Pochivalova. *Modification of the structure and properties of aluminium alloys by low energy high current electron beams*. *5th International Conference on Electron Beam Technologies*. 1997. Varna, Bulgaria.
183. S.H. Choo, S. Lee and M.G. Golkovski, *Effects of accelerated electron beam irradiation on surface hardening and fatigue properties in an AISI 4141 steel used for automotive crankshaft.* Materials Science and Engineering A, 2000. 293: p. 56-70.
184. A. Zecca, R.S. Brusa, M. Duartenaia, J. Paridaens, A.D. Pogrebnjal, A.B. Markov, G.E. Ozur, D.I. Proskurovski and V.P. Rotshtein, *Modification of α-Fe surface using low energy high current electro beam.* Physics letters A, 1993. 175: p. 433-440.
185. V.P. Rotshtein, Y.F. Ivanov, A.B. Markov, D.I. Proskurovsky, K.V. Karlik, K.V. Oskomov, B.V. Uglov, A.K. Kuleshov, M.V. Novitskaya, S.N. Dub, Y. Pauleau and I.A. Sulepov, *Surface alloying of stainless steel 316 with copper using pulsed electron beam melting of film-substrate system.* Surface and coatings technology 2006. 200: p. 6378-6383.
186. K. Zhang, J. Zou, T. Grosdidier, C. Dong and D. Yang, *Improved pitting corrosion resistance of AISI 316l stainless steel treated by high current pulsed electron beam.* Surface and coatings technology, 2006 201(3-4): p. 1393-1400.
187. M. Ahmad, J.I. Akhter, G. Ali, M. Akhtar and M.A. Choudhry, *Characterisation of electron beam modified surface of Zircaloy-4.* Journal of alloys and compounds, 2006. 426(1-2): p. 176-179.
188. B. Gao, S. Hao, J. Zou, T. Grosdidier, L. Jiang, J. Zkou and C. Dong, *High current pulsed electron beam treatment of AX31 Mg alloy.* Journal of vacuum science technology A, 2005. 23(6): p. 1548.
189. C. Dong, A. Wu, S. Hao, J. Zou, Z. Liu, P. Zhong, A. Zhang, T. Xu, J. Chen, J. Xu, Q. Lin and Z. Zhou, *Surface treatment by high current pulsed electron beam.* Surface and coatings technology 2003. 163-164: p. 620-624.
190. H. Bluhm, R. Bohme, W. Frey, H. Giese, P. Hoppe, G. Kebler, G. Muller, N. Neubert, D. Rusch, C. Schultheib, G. Schumacher, M. Sohner, H. Strabner, D. Straub, W. Vath, F. Zinnerman, V. Engelko, A. Dulson and V.I. Kurets. *Industrial applications of high voltage pulsed power techniques: Developments at Forschungszentrum Karlsruhe (FZK). 11th Pulsed Power Conference*. 1997 1 1-12: IEEE.
191. B. Gao, S. Hao, J. Zou, W. Wu, G. Tu and C. Dong, *Effect of high current pulsed electron beam treatment on surface microstructure, wear and corrosion resistance of an AZ91HP magnesium alloy.* Surface and coatings technology 2007. 201: p. 6297-6303.
192. S. Hao, B. Gao, A. Wu, J. Xou, Y. Qin, C. Dong, J. An and Q. Guan, *Surface modification of steels and magnesium alloy by high current pulsed electron beam.* Nuclear instruments and methods in physics research B 2005. 240: p. 646-652.
193. S.A. Morgan, *Summary Report TRILAP* 1999, BAE Systems Sowerby Rresearch Centre. JS 14235.
194. J. Sidhu, *Characterisation of Diffractive Lens Arrays used for beam homogenisation and ring focusing,* 1997, BAE Systems internal report Sowerby Research Centre JS13651.

195. P.J. Marsden, *Excimer Laser processing with a Microlens Array,* 1996, BAE Systems Sowerby Research Centre JS13509.
196. *Destructive tests on weld in metallic materials – bend tests*. 1996, European Standard NBNEN 910.
197. A. Vaugh, *Nd:YAG work LSM,* Unpublished work, Cranfield University, PhD.
198. J.W. Elmer and A.T. Teruya, *An enhanced faraday cup for rapid determination of power density distribution in electron beams.* American welding society, 2001: p. 288-S.
199. *Standard Practice for operating salt spray (Fog) apparatus.* ASTM international, 2004. B 117-03.
200. E. Siggs and S. Morgan, *Laser Preparation for Friction Stir Welding,* 2007, BAE Systems. TES100750.
201. S.G. Pantelakis, T.B. Kermanidis and G.N. Haidemenopoulos, *Mechanical behaviour of 2024 Al alloy specimen subjected to paint stripping by laser radiation and plasma etching.* Theoretical and applied fracture mechanics, 1996. 25: p. 139-146.
202. S.G. Pantelakis and G.N. Haidemenopoulos, *Effect of novel paint removal method processes on the fatigue behaviour of aluminium alloy 2024.* Surface and Coatings Technology, 1998. 106: p. 198-204
203. C. Padovani, A.J. Davenport and B. Connolly, *Characterisation of AA7449-T7951 after laser surface melting.* 2004, University of Birmingham Metallurgy and Materials Student Report.
204. P.L. Bonora, M. Bassoli, G. Cerisola, P.L. DeAnna, G. Buttaglin, G. DellaMea and P. Mazzoldi, *On the corrosion behaviour of laser irradiated aluminium surfaces.* Thin Solid Films 1981. 81: p. 339-345.
205. C. Padovani, A.J. Davenport and B. Connolly, *Corrosion protection of friction stir welds in high strength Aluminium alloys. Student Report.,* 2004, University of Birmingham.
206. T.M. Yue, C.F. Dong, L.J. Yan and H.C. Man, *The effect of laser surface treatment on stress corrosion cracking behaviour of 7075 Al-alloy.* Materials Letters, 2004. 58: p. 630-635.
207. E. Sicard, C. Boulmer-Leborgne, C. Andreazza-Vignolle, P. Andreazza, C. Langlade and B. Vannes, *Excimer laser treatment for aluminium alloy mechanical property enhancement.* Surface and coatings technology, 1998. 100-101: p. 440-444.
208. N.H. Prasad and R. Balasubramaniam, *Influence of laser surface treatment on oxidation behaviour of an Al-Li-Cu alloy.* Journal of Materials processing technology, 1997. 68: p. 117-120.
209. D. Dube, M. Fiset, A. Couture and I. Nakatsugawa, *Characterisation and performance of laser melted AZ91D and AM60B.* Materials Science and engineering A, 2001. 299 p. 38-45.
210. S. Tosto, P. DiLazzaro, T. Letardi and S. Martelli, *Metal surface treatments by means of high energy UV laser pulses.* Excimer lasers and applications, 1988. 1023: p. 208-215.
211. C. Spadaro, C. Sumeri and C. Dispenza, *Laser surface treatment for adhesion improvement of aluminium alloys structural joints.* Radiation physics and chemistry 2007. 76: p. 1441-1446.
212. P. Mazzoldi, G.D. Mea, G. Battaglin, A. Miotello, M. Servidori, D. Bacca and E. Jannitti, *Formation of a nanocrystalline phase in aluminium irradiated with a pulsed ruby laser.* Physics review letters, 1980. 44(2): p. 88-92.

213. P. Petrov, *Electron beam surface re-melting and alloying of aluminium alloys.* Vacuum, 1997. 48(1): p. 49-50.
214. W. Biller, D. Heyden, D. Muller and G.K. Wolf, *Modification of steel and aluminium by pulsed energetic ion beams.* Surface and coatings technology 1999. 116-119: p. 537-542.